The evolution of musculoskeletal anatomy and locomotor mode in frogs

Alice Camomile Hardy Leavey

A thesis submitted in partial fulfilment of the requirements for the degree of Doctor of Philosophy at University College London

Centre for Integrative Anatomy

Cell and Developmental Biology

University College London

&

Structure and Motion Laboratory

Comparative Biomedical Sciences

Royal Veterinary College

September 2023

Supervised by Dr Laura Porro (UCL) & Dr Christopher Richards (RVC)

Word count: 72307

Declaration

I, Alice Leavey, confirm that the work presented in this thesis is my own. Where information has been derived from other sources, I confirm that this has been indicated in the thesis.



Date: 20/09/2023

Abstract

Frogs have a highly conserved body plan, yet they employ a diverse array of locomotor modes across many environments, making them ideal organisms for investigating the relationships between morphology, function, ecology, and evolution. The biomechanical implications of anatomical variation for locomotor function are not well-understood on a broad ecological and phylogenetic scale. The overarching aim of this thesis is to improve our understanding of whether anatomical complexity is a prerequisite for functional complexity in frogs. Chapter 2 quantifies the relationship between locomotor mode, habitat type, phylogenetic history, and skeletal morphology for 164 frogs from all recognised anuran families. In Chapter 3, I use contrast-enhanced µCT imaging to digitally dissect the gross muscle anatomy of the pelvis and hindlimbs for a subset of 30 species representing all locomotor modes, forming the largest digital comparative analysis of musculoskeletal structure in frogs to date and creating a library of 3D anatomical data for use in future simulations of locomotor function. Chapter 4 presents the first digital extraction of muscle fibres in frogs using a cutting-edge automated fibre tracking algorithm to determine the relationship between locomotor mode and muscle architecture, which has important implications for the trade-off between muscle force production and contractile speed. Chapters 5 and 6 directly test the impact of different hindlimb proportions on jumping mechanics using inverse kinematics and inverse dynamics models, respectively. By quantifying the relationships between skeletal anatomy, muscle anatomy, locomotor mode, and phylogenetic history, this thesis sheds new light on how functional demands impact morphology across 160 million years of anuran evolution. This work presents crucial insights that are significant for palaeontological studies, as the shape and size of fossil bones are often used to infer the size of soft tissue structures and the behaviour of extinct taxa.

Word count: 291

Impact statement

By linking musculoskeletal dissections, biomechanical models and phylogenetic comparative methods, my thesis utilises a powerful combination of modern techniques to visualise, quantify, and compare relationships between anatomy and function across 160 million years of anuran evolution. This analysis has included some of the oldest, largest, smallest, and most evolutionarily distinct frog species in the world. I present previously unreported anatomical differences between frogs specializing in different locomotor modes, as well as examples of many-to-one and one-to-many mapping of form to function across their phylogeny. The outputs of each chapter feed directly into the following chapters, creating a workflow of research methods which enables future comparative analyses of vertebrates.

Until now, digital comparative analyses of pelvis and hindlimb skeletal proportions (Chapter 2; 164 taxa), muscle anatomy (Chapter 3; 30 taxa), fibre architecture (Chapter 4; ten taxa), and jumping kinematics (Chapter 5; 164 taxa) have never been performed on this taxonomic scale in frogs before. Chapter 3 presents the first known post-vertebral dissection for some of the world's smallest frogs, as well as the smallest hindlimb muscles (i.e., the hip and tarsals). Chapter 4 utilises a cutting-edge fibre tracking algorithm to perform the first digital analysis of frog fibre architecture. These chapters therefore provide novel insights into anatomical features that are practically impossible to extract using traditional methods. Chapters 5 and 6 employ innovative biomechanical approaches to explore how differences in hindlimb geometry impact jumping mechanics. By using hypothetical models of different anatomical proportions, I also explore the individual contribution of each hindlimb segment (Chapter 5) and joint (Chapter 6) to take-off. This powerful theoretical approach, combined with predictive models (Chapter 2), defines a path by which future studies could predict the locomotor mode of extinct taxa using fossil data. This could answer whether the ancestral anuran locomotor mode is jumping or walking, which is a long-standing debate.

Knowledge and resources have been, and continue to be, actively contributed to several different fields throughout the thesis on an international scale. So

far, this research has been presented at one museum outreach event and six conferences across Europe, North America, and Australia. Chapter 2 has been published in the Journal of Anatomy, and Chapters 3 and 4 have manuscripts in preparation. My research has also increased anatomical data accessibility, which will be crucial for the future studies of anuran anatomy and biomechanics suggested throughout this thesis. Thirty digital dissections will be made publicly available upon publication of Chapter 3 to create a valuable library of 3D musculoskeletal models. Furthermore, ten new contrastenhanced scans were uploaded to MorphoSource through a two-month research visit to the Blackburn Lab (Florida Natural History Museum), which was funded by a successful application to the UCL Bogue Fellowship.

Finally, this work provided teaching and training opportunities for undergraduate students. I designed the end-of-year assessment in two statistics modules at UCL using data from Chapter 2. Questions arising from this chapter regarding pelvic morphology led me to design and co-supervise two research projects for the third-year bio-veterinary degree at RVC.

Word count: 500

Conference presentations

Leavey, A. & Porro, L.B. Comparative analysis of musculoskeletal anatomy in relation to locomotor mode in frogs.

- In-person presentation (28 July 2 Aug 2023) International
 Conference for Vertebrate Morphology (ICVM); Cairns, Australia.
- In-person presentation (4-7 July 2023) The Society of Experimental Biology (SEB) annual meeting; Edinburgh, Scotland.

Leavey, A., Porro, L.B. & Richards, C.T. *Modelling the effect of different skeletal proportions on hindlimb kinematics in frogs.*

- In-person presentation (3-7 Jan 2023) The Society of Integrative and Comparative Biology (SICB) annual meeting; Austin, Texas, USA.
- In-person presentation (25 Nov 2022) The Centre for Ecology and Evolution (CEE) autumn symposium; London, UK.
- In-person presentation (3-7 Oct 2022) SEB early career research symposium; Helsinki, Finland.
- Virtual presentation (5 Feb 2022) The UMass Movement Research Centre (UMOVE) student research symposium; University of Massachusetts Lowell, USA.

Publications

Leavey, A., Ruta, M., Richards, C.T. & Porro, L.B. (2023). Locomotor, ecological and phylogenetic drivers of skeletal proportions in frogs. *Journal of Anatomy*, 243(3), pp.404-420.

Research paper declaration form

- 1. For a research manuscript that has already been published:
 - a. Where was the work published? Journal of Anatomy
 - b. Who published the work? Wiley Blackwell Publishing
 - c. When was the work published? 19/05/2023
 - d. Was the work subject to academic peer review? YES
 - e. Have you retained the copyright for the work? YES
- 2. For multi-authored work, please give a statement of contribution covering all authors:

Dr Laura Porro and Dr Chris Richards conceived and supervised the study. I collected all the data and, with assistance from Laura and Dr Marcello Ruta, performed the data analysis. I drafted the manuscript, and all authors provided constructive feedback.

3. In which chapter(s) of your thesis can this material be found?
Chapter 2



4. Candidate's e-signature:

Date: 19/05/2023

5. Supervisor/senior author(s) e-signature:

Date: 15/09/2023



Acknowledgements

First and foremost, I'd like to thank my primary supervisors, Dr Laura Porro (UCL) and Dr Chris Richards (RVC) for their supervision and guidance. Laura massively contributed to µCT data collection and discussions of the trends seen in anatomical data, while Chris was fundamental in building and trouble-shooting all biomechanical models. Additionally, I would like to thank Dr Ryan Felice (UCL) for his advice on comparative morphometrics and, along with Prof Susan Evans (UCL), for their feedback as Thesis Committee members.

I would like to thank the Blackburn Lab for welcoming me as one of their own during my two-month placement at the University of Florida, and for sharing many of the frog μ CT scans I used in this thesis. In particular, thanks to Dr Jaimi Gray for the training in contrast-enhanced staining and scanning protocols and digital dissection in VGStudio.

For the manuscript published based on the work in Chapter 2, I also thank Dr Marcello Ruta (University of Lincoln) for helping me perform phylogenetic statistical analyses and for comments on the manuscript; Dr Andrew Gray (Manchester Museum) for providing many of the specimens that Laura µCT-scanned from his own collection and for first-hand information on locomotor mode in various species of frog; Dr Hannes Baur (Natural History Museum of Bern) for assisting with my understanding of his Multivariate Ratio Analysis; and Dr Raúl Gómez (Universidad de Buenos Aires) and two anonymous reviewers for their comments.

Finally, I would like to thank my family and friends, without whom this would not have been possible – my husband Edd for helping me to achieve some sense of work-life balance; Rebecca Leavey for the consistent emotional support; Dr Simon Pearce for our enthusiastic discussions which made me feel proud of my work; Kevin and Lesley Leavey for providing sanctuary when life got me down; Shana Shah and all of my wonderful friends from the University of Nottingham for charging my social battery; and finally, my cat Nova, who was my work colleague, sound board, Zoom meeting buddy and serotonin supply throughout the entire PhD.

Funding

This PhD was funded by the London Interdisciplinary Doctoral (LIDo) programme, which is funded by the Biotechnology and Biological Sciences Research Council [grant number BB/M009513/1]. Costs associated with staining and scanning museum specimens (Chapter 3) were covered by the oVert project, which is funded by the National Science Foundation (grant number 1701714), while trip expenses were covered by the UCL Bogue Fellowship.

Table of Contents

Dec	laration		2
Abs	tract		3
Impa	act stater	ment	4
Con	ference p	presentations	6
Pub	lications.		6
Res	earch pa	per declaration form	7
	-	ements	
	_		
		viations	
List	of muscl	e abbreviations	17
List	of Tables	3	18
List	of Figure	es	20
1	Introduc	tion	24
2	Determi	ning the link between skeletal morphology and locomotor mo	de,
	habitat t	ype and phylogenetic history	31
2.	1	Introduction	31
2.	2	Methods	33
	2.2.1	Sampling	33
	2.2.2	Pelvic morphology	
	2.2.3	Phylogeny	35
	2.2.4	Locomotor mode	35
	2.2.5	Habitat type	35
	2.2.6	Statistical analyses	36
2.	3	Results	39
	2.3.1	Skeletal morphology across locomotor modes, habitat types a phylogenetic groups	
	2.3.2	Shape PCA spectrums for visualising the relative importance structural morphological ratios	
	2.3.3	Phylogenetic analysis	47
	2.3.4	The predictive power of skeletal morphology	48

	2.4	Discussion 5	52
	2.4.1	Body and limb proportions show distinct patterns in relation function	
	2.4.2	Skeletal pelvic morphology is important, and should be considered along a continuum	
	2.4.3	Locomotor mode has the greatest impact on morphology 5	56
	2.4.4	Skeletal morphology can be a powerful predictor of function ar ecology	
	2.4.5	Riparian morphology is influenced more by jumping the swimming	
	2.4.6	Limitations	59
	2.4.7	Future directions5	59
	2.4.8	Conclusion6	30
3	Gross n	nuscular anatomy of the anuran pelvis and hindlimb in relation	to
		tion 6	
	3.1	Introduction6	32
	3.2	Methods6	36
	3.2.1	Dataset6	36
	3.2.2	UF specimen preparation6	36
	3.2.3	μCT scanning6	38
	3.2.4	Digital dissection6	38
	3.2.5	Extracting gross anatomical muscle data	72
	3.2.6	Considering potential variation in muscle shrinkage	74
	3.2.7	Statistical analyses	75
	3.3	Results	⁷ 6
	3.3.1	Comparative anatomy of pelvis musculature	76
	3.3.2	Comparative anatomy of hindlimb musculature	30
	3.3.3	Muscle number	
	3.4	Discussion 9)5
	3.4.1	Pelvic muscles which are more strongly associated with the il are more likely to have attachment sites which differ between locomotor modes	en
	3.4.2	The size of pelvic bone crests could have functional implication for locomotion, but more evidence is needed	
	3.4.3	Locomotor modes differ in where they invest muscle mass, b not always because of relative segment length	

	3.4.4	Variation in the mass of the largest muscles is not sufficient to predict locomotor function
	3.4.5	Small muscles may have an underappreciated role in locomoto function
	3.4.6	Burrowing style does not noticeably impact pelvis and hindlimbanatomy
	3.4.7	The driver of variation in muscle anatomy depends on the hindlimb segment
	3.4.8	Increases in muscle separation could afford greater range o motion and motor control
	3.4.9	Limitations 105
	3.4.10	Future directions106
	3.4.11	Conclusion108
4		chitecture of the anuran hindlimb muscles in relation to locomotion 109
4	4.1	Introduction
4	4.2	Methods114
	4.2.1	Data selection114
	4.2.2	Exporting and preparing muscle image stacks 114
	4.2.3	Automated fibre tracking115
	4.2.4	Pennation angle116
	4.2.5	Statistical analyses117
4	4.3	Results118
	4.3.1	Comparisons of relative fibre length 118
	4.3.2	Comparisons of PCSA
	4.3.3	The relationship between muscle size and architecture 124
4	4.4	Discussion
	4.4.1	Jumpers may increase performance via modifications in fibre architecture more than other locomotor modes
	4.4.2	Fibre architecture may be an example of many-to-one mapping of morphology to function
	4.4.3	Frogs with a minute body size may experience different selection pressures on fibre architecture
	4.4.4	Where species place in functional space depends on the muscle being examined
	4.4.5	Reducing fibre length to amplify force production could reduce the need to grow and maintain high muscle mass, regardless of the degree of pennation

	4.4.6	Pennation angle: to measure or not to measure? 133
	4.4.7	Limitations
	4.4.8	Future directions135
	4.4.9	Conclusion137
5	Modellir	ng the effect of different skeletal proportions on hindlimb
	kinemat	tics138
	5.1	Introduction
	5.2	Methods
	5.2.1	Model organism
	5.2.2	Inverse kinematics model construction and validation 141
	5.2.3	Modelling different frog species
	5.2.4	Hypothetical models147
	5.2.5	Statistical analyses 148
	5.3	Results
	5.3.1	Simulated versus observed kinematics 149
	5.3.2	Comparative analysis of hindlimb kinematics in real frogs 150
	5.3.3	The effect of different hindlimb proportions on kinematics in hypothetical frog models
	5.4	Discussion
	5.4.1	Take-off kinematics varies with hindlimb proportions, but not entirely as hypothesised
	5.4.2	Kinematic trade-offs between segments may be key to optimising the take-off sequence
	5.4.3	Hindlimb proportions affect joint positioning and direction of movement, potentially influencing jumping dynamics 174
	5.4.4	The route to take-off differs significantly between locomotor modes
	5.4.5	Testing unoccupied areas of morphospace 176
	5.4.6	Limitations
	5.4.7	Future directions179
	5.4.8	Conclusion
6	Modellir	ng the effect of different skeletal proportions on hindlimb joint
	dynami	cs182
	6.1	Introduction
	6.2	Methods 184

	6.2.1	Model set up1	184
	6.2.2	Running the dynamics simulation1	187
	6.3	Results1	190
	6.3.1	Ground reaction forces 1	190
	6.3.2	Proximity to the ground reaction force 1	192
		197	
	6.3.3	External joint torques1	198
	6.4	Discussion1	198
	6.4.1	A longer shank, but not proximal foot, reduces the forces need to take off	
	6.4.2	Segment length relative to total hindlimb length has significal impacts on joint dynamics, even if proportions are similar 2	
	6.4.3	The ground reaction force vector orientation changes we different hindlimb proportions	
	6.4.4	Additional factors may be influencing the relationship betwee hindlimb anatomy and dynamics	
	6.4.5	Limitations	202
	6.4.6	Future directions	204
	6.4.7	Conclusion	
7	Thesis	discussion2	207
	7.1	Thesis summary	207
	7.2	Key findings2	208
	7.2.1	Novel insights into how musculoskeletal anatomy different frogs specialising in different locomotor functions co provide the means to predict the lifestyle of extinct specialisms.	uld ies
	7.2.2	Frogs demonstrate high anatomical complexity that could linked to 'many-to-many' mapping of form to function	
	7.2.3	The effect of hindlimb geometry on jumping biomechan depends on which segment of the hindlimb is varied	
	7.3	Future directions	214
	7.3.1	Musculoskeletal dynamics models	214
	7.3.2	Predicting the behaviour of extinct taxa	216
	7.3.3	Assigning categories to continuous data	220
	7.3.4	Generalist versus specialist2	221
	7.3.5	Macroevolutionary relationships between anatomy and funct	

The evolution of musculoskeletal anatomy and locomotor mode in frogs

7.4	Conclusion	224
References		225
Appendices		238
Supplementa	ary Datasets	284

List of abbreviations

AJ: Arboreal jumper

AQ: Aquatic swimmer

BWH: Burrower-walker-hopper

COM: Centre of motion

CSA: Cross-sectional area

DF: Distal foot

DiceCT: Diffusible iodine contrast enhanced computed tomography

EMG: Electromyography

ESD: Expansion of the sacral diapophyses

GRF: Ground reaction force

ID: Inverse dynamics

IK: Inverse kinematics

LDA: Linear discriminant analysis

MBL: Muscle belly length

MBM: Muscle belly mass

MBV: Muscle belly volume

PCA: Principal component analysis

PCSA: Physiological cross-sectional area

PERMANOVA: Permutational multivariate analysis of variance

PF: Proximal foot

pFDA: Phylogenetic flexible discriminant analysis

SVL: Snout-vent length

List of muscle abbreviations

Pelvis STd: Semitendinosus dorsal head

CI: Coccygeoiliacus STv: Semitendinosus ventral head

CS: Coccygeosacralis TFL: Tensor fascia latae

IE: Iliacus externus Shank

LD: Longissimus dorsi ECB: Extensor cruris brevis

PY: Pyriformis PER: Peroneus

Thigh PL: Plantaris longus

AL: Adductor longus TiAB: Tibialis anterior brevis

AMd: Adductor magnus dorsal TiAL: Tibialis anterior longus

AMv: Adductor magnus ventral TiP: Tibialis posticus

CR: Cruralis <u>Tarsals</u>

GE: Gemellus AbdV: Adductor brevis dorsalis V

GM: Gluteus magnus EBS: Extensor brevis superhallucis

GRM: Gracilis major EDCL: Extensor digitorum communis

Iongus GRm: Gracilis minor

FDBS: Flexor digitorum brevis

superficialis

INT: Intertarsalis

II: Iliacus internus
PP: Plantaris profundus

TaA: Tarsalis anticus

OI: Obturator internus

TaP: Tarsalis posticus

PT: Pectineus TP: Transversus plantae

QF: Quadratus femoris

SM: Semimembranosus

SA: Sartorius

IFem: Iliofemoralis

OE: Obturator externus

List of Tables

Table 2.1 - Summary of the variables used in each dataset for the shape PCA
analysis38
Table 2.2 - Descriptive statistics of the key morphometric measurements and ratios
discussed in this chapter41
Table 2.3 - Coefficients from the best PGLS models describing the relationship
between variation in skeletal morphology (PC1 scores and PC2 scores from the full
dataset) and locomotor mode (LM) and habitat type for 164 frog species48
Table 2.4 - Classification results from the linear discriminant analysis49
Table 2.5 - Classification results from the phylogenetic flexible discriminant analysis
50
Table 3.1 - Summary of the thigh and shank muscles which have similar functions
according to Přikryl et al. (2009) and Duellman & Trueb (1986)74
Table 3.2 - Summary of the locomotor pairs which differ significantly in muscle
anatomy according to PERMANOVA tests of the principal components (PC) for each
hindlimb segment86
Table 3.3 - PGLS coefficients for shank muscle count
Table 4.1 - Pairwise Tukey results from the best ANOVA model for size-corrected
physiological cross-sectional area123
Table 4.2 - Pairwise Tukey results from the best ANOVA model for size-corrected
anatomical cross-sectional area124
Table 5.1 - Summary of the relationship between average relative hindlimb segment
length and locomotor mode141
Table 5.2 - Relative hindlimb proportions for each hypothetical frog model148
Table 5.3 - The range of hindlimb segment ratios for the 164 study species148
Table 5.4 - A summary of the most prominent kinematic effects of elongating or
shortening each hindlimb segment156
Table 5.5 - The results of the permutational phylogenetic ANOVAs testing the
relationships between angle change and locomotor mode for 164 frogs158
Table 5.6 - The difference between maximum and minimum protraction-retraction
(PR) and abduction-adduction (AA) polar angles in each model of hypothetical
hindlimb proportions170
Table 5.7 - The difference between maximum and minimum 3D joint angles in each
model of hypothetical hindlimb proportions171

The evolution of musculoskeletal anatomy and locomotor mode in frogs

List of Figures

Figure 1.1 - The complex relationships between anatomy and function25
Figure 1.2 - Three distinct pelvic types
Figure 2.1 - Morphometric measurements used in analysis
Figure 2.2 - pPCA of morphometric measurements for the full dataset, coloured-
coded according to three alternative groupings of locomotor mode (A), habitat type
(B) and phylogenetic group (C)44
Figure 2.3 - Shape PCA ratio spectra for PC1 and PC2 for the structural dataset
containing total body and limb lengths46
Figure 2.4 - Shape PCA ratio spectra for PC1 and PC2 for the full dataset47
Figure 2.5 - Phylogeny of 164 frog species
Figure 2.6 - Examples of the broad variation found in pelvis anatomy in relation to
the three 'distinct' morphotypes56
Figure 3.1 - 3D digital dissection of Hemisus guineensis with annotation of the
skeleton and pelvis muscles in dorsal view70
Figure 3.2 - 3D digital dissection of the right hindlimb of Hemisus guineensis71
Figure 3.3 - Techniques for measuring the length of curved muscles73
Figure 3.4 - The length of longissimus (LD), coccygeosacralis (CS), coccygeoiliacus
(CI) and iliacus externus (IE) relative to their associated bone(s)77
Figure 3.5 - Average mass across locomotor modes for muscles in the pelvis79
Figure 3.6 - A phylomorphospace plot using the principal component (PC) scores
for the pelvic muscles80
Figure 3.7 - Average muscle mass in each hindlimb segment across locomotor
modes81
Figure 3.8 - Average relative mass of each muscle in the thigh across locomotor
modes83
Figure 3.9 - A phylomorphospace plot using the principal component (PC) values
for the muscles in each hindlimb segment86
Figure 3.10 - Average relative mass of each functional muscle group in the thigh
88
Figure 3.11 - Average relative mass across locomotor modes for muscles in the
shank90
Figure 3.12 - Average relative mass of each functional muscle group in the shank
91
D 00 (000

Figure 3.13 - Average relative mass across locomotor modes for muscle	s in the
proximal foot	92
Figure 3.14 - Phylogeny of study taxa derived from Jetz & Pyron (2017) where
branch colours represent muscle count for the thigh (left) and shank (right)	94
Figure 4.1 - Functional space plots hypothesising how the trade-off between	en fibre
length and physiological cross-sectional area (PCSA) can differ betwe	en both
locomotor modes (hypothesis 1) and muscles specialising in different for	unctions
(hypothesis 2)	113
Figure 4.2 - The process of muscle image stack preparation	115
Figure 4.3 - 3D visualisation of Arthroleptis tanneri fibres from the four	muscles
used for analysis	116
Figure 4.4 - Measurement of pennation angle along the force-producing ax	is of the
cruralis and plantaris longus, using Arthroleptis tanneri	117
Figure 4.5 - The relationship between relative fibre length and muscle bell	y length
	120
Figure 4.6 - The relationship between size-corrected physiological cross-s	ectional
area (PCSA) and relative fibre length	123
Figure 4.7 - The relationship between relative fibre length and relative musc	le mass
	126
Figure 4.8 - The relationship between average pennation angle and relative	muscle
mass	128
Figure 5.1 - Hierarchy of system properties in limb modelling	139
Figure 5.2 - Dorsal view of the frog 'stick-figure' model	142
Figure 5.3 - A flow diagram depicting the process of building and valida	iting the
kinematics model	143
Figure 5.4 - A flow diagram depicting the process of building the model fo	r testing
the effect of different segment proportions on hindlimb kinematics	146
Figure 5.5 - Polar angle graphs from validation of the inverse kinematics (Ik	() model
	150
Figure 5.6 - The first and final frames of the take-off sequence for two sets	of three
species exemplifying variation in A) thigh:shank length ratio and B) p	oroximal
foot:total hindlimb length ratio	152
Figure 5.7 - Hindlimb segment kinematics for three species exemplifying v	/ariation
in thigh:shank length ratio	153

Figure 5.8 - Hindlimb segment kinematics for three species exemplifying variation
in proximal foot (PF):total hindlimb length ratio154
Figure 5.9 - 3D joint angles for two sets of three species exemplifying variation in
the ratio between A) thigh and shank length, and B) proximal foot (PF) and total
hindlimb length155
Figure 5.10 - Maximum-minimum protraction-retraction (PR) angle against relative
segment length
Figure 5.11 - Maximum-minimum abduction-adduction (AA) angle against relative
segment length161
Figure 5.12 - Maximum-minimum 3D joint angle for in degrees against relative
segment length
Figure 5.13 - The first frame of the take-off sequence for hypothetical thigh (A),
shank (B) and proximal foot (PF) (C) proportions
Figure 5.14 - Hindlimb segment kinematics for hypothetical thigh proportions
Figure 5.15 - Hindlimb segment kinematics for hypothetical shank proportions
Figure 5.16 - Hindlimb segment kinematics for hypothetical proximal foot (PF)
proportions
Figure 5.17 - 3D joint angles for hypothetical thigh (A), shank (B) and proximal foot (PF) (C) proportions
Figure 5.18 - A visual representation of the hindlimb in the two sets of
'complementary' hypothetical models
Figure 6.1 - A flow diagram depicting the process of building the inverse dynamics model for testing the effect of different segment proportions on hindlimb dynamics
Figure 6.2 - The take-off sequence for <i>Phlyctimantis maculatus</i> with the ground
reaction force and joint torques189
Figure 6.3 - Resultant ground reaction forces for hypothetical hindlimb proportions191
Figure 6.4 - External moment arms and resultant joint torques for each model of
hypothetical thigh proportions195
Figure 6.5 - External moment arms and resultant joint torques for each model of
hypothetical shank proportions

The evolution of musculoskeletal anatomy and locomotor mode in frogs

Figure 6.6 - External moment arms and resultant joint torques for	each model of
hypothetical proximal foot (PF) proportions	197
Figure 7.1 - A prediction of where three extinct frog species (†)	might place in
skeletal morphospace and on a plot of total change in hindlimb orie	entation during
take-off	220

1 Introduction

The complex relationship between form and function, and how it influences animal behaviour has posed a major, long-standing challenge in evolutionary biology. For example, the behaviour and ecology of extinct animals must be inferred from limited fossilised remains; thus, a tight correlation between bone and soft-tissue anatomy, and how this relates to function, is most often assumed (Bates et al., 2021). To better understand the strength of the relationship between form and function in extinct taxa, anatomical characteristics must be measured in living species for which behaviour and ecology is known (Perry & Prufrock, 2018). However, even this approach faces difficulty due to the ability of one trait to influence multiple functions (i.e., 'one-to-many mapping', Figure 1.1A) and multiple morphological configurations to enable the same function (i.e., 'many-to-one mapping', Figure 1.1B) (Wainwright et al., 2005; Holzman et al., 2011; Bergmann & Elroy, 2014; Moen, 2019). Therefore, both detailed descriptions of how anatomy varies between species and quantitative tests of how this can impact function must be carried out to fully understand the evolutionary origins of biological niches. Using this approach, this thesis will advance our understanding of how form-function-behaviour relationships map onto evolutionary relationships.

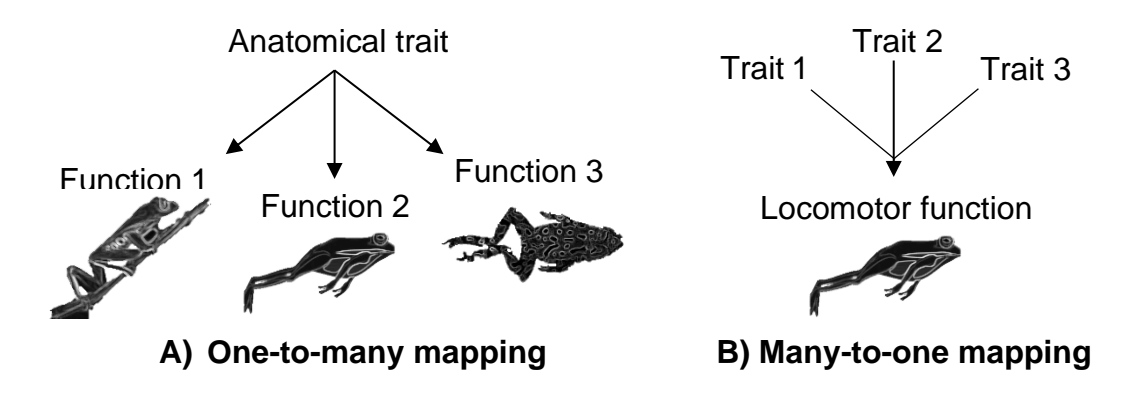


Figure 1.1 - The complex relationships between anatomy and function. A) A morphological feature, such as long hindlimbs, could benefit multiple locomotor modes in different ways. However, this could result in functional trade-offs which cause suboptimal performance, e.g., the selection pressure for limb symmetry in climbers could impede their ability to jump (de Oliveira-Lagôa et al., 2019). B) Multiple anatomical features can enhance the performance of one function, such as long hindlimbs, narrow sacral expansion and short forelimbs for jumping. However, all traits do not necessarily need to be present for that function to be performed optimally, e.g., *Litoria nasuta* holds the record for longest jump distance, yet it has a relatively wide sacral expansion that is not typically associated with strong jumping ability in frogs (James & Wilson, 2008). As one-to-many and many-to-one mapping of form to function can impact performance, and therefore an individual's chances of survival, these complex relationships will have evolutionarily significant consequences.

Anura, part of the Class Amphibia, are ideal model organisms for tackling this fundamental challenge. Frogs are spread across the world, excluding only Antarctica, a few oceanic islands, and the ocean (Wake & Koo, 2018; Amphibiaweb.org, 2022). Many distinctive features separate frogs from even their closest relatives - a shortened and inflexible spinal column of nine or fewer vertebrae, absent tail, an elongated pelvic girdle with a mobile sacro-urostylic joint, and relatively long hindlimbs with elongated ankle bones and fusion of the tibia and fibula, as well as the radius and ulna in the forelimb (Duellman & Trueb, 1986). Relatively small anatomical differences in this largely conserved body plan enable frogs to respond to various mechanical challenges and inhabit numerous ecological niches (Nauwelaerts *et al.*, 2007; Gomes *et al.*, 2009; Moen *et al.*, 2013; Vidal-García *et al.*, 2014; Lires *et al.*, 2016; Tulli *et al.*, 2016; Soliz *et al.*, 2017; Citadini *et*

al., 2018; Moen, 2019). For example, their variation in anatomy is largely linked to the wide array of strategies frogs utilise for feeding, reproducing, and escaping predation (Wells, 2007). Frogs use a range of locomotor modes including walking, hopping, jumping, swimming, burrowing, and climbing to traverse different terrestrial, aquatic, arboreal and subterranean environments (Wells, 2007; the distinction between each locomotor mode and habitat is defined in Chapter 2). In addition, frogs show repeated independent evolution of similar phenotypes on a global scale due to similar microhabitat requirements, suggesting that there are a limited number of ways in which frogs can respond to selection (Moen et al., 2016). This makes them ideal organisms for investigating the relationships between morphology, function, ecology, and evolutionary history.

While the anuran body plan was originally assumed to represent specialisations for jumping (Shubin & Jenkins, 1995; Gans & Parsons, 1966, Přikryl et al., 2009), the most basal extant taxa demonstrate it may have originally evolved for swimming (Astley, 2016) or walking and hopping (Reilly & Jorgensen, 2011). To predict locomotor performance, frog morphometric studies have typically examined total hindlimb length and how it compares to the length of the forelimb and body (Rand, 1952; Zug, 1972; Emerson, 1978; Choi et al., 2003; James et al., 2005; James & Wilson, 2008; Gomes et al., 2009; Herrel et al., 2016; Hudson et al., 2016; Reynaga et al., 2018). For instance, while both terrestrial and arboreal jumpers have long hindlimbs, arboreal jumpers are said to have similarly elongated forelimbs to meet the biomechanical requirements for both climbing and jumping (Simons, 2008), or to compensate for the potential problem of requiring a displaced centre of gravity (de Oliveira-Lagôa et al., 2019). Similarity in fore- and hindlimb length is also associated with frogs that are specialised in walking (Reynaga et al., 2018). Comparatively few studies have investigated how locomotor mode depends on the relative length of each part of the hindlimb, which may play different functional roles in locomotion (Dobrowolska, 1973; Enriquez-Urzelai et al., 2015; Lires et al., 2016; Gómez & Lires, 2019). Therefore, hindlimb segment proportions, and their effect on the relationship between bone and muscle morphology, are an example of anatomical complexity which can impact locomotor performance in frogs.

Anuran pelvis structure has also been key to determining the link between variations in morphology and locomotor performance (Emerson, 1979; 1982; Pugener & Maglia, 2009; Reilly & Jorgensen, 2011; Jorgensen & Reilly, 2013; Soliz *et al.*, 2017; Page 26 of 286

Buttimer et al., 2020). The degree of expansion and shape of the sacral diapophyses, the absence or presence of dorsal ridges on the urostyle and ilia, and the morphology of the sacro-urostylic joint have all been associated with particular locomotor styles and are additional examples of anatomical complexity in frogs. These features are widely used to distinguish three pelvic types (Figure 1.2), which are named after the movements they permit - 'lateral-bending', 'fore-aft sliding' and 'sagittal-hinge' (Emerson, 1979). Previous studies have proposed that these pelvic types are associated with walking, swimming, and jumping, respectively (Emerson, 1979; 1982; Reilly & Jorgensen, 2011; Jorgensen & Reilly, 2013). More recently, it has been demonstrated that frog families (Manzano & Barg, 2005) and locomotor modes (Simons, 2008; Soliz et al., 2017) do not fall neatly into these groups. For example, Litoria nasuta, the pelodryadinine hylid currently holding the record for best jumping performance (equivalent of 55.2 times its body length; James & Wilson, 2008) has a lateral-bender pelvic type typically associated with walking. Recent research suggests that a sagittal-hinge mechanism is not obligatory for jumping, and it may be mostly used to fine-tune jump trajectory (Richards et al., 2018). It is therefore uncertain whether Emerson's three pelvic types accurately represent species-level complexity in pelvic morphology, suggesting that their correlation with particular locomotor modes should be investigated more thoroughly.

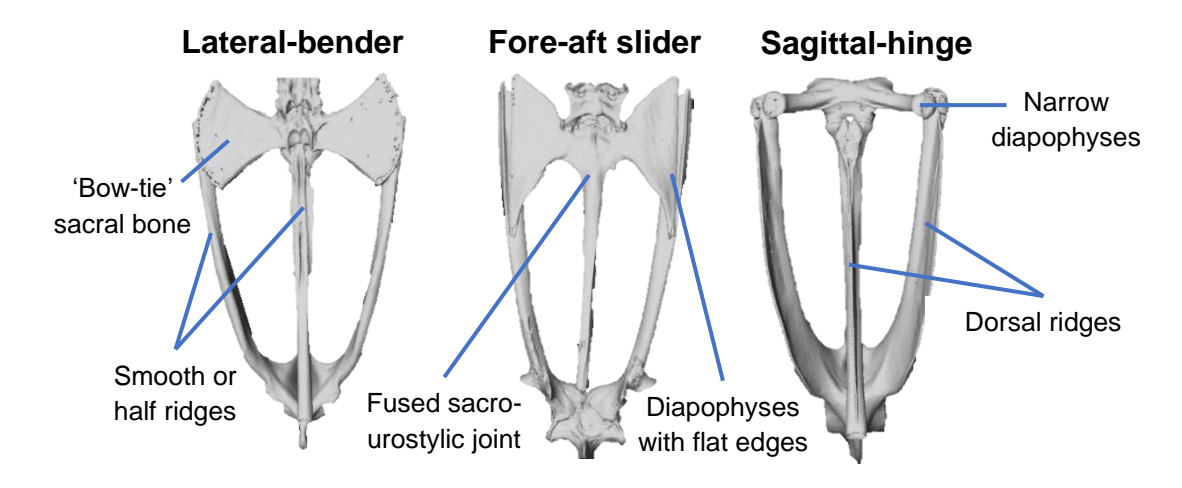


Figure 1.2 - Three distinct pelvic types following the work of Reilly & Jorgensen (2011) and Emerson (1979; 1982) from a dorsal view. Images were extracted from the μCT scans used in Chapter 2. Lateral-bender: *Ansonia mcgreggori* (voucher number: KU:KUH:334742) – walker-hopper in the Hyloidea; Fore-after-slider: *Xenopus calcaratus* (CAS:HERP:207759) – swimmer in the Archaeobatrachia; Sagittal-hinge: *Ptychadena oxyrhynchus* (CAS:HERP:256862) – terrestrial jumper in the Ranoidea.

Comparative analyses of muscle anatomy, and how this relates to locomotor function, are rather limited in frogs. Where the musculature of multiple species has been described, comparisons are largely qualitative (Přikryl et al., 2009). Detailed functional analyses of muscle structures are limited either to multiple muscles in just one species (Kargo & Rome, 2002; Collings et al., 2022), or to a couple of muscles compared across multiple species, which tend to focus on its relevance to jumping and/or swimming (Gillis & Biewener, 2000; Richards & Biewener, 2007; James & Wilson, 2008; but see Astley, 2016; Vera et al., 2022). Additionally, anuran hindlimb muscles have been observed to vary in the degree of muscle head separation, especially in the thigh (Přikryl et al., 2009), which is likely to have functional consequences for motion (Collings & Richards, 2019) but this is yet to be quantified. Frog muscles have also been shown to vary at an architectural level, but again this is rarely described across more than a handful of species and/or muscles (Lieber & Brown, 1992; Lieber & Fridén, 2000; Kargo & Rome, 2002; Mendoza & Azizi, 2021). A detailed comparative analysis of muscle anatomy for all hindlimb segments across multiple representative species for each of the five primary locomotor modes has

not been performed, thus preventing comprehensive evaluations of the functional effects of anatomical complexity.

Even more enigmatic are the biomechanical implications of changes in musculoskeletal anatomy, due to the complexity of tetrapod locomotor systems (Richards, 2019). There are multiple degrees of freedom about limb joints, simultaneous interactions between limb posture and limb structure, and a distal accumulation of joint motion from the hip to the foot, which generates thousands of possible solutions to how a frog might move its hindlimb to achieve specific locomotor functions (Kargo & Rome, 2002). This means that the function(s) that a morphological trait is capable of are not always clear. Rather than investigating a structure's suitability for locomotor multi-functionality (Kargo & Rome, 2002; Nauwelaerts *et al.*, 2007; Figure 1.1A), and why such traits vary across evolution, biomechanical studies have focused largely on how frog morphology is specialised towards a specific locomotor function (James & Wilson, 2008; Roberts *et al.*, 2011; Robovska-Havelkova *et al.*, 2014; Reynaga *et al.*, 2018). Overcoming these challenges will require computational modelling tools capable of acquiring the quantitative evidence needed to untangle the links between form and function.

In summary, the relative impacts of the various constraints and demands associated with locomotor function, habitat type and phylogenetic history on the anuran body plan are understudied (Gomes *et al.*, 2009; Moen *et al.*, 2013; Vidal-García *et al.*, 2014; Soliz *et al.*, 2017; Citadini *et al.*, 2018; Ponssa *et al.*, 2018; Buttimer *et al.*, 2020). My research builds upon prior work by contributing knowledge to one of the most prominent gaps in this field – to what extent is anuran functional complexity (e.g., the ability to perform different locomotor modes) related to complexity in musculoskeletal anatomy (e.g., hindlimb proportions, the size of pelvic features, muscle structure, muscle number, fibre architecture). By mapping these relationships onto the anuran phylogeny, this thesis will contribute knowledge towards a central question in evolutionary biology – whether complexity increases as organisms evolve (McShea, 2000; Adami, 2002). I will analyse anatomical, experimental, and simulated data to:

 Determine the link between skeletal structure and locomotor mode, habitat type and phylogenetic history (Chapter 2).

- Comparatively analyse the gross musculoskeletal anatomy of the hindlimb and pelvis in relation to locomotor mode and phylogenetic history (Chapter 3).
- Extract properties of muscle architecture (i.e., fibre length, pennation angle, physiological cross-sectional area) and analyse them in relation to locomotor mode (Chapter 4).
- Assess the functional significance of differences in hindlimb segment proportions for jumping kinematics (Chapter 5) and joint dynamics (Chapter 6) during take-off.

Combined, these chapters utilise a novel and highly interdisciplinary combination of cutting-edge techniques to bridge the gap in our understanding of how anuran musculoskeletal anatomy, locomotor function, and phylogenetic history are related across 160 million years of anuran evolution.

2 Determining the link between skeletal morphology and locomotor mode, habitat type and phylogenetic history

Dr Laura Porro and Dr Chris Richards assisted in the design of the project and, along with Dr Marcello Ruta, have provided comments on the manuscript published as in Journal of Anatomy result of this the а work (https://doi.org/10.1111/evo.14336). Dr Marcello Ruta assisted with phylogenetic analyses and Dr Laura Porro provided several µCT scans and training in the processing and 3D visualisation of µCT data.

2.1 Introduction

The history of anuran morphometrics is dominated by a focus on the relationship between total limb lengths and jumping performance (Rand, 1952; Zug, 1972; Dobrowolska, 1973; Choi et al., 2003; James et al., 2005; James & Wilson, 2008). In contrast, locomotor modes other than jumping (i.e., walking, hopping, swimming, burrowing, and climbing) have received comparatively less attention (Robovska-Havelkova et al., 2014; Hudson et al., 2016; Reynaga et al., 2018; Vassallo et al., 2021). Even fewer studies have considered how individual hindlimb segments have different functions during locomotion (Dobrowolska, 1973; Enriquez-Urzelai et al., 2015; Lires et al., 2016; Gómez & Lires, 2019). Furthermore, comparative analyses of limb robustness, represented by bone width:length ratio, could also be a potential indicator of locomotor function. For example, larger humeral crests can afford broader attachment sites for forelimb muscles and thus better digging performance, implying that the thickness of the forelimb relative to its length may be a predictor of fossoriality (Emerson, 1976; Keeffe & Blackburn, 2020; Keeffe & Blackburn, 2022). Similarly, hindlimb thickness in aquatic species is associated with large muscles used for underwater propulsion (Gillis & Biewener, 2000). The lack of comparative morphometric studies utilising ratios in addition to measurements of absolute lengths may be hampering conclusions about how locomotor function and skeletal proportions covary (Petrović et al., 2017).

Despite the important progress made by previous studies, disentangling the relationships between anuran morphology, habitat type and locomotor mode remains challenging due to inconsistencies in the taxa examined, skeletal measurement definitions, analytical methods, and allocation of locomotor

categories. For example, Buttimer *et al.* (2020) considered 'burrowing' as a habitat type, but not a locomotor mode, which would have a considerable impact on one of their major findings - that burrowing drove many morphological trends in anurans. This lack of consistency across studies makes it difficult to make conclusive statements about the functional effects of different morphologies.

To address the challenges outlined above, this chapter investigates the relationships between skeletal anatomy, locomotor mode and habitat type for 164 frog species spanning all extant families. Based on the findings of previous literature described in Chapter 1, I hypothesise that:

- H1) jumpers have the largest hindlimb length:snout-vent length (SVL) ratio, while burrowers have the smallest (Gomes *et al.*, 2009; Vidal-García *et al.*, 2014).
- H2) terrestrial jumpers have the largest hindlimb:forelimb length ratio, whereas this ratio is close to 1:1 in walker-hoppers (Reynaga *et al.*, 2018).
- H3) hindlimb:forelimb length ratio is closer to 1:1 in arboreal jumpers than in terrestrial jumpers (Simons, 2008; de Oliveira-Lagôa *et al.*, 2019).
- H4) the relative lengths of individual segments of the hindlimbs will differ between locomotor modes. Specifically, the tibiofibula:femur ratio will be highest for jumpers and lowest in burrowers (Simons, 2008; de Oliveira-Lagôa *et al.*, 2019).
- H5) burrowers have the widest, and therefore the most robust, forelimb bones (Emerson, 1976; Keeffe & Blackburn, 2020), while aquatic species have the most robust hindlimb bones (Gillis & Biewener, 2000).
- H6) terrestrial jumpers have a narrow expansion of the sacral diapophyses (ESD), while swimmers have a wide ESD (Emerson, 1979; 1982; Reilly & Jorgensen, 2011; Jorgensen & Reilly, 2013).

This chapter uses a novel combination of newly acquired µCT data, comparative analyses of anatomical ratios, and predictive methods to comprehensively quantify and explore how skeletal anatomy is correlated with locomotor mode and habitat type across a broad and unique range of anurans. By applying two types of predictive analyses using extant taxa, I demonstrate how skeletal morphology could be used to predict the primary locomotor mode and potential ecology of extinct species in future studies, with or without phylogenetic history. The reliability of

discrete pelvic types in identifying species and predicting locomotor mode and habitat type is also explored.

2.2 Methods

2.2.1 Sampling

Microcomputed tomography (µCT) scans of adult frogs were obtained from the online repository MorphoSource and Dr Laura Porro's collections for 3D visualisation of the skeleton in Amira (Version 2020.2; Thermo Fisher Scientific, USA). I extracted 22 skeletal measurements (Appendix Table A.1) from 164 species which cover all 54 recognised families (AmphibiaWeb, 2021). These include measurements of bones that have not been widely considered in previous studies, such as the calcaneum (tarsal segment) and various elements of the hand and foot. Sampling size ranged from several species for large families (e.g., Hylidae) to one representative for small families (e.g., Ascaphidae). Measurements were taken in dorsal view on the left side, except where bones were broken or missing, in which case the right side was measured (19 out of 164 scans). In 23 specimens, the extremities of long bones were poorly ossified, despite using adult specimens. Therefore, maximum length measurements in these specimens relied upon the ossified portions of each bone that could be detected in the scans. Femoral and humeral width at midshaft were used as proxies for hindlimb and forelimb robusticity, respectively. Total lengths for the body, hindlimb, foot, forelimb, and hand, as well as the iliac angle (Appendix Figure A.1) were calculated from raw measurements (Appendix Table A.1). Overall, 16 morphological variables were analysed (Figure 2.1), along with ten ratios which have been utilised in previous studies (Enriquez-Urzelai et al., 2015; Petrović et al., 2017; de Oliveira-Lagôa et al., 2019) to compare relative lengths of individual limb segments, entire limbs, and body length. As the sex of most specimens was unknown, measurements were size-corrected prior to analysis to mitigate the effects of dimorphism (see section 2.2.6), as females are larger in approximately 90% of frog species (Nali et al., 2014).

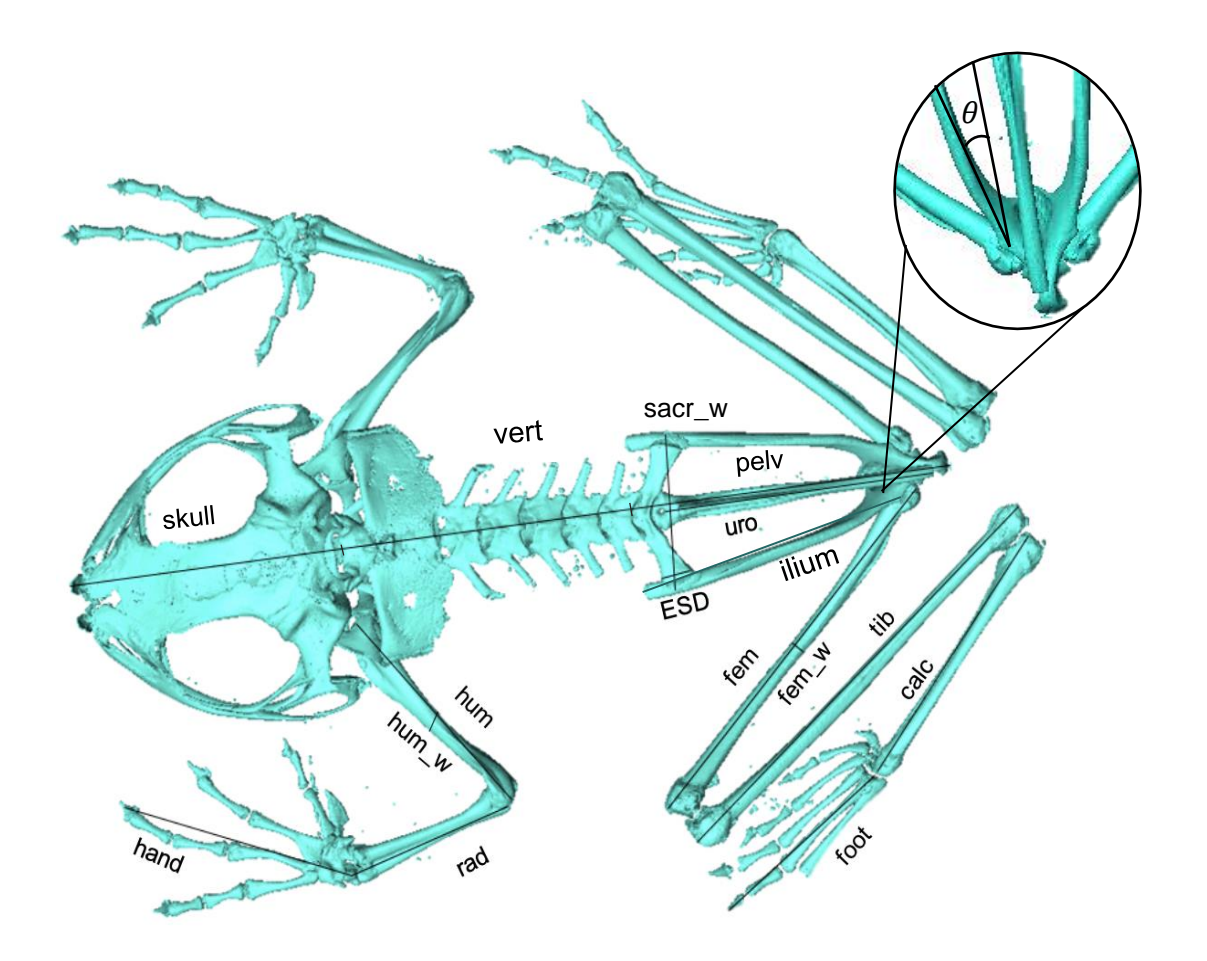


Figure 2.1 - Morphometric measurements used in analysis in the full dataset using *Amnirana albolabris* (voucher number: CAS:HERP:258101) as an example (see Table 2.1 for the full names of abbreviations). For the shape PCA analysis of the 'structural dataset', some measurements were combined to calculate total snoutvent length, hindlimb length, forelimb length and iliac angle [θ] (see Table A.1 for full measurement descriptions).

2.2.2 Pelvic morphology

Initially, taxa were to be categorized according to Emerson's (1979; 1982) pelvic types using the shape of the sacral diapophyses and the absence/presence of dorsal crests on the iliac shaft and the urostyle. However, separation between pelvic types was not straightforward, particularly between sagittal-hinge and lateral-bending types, which appear to blend along a morphological continuum (see section 2.4.4). Instead, ESD was considered as a continuous variable in the analyses of skeletal data (Figure 2.1) and the size of the dorsal crests were described according to previous literature (e.g., Emerson, 1979; Reilly & Jorgensen, 2011) before being converted to numerical values (i.e., smooth bone = 0, half-length crest = 0.5 and full-length crest = 1) for a separate analysis.

2.2.3 Phylogeny

To determine the importance of phylogenetic history in the evolution of skeletal structures, Jetz & Pyron's (2017) phylogeny was trimmed down to the taxa used in the present study using the 'keep.tip' function in *ape* (Paradis & Schliep, 2019; R Version 1.3.9, 2020). The nomenclature was updated (IUCN, 2020) and, for the three species not in the tree, I replaced the most closely related congeneric taxa to preserve branch lengths (Appendix Table B.1). This tree was used to allocate each species to broad phylogenetic groups for statistical analyses – Archaeobatrachia (i.e., taxa from before the evolution of the suborder Neobatrachia), the Ranoidea clade, or the Hyloidea clade. The Calyptocephalellidae, Myobatrachidae, Sooglossidae and Nasikabatrachidae are not within the Hyloidea or Ranoidea, nor amongst the earliest evolving taxa (Jetz & Pyron, 2017), so the species from these families (n = 10) were grouped under their suborder 'Neobatrachia'.

2.2.4 Locomotor mode

Information on locomotor mode was gathered from the literature (e.g., Jorgensen & Reilly, 2013; Keeffe & Blackburn, 2020) and through exchanges with researchers who have conducted first-hand behavioural observations in the field (Andrew Gray and David Blackburn, pers. comms.). The locomotor categories were swimmers (AQ), walker-hoppers (WH), burrower-walker-hoppers (BWH), terrestrial jumpers (TJ) and arboreal jumpers (AJ) (Wells, 2007). In line with previous literature, jumpers are defined as frogs which can perform a leap greater than eight times their SVL and choose to jump and hop more often than they walk (Emerson, 1979; Reilly et al., 2015; Soliz et al., 2017). Primary locomotor mode was unknown for 28 species, so closely related species from the same habitat were substituted. Additionally, twenty taxa appeared to perform two different principal locomotor modes. It can be difficult to assign a single locomotor category to a frog as their behaviour depends on habitat type (Enriquez-Urzelai et al., 2015). Therefore, one primary locomotor mode was assigned to every species, but I examined the case-wise statistics of predictive analyses to consider any potential secondary locomotor mode (see section 2.2.6).

2.2.5 Habitat type

Each species was assigned to one of the four main habitat types (Gomes *et al.*, 2009; Soliz, *et al.*, 2017) according to AmphibiaWeb and the IUCN (2021): arboreal,

terrestrial, aquatic, or riparian (i.e., frogs that spend comparable amounts of time in water and on land; Nauwelaerts *et al.*, 2007).

2.2.6 Statistical analyses

All raw data can be found in the 'full dataset' (Supplementary Dataset 1) and all analyses were performed in R (Version 1.3.9, 2020). The effect of size was adjusted by dividing each measurement by the geometric mean of each specimen (i.e., the 16th root of the product of the 16 skeletal measurements), resulting in dimensionless ratios known as Mosimann shape variables. These ratios are suggested to perform better than residuals as size-adjusted shape variables (Mosimann, 1970; Jungers et al., 1995). Furthermore, unlike residuals, Mosimann shape variables do not rely on trends from other individuals - they correct for scaling using information that relates solely to the specimen being measured (Sakamoto & Ruta, 2012). For each locomotor mode, habitat type and major phylogenetic group, the means, standard errors, and ratios involved in each hypothesis were examined to reveal morphological patterns and indicate which groups have more conserved anatomical features. The Mosimann shape variables were then log-transformed for further analyses. A phylogenetic principal component analysis (pPCA) was performed under a Brownian motion model of evolution on the covariance matrix (phyl.pca function in phytools; Revell, 2012) to find the principal axes of variation. A permutational multivariate analysis of variance (PERMANOVA) tested the significance of differences between group means for locomotor mode, habitat type and phylogenetic group by performing pairwise comparisons (pairwiseAdonis package; Anderson, 2005). Using *nlme* (Pinheiro et al., 2017), ape (Paradis & Schliep, 2019), and the species' scores from PC1 and PC2 as the dependent variables, a phylogenetic least squares (PGLS) analysis was used to determine how much variation in skeletal morphology is driven by locomotor mode, habitat type and phylogeny. The phylogenetic signal was extracted using Pagel's lambda (λ ; Pagel, 1999). Phylogenetic trees mapping the scores for PC1 and PC2 were constructed and visualised using RColorBrewer (Neuwirth & Neuwirth, 2011) and the 'contMap' function in phytools (Revell, 2012). A Dunn's test with a Bonferroni correction for pairwise comparisons was used to test for associations between dorsal crest length, locomotor mode and phylogenetic group for the ilia and urostyle, as these data are not normally distributed.

Few studies have investigated the relationship between skeletal morphology and locomotor function using individual limb segment lengths (Dobrowolska, 1973; Enriquez-Urzelai et al., 2015; Lires et al., 2016; Gómez & Lires, 2019). To demonstrate the importance of analysing the length of each limb segment rather than just overall limb length, I created a subset of the full dataset (Table 2.1), which combines some measurements to calculate total lengths for the body, hindlimb and forelimb (Table S1). Any variables that are not involved in these calculations remain unchanged. This is referred to as the 'structural dataset' (Table 2.1; Supplementary Dataset 2). Then, I performed one shape PCA (SPCA; Baur & Leuenberger, 2011) for each dataset. SPCA interprets a PCA in terms of ratios of body measurements by performing it in isometry-free shape space and produces a PCA ratio spectrum which visualises the proportions that are most important when explaining the variance in each principal component (Baur & Leuenberger, 2011; Petrović et al., 2017). If individual hindlimb segments differ in explanatory power, then this illustrates that they are important to consider in analyses of skeletal morphology compared to total hindlimb length alone.

Table 2.1 - Summary of the variables used in each dataset for the shape PCA analysis.

Measurement	Abbreviation	Full dataset	Structural dataset
Snout-vent length	SVL		X
Skull	skull	X	
Vertebrae	vert	X	
Pelvis	pelv	X	
Sacral expansion	ESD	X	X
Sacral width	sacr_w	X	X
llium	ilium	X	X
Urostyle	uro	X	X
Iliac angle	θ	X	Χ
Hindlimb length	HL		Χ
Femur	fem	X	
Femur width	fem_w	X	Χ
Tibiofibula	tib	X	
Calcaneum	calc	X	
Foot	foot	X	
Forelimb length	FL		X
Humerus	hum	X	
Humerus width	hum_w	X	Χ
Radioulna	rad	X	
Hand	hand	X	

I also tested how well skeletal morphology predicts the designation of each frog to its locomotor mode, habitat type and phylogenetic group, with and without incorporation of phylogenetic history. Two types of predictive analyses were performed: linear discriminant analyses (LDA; Ida function in the MASS package) and phylogenetic flexible discriminant analysis (pFDA; phylo.fda function; Motani & Schmitz, 2011). Both aim to establish whether the measurement data are able to retrieve the same categories of locomotor mode, habitat type, or phylogenetic group or, with regards to taxa with debateable primary locomotor modes, the alternative locomotor mode (see section 2.2.3). Misclassifications indicate that the morphology of that species falls outside the range estimated for that locomotor mode, habitat type or phylogenetic group based on the data provided. Data from the ten neobatrachian species which are not within the clades Hyloidea and Ranoidea were not included as inputs, but these analyses were used to predict which phylogenetic group they would be associated with, given their skeletal morphology. For the pFDA, the optimal Pagel's lambda was used, which maximises the correlation between locomotor mode/habitat type and the morphological variables (Motani & Schmitz,

2011). The rationale behind using both analyses was to see the difference in the predictive power of morphological variables with and without the incorporation of phylogenetic history, and to investigate whether this approach has the potential to determine these categories (especially locomotor mode and habitat type) in fossil frogs.

2.3 Results

2.3.1 Skeletal morphology across locomotor modes, habitat types and phylogenetic groups

Descriptive statistics for the size-corrected measurements and key ratios can be found in Table 2.2. Five PC axes are required to explain ~80% of the total variance. The first two principal components (PCs) from the pPCA explain 34.2% and 21.9% of the total variance in the data respectively (Appendix Table A.2). Along PC1, species with larger sacral expansions have more positive loadings (Appendix Table A.2; Figure 2.2). Positive loadings on the second PC axis indicate species with a long tibiofibula and calcaneum, and the most negative loadings correspond to species with large humeral ridges. In terms of morphospace occupations, all groups appear to overlap considerably, but PERMANOVA tests indicate that locomotor mode, habitat type, and phylogenetic group all have significant effects on skeletal morphology (Appendix Table A.3). Regarding locomotor mode, AJ and TJ are significantly separate from each other, as well as from all non-jumpers, which show a much broader spread across morphospace. There is no significant separation between AQ, BWH and WH. For habitat type, arboreal taxa are significantly separate from all other taxa, and riparian and aquatic taxa are significantly different from each other (Appendix Table A.3). There is no significant separation between terrestrial and aquatic taxa. When grouped according to phylogeny, Hyloidea and Ranoidea are not significantly different from each other, nor the ten Neobatrachia species, but the Archaeobatrachia are distinct from all of the more phylogenetically derived groups (Appendix Table A.3). Regarding the dorsal pelvic crests, all models show that there are significant differences between locomotor modes (Iliac crest Kruskal-Wallis: Chi-squared₍₄₎ = 30.42, p < 0.0001; Urostylic crest Kruskal-Wallis: Chi-squared₍₄₎ = 21.87, p < 0.001) and phylogenetic groups (Iliac crest Kruskal-Wallis: Chi-squared₍₃₎ = 15.26, p = 0.002; Urostylic crest Kruskal-Wallis: Chisquared₍₃₎ = 14.06, p = 0.003). TJ have longer iliac crests than BWH and AJ, and Page 39 of 286

longer urostylic crests than BWH and WH (Appendix Table A.4). The more phylogenetically derived groups have significantly longer crests than the Archaeobatrachia.

Page 41 of 28

Table 2.2 - Descriptive statistics of the key morphometric measurements and ratios discussed in this chapter for locomotor mode, habitat type and major phylogenetic group (Arch. = Archaeobatrachia). Light and dark boxes indicate the highest and lowest values respectively. Measurement abbreviations can be found in Table 2.1. The values are displayed as the mean ± standard error, and the number in brackets indicates the number of species in each group. The iliac angle is a raw measurement, whereas all other anatomical measurements shown have been corrected for size (see section 2.2.6) but not log-transformed for ease of interpretation.

	LOCOMOTOR MODE					HABITAT				PHYLOGENETIC GROUP		
Measurement	BWH (33)	WH (26)	TJ (66)	AJ (30)	AQ (9)	Terrestrial (96)	Riparian (31)	Arboreal (28)	Aquatic (9)	Arch. (16)	Hyloidea (72)	Ranoidea (65)
SVL	5.930 ± 0.478	5.646 ± 0.669	4.944 ± 0.370	6.310 ± 0.470	7.265 ± 0.975	5.003 ± 0.278	6.470 ± 0.662	6.329 ± 0.481	7.265 ± 0.975	6.829 ± 0.601	5.362 ± 0.336	5.491 ± 0.387
ESD	2.291 ± 0.185	2.141 ± 0.264	1.856 ± 0.148	2.382 ± 0.191	2.815 ± 0.377	1.898 ± 0.107	2.461 ± 0.276	2.382 ± 0.195	2.815 ± 0.377	2.667 ± 0.268	2.010 ± 0.131	2.072 ± 0.149
sacr_w	0.414 ± 0.049	0.357 ± 0.064	0.161 ± 0.014	0.310 ± 0.036	0.665 ± 0.168	0.275 ± 0.026	0.247 ± 0.042	0.315 ± 0.038	0.665 ± 0.168	0.796 ± 0.118	0.266 ± 0.023	0.209 ± 0.018
HL	7.384 ± 0.720	7.164 ± 0.780	7.505 ± 0.604	9.673 ± 0.777	8.771 ± 0.959	6.653 ± 0.376	9.913 ± 1.073	9.624 ± 0.765	8.771 ± 0.959	8.566 ± 0.685	7.656 ± 0.483	7.788 ± 0.603
foot	2.206 ± 0.200	2.063 ± 0.230	2.120 ± 0.171	2.284 ± 0.179	2.742 ± 0.320	1.922 ± 0.108	2.800 ± 0.300	2.268 ± 0.175	2.742 ± 0.320	2.486 ± 0.191	2.068 ± 0.125	2.188 ± 0.170
FL	4.097 ± 0.333	4.174 ± 0.493	3.549 ± 0.261	4.629 ± 0.342	4.870 ± 0.786	3.562 ± 0.202	4.683 ± 0.449	4.633 ± 0.347	4.870 ± 0.786	4.708 ± 0.380	3.971 ± 0.257	3.852 ± 0.268

hand	1.366 ± 0.109 8.865	1.419 ± 0.172 9.924	3.549 ± 0.261 7.952	1.805 ± 0.141 9.474	1.696 ± 0.274 8.574	1.212 ± 0.070	1.663 ± 0.158	1.810 ± 0.144	1.696 ± 0.274	1.601 ± 0.122	1.441 ± 0.099	1.350 ± 0.268	The evolution
lliac angle (°)	± 0.403	± 0.548	± 0.209	± 0.394	± 0.794	8.593 ± 0.229	8.690 ± 0.471	9.476 ± 0.414	8.574 ± 0.794	8.664 ± 0.653	9.317 ± 0.285	8.159 ± 0.255	
Ratio													of 1
HL/FL	1.807 ± 0.062	1.748 ± 0.044	2.105 ± 0.035	2.071 ± 0.031	1.946 ± 0.132	1.917 ± 0.035	2.071 ± 0.052	2.070 ± 0.028	1.946 ± 0.132	1.848 ± 0.074	1.962 ± 0.037	2.010 ± 0.039	of musculoskeletal anatomy
HL/SVL	1.224 ± 0.038	1.290 ± 0.037	1.507 ± 0.023	1.526 ± 0.032	1.249 ± 0.050	1.351 ± 0.024	1.510 ± 0.034	1.523 ± 0.031	1.249 ± 0.050	1.275 ± 0.047	1.440 ± 0.027	1.405 ± 0.028	skeletal
ESD/HL	0.061 ± 0.006	0.048 ± 0.006	0.023 ± 0.001	0.033 ± 0.003	0.075 ± 0.019	0.042 ± 0.003	0.027 ± 0.003	0.033 ± 0.003	0.075 ± 0.019	0.092 ± 0.012	0.035 ± 0.002	0.031 ± 0.003	anatom
fem/HL	0.276 ± 0.003	0.269 ± 0.004	0.272 ± 0.004	0.281 ± 0.002	0.285 ± 0.011	0.274 ± 0.003	0.267 ± 0.003	0.281 ± 0.002	0.285 ± 0.011	0.272 ± 0.005	0.277 ± 0.004	0.274 ± 0.002	y and lo
tib/HL	0.272 ± 0.004	0.282 ± 0.003	0.299 ± 0.004	0.304 ± 0.002	0.273 ± 0.006	0.287 ± 0.003	0.293 ± 0.003	0.305 ± 0.002	0.273 ± 0.006	0.277 ± 0.005	0.296 ± 0.004	0.289 ± 0.002	and locomotor mode
calc/HL	0.151 ± 0.003	0.163 ± 0.004	0.177 ± 0.003	0.177 ± 0.003	0.155 ± 0.008	0.159 ± 0.003	0.156 ± 0.003	0.177 ± 0.003	0.155 ± 0.008	0.165 ± 0.004	0.169 ± 0.003	0.149 ± 0.006	r mode i
foot/HL	0.302 ± 0.006	0.285 ± 0.007	0.282 ± 0.005	0.237 ± 0.003	0.313 ± 0.015	0.288 ± 0.004	0.285 ± 0.006	0.237 ± 0.003	0.313 ± 0.023	0.293 ± 0.009	0.274 ± 0.006	0.282 ± 0.004	in frogs

tib/fem	0.989 ± 0.017	1.055 ± 0.018	1.101 ± 0.009	1.084 ± 0.008	0.994 ± 0.021	1.050 ± 0.010	1.102 ± 0.015	1.083 ± 0.009	0.994 ± 0.021	1.025 ± 0.034	1.076 ± 0.009	1.061 ± 0.010	
fem_w/fem	0.074 ± 0.004	0.064 ± 0.002	0.053 ± 0.001	0.044 ± 0.001	0.074 ± 0.006	0.062 ± 0.002	0.055 ± 0.002	0.045 ± 0.001	0.074 ± 0.006	0.071 ± 0.006	0.055 ± 0.002	0.057 ± 0.002	
hum_w/hum	0.132 ± 0.009	0.110 ± 0.004	0.096 ± 0.003	0.130 ± 0.012	0.130 ± 0.023	0.111 ± 0.004	0.098 ± 0.003	0.089 ± 0.002	0.130 ± 0.023	0.142 ± 0.012	0.103 ± 0.004	0.097 ± 0.003	

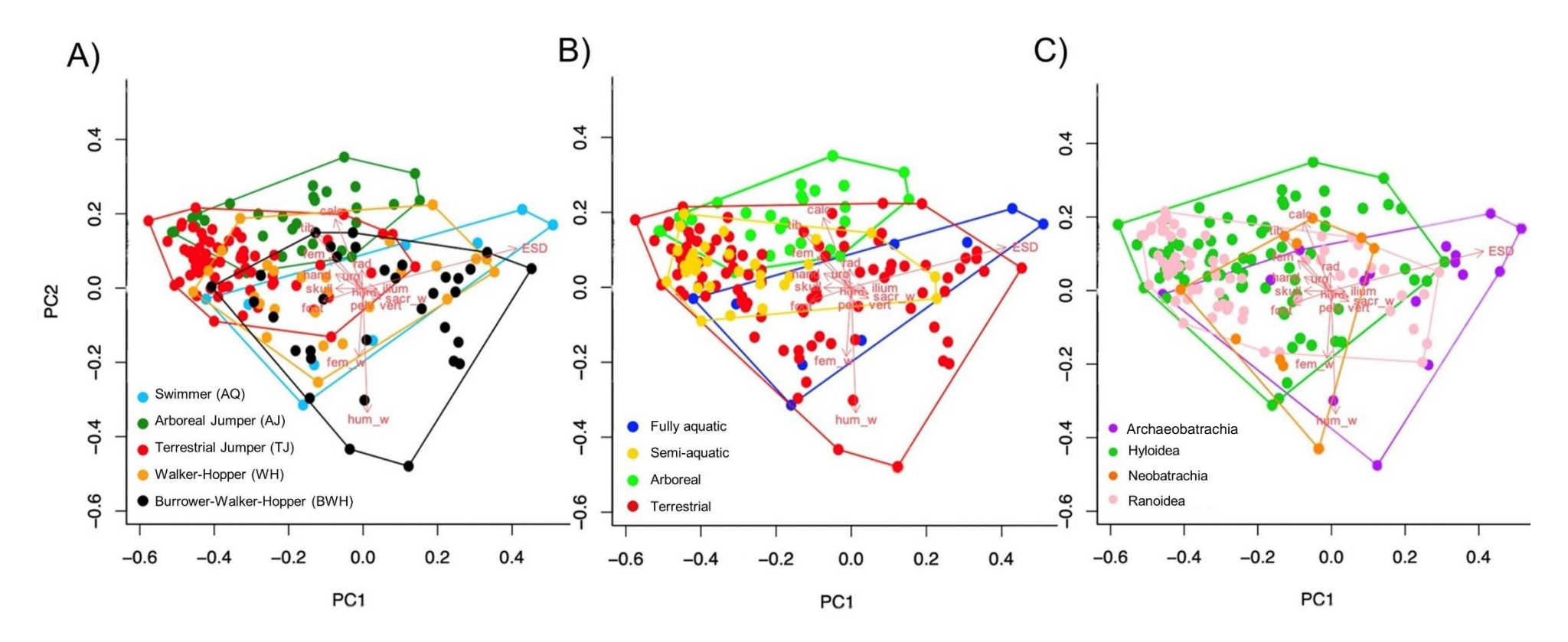


Figure 2.2 - pPCA of morphometric measurements for the full dataset, coloured-coded according to three alternative groupings of locomotor mode (A), habitat type (B) and phylogenetic group (C). The red arrows represent the pPCA loadings, which can be found in Appendix Table A.2.

2.3.2 Shape PCA spectrums for visualising the relative importance of structural morphological ratios

For the SPCA analysing the structural dataset (i.e., the subset of nine variables describing total body and limb lengths), the first two principal components (PCs) explain 67.1% and 16.5% of the total variance. Most of the variation in shape PC1 is explained by the ratio between hindlimb length and sacral expansion (Appendix Table A.5), which corresponds to the position of these two variables at the opposite ends of the PC1 ratio spectrum (Figure 2.3). The width of the humerus and length of the hindlimb is the most important ratio driving shape PC2 (Appendix Table A.5; Figure 2.3). In the full dataset, shape PC1 explains 56.7% of variance, and shape PC2 explains 16%. The ratio between tibiofibula length and sacral expansion explains most of the variation in shape PC1, while the ratio between humerus width and calcaneum length is the most important ratio driving shape PC2 (Appendix Table A.6; Figure 2.4). However, note that the PC2 ratio spectrums for both datasets have wider error bars, which occurs when PC values are less significantly separated from each other. Therefore, the wider error bars indicate that less definitive conclusions can be made from PC2 (Baur & Leuenberger, 2011). Allometry ratio spectrums show that shape is not significantly correlated with size for both datasets (Appendix Figure A.2).

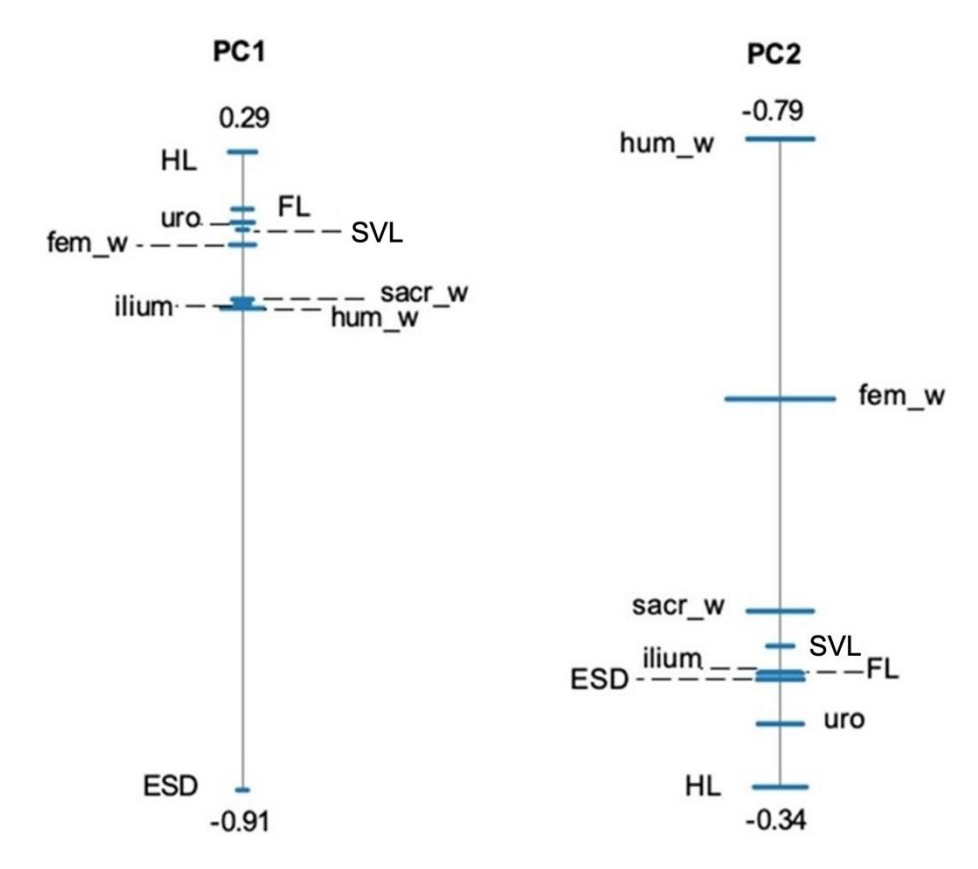


Figure 2.3 - Shape PCA ratio spectra for PC1 and PC2 for the structural dataset containing total body and limb lengths. A SPCA spectrum visualises the proportions that are most important when explaining the variance in each principal component (Baur & Leuenberger, 2011; Petrović *et al.*, 2017). Bars represent 68% confidence intervals based on 999 bootstrap replicates. Variable labels alternate from left to right; dashed lines are used to distinguish between those that are very closely positioned. Variables positioned close to each other depict ratios that explain little variation, whereas those at the most opposite ends of each spectrum represent a ratio with high explanatory power. In this case, the ratio of hindlimb length/sacral expansion and humerus width/hindlimb length have the highest explanatory power for PC1 and PC2, respectively. The numbers at each end of the spectrum represent the highest and lowest PC loadings of the two most opposite variables. See Table 2.1 for abbreviations.

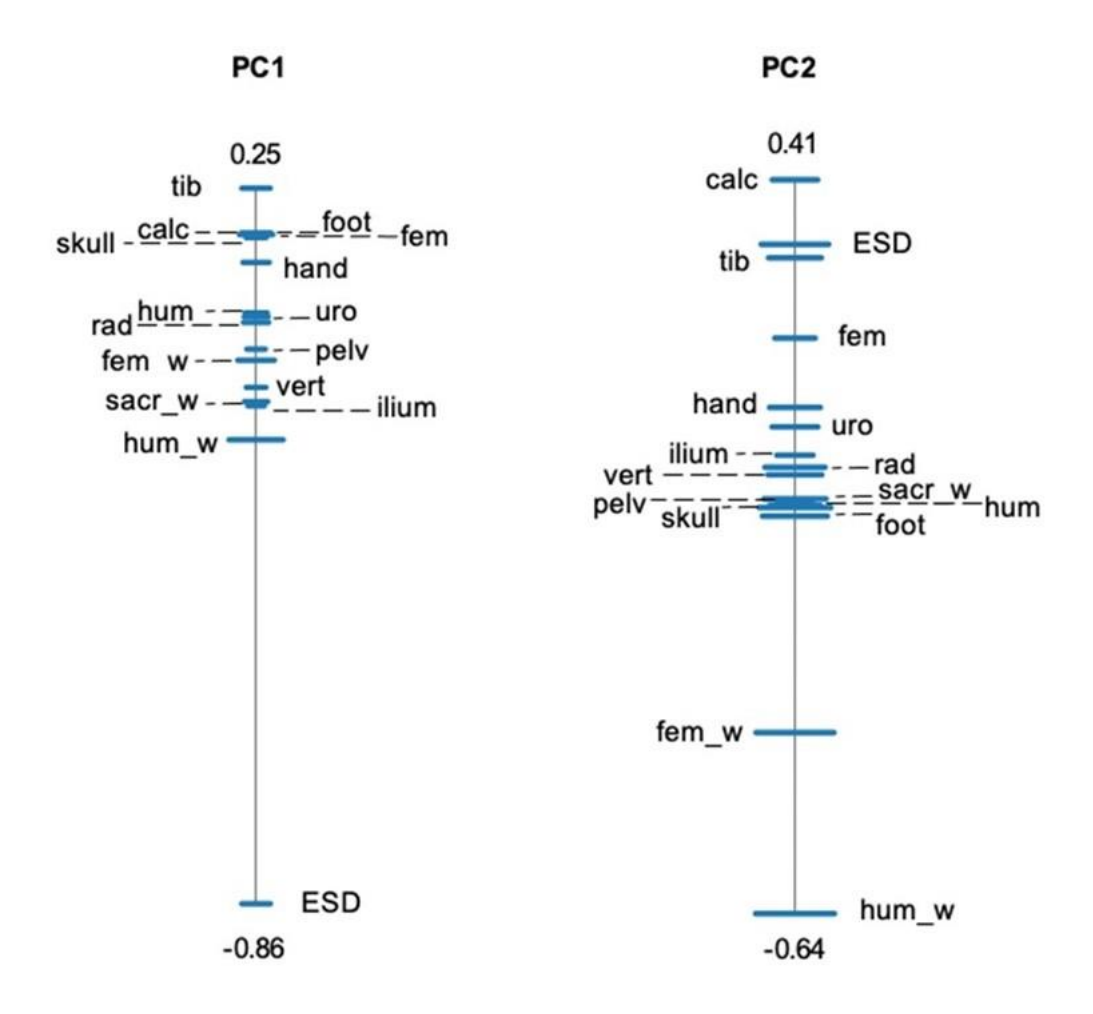


Figure 2.4 - Shape PCA ratio spectra for PC1 and PC2 for the full dataset. In this case, the ratio of tibiofibula length/snout-vent length and calcaneum length/humerus width have the highest explanatory power for PC1 and PC2, respectively. The numbers at each end of the spectrum represent the highest and lowest PC loadings of the two most opposite variables. See Table 2.1 for abbreviations.

2.3.3 Phylogenetic analysis

By plotting the scores obtained from the pPCA onto the trimmed phylogeny, the evolution of skeletal morphology can be visualised (Figure 2.5). The strongest PGLS model includes both locomotor mode and habitat type for PC1, but only locomotor mode for PC2 (Appendix Table A.7). The most significant predictor of skeletal morphology is locomotor mode in both analyses (Table 2.3). The phylogenetic signal is greater than one for PC1 scores, indicating the signal is stronger near the root of the phylogeny compared to the tips (Pagel, 1999), while the phylogenetic signal is weaker for PC2 (Table A.7).

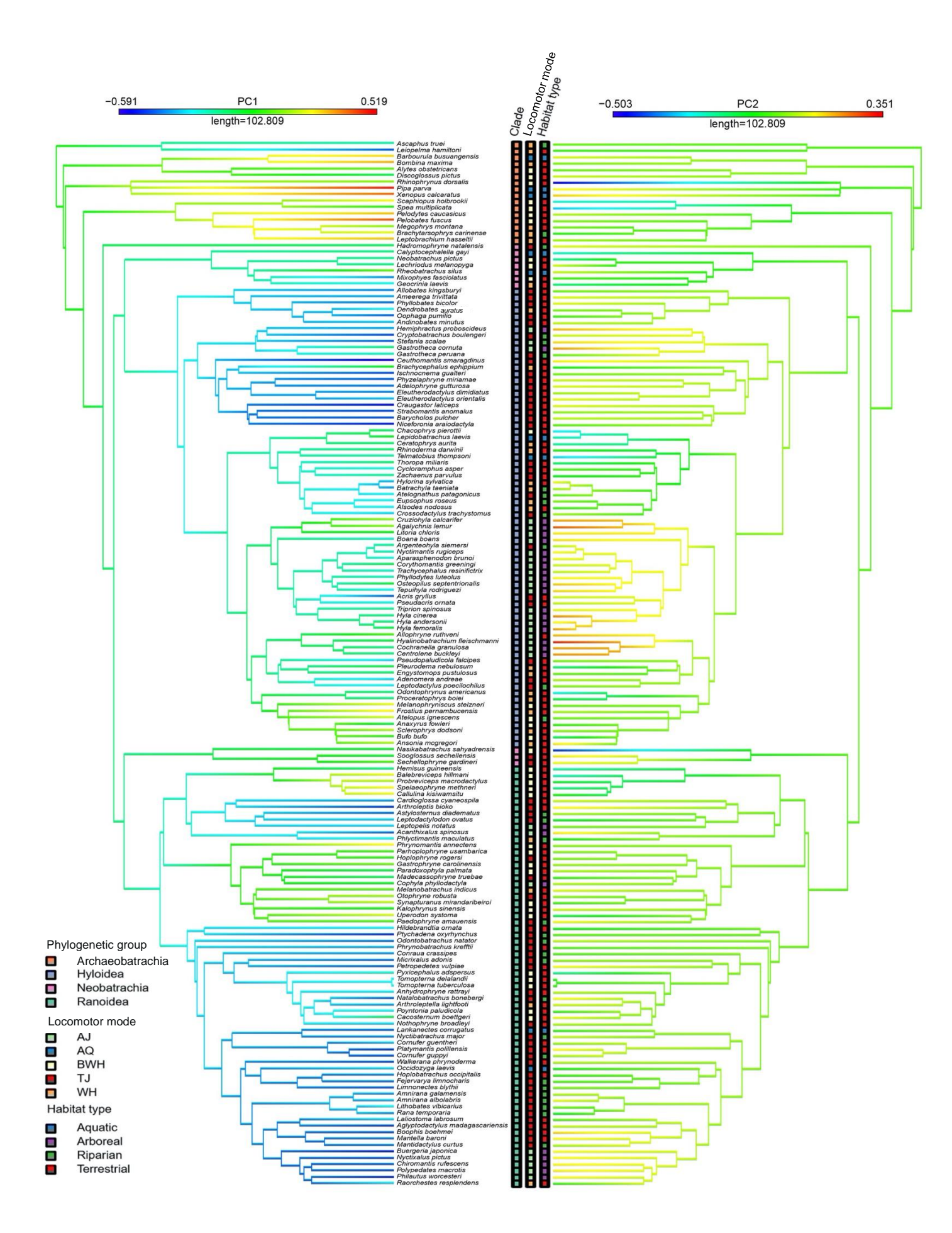


Table 2.4 - Classification results from the linear discriminant analysis (LDA) of the full dataset for locomotor mode, habitat type and phylogenetic group. The ten species in the Neobatrachia group were not used as inputs for the predictive model.

	Locomotor	Predicted group accuracy – 77.4%						
	mode	WH	BWH	TJ	AJ	AQ	Total	
	WH	14	6	5	0	1	26	
	BWH	6	20	6	0	1	33	
Count	TJ	3	1	60	2	0	66	
- Court	AJ	0	0	1	29	0	30	
	AQ	1	2	2	0	4	9	
	WH	53.8	23.1	19.2	0.0	3.8	100	
%	BWH	18.2	60.6	18.2	0.0	3.0	100	
	TJ	4.5	1.5	90.9	3.0	0.0	100	
	AJ	0.0	0.0	3.3	96.7	0.0	100	
	AQ	11.1	22.2	22.2	0.0	44.4	100	
	Habitat type	Predicted g	roup accur	acy – 76.8%	, o			
	,	Terrestrial	Riparian	Arboreal	Aquatic	Total		
	Terrestrial	85	5	4	2	96		
0	Riparian	18	11	2	0	31		
Count	Arboreal	1	1	26	0	28		
	Aquatic	3	2	0	4	9		
	Terrestrial	88.5	5.2	4.2	2.1	100		
0/	Riparian	58.1	35.5	6.5	0.0	100		
%	Arboreal	3.6	3.6	92.9	0.0	100		
	Aquatic	33.3	22.2	0.0	44.4	100		
	Phylogenetic group	Predicted 75.3% (exc						
		Archaeo- batrachia	Hyloidea	Ranoidea	Total			
	Archaeo- batrachia	11	5	0	16			
Count	Hyloidea	0	54	18	72			
	Ranoidea	1	15	50	66			
	Neobatrachia	1	6	3	10			
	Archaeo- batrachia	68.8	31.3	0.0	100			
%	Hyloidea	0.0	75.0	25.0	100			
	Ranoidea	1.5	22.7	75.8	100			
	Neobatrachians	10.0	60.0	30.0	100			

Table 2.5 - Classification results from the phylogenetic flexible discriminant analysis (pFDA) of the full dataset for locomotor mode, habitat type and phylogenetic group. The ten species in the Neobatrachia group were not used as inputs for the predictive model.

	Locomotor	Predicted g					
	mode	WH	BWH	TJ	AJ	AQ	Total
	WH	12	5	8	0	1	26
	BWH	6	16	6	1	4	33
Count	TJ	6	6	51	3	0	66
	AJ	1	4	5	19	1	30
	AQ	1	3	0	0	5	9
	WH	46.2	19.2	30.8	0.0	3.8	100
	BWH	18.2	48.5	18.2	3.0	12.1	100
%	TJ	9.1	9.1	77.3	4.5	0.0	100
	AJ	3.3	13.3	16.7	63.3	3.3	100
	AQ	11.1	33.3	0.0	0.0	55.6	100
	Habitat type	Predicted group accuracy – 65.2%					
	• •	Terrestrial	Riparian	Arboreal	Aquatic	Total	
	Terrestrial	80	7	2	7	96	
0	Riparian	20	11	0	0	31	
Count	Arboreal	15	0	12	1	28	
	Aquatic	5	0	0	4	9	
	Terrestrial	83.3	7.3	2.1	7.3	100	
0/	Riparian	64.5	35.5	0.0	0.0	100	
%	Arboreal	53.6	0.0	42.9	3.6	100	
	Aquatic	55.6	0.0	0.0	44.4	100	
	Phylogenetic group	(excl. Neob	•	acy – 71.4%			
		Archaeo- batrachia	Hyloidea	Ranoidea	Total		
	Archaeo- batrachia	11	5	0	16		
Count	Hyloidea	2	52	18	72		
	Ranoidea	0	19	47	66		
	Neobatrachia	10	0	0	10		
	Archaeo- batrachia	68.8	31.3	0.0	100		
%	Hyloidea	2.8	72.2	25.0	100		
	Ranoidea	0.0	28.8	71.2	100		
	Neobatrachia	100.0	0.0	0.0	100		

Based on the literature, locomotor mode is uncertain for 28 taxa (see section 2.2.4). Therefore, I examined the case-wise statistics of each predictive analysis to see if the alternative locomotor mode is correctly predicted. In the LDA and pFDA, respectively, 14 and ten species have had their primary locomotor mode predicted correctly, while eight and nine species are predicted to have the alternative locomotor mode, which supports the predictive power of the model. Additionally, where the locomotor mode from a closely related proxy species is used, the LDA and pFDA correctly predict the locomotor mode for 23 and 15 out of the 28 species, respectively. These findings highlight why entire families should not be grouped under a single locomotor type, as this could vary at the genus or species-level. Additionally, the pFDA made more incorrect classifications (48) than the LDA (28) where locomotor mode is certain, suggesting that the inclusion of phylogenetic history weakens the predictive power of skeletal morphology.

For habitat type, LDA1 explains 79% of the variance in the data, and LD2 explains 12.4%. pFDA1 and pFDA2 explain 60.2% and 23.6%, respectively. Classification is successful in 76.8% of species in the LDA (Table 2.4) and 65.2% in the pFDA (Table 2.5). For the LDA, arboreal (92.9%) and terrestrial (88.5%) taxa are classified correctly most often, but riparian species are frequently misclassified as terrestrial (58.1%). Similar conclusions hold true for the pFDA, except that arboreal species are often mistaken for being terrestrial (53.6%). In the 17 cases of habitat type uncertainty, the primary habitat type is predicted correctly for seven species in the LDA and six species in the pFDA, and the potential alternative habitat type is predicted in six and four species, respectively. There are 28 (LDA) and 45 (pFDA) cases where habitat type is classified incorrectly despite certainty.

When categorised by phylogenetic group, LD1 explains 78.3% of the variance in the data and LD2 explains 21.7%. pFDA1 and pFDA2 explain 85.1% and 14.9%, respectively. Correct categorisations are almost equal across the phylogenetic groups in the LDA, where 75.3% of species are correctly categorised overall (Table 2.4). For the pFDA, Ranoidea and Hyloidea are correctly classified most often, with an overall accuracy of 71.4% (Table 2.5). The ten species in the Neobatrachia group are mainly categorised as Hyloidea and Ranoidea, with *Calyptocephalella gayi* being classified as Archaeobatrachia in the LDA, while the pFDA suggests that all

neobatrachians belong in the Archaeobatrachia group based their skeletal morphology.

2.4 Discussion

This chapter examines important correlations between anuran skeletal proportions and locomotor mode, habitat type and phylogenetic history across an extensive taxonomic scope by utilising a combination of 3D dissection data from µCT scans, comparative morphometrics, and two forms of predictive analyses. In summary, the impact of locomotor function on the evolution of frog anatomy is reflected mostly in the differences in sacral expansion and hindlimb proportions between locomotor modes and habitat types. Examining the levels of variation within groups has shown that some locomotor modes are associated with less conserved skeletal morphologies than others, suggesting multiple anatomical solutions for achieving the same function. Additionally, pelvic morphology is shown to form a morphological continuum. Therefore, Emerson's (1979; 1982) three pelvic morphotypes are unlikely to be reliable for predicting locomotor mode and habitat type for individual species, let alone entire families. Additionally, by testing two types of predictive analyses using extant taxa, this chapter has shown that skeletal morphology could be used to predict the lifestyle of extinct species in future studies.

2.4.1 Body and limb proportions show distinct patterns in relation to function

As expected, the hindlimb length:SVL ratio is lowest in burrowers, then increases across walker-hoppers, swimmers, terrestrial jumpers, and then arboreal jumpers (supporting hypothesis 1). This result corroborates findings from previous studies that that proportionately longer hindlimbs likely evolved to enable better jumping performance (Choi *et al.*, 2003; James & Wilson, 2008; Gomes *et al.*, 2009; Vidal-García *et al.*, 2014; Herrel *et al.*, 2016). On average, terrestrial jumpers have 2.1x longer hindlimbs relative to forelimbs, while walker-hoppers have a hindlimb:forelimb length ratio closer to 1:1, supporting hypothesis 2. Arboreal jumpers are also expected to have a hindlimb:forelimb ratio closer to 1:1, as this locomotor mode was thought to be constrained by a functional trade-off between jumping versus climbing demands (Simons, 2008; Enriquez-Urzelai *et al.*, 2015; de Oliveira-Lagôa *et al.*, 2019). Contrary to hypothesis 3, arboreal jumpers have the second highest hindlimb:forelimb length ratio. This suggests that while the optimal

forelimb length for climbing is likely higher than the optimal forelimb length for jumping, both sets of limbs do not need to be equally elongated to enable tree frogs to reach distant branches. This is potentially because jumping may be used as an escape mechanism, and therefore has more important consequences for survival, while climbing is more important for slowly traversing the canopy. Alternatively, it is possible that the measurements included in the present study may not capture morphology particularly adapted for climbing (e.g., toes pads).

As predicted, the relative lengths of different hindlimb segments vary between locomotor modes and habitat types (supporting hypothesis 4). Hindlimb elongation occurs primarily in the femur for swimmers, while the lengths of the tibiofibula and calcaneum drives hindlimb elongation in jumpers (Table 2.2), corroborating the findings of previous studies (Nauwelaerts et al., 2007; James & Wilson, 2008; Jorgensen & Reilly, 2013; Lires et al., 2016; Gómez & Lires, 2019). Support for hypothesis 5 is less clear. Burrowers have both the most robust forelimb and hindlimb bones, thus permitting the evolution of large muscles for forward- and backward-burrowing (Emerson, 1976; Keeffe & Blackburn, 2020). In terms of habitat type, aquatic taxa have the most robust hindlimbs and forelimbs. However, when interpreting any trends in habitat type, it is important to note that terrestrial taxa are comprised of a mix of walker-hoppers, burrowers, and terrestrial jumpers, which all have contrasting morphologies. Terrestrial taxa have relatively average means for most anatomical variables, indicating that some effects are being cancelled out. This emphasises the importance of considering more than just broad habitat types when investigating correlations between morphology, function, and ecology.

The least amount of variation across all ratios is exhibited by both arboreal and terrestrial jumpers, indicating either that convergent evolution occurred (Moen *et al.*, 2016), or that the skeletal proportions of jumping frogs are more conserved. In contrast, swimmers have the most variable skeletal morphology, suggesting that there are more anatomical solutions to achieve satisfactory swimming performance compared to jumping. This supports findings by previous studies, which found differences in swimming kinematics between species, particularly those occupying different habitat types (Richards, 2010; Robovska-Havelkova *et al.*, 2014). This variation in swimming strategies combined with the finding that swimmers exhibit the most variation in skeletal proportions suggest that swimming is a less

functionally (and morphologically) constrained type of locomotion than jumping, although future functional studies are needed to test such a hypothesis explicitly.

2.4.2 Skeletal pelvic morphology is important, and should be considered along a continuum

Both the pPCA (Figure 2.2; Appendix Table A.2) and ratio spectrum analyses (Figure 2.4; Appendix Table A.5; Appendix Table A.6) show that sacral expansion is the key driver of morphological variation in frogs and the primary determinant of locomotor mode (Emerson 1979; 1982; Jorgensen & Reilly, 2013; Buttimer et al., 2020). A narrow ESD and low ESD:hindlimb length ratio are associated with terrestrial jumpers, and high values are associated with swimmers, supporting hypothesis 6. Sacral width, pelvis length and iliac angle are also expected to vary with locomotor mode (Simons, 2008; Jorgensen & Reilly, 2013). Burrowers and walker-hoppers have a wider and longer pelvis (Table 2.2) to enable lateral rotation (Emerson, 1982). These features, plus the larger iliac angle, indicate that the pelvis of burrowers and walker-hoppers has room for larger muscles and the potential for longer external moment arms about the iliosacral joint. In contrast, jumpers have the narrowest sacral width and smallest iliac angle (Table 2.2). Jumpers may instead allow for the attachment of larger pelvis muscles via significantly longer dorsal crests on the ilia and urostyle compared to burrowers and walker-hoppers (Appendix Table A.4).

Walker-hoppers, swimmers, and jumpers have been associated with 'lateral-bending', 'fore-aft sliding' and 'sagittal-hinge' pelvic types, respectively (Emerson, 1979; 1982; Reilly & Jorgensen, 2011). Jorgensen & Reilly (2013) found that all except one species of terrestrial jumpers in their study have a sagittal-hinge pelvic type. However, the record for best jumping performance (the equivalent of 55.2 times body length) is currently held by the pelodryadinine hylid *Litoria nasuta* (James & Wilson, 2008), which has a large sacral expansion, atypical for jumping species. It does, however, have hindlimbs which are more than twice as long as its SVL on average (2.02 +/- 0.07; James & Wilson, 2008), suggesting that frogs could hypothetically attain greater jumping performance through extreme elongation of the hindlimbs to compensate for the lack of a sagittal-hinge pelvis type. Computational simulations suggest that a sagittal-hinge mechanism is not obligatory for jumping as it may be mostly used to fine-tune jump trajectory (Richards *et al.*, 2018).

Additionally, species that have already attained the theoretically optimal (for jumping) sagittal-hinge pelvic morphology may only be able to improve jumping performance by further elongating their hindlimbs. Ultimately, the significance of pelvic morphology cannot be determined until more functional studies are done which consider the pelvis and hindlimb as a whole unit.

This chapter initially aimed to explore relationships among pelvic morphology and locomotor mode in more detail, but locomotor categories did not neatly align with Emerson's pelvic types, an observation also made in previous studies (Simons, 2008; Soliz et al., 2017). In particular, lateral-bending and sagittal-hinge pelvic types appear to blend along a morphological continuum, especially in the shape of the sacral diapophyses (Figure 2.6; 1a-2b). These findings suggests that there are more complex links between form and function in anuran pelvic structures than previously thought. For example, the sacral shape in *Batrachyla taeniata* differs significantly from that of Ansonia mcgregori, both of which are walker-hoppers in the Hyloidea classed as having a lateral-bending pelvis type in previous literature. Sacral shape in B. taeniata appears more similar to that of Ptychadena oxyrhynchus, which has a sagittal-hinge pelvis type according to Reilly & Jorgensen (2011). In comparison, fore-aft slider pelvic types appear relatively consistent in shape (Figure 2.6; 3a-3b). These observations support the aforementioned conclusion that multiple anatomical solutions are potentially available to achieve particular locomotor modes and functional performance, or access particular habitats.

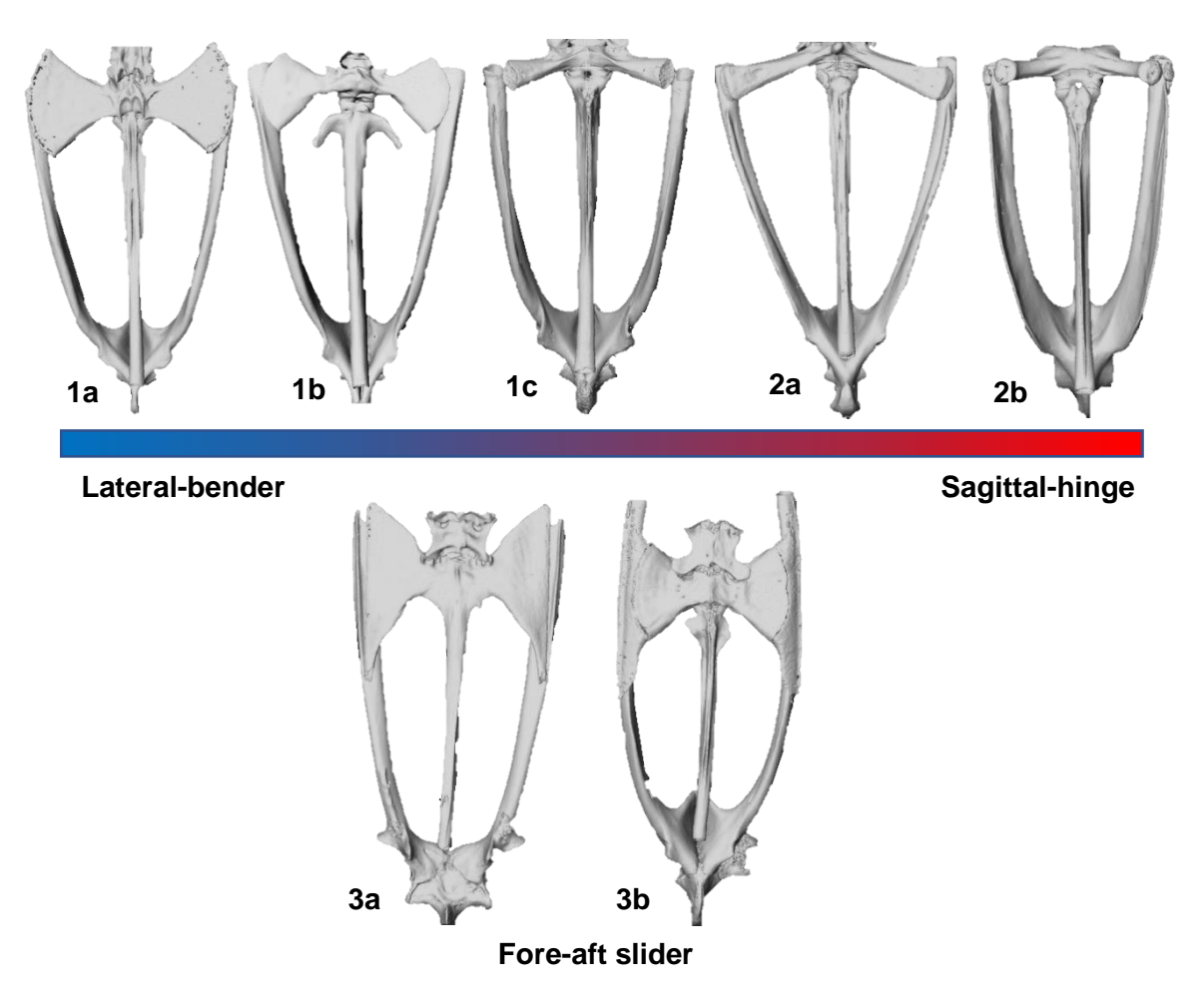


Figure 2.6 - Examples of the broad variation found in pelvis anatomy in relation to the three 'distinct' morphotypes described by Emerson (1979; 1982). Lateral-bender and sagittal-hinge morphs appear occupy a morphological continuum (coloured bar), while fore-aft sliders are distinct in their morphology. 1a) Ansonia mcgregori (voucher number: KU:KUH:334742) - WH, Hyloidea; 1b) Alytes obstetricians BWH, Archaeobatrachia; (CAS:SUA:21691) -1c) Batrachyla taeniata (CAS:HERP:85253) – WH, Hyloidea; 2a) Hemiphractus proboscideus (UF:Herp:43204) AJ, Hyloidea; 2b) Ptychadena oxyrhynchus (CAS:HERP:256862) TJ, Ranoidea; 3a) Xenopus calcaratus (CAS:HERP:207759) - AQ, Archaeobatrachia; 3b) Callulina kisiwamsitu - BWH, Ranoidea.

2.4.3 Locomotor mode has the greatest impact on morphology

Several ecomorphometric studies suggest that the frog body plan enables responses to a broad array of mechanical challenges and environmental uncertainty, and therefore allows them access to a variety of locomotor styles and habitats (Nauwelaerts *et al.*, 2007; Gomes *et al.*, 2009; Moen *et al.*, 2013; Vidal-

García et al., 2014; Tulli et al., 2016; Soliz et al., 2017). Though this generalised morphology could represent a morphological optimum that is constrained by phylogenetic inertia (Soliz et al., 2017), strong correlations have been found between performance, morphology, and microhabitat, regardless of phylogeny or geographical location (Gomes et al., 2009; Moen et al., 2013). Similar morphological structures and locomotor functions occur across unrelated taxa, especially for terrestrial and arboreal jumpers, suggesting that locomotor mode is a more important driver of morphological evolution than phylogeny (Appendix Table A.3; Emerson, 1988; Reilly & Jorgensen, 2011; Moen et al., 2013). Habitat type is a weaker driver of morphological evolution, demonstrated by the disappearance of locomotor trends when grouped by habitat type. For example, burrowers have the most robust forelimb and hindlimb, but this is hidden when grouped by habitat as terrestrial jumpers, walker-hoppers and burrowers have contrasting morphologies (Table 2.2). However, this is not to say that habitat type plays no role in shaping morphology. For example, the terrestrial group are correctly predicted most often (LDA: 88.5%; pFDA: 83.3%), indicating that common functional requirements and constraints involved with living a terrestrial lifestyle, such as similar weight-bearing compared to arboreal and aquatic taxa, could result in a predictably similar morphology. In summary, future research should take caution, as using broad habitat categories alone is not sufficient for explaining morphological variation in anurans (Figure 2.2).

2.4.4 Skeletal morphology can be a powerful predictor of function and ecology

As Neobatrachia is comprised largely of the clades Ranoidea and Hyloidea, the ten species within the Neobatrachia which are sister taxa to these clades are expected to be predicted as belonging to one of these groups, which is the outcome of the LDA. The pFDA yielded an unexpected result in that each one is categorised as Archaeobatrachia according to their skeletal morphology. In the Jetz & Pyron (2017) tree, these species are in the basal position outside of Hyloidea or Ranoidea, indicating that the specialised morphology that distinguishes the more derived members of that group have not yet evolved. Figure 2.2 demonstrates how these ten neobatrachians are central within phylogenetic group morphospace. Their phylogenetic position relative to the Hyloidea and Ranoidea implies that these

species have always been difficult to classify based on their skeletal morphology alone, so the pFDA may be reflecting this.

Asides from this, predictive models yielded very similar results, regardless of whether they incorporated phylogenetic history. Almost every species has the same group predicted in both the pFDA and LDA for their locomotor mode (96.3%), habitat type (97%) and phylogenetic group (94.5%). Although these predictions occasionally differed to the locomotor (41.5%) or habitat (35.4%) group allocated in the dataset, several of the disagreements in the predictive models are when the alternative group is correctly predicted. Furthermore, the significant separation of jumpers versus non-jumpers and the Archaeobatrachia versus more derived groups in the pPCA PERMANOVA analyses indicates that future studies should be able to determine whether extinct taxa are good jumpers from their skeletal anatomy using fossil measurements, which is a long-debated area of anuran biology (Přikryl *et al.*, 2009; Reilly & Jorgensen, 2011; Herrel *et al.*, 2016; Lires *et al.*, 2016; Gómez & Lires, 2019).

2.4.5 Riparian morphology is influenced more by jumping than swimming

Previous studies have stated there is little difference in the morphology of jumpers and swimmers (Vidal-García et al., 2014; Lires et al., 2016; Buttimer et al., 2020), a finding not reflected by my analyses. Incorporating a semi-aquatic habitat type permits useful insight into the role of locomotor mode in determining morphology and suggests why the results of this chapter differ from the cited studies (Nauwelaerts et al., 2007). Even though riparian species spend approximately half their time in an aquatic environment (Nauwelaerts et al., 2007), their skeletal measurements indicate morphology that is more suited to jumping than swimming. Similar to terrestrial jumpers, riparian taxa have the smallest sacral expansion, longest tibiofibula relative to femur, and the longest hindlimb relative to forelimb. They also have the lowest ratio of femur to total hindlimb length, while aquatic frogs have the highest. The PERMANOVA shows that riparian frogs have a more significantly different morphology from aquatic taxa than terrestrial taxa (Appendix Table A.3). Riparian species are also most often mistaken for inhabiting terrestrial environments according to both the LDA (58.1%; Table 2.4) and pFDA (64.5%; Table 2.5), even though terrestrial taxa have the most frequently correct classifications (LDA 88.5%; pFDA 83.3%). Additionally, in terms of locomotor mode,

terrestrial jumpers are never misclassified as swimmers, contrasting previous findings (Lires *et al.*, 2016). These results all suggest that riparian skeletal morphology may be less strongly influenced by the functional demands for swimming than jumping performance.

Despite these significant differences in morphology, there is unlikely to be a performance trade-off between the two locomotor modes (Nauwelaerts *et al.*, 2007; Herrel *et al.*, 2014; Soliz *et al.*, 2017), potentially due to many-to-many mapping (Bergmann & Elroy, 2014); i.e., several anuran characteristics are advantageous for both jumping and swimming. For example, the riparian taxa in the present study have the longest feet (Table 2.2), potentially to increase surface area of the 'paddle' for underwater propulsion, as well as for generating a larger force during jumping. Over half of extant anuran species are dependent on water bodies for reproduction (Gomez-Mestre *et al.*, 2012), so the ability to swim is unlikely to be eliminated from a frog's locomotor repertoire by the evolution of novel anatomical modifications specific to other locomotor modes. Furthermore, as previously noted, studies of swimming kinematics across frog species have demonstrated that taxa with different ecologies may employ different swimming strategies, potentially reflecting differences in morphology (Richards, 2010; Robovska-Havelkova *et al.*, 2014).

2.4.6 Limitations

One important limitation in this chapter is that μ CT scanning of unstained specimens does not permit visualization of lower density tissues (muscles, cartilage, tendons, etc.), as all soft tissues typically present the same grayscale value in the data and cannot be distinguished from each other. Thus, poorly mineralised cartilaginous and ligamentous structures that form an integral part of the sacro-iliac joint (Emerson, 1979; Manzano & Barg, 2005; Reilly & Jorgensen, 2011), as well as any unossified ends of long bones, may not be clear in these data. Subtle but important anatomical differences between taxa may have therefore been missed in this study. For example, swimmers and burrowers are hypothesized to have evolved a fused urostyle to limit lateral bending and create greater force through the hindlimbs, while a bicondylar sacro-urostylic junction may play a similar role in jumping frogs (Pugener & Maglia, 2009; Jorgensen & Reilly, 2013).

2.4.7 Future directions

Daily habitual use of muscle results in larger entheses, the attachment sites of muscle to bone, due to the mechanical stress or force experienced by the surface area of bone (Zumwalt, 2006). As a response, prior to skeletal maturity, bone growth increases. A particularly rugose enthesis can also indicate larger, more pinnate, or more forceful muscles (Perry & Prufrock, 2018). Therefore, a species with a larger bone is expected to reflect larger associated muscles and forces, predominantly in structures important for the locomotor mode of that species. This assumption forms the basis of functional interpretations of fossil data (Bates et al., 2021). However, as bony responses vary between stimuli, and bone and muscle can scale differently to body mass, bone size and shape cannot necessarily be used as a reliable predictor for muscle attachment area, muscle volume, force produced, or architectural properties (Rabey et al., 2015; Perry & Prufrock, 2018; Bates et al., 2021). Therefore, studies cannot infer differences in muscle force production between muscles, species, or locomotor modes with skeletal data alone. To be able to determine if an extinct frog was a good jumper based purely on the size of their bones, studies must first demonstrate that the associated muscle and its attachment site are proportionately larger in good jumpers, i.e., that the size of that muscle is an adaptation for long-distance jumping. This observation and the findings of this chapter have therefore inspired the natural next step in this thesis - comparative analyses of muscle anatomy (Chapters 3 and 4).

2.4.8 Conclusion

This chapter has comprehensively addressed its aim of determining the link between skeletal anatomy and locomotor mode, habitat type and phylogenetic history in anurans. Sacral expansion, hindlimb segment proportions, and humeral width are found to be the strongest drivers of morphological variation. The ability of key skeletal features to predict locomotor mode and habitat type is established, indicating that skeletal morphology may be useful for determining the lifestyle of rarely observed extant taxa, as well as extinct taxa using fossil data. My findings also suggest that jumping morphology is conserved across terrestrial, arboreal, and semi-aquatic habitats, while there is a wide range of anatomical solutions to performing swimming, burrowing, or walking. This chapter also presents novel evidence that pelvic characteristics are best considered as a continuum across a broad range of anuran families, locomotor modes and habitat types. Establishing directly how these differences in skeletal proportions relate to muscle morphology Page 60 of 286

and impact locomotor function will require further anatomical dissections, as well as biomechanical analyses. Therefore, the findings from this research have inspired the work carried out throughout the remainder of this thesis.

3 Gross muscular anatomy of the anuran pelvis and hindlimb in relation to locomotion

Dr Laura Porro provided Amira tutorials, guidance regarding anatomical measurements and, along with Dr Chris Richards, comments on draft versions of this chapter. The work carried out at the University of Florida was supported by the oVert project, which is supervised by Dr David Blackburn, and the UCL Bogue Fellowship. Dr Jaimi Gray designed the staining and scanning protocols and, along with Dr Ed Stanley, provided tutorials in VGStudio Max.

3.1 Introduction

Interspecific variation in pelvic and hindlimb myology has been long assumed to indicate differences in locomotor behaviour (Nauwelaerts et al., 2007; Fabrezi et al., 2014; Rabey et al., 2015; Ponssa et al., 2018; Collings & Richards, 2019). Essentially, a larger muscle indicates higher functional importance, as more energy has been invested into its growth despite the associated physiological and anatomical costs (e.g., daily energy expenditure; Perry & Prufrock, 2018). Several studies have investigated how total hindlimb mass is associated with locomotor performance in frogs (Marsh & John-Alder, 1994; Choi et al., 2003; Moen, 2019), but there are no studies comparing the relative proportions of total muscle mass within each hindlimb segment. Jumpers and swimmers may invest more strongly in shank muscles, as the sizes of ankle extensors are linked to jump force and propulsive foot rotations during swimming (Gillis & Biewener, 2000; James et al., 2005; Astley, 2016). Since backwards-burrowing frogs need to scoop dense substrate with their feet (Emerson, 1976), they may invest more in proximal foot muscles than non-burrowers. It is not known whether this also applies to forwards burrowers, which have evolved more recently. Moreover, relatively few studies compare the gross anatomical properties of more than just the largest muscles (Nauwelaerts et al., 2007; Přikryl et al., 2009; Vera et al., 2022), despite the knowledge that muscles are not mechanically independent, i.e., the function of a single muscle often depends on the configuration of joints, and therefore the actions of other muscles (Roberts, 2002; Collings & Richards, 2019). Studies that directly measure the correlation between muscle activity and locomotor performance are limited to a few major muscles, with a sample size that does not adequately

represent all locomotor modes (Peplowski & Marsh, 1997; Gillis & Biewener, 2000; James *et al.*, 2005; Nauwelaerts *et al.*, 2007; Azizi & Roberts, 2010; Astley, 2016; Reynaga *et al.*, 2019; Mendoza & Azizi, 2021; Marsh, 2022). One of the biggest knowledge gaps remaining is how investment into each group of post-sacral muscles with similar functions (herein referred to as 'functional muscle groups') differs between locomotor modes.

Differences in locomotor behaviour can also impact the point at which muscles originate and insert onto bone, as well as the size of their attachment sites. There is currently a large debate about the extent to which bone size and shape can be used to predict locomotor performance and muscle properties, particularly in fossil taxa (Rabey et al., 2015; Perry & Prufrock, 2018; Bates et al., 2021). Subtle differences in bone shape could alter the origins and/or insertions of muscles enough to change their moment arms (Collings & Richards, 2019). Pelvic muscles, for example, have been observed to vary in the extent to which they insert onto the ilia and urostyle (Přikryl et al., 2009; Fabrezi et al., 2014; Collings & Richards, 2019), but the functional implications of this variation are yet to be quantified. The presence/absence of dorsal crests on the ilia and urostyle is an understudied area of anuran morphology that provides the ideal model system to explore these relationships in detail (Emerson, 1979, 1982; Reilly & Jorgensen, 2011; Jorgensen & Reilly, 2013). Chapter 2 quantified how these osteological features differ across the largest range of species to date (Appendix Table A.4), but how dorsal crest size is linked pelvic muscle anatomy has only been quantified in one genus (Ponssa et al., 2018).

Traditionally, physical dissections have been used to record and compare musculoskeletal anatomy (Dunlap, 1960; Emerson, 1979; Duellman & Trueb, 1986; Nauwelaerts *et al.*, 2007; Přikryl *et al.*, 2009). There are several limitations associated with this invasive technique. Primarily, its destructive nature means that it is often not a suitable method for collecting data from museum specimens, closing off a vast source of potential knowledge. The damage means that data collection is not repeatable, and the 3D musculoskeletal topology is almost impossible to preserve and analyse. This makes modelling the complexity of 3D muscle pathways challenging, especially for muscles which pass through or wrap around other structures. Identifying muscle origins, insertions and lines of action is crucial for functional analyses as these variables determine how a muscle contributes to the

production of joint torque (Collings *et al.*, 2022). Additionally, data can be easily lost, particularly for fragile or small structures, or those with large attachments, such as the small hip muscles, which are difficult to separate from the bone's surface intact (Appendix Figure C.1).

Diffusible iodine contrast enhanced computed tomography (diceCT) has recently made possible the non-destructive, high-resolution digital dissection of soft tissues, with preservation of the 3D topology in vertebrates (Gignac & Kley, 2014; Gignac et al., 2016; Holliday et al., 2022). Crucially, this has enabled dissection of rare and recently extinct specimens from museum collections, as diffusible iodine staining is largely reversible (Hedrick et al., 2018; Yapuncich et al., 2019; Early et al., 2020; Lanzetti & Ekdale, 2021; Leonard et al., 2022). This technique has also facilitated the study of minute anatomical structures that are not possible to extract using traditional techniques (e.g., bird cranial and pectoral muscles: Jones et al., 2019; To et al., 2021; Widrig et al., 2023). Additionally, diceCT data has been used to create 3D interactive models (Tsai & Holliday, 2011; Holliday et al., 2013; Lautenschlager et al., 2014; Bribiesca-Contreras & Sellers, 2017), which can be used for educational materials and further research (Gray et al., 2023). For example, subsequent biomechanical models have been created to investigate the impact of different morphologies on mechanical performance, including limb motion in reptiles (Wilken et al., 2019; Tsai et al., 2020; Demuth et al., 2022) and feeding mechanics in rodents (Cox & Faulkes, 2014), frogs (Kleinteich & Gorb, 2015), primates (Orsbon et al., 2020) and bats (Santana, 2018). Even studies of extinct taxa have benefited from diceCT through increased contrast of internal fossil structures (Bailleul et al., 2021) and reconstructions of soft tissues supplemented with inferences of bony correlates (Lautenschlager, 2016). However, there are relatively few comparative studies incorporating enough diceCT data to analyse the relationship between soft tissue anatomy, ecology, behaviour, and phylogenetic history across more than just a handful of species. Studies include the investigation of hindfoot drumming in molerats (Sahd et al., 2022), bat diet (Santana, 2018), bat flight performance (Stanchak & Santana, 2018), and masticatory mechanics in rodents (Hautier et al., 2012). For frogs, diceCT has only recently been applied to exploring frog anatomy (Porro & Richards, 2017; Collings & Richards, 2019). The novel combination of the resulting 3D muscloskeletal models with biomechanical modelling of frog locomotion is rarer still (Collings et al., 2022). Only one study has used diceCT to compare muscle anatomy across taxa in relation to locomotor behaviour, which was specifically in relation to the role of the forelimbs and pectoral girdle in determining burrowing style for five species (Keeffe & Blackburn, 2020).

The overarching aim of this chapter is to quantify the size of muscles in the pelvis and hindlimb using digital dissection and compare them across all five primary locomotor modes spanning all major phylogenetic groups. Based on the findings of Chapter 2 and the literature, I propose a set of hypotheses:

- H1) The length of the pelvis muscles relative to the iliac shaft and urostyle will differ between locomotor modes.
- H2) There will be a correlation between pelvis muscle size and the length of the dorsal iliac and urostylic crests.
- H3) The relative total mass of muscle in the pelvis and each segment of the hindlimb will differ between locomotor modes.
- H4) Locomotor modes will invest differently into the mass of each functional muscle group.

Furthermore, previous anatomical studies have noticed that frogs differ in the amount of muscle separation (Dunlap, 1960; Přikryl *et al.*, 2009), but this has never been quantitatively analysed. For example, *Xenopus*, a highly specialised aquatic frog, has a low degree of muscle separation in the thigh (Porro & Richards, 2017). It is unknown whether this is due to its locomotor specialisation, or more basal position in the anuran phylogeny. I hypothesise that these observed differences in muscle number could have three potential explanations:

- H5.1) Differences in phylogenetic position, particularly Archaeobatrachia versus more derived species.
- H5.2) Differences in locomotor mode.
- H5.3) A mixture of phylogenetic history and selection pressures from different locomotor modes.

If the hypothesis 5.1 is true, I would expect to see an increase in muscle separation over evolutionary time. If hypothesis 52 is true, then muscle number may decrease in taxa that are more specialised in their locomotor function, as removing anatomical complexity could optimise functional performance (McShea & Hordijk, 2013). In this

case, a locomotor generalist, like *Phlyctimantis maculatus*, would be expected to have a higher number of muscles than locomotor specialists like *Xenopus* (swimming) or *Litoria* (jumping), for example. Alternatively, hypothesis 5.3 would be that both evolutionary history and locomotor mode influence muscle number - more recently evolved species with a locomotor specialisation may be constrained by phylogenetic inertia. Support for each hypothesis could also vary between pelvis and hindlimb anatomy. In this chapter, I plot the relationship between locomotor mode and pelvis, thigh, and shank muscle number on the frog phylogeny to directly address these hypotheses.

3.2 Methods

3.2.1 Dataset

Thirty taxa are used in this chapter, six from each locomotor mode (terrestrial jumper [TJ], arboreal jumper [AJ], swimmer [AQ], walker-hopper [WH] and burrower [BWH]). Locomotor mode, phylogenetic group (Archaeobatrachia, Neobatrachia, Hyloidea, and Ranoidea), skeletal proportions, and the length of dorsal crests were recorded in the same way as in Chapter 2. Twenty-four contrast-enhanced µCT scans were obtained from MorphoSource and Dr Laura Porro's collection, 13 of which had already been digitally dissected for previous studies (e.g., Porro & Richards, 2017; Collings & Richards, 2019). To bolster the coverage of locomotor modes and families, I stained and scanned ten additional specimens from the Florida Natural History Museum, in collaboration with the Blackburn Lab (University of Florida, USA). Six 'UF specimens' are used in the present study. All specimen information, staining durations and scanning parameters can be found in Supplementary Dataset 4.

3.2.2 UF specimen preparation

Where possible, specimens were chosen from containers with many individuals from the same locality, avoiding frogs that were relatively small (i.e., potentially juveniles), had signs of damage (i.e., broken bones, previous physical dissection) or had any limbs bent into unnatural positions (frogs are occasionally fixed with their hindlimbs outstretched). As specimens had been fixed in formalin and stored in 70% ethanol, and the staining solution is water-based, they were then placed in a new glass jar containing 50% ethanol to begin gradually reducing the ethanol

concentration to avoid osmotic shock (Gray *et al.*, 2023). The concentration was then reduced to 30% ethanol for two to three days before filling the jars with staining solution.

Lugol's iodine enables visualisation of soft tissues which would otherwise be indistinguishable from each other by increasing their radiopacity (Metcher, 2009; Gignac et al., 2016). The iodine selectively binds to the glycogen molecules and lipids within the muscles (Li et al., 2016). This process has been reported to cause varied levels of muscle shrinkage during staining at high concentrations (>10%) and long durations (Vickerton et al., 2013; Hedrick et al., 2018; Brocklehurst et al., 2019; Lanzetti & Ekdale, 2021). The mechanism of shrinkage has only recently been diagnosed as being caused by the acidification of the iodine (Dawood et al., 2021). Therefore, 1.25% buffered Lugol's was used here, which stabilises the pH and significantly reduces shrinkage due to staining whilst preserving the high-resolution contrast (Gray et al., 2023). Prior to staining, snout-vent length, and the width and depth of the body and head were measured using digital callipers to enable quantification of any potential shrinkage after staining. A stock solution of 15% Lugol's iodine (50g iodine and 100g potassium iodine per litre of de-ionised water) was combined with Sorensen's buffer (18.88g of sodium phosphate dibasic and 18.1g of potassium phosphate monobasic per litre of de-ionised water) to create a solution of buffered Lugol's iodine with a pH of 7.2 (Gray et al., 2023). The solution was diluted using de-ionised water so that the concentration of Lugol's iodine was 1.25%. During staining, the specimens were stored in a dark room, as iodine can react to light. Staining time varied depending on the size of the specimen, but as frogs are relatively small, it was around one to two weeks (Supplementary Dataset 4).

Although sodium thiosulfate has been shown to chemically reverse the colour staining caused by the iodine, this compound does not remove the iodine, and has been known to occasionally cause tissue damage if it crystalises, as well as bone decalcification (Gignac *et al.*, 2016). Therefore, after the final scan was complete, specimens were removed from the staining solution and placed in fresh 30% ethanol, where the concentration was gradually increased to the same level as the original solution over one week. Then, the solution was refreshed every few days until it ran clear. Staining is not entirely reversible as soft tissues can remain more radiopaque than before (Appendix Figure C.3; Early *et al.*, 2020) but this method

removes the physical stain to a sufficient level to return the specimen to the museum collection.

3.2.3 µCT scanning

All UF specimen scans were carried out with the Phoenix v|tome|x µCT scanner at the Nanoscale Research Facility, University of Florida. Specimens were scanned prior to staining to better visualise the skeletal structures, as they can be more difficult to segment after the contrast of soft tissues has been enhanced. For stained specimens, the iodine solution can accumulate at the boundary between the skin and the muscles due to differences in binding abilities and rates of transport between types of soft tissue, which can decrease scan quality (Li et al., 2016). Therefore, specimens were all submerged in a water bath at room-temperature for at least half an hour prior to scanning to remove unbound iodine (Gray et al., 2023). A small aluminium rod was placed in the scanner alongside each specimen to act as an object of known density. A three-minute 'fast scan' was carried out first to check that the stain had permeated the deeper areas of all of the muscles (Appendix Figure C.2). An X-ray filter was used if the specimen was particularly large or dense. Most contrast-enhanced scans were conducted at 100kV and 200µA as a series of overlapping 'panels' along the same vertical axis to achieve high resolution (<20µm/voxel) for each region of interest (Supplementary Dataset 4). Scans were then reconstructed using the Phoenix Datos|x 2 acquisition software. The scan optimiser was used to correct for movement of the specimen during scanning. Beam hardening correction was set at level 7 to correct for how x-ray beams soften as they move through dense material. Scans were then imported into VGStudio Max (Version 3.4), where the aluminium rod was set as the object with the highest grayscale value, and black air voxels as the lowest grayscale value so that all scans were calibrated to fit in a similar range. Overlapping scans were stitched together by aligning the volumes as much as possible using the transformation tools, then snapping them together using the 'best fit regression tool'. The 'merge volumes' tool was then used to create a single volume. Voxels outside of the region of interest (ROI) were removed using the 'surface determination' and 'split ROI' tools so that only the frog is remaining to reduce file size. The resulting volume is exported as a VGL project file for digital dissection.

3.2.4 Digital dissection

I digitally dissected the UF specimens in VGStudio Max (Version 3.4), and eleven MorphoSource scans in Amira (Version 2020.2). Thirteen scans had been digitally dissected by Dr Laura Porro in Avizo (Version 8.0) for previous work. Digital dissection was carried out from the pelvis (excluding the iliolumbaris, as it extends from the sacral bone anteriorly) to the proximal foot (excluding small foot muscles that originate at the tarsometatarsal joint) for whichever hindlimb showed the least damage (Figure 3.1; Figure 3.2). Muscle topology, variation in muscle fibre orientation and differences in density between tissues was used to discriminate between structures. Muscle nomenclature and abbreviations are consistent with previous literature on frog dissection (Dunlap, 1960; Přikryl *et al.*, 2009; Porro & Richards, 2017; Collings & Richards, 2019).

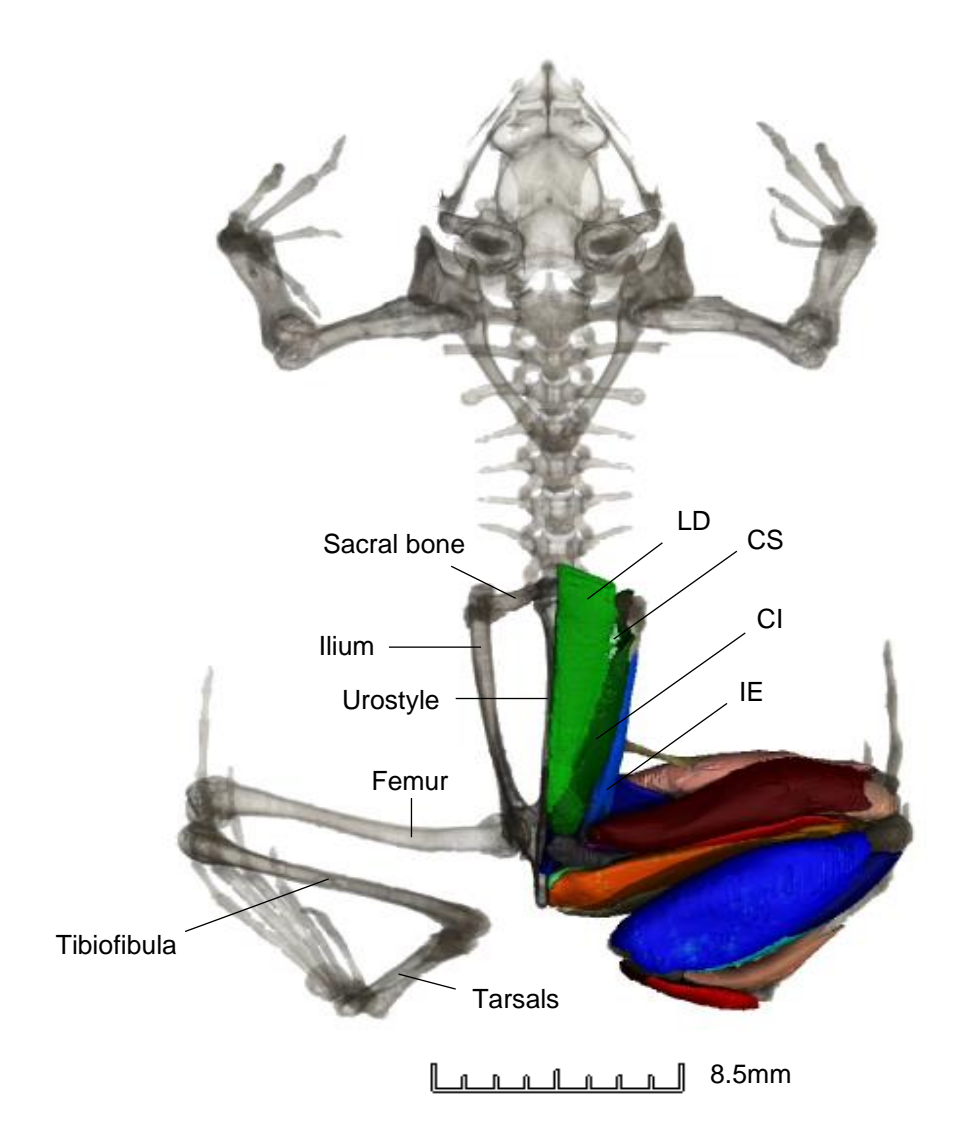


Figure 3.1 - 3D digital dissection of *Hemisus guineensis* (voucher number: CAS-herp-258533) in VGStudio Max (Version 3.4), with annotation of the skeleton and pelvis muscles in dorsal view. The view of the coccygeosacralis (CS) is partially obscured as it is positioned behind the longissimus dorsi (LD). See 'List of muscle abbreviations' for the full names of each muscle.

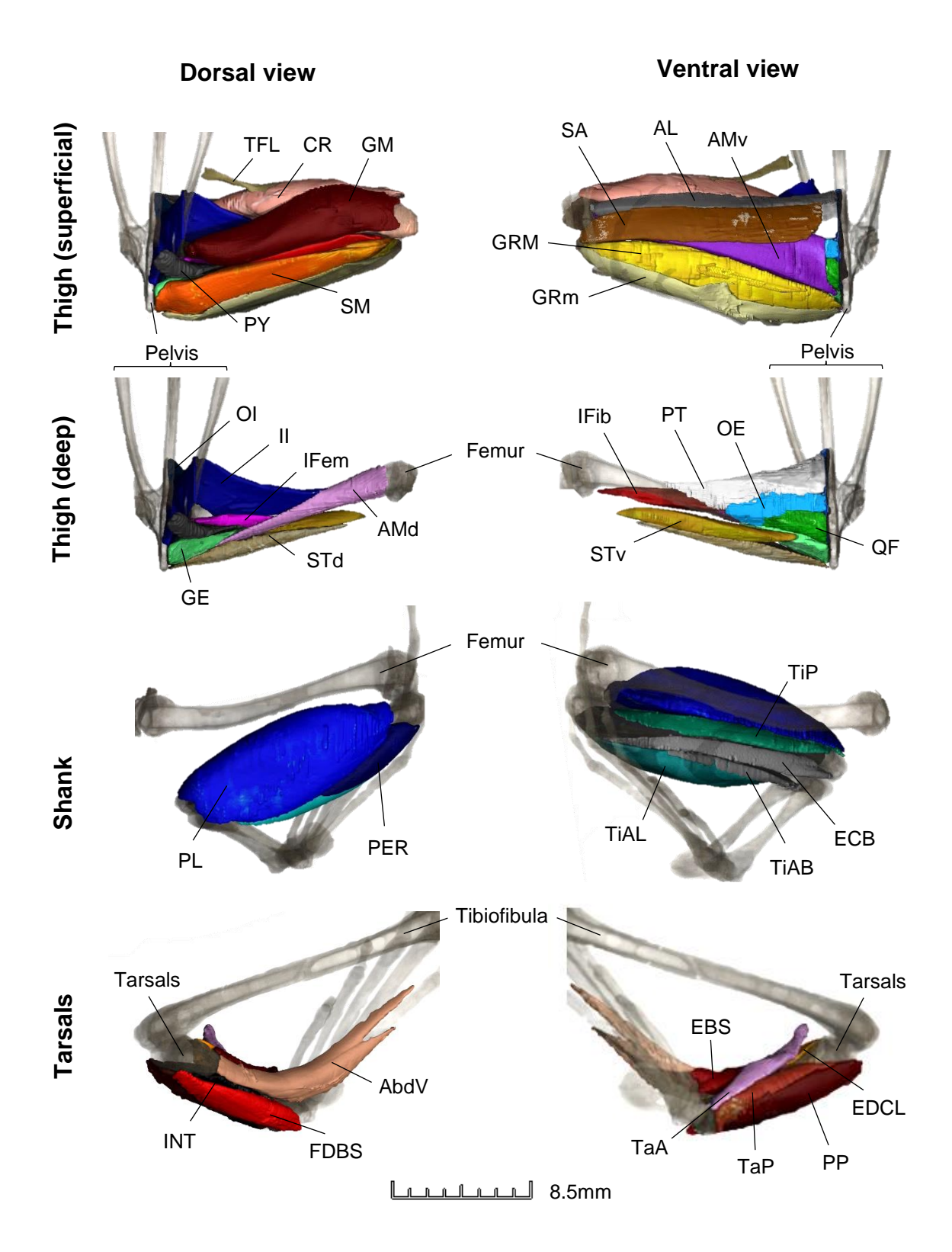


Figure 3.2 - 3D digital dissection of the right hindlimb of *Hemisus guineensis* (voucher number: CAS-herp-258533) in VGStudio Max (Version 3.4). See the 'List of muscle abbreviations' for the full names of each muscle.

In Amira, the threshold tool in the segmentation editor was used to isolate bone and soft tissue. Individual structures were selected using the paintbrush tool no more than every five scan slices, before using the interpolation tool. Once segmentation of a structure was completed, the volume model was viewed to check placement and visualise any abnormalities. In VGStudio Max, a combination of the draw, region growing, opening/closing, erode/dilate, smoothing, and refinement tools were used to digitally dissect each of the UF specimens. The software interpolates the changes across all three planes of view and updates the 3D rendering automatically.

3.2.5 Extracting gross anatomical muscle data

The muscle belly length (MBL), defined as the longest distance between the proximal origin and distal insertion points (Lieber & Fridén, 2000), for each muscle in the pelvis and hindlimb was measured from the volume model using the 3D line tool in Amira and the polyline tool in VGStudio Max. All 30 specimens appeared to have a 'relaxed' or 'natural' pose, so MBL is unlikely to be overestimated from overly stretched muscles. The longissimus can originate as far anteriorly as the pectoral girdle in some species (Přikryl et al., 2009), but this was often too difficult to dissect completely due to the presence of many layers of muscle divided by transverse tendinous inscriptions. Therefore, the longissimus was measured from its point of attachment on the anterior side of the sacral bone to its point of insertion on the urostyle since this area of anatomy was most important for addressing the aims of this chapter. Most curved muscles were measured using the sum of two parts to reduce the chances of measurement error – a straight line measurement from each end of the muscle, meeting on the outer edge of the centre of the curve (Figure 3.3). The obturator internus (OI) originates from the ischium and wraps around the proximal head of the femur to form an incomplete circle of muscle (Přikryl et al., 2009). The length of the OI was calculated by multiplying the radius and the central angle that is formed when measured between the two ends of the muscle (Figure 3.3). This was done to obtain more replicable results across scans compared to a series of short straight-line measurements. Muscle belly volume (MBV) was extracted from the 'Material statistics' module in Amira, or by selecting the relevant region of interest in VGStudio Max. Muscle belly mass (MBM), a measure for the muscle's inertial resistance against translation (Nauwelaerts et al., 2007), was calculated by multiplying MBV by the standard value for vertebrate skeletal muscle density (1.056 g/cm³; Mendez & Keys, 1960).

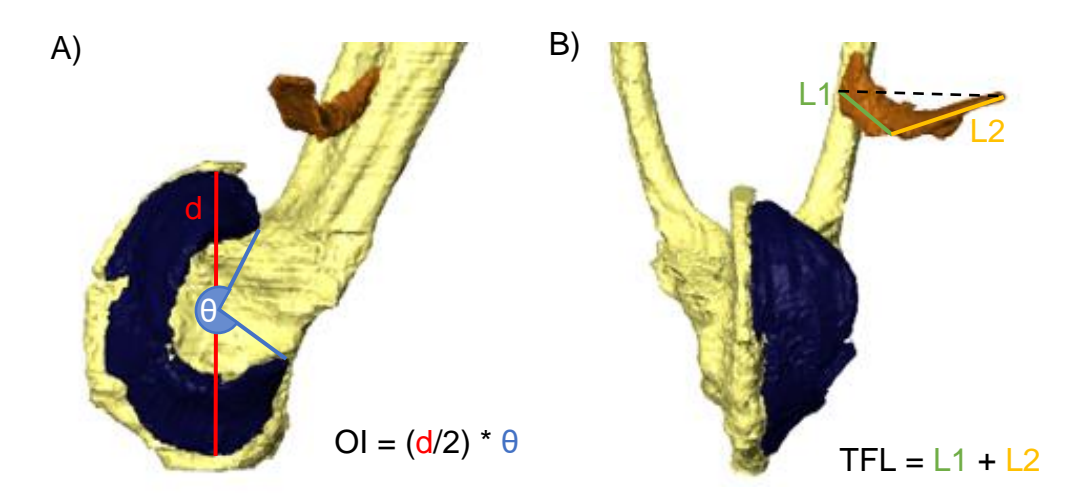


Figure 3.3 - Techniques for measuring the length of curved muscles A) for obturator internus (OI) (side view) and B) all other curved muscles, using tensor fascia latae (TFL) as an example (ventral view), shown in Amira (Version 2020.2) using *Phlyctimantis maculata* (specimen from Porro & Richards, 2017). The longest possible distance between the proximal and distal end of the muscle (dashed line) is used to determine the two points to measure from.

To address hypothesis 3, the mass of each muscle was added together according to the functional muscle groups in the thigh and shank described in the literature (Table 3.1). To address hypotheses 5.1-5.3, muscle heads were counted for the pelvis, thigh, and shank. Separate muscle heads were defined as when there is a distinct and consistent area of lower grayscale values between two (or more) areas of muscle that could be traced in all planes of view. A muscle head was considered separate if this occurred throughout at least one third of the length of the muscle, as there could be variation in muscle function even when there is separation at only one end of the muscle (Collings & Richards, 2019). Where possible, the literature was consulted to check if muscle separation had been found during traditional dissection (Přikryl et al., 2009; Porro & Richards, 2017; Collings & Richards, 2019). The semimembranosus and gracilis major thigh muscles were not considered reliable to assess for this step as they are known to have oblique tendinous inscriptions (Přikryl et al., 2009; Collings & Richards, 2019), and tendons cannot be visualised in iodine-stained scans. The proximal foot was excluded from the muscle count analysis because the distal part of the hindlimb is where scan resolution

tended to be lowest, making the ability to distinguish between different muscles difficult, let alone different muscle heads.

Table 3.1 - Summary of the thigh and shank muscles which have similar functions according to electrical stimulation (Přikryl *et al.*, 2009).

Functional group	Muscles				
Thigh					
Femur retraction	Semimembranosus, iliofibularis, gemellus,				
	obturator externus, quadratus femoris				
Femur protraction and	Adductor magnus, sartorius, adductor longus				
adduction					
Femur retraction and adduction	Gracilis major, iliofemoralis, gracilis minor				
Femur protraction and	Iliacus internus				
abduction					
Femur long-axis rotation	Obturator internus				
Femur stabilisation (i.e.,	Pectineus				
resistance to long-axis rotation)					
Knee flexion	Semitendinosus				
Knee extension	Cruralis, gluteus magnus, tensor fascia latae				
Shank					
Ankle extension	Plantaris longus, tibialis anticus longus, tibialis				
	posticus				
Knee extension	Peroneus, extensor cruris brevis				
Dorsiflexion and inversion of the	Tibialis anticus brevis				
ankle					

3.2.6 Considering potential variation in muscle shrinkage

Specimens stored in alcohol-based solutions are more likely to exhibit muscle shrinkage than those which are scanned after being thawed from frozen (Leonard *et al.*, 2021). Higher concentrations of iodine, staining for longer durations, and/or using Lugol's iodine without a buffer also increases the extent of muscle shrinkage (Vickerton *et al.*, 2013; Dawood *et al.*, 2021). The specimens used in the present study differed in the duration of storage, the type of solution they were stored in, and the concentration and duration of staining, meaning that there is likely variation in the mass and density of muscles between specimens caused by shrinkage (Levy, 2018). This variation will have consequences for inferring the functional capabilities of the muscles in each specimen. Additionally, total body mass was only available for six out of 30 specimens, so shrinkage corrections suggested by previous studies could not be performed (Leonard *et al.*, 2021). Therefore, the mass of each muscle was converted into relative percentages of total hindlimb segment mass. Using

relative percentages also reduces the effect of sexual dimorphism, as a mix of sexes had to be used and females are larger in approximately 90% of frog species (Nali *et al.*, 2014).

3.2.7 Statistical analyses

All analyses were carried out in R (Version 4.3.1). All continuous data (excluding muscle head count, see below) was transformed (log+1) prior to any statistical analyses. Shapiro-Wilk tests were used to evaluate the normality of the residuals for all variables while controlling for phylogeny. To address hypothesis 1, ANOVA/Kruskal-Wallis tests, followed by Tukey/Dunn's tests, were used to determine whether there are significant differences between locomotor modes in the length of each pelvis muscle relative to its associated long bone, i.e., the ilium and/or urostyle. The Tukey test automatically accounts for testing multiple pairs; a Bonferroni correction was integrated into all Dunn's tests. The pyriformis was excluded from this stage of analysis as it originates at the posterior tip of the urostyle. The total pelvis muscle mass relative to the total mass of the pelvis and hindlimb muscles combined was also compared to gauge how much each locomotor mode invests into pelvis versus hindlimb muscle size. To address hypothesis 2, Spearman's rank tests were used to evaluate the relationship between dorsal crest length and the size of the associated muscles. As in Chapter 2, a Dunn's test was used to determine whether crest length differed significantly between locomotor modes in this dataset.

To address hypotheses 3 and 4, ANOVA/Kruskal-Wallis and the same post-hoc tests were used to analyse the differences between locomotor modes for total hindlimb muscle composition and each functional muscle group. Phylogenetic principal component analyses (pPCAs) were performed under a Brownian motion model of evolution on the covariance matrix (phyl.pca function in *phytools*; Revell, 2012) to find the principal axes of variation in the muscle composition within the pelvis and each hindlimb segment. Pagel's lambda was obtained for each principal component to examine the impact of evolutionary history on muscle anatomy (phylosig function in *phytools*; Pagel, 1999). A phylomorphospace plot for the first two principal components from each analysis was used to examine how species cluster according to phylogenetic group and locomotor mode (phylomorphospace function in *phytools*). A permutational multivariate analysis of variance

(PERMANOVA) was then used to test whether the differences between the means for each locomotor mode and phylogenetic group were significant by performing pairwise comparisons (*pairwiseAdonis* package; Anderson, 2005). All PERMANOVAs used 999 permutations and corrected for multiple testing by adjusting the *p*-values using a Bonferroni correction.

Muscle head count was treated as continuous data (but left un-transformed), rather than discrete data, because partial fusion/separation was observed at the proximal or distal ends of muscles in some species. This approach preserves the order of the data, as well as the upper and lower bounds (e.g., you cannot have less than 17 and more than 23 thigh muscles). To address hypothesis 5.1, linear models were fit between pelvis, thigh, and shank muscle numbers and locomotor mode. An identical set of phylogenetic generalised least squares (PGLS) models were used to address hypotheses 5.2 and 5.3, i.e., to incorporate phylogenetic history as a potential explanatory factor. Voxel size was also included as a random factor in the hindlimb composition and muscle count analyses to test whether high voxel size due to a low resolution scan relative to actual structure size might cause over-estimations of object size in smaller specimens (Broeckhoven & du Plessis, 2018).

3.3 Results

3.3.1 Comparative anatomy of pelvis musculature

The only significant difference in relative pelvis muscle length between locomotor modes (hypothesis 1) is for the coccygeoiliacus, relative to both the ilium (Kruskal: Chi-squared₍₄₎ = 12.63, p = 0.013) and urostyle (Kruskal: Chi-squared₍₄₎ = 13.52, p = 0.009) (Figure 3.4). The coccygeoiliacus was a significantly longer relative to the ilium in TJ compared to AJ (Dunn's: z = 3.064, p-adjusted = 0.022) and BWH (Dunn's: z = 2.806, p-adjusted = 0.045). When uncorrected for multiple testing, there is a significantly longer coccygeoiliacus-ilium relationship in TJ compared to WH (Dunn's: z = 2.127, p = 0.033), and AQ compared to AJ (Dunn's: z = 1.966, p = 0.049). Relative to the urostyle, the coccygeoiliacus was shorter in AJ than all other locomotor modes, but only the difference from BWH is significant (Dunn's: z = 3.424, p-adjusted = 0.006). When uncorrected for multiple testing, AJ also have a smaller coccygeoiliacus-urostyle relationship than AQ (Dunn's: z = 2.170, p = 0.03) and TJ (Dunn's: z = 2.722, p = 0.007). Qualitative observations for the other pelvis muscles

include the longissimus inserting further down the length of the urostyle on average in non-jumpers, WH having a slightly longer coccygeosacralis relative to urostyle length, and both swimmers and jumpers having a longer iliacus externus than other locomotor modes (Figure 3.4).

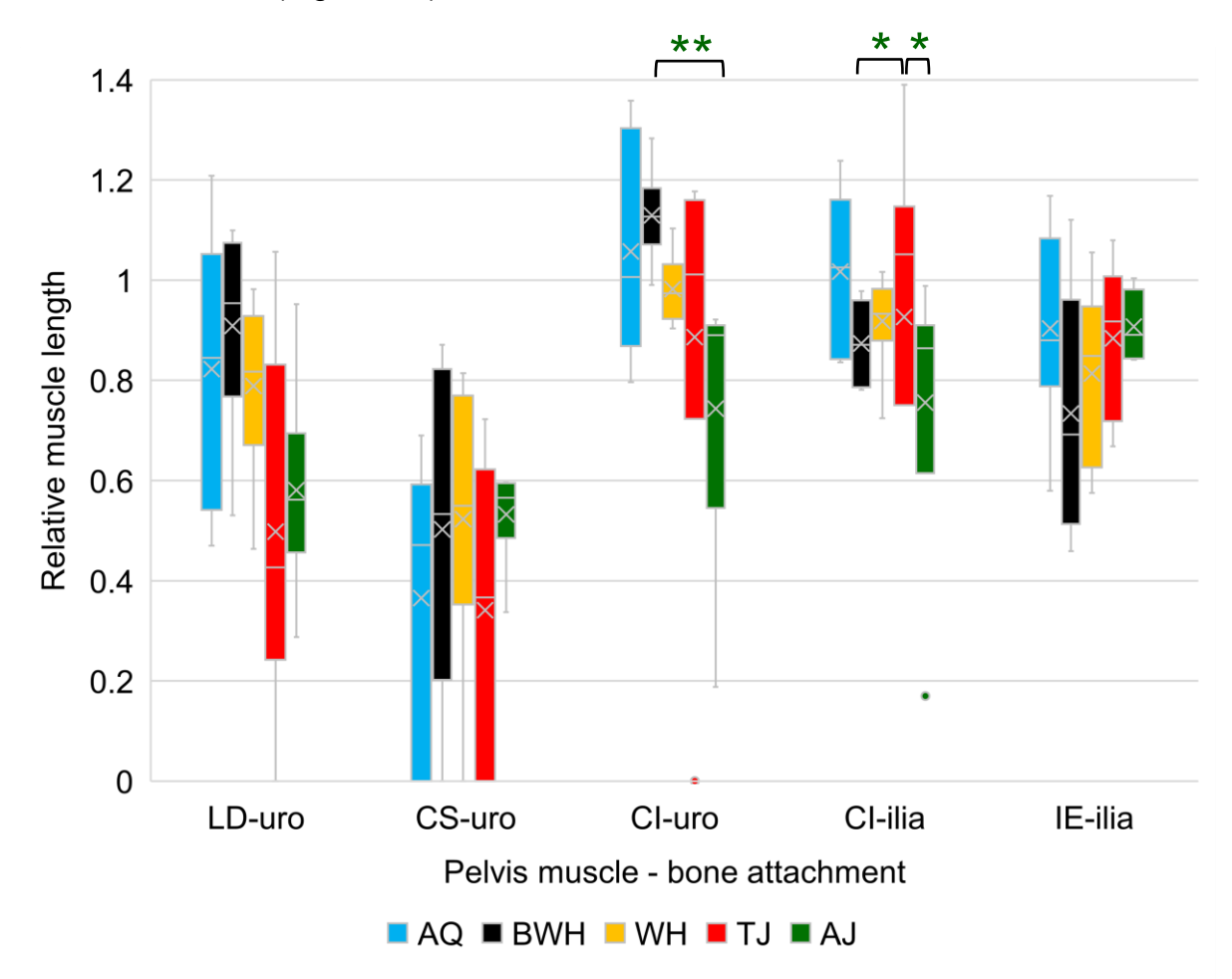


Figure 3.4 - The length of longissimus (LD), coccygeosacralis (CS), coccygeoiliacus (CI) and iliacus externus (IE) relative to their associated bone(s) – the urostyle (uro) or ilium – across locomotor modes. The pyriformis is excluded since it originates at the posterior tip of the urostyle and inserts onto the thigh. The error bars represent standard deviation. Dunn's test significance values are represented by ** = p <0.01 and * = p <0.05.

When testing the relationship between muscle mass and the length of the dorsal crests on the ilium and urostyle (hypothesis 2), the longissimus dorsi shows a significant negative relationship with urostyle crest length (Spearman's rank: rho = -0.469, p = 0.01). The coccygeoiliacus has significant positive relationships with both ilium (Spearman's rank: rho = 0.413, p = 0.026) and urostyle (Spearman's rank: rho = 0.394, p = 0.034) crest length. The size of the coccygeosacralis and the iliacus

externus is not significantly correlated with the urostyle and ilium, respectively. There are no significant differences between locomotor modes regarding crest lengths for both the urostyle and ilium.

Pelvic muscle composition (Figure 3.5) is primarily determined by the relative mass of the coccygeoiliacus and iliacus externus in PC1, and the longissimus dorsi and coccygeosacralis in PC2 (Figure 3.6; Appendix Table D.1). The first three PCs explain 97.4% accumulative variance. AQ have the largest variation in pelvis muscle anatomy, while BWH have the smallest (Figure 3.5; Figure 3.6). There are no significant differences in the morphospace occupied by each locomotor mode along either axis. There is a significant difference between Archaeobatrachia and the Hyloidea along PC1, but only when the p-values are not adjusted for multiple testing (PERMANOVA: F = 3.745, R² = 0.19, p = 0.009). This observation is exemplified best by AQ, as the Archaeobatrachia in this locomotor group have a considerably larger iliacus externus (Figure 3.6). The phylogenetic signal of the principal components is moderate, but not significantly different from zero in both cases (PC1: h = 0.504, p = 0.473; PC2: h = 0.753, p = 0.377).

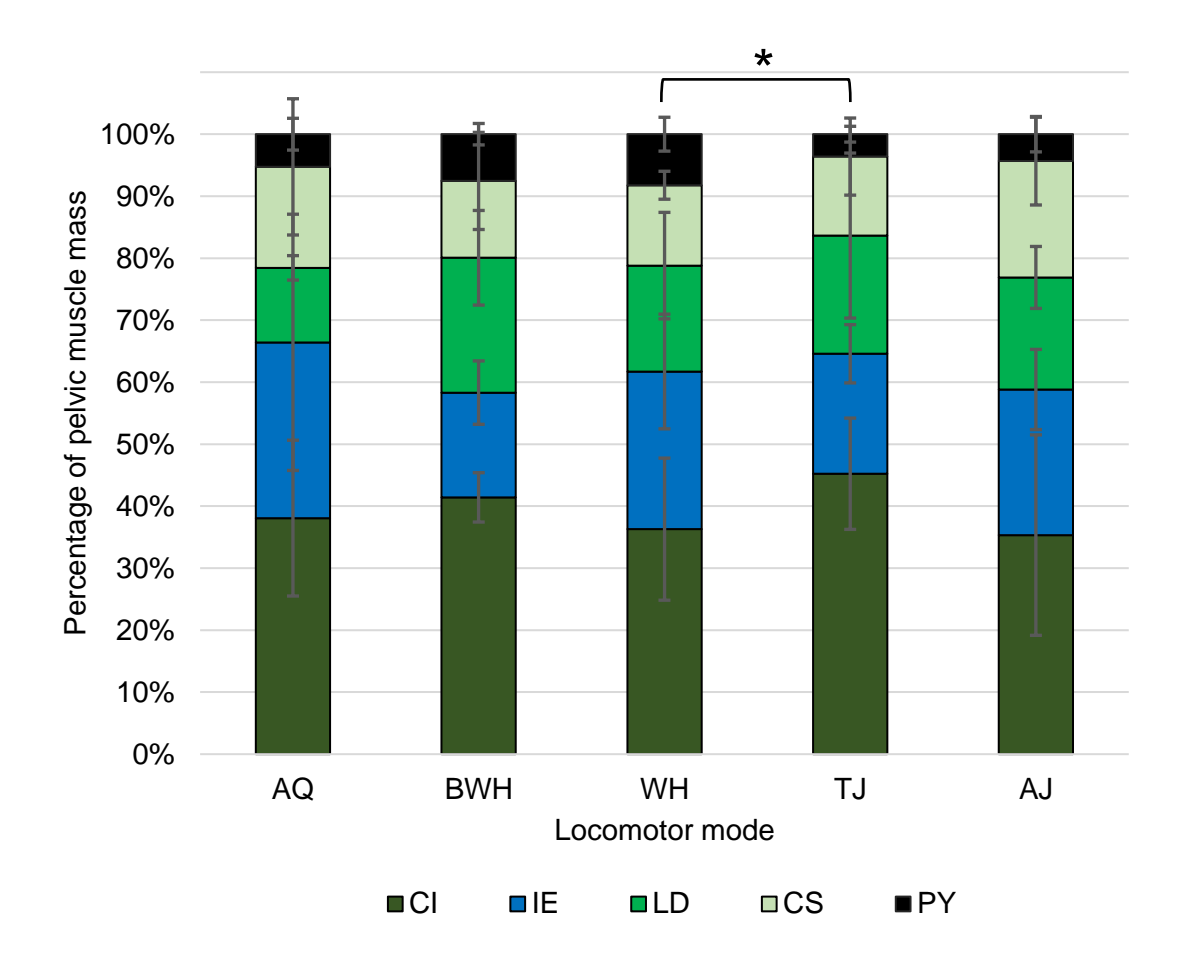


Figure 3.5 - Average mass across locomotor modes for muscles in the pelvis – coccygeoiliacus (CI), iliacus externus (IE), longissimus dorsi (LD), coccygeosacralis (CS), and pyriformis (PY). The error bars represent standard deviation from the mean. The pyriformis is the only muscle which shows a significant difference, indicated by the Tukey test where * signifies *p-adjusted* < 0.05.

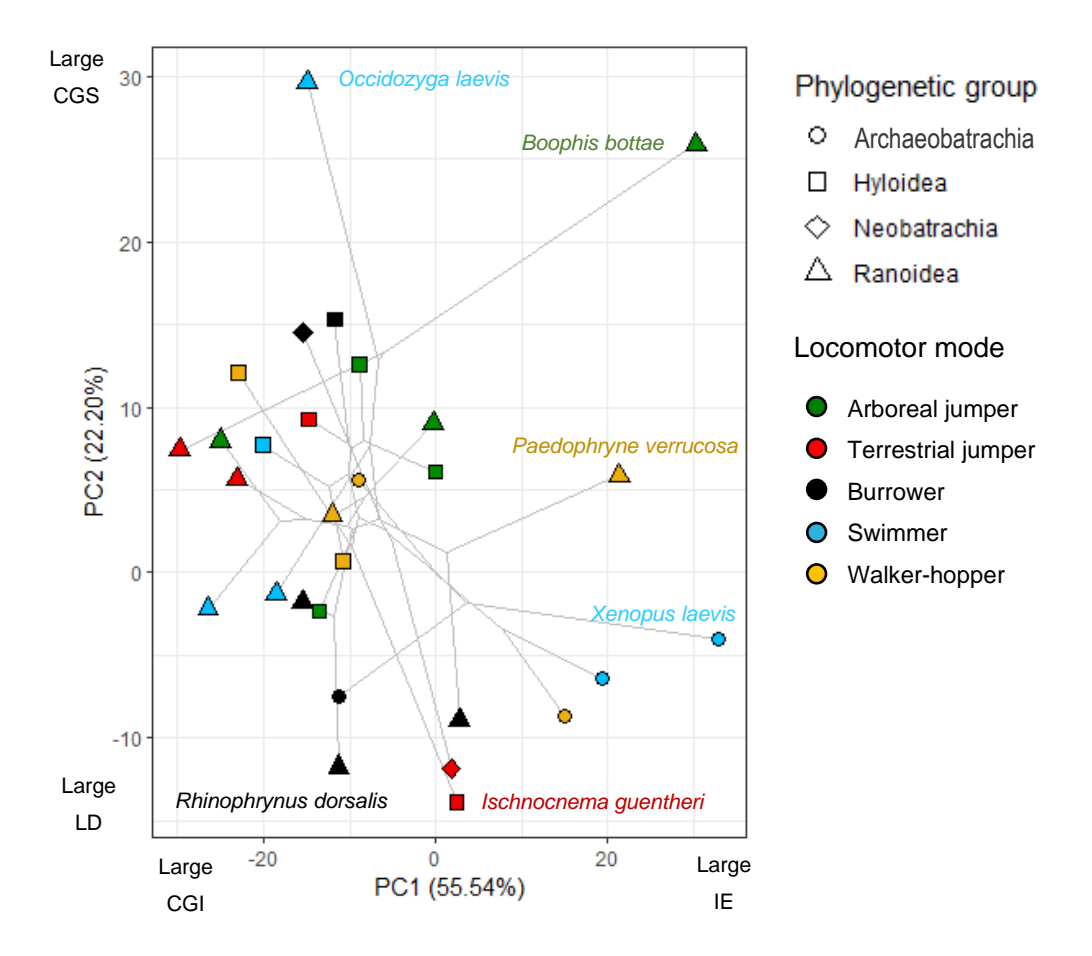


Figure 3.6 – A phylomorphospace plot using the principal component (PC) scores for the pelvic muscles, coded by phylogenetic group and locomotor mode. Axes are labelled with the muscles most strongly influencing the positive and negative loadings (Appendix Table D.1). See Figure 3.5 for the full names of anatomical abbreviations.

3.3.2 Comparative anatomy of hindlimb musculature

In terms of overall hindlimb composition, relative segment length and total relative segment muscle mass are positively and significantly correlated for the shank (Spearman's correlation: rho = 0.433, p = 0.018) and proximal foot (Pearson's correlation: cor = 0.464, p = 0.01), but not the thigh (Pearson's correlation: rho = 0.114, p = 0.459). WH, AJ, and BWH have the highest relative thigh, shank, and proximal foot muscle masses, respectively (Figure 3.7). Based on the standard deviation in the mass of each hindlimb segment across all taxa, differences in hindlimb composition are driven mostly by the thigh (4.44%) and shank (4.43%), while the proximal foot is relatively uniform (2.26%). WH have the most variable hindlimb composition, while AJ deviates least from the average. The shank is the

only segment which shows any significant differences in total muscle mass between locomotor modes (ANOVA: $F_{(4, 25)} = 3.27$, p = 0.027). The only locomotor modes which differ significantly from each other are AJ and WH, where AJ have a higher relative shank mass (Tukey: difference in means = 6.71%, p = 0.048; Figure 3.7). This effect is not driven by evolutionary history as the phylogenetic signal of the residuals is zero. Adding voxel size as another model parameter does not improve the fit to the data, indicating that scan resolution does not significantly impact these findings (Appendix Table C.1).

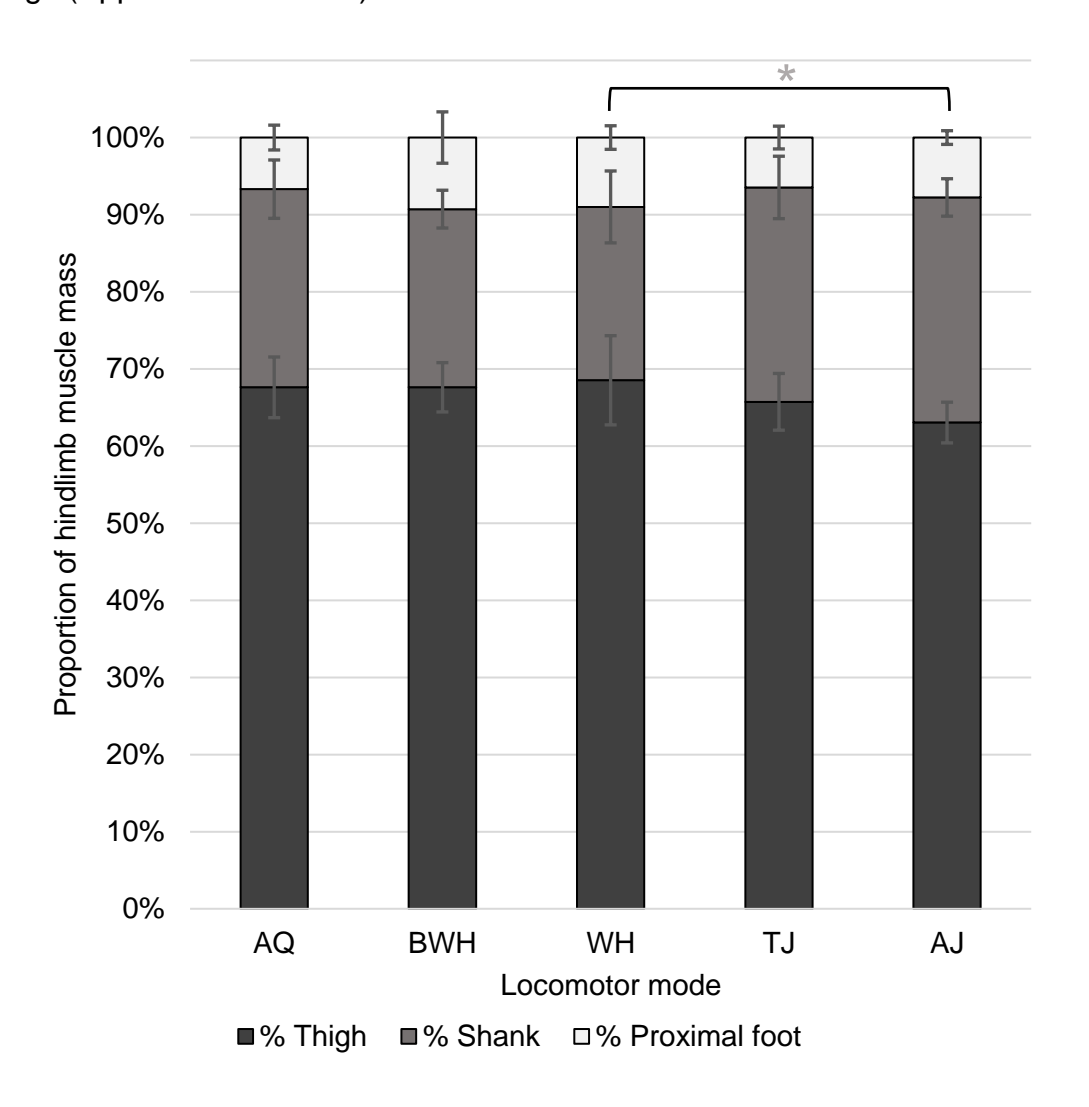


Figure 3.7 - Average muscle mass in each hindlimb segment across locomotor modes. The error bars represent standard deviation from the mean. The shank is the only segment which shows a significant difference, indicated by the Tukey test where * signifies p-adjusted < 0.05.

The composition of the thigh (Figure 3.8) is primarily determined by the relative mass of the cruralis and semimembranosus in PC1, and the pectineus, adductor

longus, and adductor magnus in PC2 (Figure 3.9; Appendix Table D.1). The first four PCs explain 84.1% of the total variance. There are no significant differences in the distribution of locomotor modes along PC1 unless p-values are not adjusted for multiple testing, in which case TJ PC1 values are significantly lower than WH (Table 3.2), as TJ tend to have a larger cruralis muscle (Figure 3.8; Figure 3.9). For PC2, BWH have significantly lower values than TJ and AJ (Table 3.2), as BWH have larger pectineus and adductor longus muscles (Figure 3.8; Figure 3.9). Without p-value adjustment, BWH PC2 values are also significantly lower than WH. BWH have the most variation in thigh musculature, while WH are the most densely clustered around the average (Figure 3.8; Figure 3.9). There are no significant differences between phylogenetic groups along either axis. The phylogenetic signal of PC1 is one, while lambda for PC2 is almost equal to zero, but neither are significant (p = 0.42 and p = 1, respectively).

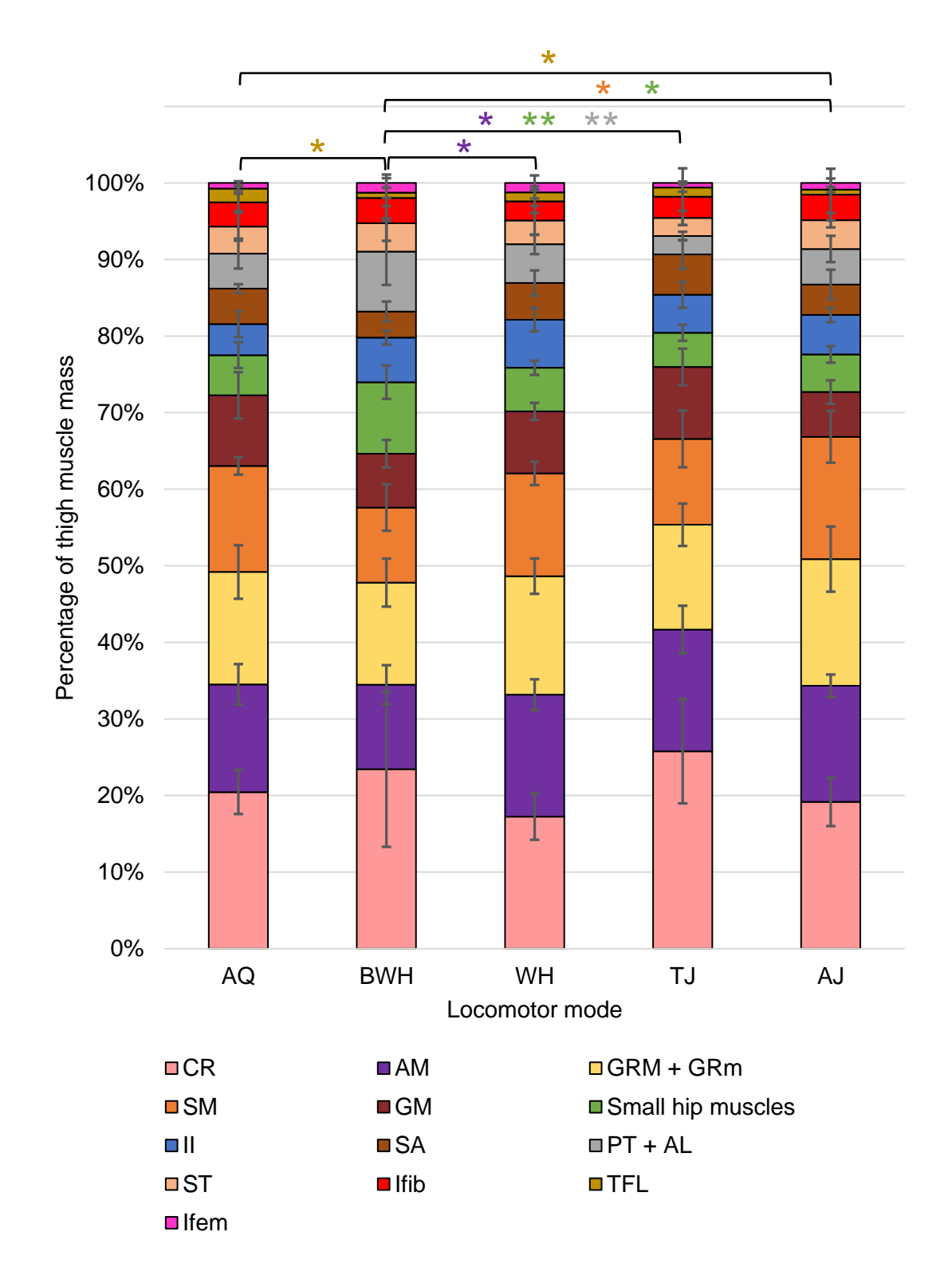


Figure 3.8 - Average relative mass of each muscle in the thigh across locomotor modes – cruralis (both deep and superficial heads; CR), adductor magnus (both dorsal and ventral heads; AM), gracilis major and minor (GRM + GRm), semimembranosus (SM), gluteus magnus (GM), small hip muscles (sum of the obturator internus, obturator externus, gemellus, and quadratus femoris), iliacus internus (II), sartorius (SA), pectineus and adductor longus (PT + AL),

semitendinosus (both dorsal and ventral heads; ST), iliofibularis (Ifib), tensor fascia latae (TFL), and iliofemoralis (IFem). The error bars represent standard deviation from the mean. Tukey and Dunn's test significance values are represented by ** = p-adjusted <0.01 and * = p-adjusted <0.05.

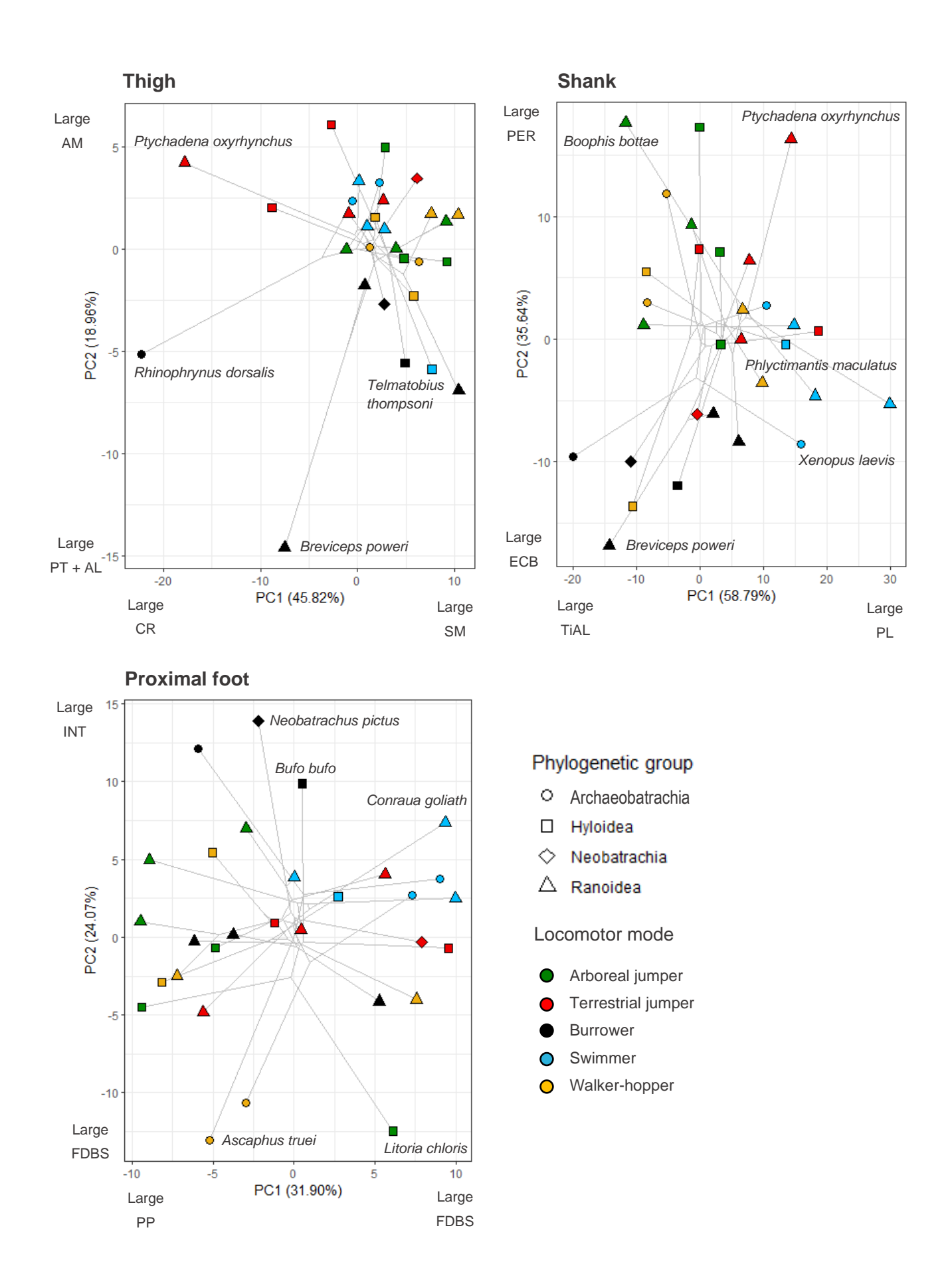


Figure 3.9 - A phylomorphospace plot using the principal component (PC) values for the muscles in each hindlimb segment, coded by phylogenetic group and locomotor mode. Axes are labelled with the muscles most strongly influencing the positive and negative loadings (Appendix Table D.1). Significant differences in PC values between locomotor modes can be found in Table 3.2. See Figures 3.8, 3.11 and 3.13 for the full names of anatomical abbreviations.

Table 3.2 - Summary of the locomotor pairs which differ significantly in muscle anatomy according to PERMANOVA tests of the principal components (PC) for each hindlimb segment. The first locomotor mode described in the pairing has the higher PC value. Pairs highlighted in bold are significantly different even after the p-value has been adjusted for multiple testing. The pelvis is not included here because none of the pairs have any significant p-values. PF = proximal foot.

Model	Pairs	F model	R ²	<i>p</i> -value	Adjusted p-value
Thigh PC1	WH vs TJ	5.681	0.362	0.025	0.25
	AJ vs TJ	4.672	0.318	0.046	0.46
Thigh PC2	TJ vs BWH	22.714	0.694	0.002	0.02
	AJ vs BWH	11.66	0.538	0.002	0.02
	WH vs BWH	11.336	0.531	0.006	0.06
	TJ vs WH	8.25	0.452	0.006	0.06
	AQ vs BWH	8.863	0.47	0.021	0.21
Shank PC1	AQ vs AJ	27.437	0.733	0.004	0.04
	AQ vs BWH	23.33	0.7	0.003	0.03
	AQ vs WH	19.382	0.66	0.003	0.03
	TJ vs BWH	7.95	0.443	0.023	0.23
	TJ vs AJ	6.621	0.398	0.028	0.28
	AQ vs TJ	5.053	0.336	0.043	0.43
Shank PC2	AJ vs BWH	30.145	0.751	0.004	0.04
	TJ vs BWH	17.351	0.634	0.002	0.02
	AQ vs BWH	11.742	0.54	0.009	0.09
	WH vs BWH	8.684	0.465	0.028	0.28
PF PC1	AQ vs BWH	11.953	0.544	0.008	0.08
PF PC2	AQ vs WH	9.073	0.476	0.01	0.1
	BWH vs WH	5.831	0.369	0.01	0.1

When thigh anatomy is evaluated in terms of functional muscle groups (Table 3.1), TJ show the most deviation from group averages, while WH show the least (Figure 3.10). Femur stabilisers (ANOVA: $F_{(4, 25)} = 4.25$, p = 0.009) and femur long-axis rotators (Kruskal-Wallis: Chi-square₍₄₎ = 14.76, p = 0.005) show significant

differences across locomotor modes (Figure 3.10). TJ have significantly larger femur stabilisers than both AJ (Tukey: difference in means = 2.17%, p-adjusted = 0.035) and WH (Tukey: difference in means = 2.36%, p-adjusted = 0.019). The long-axis rotators are significantly smaller in BWH compared to AJ (Dunn's: z = 2.98, p-adjusted = 0.014), TJ (Dunn's: z = 2.98, p-adjusted = 0.014) and WH (Dunn's: z = 3.02, p-adjusted = 0.013). When not corrected for multiple testing, AQ also have significantly larger long-axis rotators than WH (Dunn's: z = 1.67, p = 0.047). While knee extensors do not show significant differences overall (Kruskal: Chi-square(4) = 8.082, p = 0.09), there are significant differences between some locomotor groups when not adjusted for multiple testing - TJ have significantly larger knee extensors in the thigh than AJ (Dunn's: z = 2.43, p = 0.015), BWH (Dunn's: z = 1.69, p = 0.046), and WH (Dunn's: z = 2.03, p = 0.042; Figure 3.10).

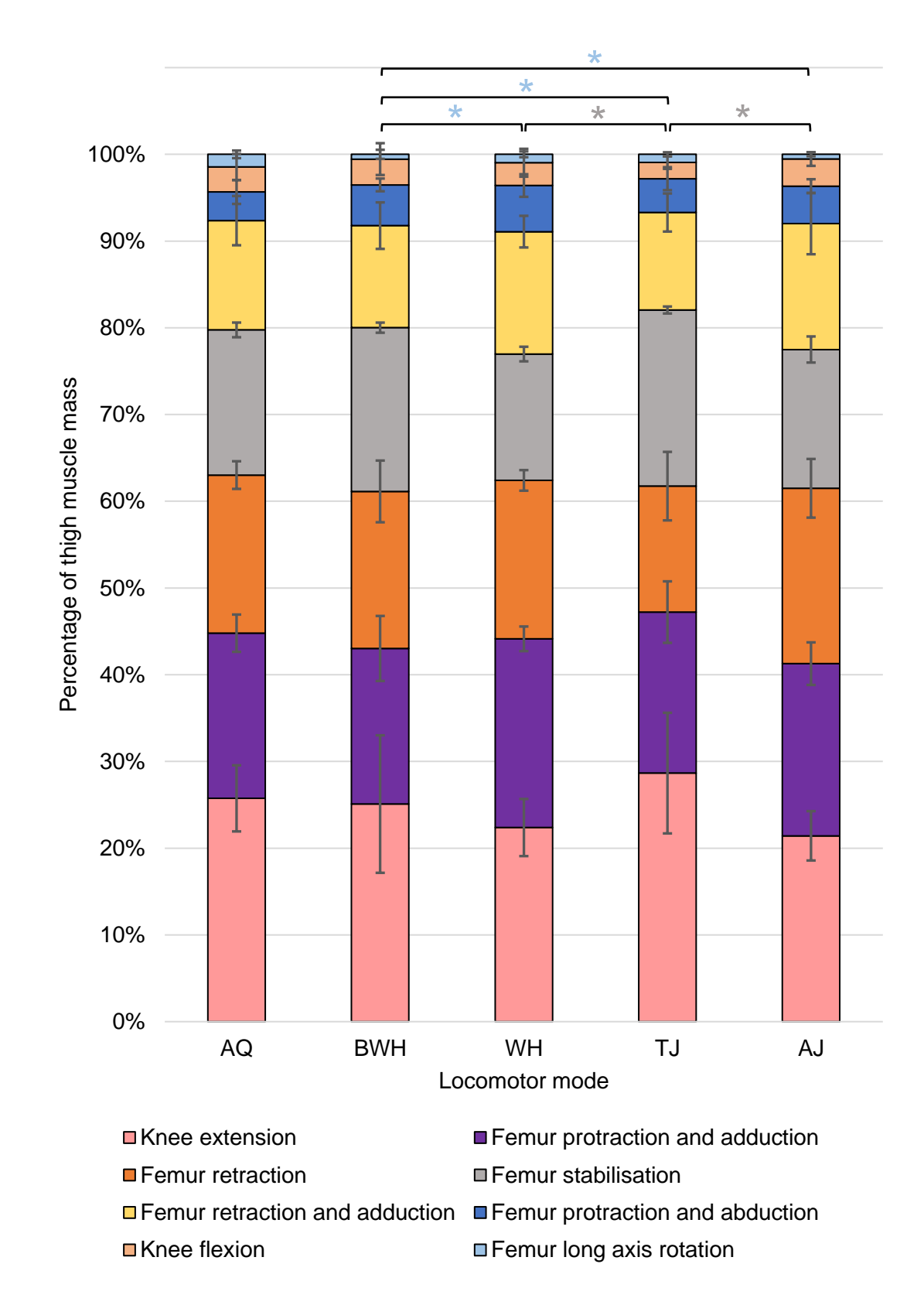


Figure 3.10 - Average relative mass of each functional muscle group in the thigh. The error bars represent standard deviation from the mean. See Table 3.1 for the muscles within each functional group. Colours match the muscle in Figure 3.8 that

contributes the most mass to each functional group. Tukey and Dunn's test significance values are represented by * = p-adjusted < 0.05.

The shank is the segment with the most significant differences between locomotor modes (Figure 3.11). AQ have the smallest total amount of variation in muscle anatomy, as indicated by the small error bars in Figure 3.11 and distinct clusters of AQ taxa in phylomorphospace (Figure 3.9), while WH have the largest. Shank muscle composition is primarily determined by the relative mass of the tibialis anticus longus and plantaris longus in PC1, and the extensor cruris brevis and peroneus in PC2, which explains 94.4% of the total variance (Figure 3.9). For PC1, AQ values are significantly higher than AJ, BWH and WH, while PC2 values are significantly higher in AJ and TJ compared to BWH (Table 3.2). There are no significant differences between phylogenetic groups along either axis, which is reflected in the phylogenetic signals (both PC1 and PC2: $\lambda = 0.00006$, p = 1).

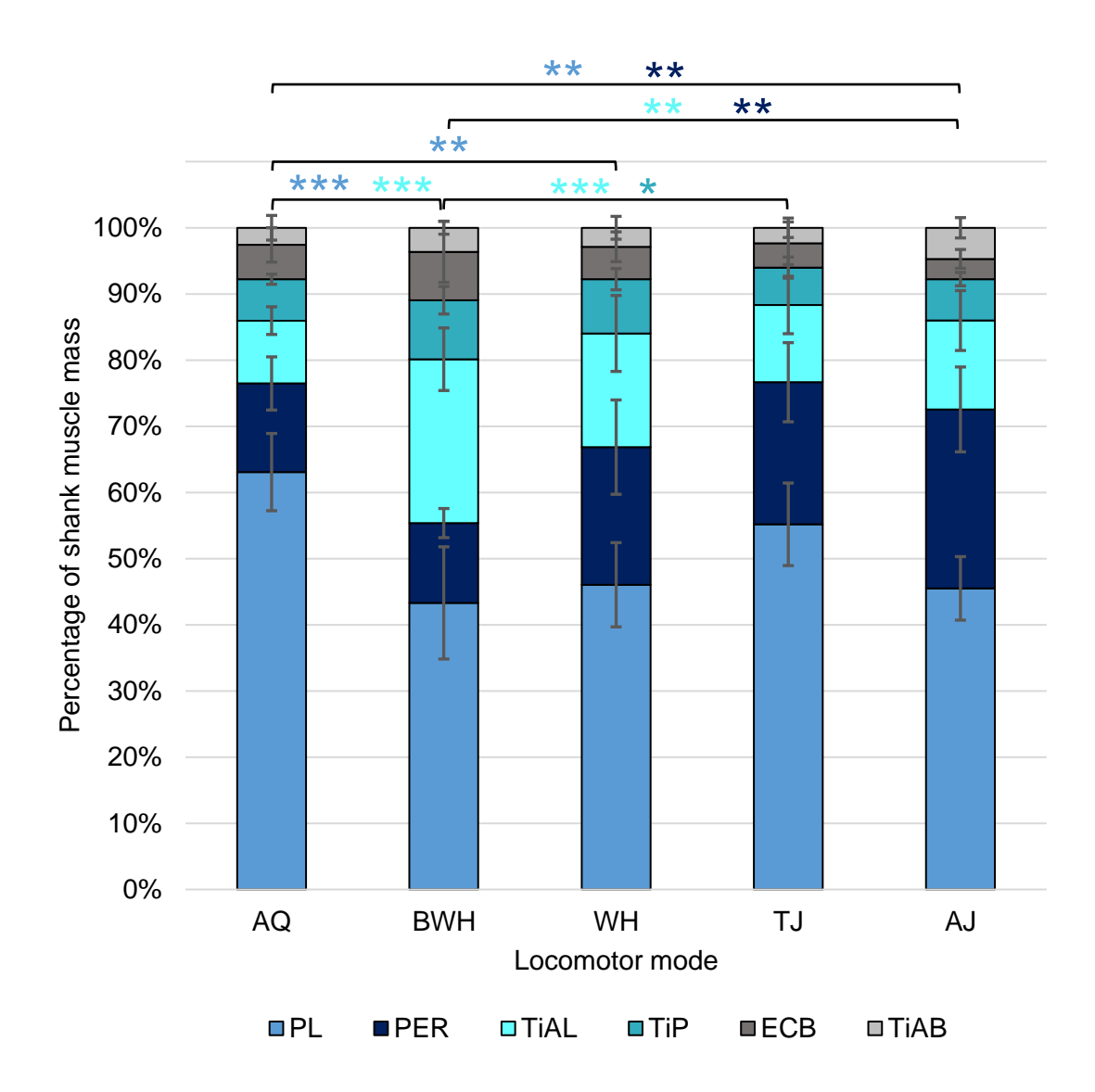


Figure 3.11 - Average relative mass across locomotor modes for muscles in the shank – plantaris longus (PL), peroneus (PER), tibialis anticus longus (sum of both heads; TiAL), tibialis posticus (TiP), extensor cruris brevis (ECB), and tibialis anticus brevis (TiAB). The error bars represent standard deviation from the mean. Tukey test significance values are represented by *** = p-adjusted < 0.001, ** = p-adjusted < 0.05.

For the shank functional muscle groups, ankle extensors (ANOVA: $F_{(4, 25)} = 5.06$, p = 0.004) and knee extensors (ANOVA: $F_{(4, 25)} = 4.22$, p = 0.010) show significant differences between locomotor modes (Figure 3.12). AJ have significantly smaller ankle extensors than both AQ (Tukey: difference in means = 13.63%, p-adjusted = 0.003) and BWH (Tukey: difference in means = 11.79%, p-adjusted = 0.013). AJ instead has significantly larger knee extensors than both AQ (Tukey: difference in means = 11.52%, p-adjusted = 0.014) and BWH (Tukey: difference in means =

10.71%, p-adjusted = 0.025). While the ankle dorsiflexion group does not show significant differences overall (Kruskal-Wallis: Chi-square₍₄₎ = 8.461, p = 0.08), AJ have significantly larger values than AQ (Dunn's test: z = 2.25, p = 0.012) and TJ (Dunn's test: z = 2.48, p = 0.007) when not corrected for multiple testing (Figure 3.12).

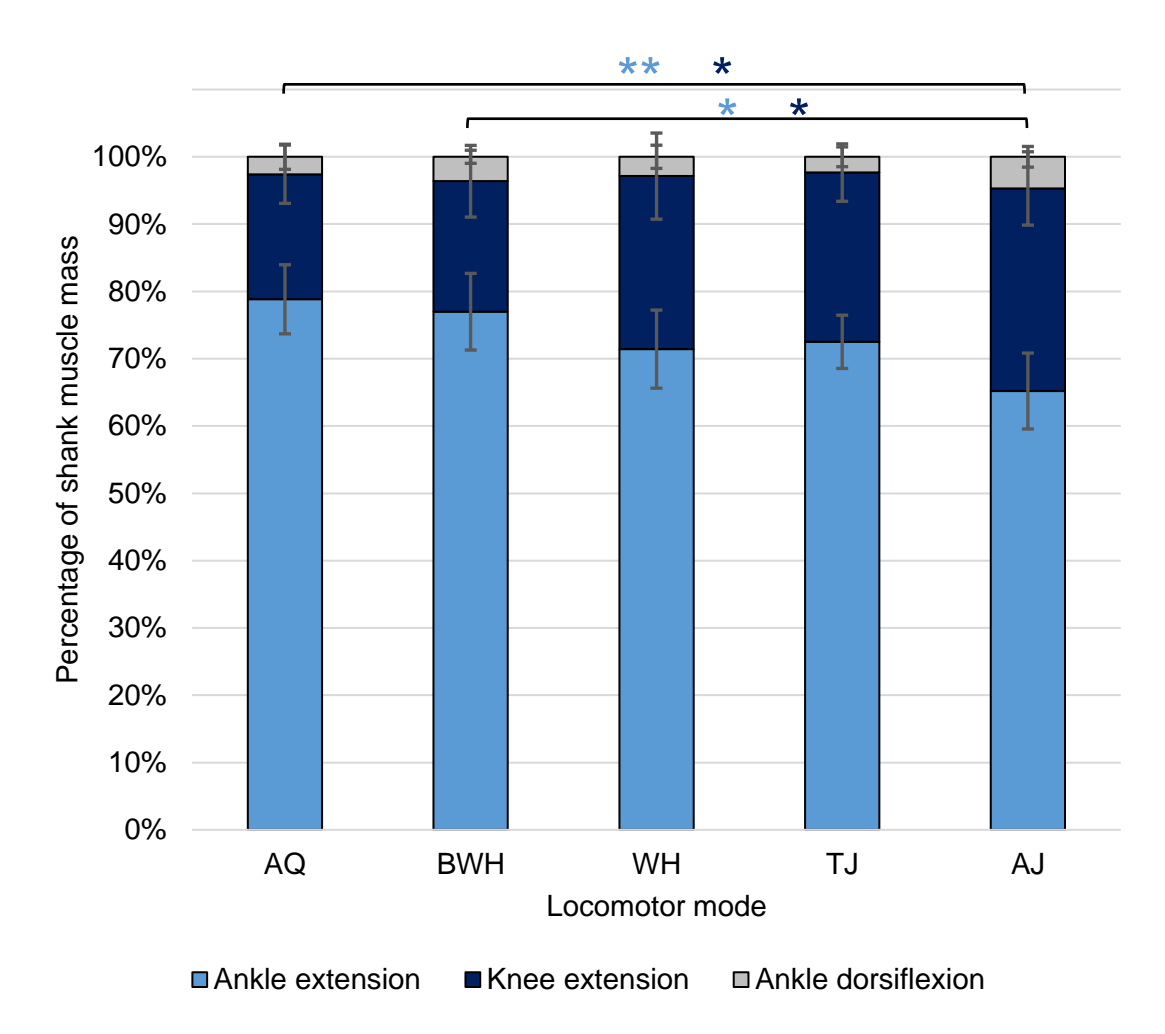


Figure 3.12 - Average relative mass of each functional muscle group in the shank. The error bars represent standard deviation from the mean. See Table 3.1 for the muscles within each functional group. Colours match the muscle in Figure 3.11 that contributes the most mass to each functional group. Tukey test significance values are represented by ** = p-adjusted < 0.01, and * = p-adjusted < 0.05.

WH have the most variation in proximal foot muscle anatomy, while AJ have the least (Figure 3.13). The muscle composition is primarily determined by the relative mass of the plantaris profundus and flexor digitorum brevis superfiscialis (FDBS) in PC1, and the FDBS and intertarsalis in PC2 (Figure 3.9). The first four PCs explain 84.2% of the variance. None of the locomotor modes are significantly different from

each other unless the p-value is not adjusted for multiple testing, in which case AQ have significantly higher values for PC1 than BWH, and both AQ and BWH have significantly higher values for PC2 than WH (Table 3.2). There are no significant differences between phylogenetic groups along either axis, which is reflected in the phylogenetic signals (both PC1 and PC2: $\lambda = 0.0001$, p = 1).

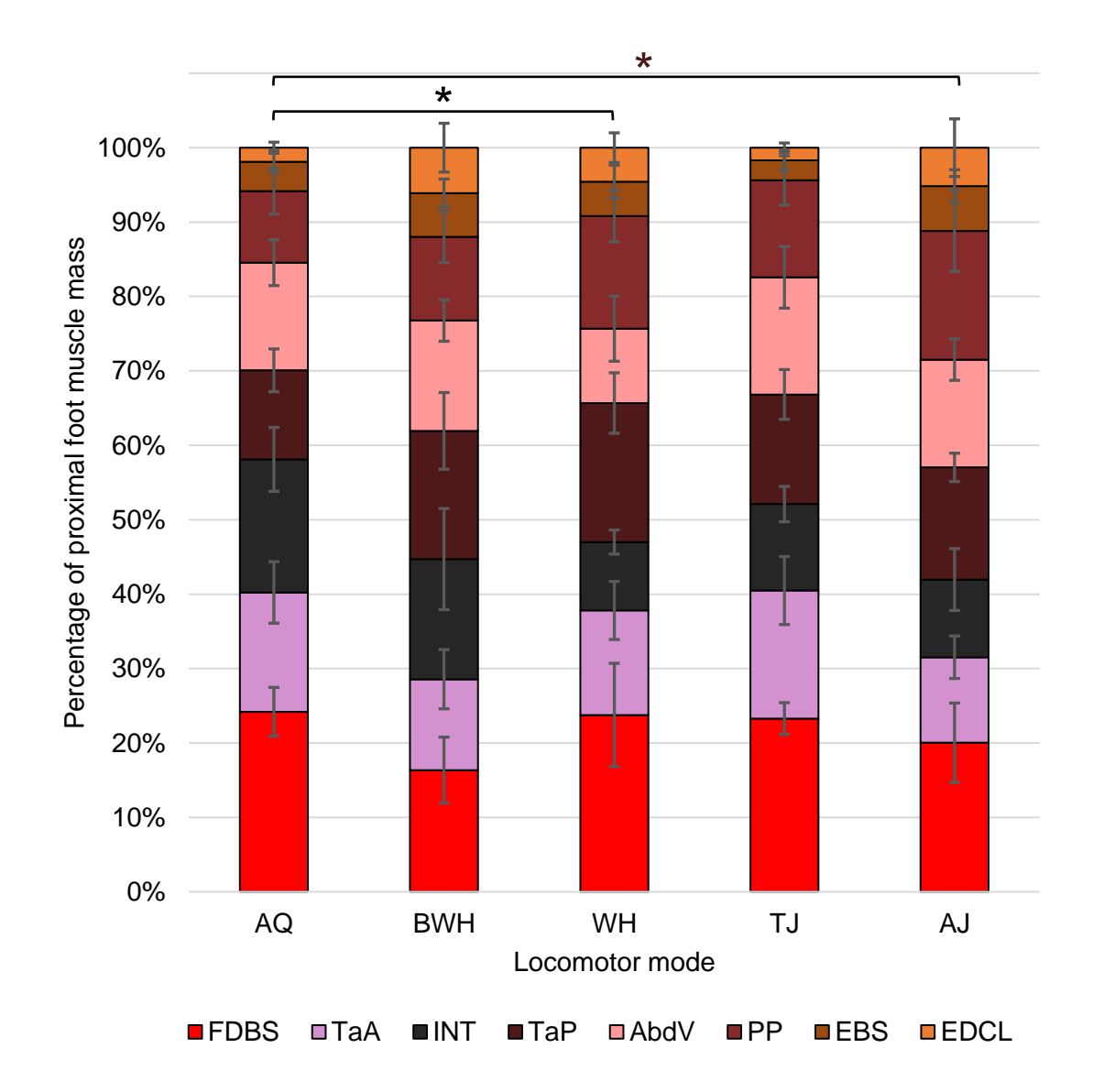


Figure 3.13 - Average relative mass across locomotor modes for muscles in the proximal foot – flexor digitorum brevis superfiscialis (FDBS), tarsalis anticus (TaA), intertarsalis (INT), tarsalis posticus (TaP), adductor brevis dorsalis V (AbdV), plantaris profundus (PP), extensor brevis superhallucis (EBS), and extensor digitorum communis longus (EDCL). The error bars represent standard deviation from the mean. Tukey and Dunn test significance values are represented by * = p-adjusted < 0.05.

3.3.3 Muscle number

All information on muscle head count is available in Supplementary Dataset 5. None of the best fit models include voxel size as an explanatory factor, meaning that scan resolution does not significantly impact muscle counts (Appendix Table C.2). The pelvis, thigh and shank usually contain five, 17, and six muscles respectively, which aligns with previous findings (Přikryl *et al.*, 2009; Collings & Richards, 2019). Regarding pelvis muscle count, there are no significant differences between locomotor modes. Phylogenetic signal is high ($\lambda = 0.981$), but not significantly different from zero (p = 0.402) nor one (p = 0.963). The only differences in the degree of muscle separation in the pelvis in this dataset is for the coccygeosacralis (absent in *Alytes obstetricans*, *Barbourula busuangensis*, *Breviceps poweri*, *Sechellophryne gardineri*, and *Xenopus laevis*), the iliacus externus (four layers in *X. laevis*, two heads in *A. obstetricans*), and the pyriformis (missing in *X. laevis*; Porro & Richards, 2017).

In the thigh, the separation of muscles into distinct parts occurs for all species in the adductor magnus (dorsal and ventral heads). The next most common cases of muscle separation are in the adductor longus (distinct from the pectineus in 20 species), semitendinosus (dorsal and ventral heads in 19 species) and cruralis (deep and superficial layers in 14 species). Additionally, the tensor fascia latae is missing in B. poweri and Hyperolius ocellatus, while it has two distinct heads in Occidozyga laevis. In Ptychadena oxyrhynchus and Stephania scalae, the semimembranosus appears to have two very distinct heads rather than the oblique tendinous inscription described in previous studies (Collings & Richards, 2019), but these cases are not counted for analysis since the tendons could not be visualised to confirm this. The gracilis minor is not distinguishable from the gracilis major in Sechellophryne gardineri. Thigh muscle number is more variable compared to pelvis and shank muscle number, ranging from 17 to 23 muscle heads, and is often lower in earlier diverging taxa (Figure 3.14). This is reflected in the high phylogenetic signal (0.989), which is almost significantly different from zero (p = 0.054) and not significantly different from one (p = 0.976). There are no significant differences in thigh muscle count between locomotor modes.

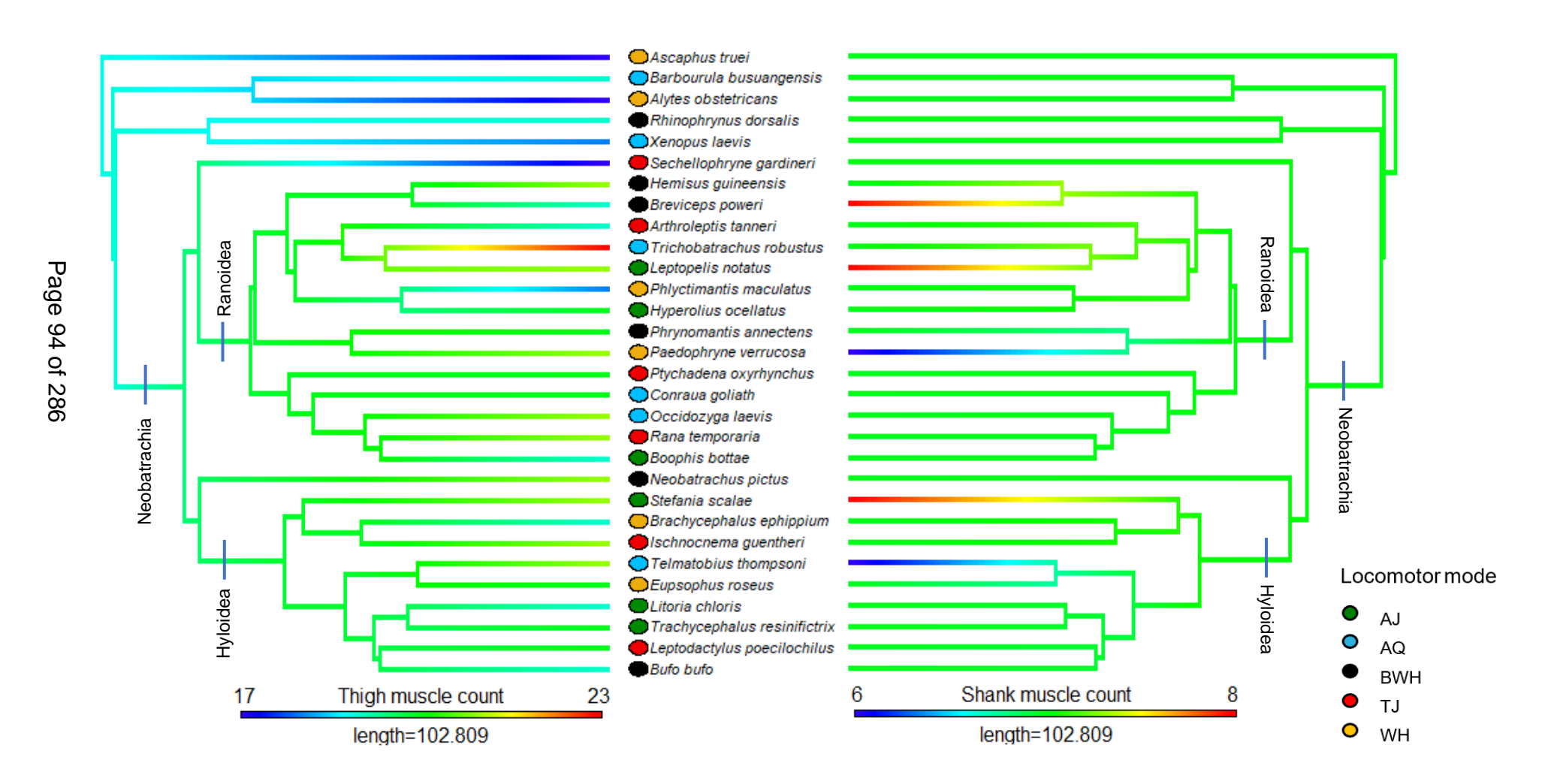


Figure 3.14 - Phylogeny of study taxa derived from Jetz & Pyron (2017) where branch colours represent muscle count for the thigh (left) and shank (right). The coloured dots at the tip labels represent the locomotor mode for each species.

Muscle count is the most uniform in the shank (Figure 3.14). The tibialis anticus longus is separated into two distinct heads for all species excluding Paedophryne verrucosa and Telmatobius thompsoni. In line with previous studies (e.g., Collings & Richards, 2019), this muscle varies greatly in the point at which the muscle belly splits, and how much the heads differ in size. For example, Litoria chloris has the greatest size difference (0.28:1), while S. scalae has the smallest (0.99:1). The extensor cruris brevis and the plantaris longus have only one case each where the muscles are separated into two distinct heads (Leptopelis notatus and S. scalae, respectively). Shank muscle count is the only variable in this analysis to show significant differences between locomotor modes (Table 3.3), and the phylogenetic signal is zero (p = 0.01).

Table 3.3 - PGLS coefficients for shank muscle count. *P*-values highlighted in bold indicate significance values below 0.05.

Coefficients	Estimate	Standard	t-value	<i>p-</i> value
		error		
Intercept	7.333	0.16	45.873	<0.001
AQ	-0.5	0.226	-2.212	0.036
BWH	-0.167	0.226	-0.737	0.468
TJ	-0.333	0.226	-1.474	0.153
WH	-0.5	0.226	-2.212	0.036

3.4 Discussion

This chapter aims to relate the muscle anatomy of the pelvis and hindlimb in frogs to their locomotor mode and evolutionary history to enhance our understanding of the relationship between form and function in vertebrates. It is essential to identify osteological correlates of muscle anatomy to be able to infer behaviour using fossils in future studies of extinct taxa (Perry & Prufrock, 2018). This detailed study of anatomical structures aims to address seven hypotheses, four of which investigate variation in muscle sizes, while the other three examine differences in muscle separation. I found many interesting avenues for future exploration using functional analyses, particularly for the muscles which discriminate between arboreal and terrestrial habitats for jumping, and between burrowers and non-burrowers. DiceCT has enabled the discovery that locomotor modes differ significantly in the size of some small hip and shank muscles, providing novel evidence of their functional significance. This chapter also marks the first quantitative analysis of how the

degree of muscle separation can differ between frogs. Phylogenetic history appeared to be the key contributing factor to muscle separation/fusion in the pelvis and thigh, while the number of separate shank muscles is influenced more strongly by locomotor mode. This chapter has also provided the 3D anatomical models of the pelvis and hindlimbs required for future biomechanical simulations to determine what consequences the observed variation in muscle size and intramuscular separation could have for the functional workspace of the limb.

3.4.1 Pelvic muscles which are more strongly associated with the ilia are more likely to have attachment sites which differ between locomotor modes

In line with previous studies (Přikryl *et al.*, 2009; Fabrezi *et al.*, 2014; Collings & Richards, 2019), I found pelvis myology to be highly variable, displaying a wide range of origins, insertions, and sizes. In support of hypothesis 1, there is a significant difference between locomotor modes in length of the coccygeoiliacus relative to the ilium and urostyle. The length of the coccygeoiliacus relative to the ilium is larger in terrestrial jumpers and swimmers than other locomotor modes (Figure 3.4). This generally aligns with the findings of functional analyses, as the coccygeoiliacus muscle is responsible for gliding the ilia along the anteroposterior plane, which is important for transmitting thrust to the sacrum during the jump launch phase (Ponssa *et al.*, 2018) and for shifting the pelvis posteriorly during swimming (Přikryl *et al.*, 2009). However, it is interesting that this muscle is significantly smaller in arboreal jumpers (Figure 3.4; Figure 3.5). This result implies that the coccygeoiliacus is influenced by the functional requirements of occupying different habitats, i.e., a large coccygeoiliacus may inhibit the ability to climb, or the pliability of the substrate may influence how this muscle is activated (Reynaga *et al.*, 2019).

Besides the coccygeoiliacus, the iliacus externus was the second largest driver of variation in pelvic morphospace (Figure 3.6). It varies widely in its functional capabilities depending upon its length and hindlimb posture (Přikryl *et al.*, 2009), but is generally essential as a femur protractor and hip flexor for the swing phase of walking and climbing (Collings & Richards, 2019), recovery phase of swimming, and crouched position in jumping (Nauwelaerts *et al.*, 2007). In terms of relative length, the iliacus externus is, on average, longest in jumpers and swimmers, and shorter in burrowers and walker-hoppers (Figure 3.4). It is also generally shorter in species

within the phylogenetic group Hyloidea (Figure 3.6), supporting the phylogenetic analysis by Fabrezi *et al.* (2014). When looking at relative mass, the iliacus externus is largest in swimmers and walker-hoppers, and smallest in burrowers (Figure 3.5). The lack of statistical significance in these results could be explained by an observation made by Collings & Richards (2019) – that the functional implications of the iliacus externus could be related more to its shape than its size. As longer muscles allow a greater range of motion (Lieber & Bodine-Fowler, 1993), while shorter muscles with a larger volume generally results in higher cross-sectional area and force output, there could be a trade-off in the shape of the iliacus externus relating to locomotor function. In *Phlyctimantis maculatus*, the iliacus externus is long and rather cylindrical, affording it the range of motion required to bring the leg upwards and forwards while running (Collings & Richards, 2019). Similar to the coccygeoiliacus, the considerable difference in both the size and length of the iliacus externus between arboreal and terrestrial jumpers could reflect different selection pressures in different habitats (Enriquez-Urzelai *et al.*, 2015).

Despite the shape of the sacral bone driving the most variation in post-vertebral skeletal anatomy (Chapter 2; Emerson, 1982; Reilly & Jorgensen, 2011; Petrović et al., 2017; Buttimer et al., 2020), there is little support for hypothesis 1 from its most closely associated muscle - the coccygeosacralis. On average, this muscle is longest in walkers (Figure 3.4), but most voluminous in swimmers (Figure 3.5). The longissimus dorsi also does not show any significant differences between locomotor modes. In general, the longissimus tends to be longer in non-jumpers, but has the largest mass in terrestrial jumpers. A lack of significant differences may have something to do with the pattern of ontogeny. Frogs achieve tetrapod locomotion at the beginning of metamorphosis before their urostyle has formed and its associated muscles have been differentiated, while the iliac shaft muscles develop during the larval stage (Fabrezi et al., 2014). However, this does not explain why the coccygeoiliacus would show significant differences, as it is one of the last muscles to become differentiated. An alternative explanation is because these two pelvis muscles have relevant roles in all locomotor behaviours. For instance, the longissimus dorsi and coccygeosacralis are important for lateral bending during walking, fore-aft gliding during swimming (Collings & Richards, 2019), and extension of the sacrum during the initial jump phase (Ponssa et al., 2018), as they function by dorsally rotating the urostyle and bending or stiffening the trunk, respectively

(Přikryl *et al.*, 2009). Similarly, as the lateral and long-axis rotator of the urostyle, the pyriformis is said to be involved in multiple functions (Přikryl *et al.*, 2009), though it was significantly larger in burrowers compared to terrestrial jumpers (Figure 3.5).

3.4.2 The size of pelvic bone crests could have functional implications for locomotion, but more evidence is needed

While working on Chapter 2, I observed that the length of dorsal crests on the iliac shaft and urostyle varied significantly between locomotor modes and phylogenetic groups. The results aligned with the observation made by previous studies - that jumpers and more derived groups tend to have larger crests (Appendix Table A.4; Emerson, 1979; Reilly & Jorgensen, 2011; Ponssa et al., 2018). Therefore, I predicted that there would be a correlation between crest size and the size of their associated muscles (hypothesis 2). The only other study to directly quantify this relationship found that leptodactylid jumpers with larger crests have larger muscles compared to walkers (Ponssa et al., 2018), thus supporting the concept that pelvic bone and muscle morphology are linked to locomotor function. However, the species analysed in this chapter do not entirely support this conclusion. The only muscle which has a significant positive relationship between crest length and muscle mass is the coccygeoiliacus, and there is a negative correlation between longissimus mass and urostylic crest length. Additionally, there are no significant differences in crest sizes between locomotor modes, which contradicts my findings from Chapter 2 (Appendix Table A.4). This could be because approximate crest length is not sufficient to infer locomotor function for the sample size of the muscle dataset. The height of the crests, and therefore the size of the attachment area, could also be more meaningful for locomotor function, i.e., even if the crest is long, a muscle may only attach to a small section of it. Additionally, some species (e.g., Ascaphus, Barbourula, Paedophryne, Sechellophryne) have lateral urostylic crests which were not analysed here but might provide scaffolding for larger pelvic muscles. Given the significant match between the results from Chapter 2 (Appendix Table A.4) and previous literature, the results from this present chapter may not provide enough evidence to accept or reject hypothesis 2 at this time.

3.4.3 Locomotor modes differ in where they invest muscle mass, but not always because of relative segment length

This chapter investigates whether the total muscle mass invested into each segment of the hindlimb differs across locomotor modes in frogs (hypothesis 3). While the shank and proximal foot do show a significant, positive relationship between total relative muscle mass and length, the thigh does not, meaning that femur length is not an appropriate proxy for muscle mass in this segment. Furthermore, if muscle mass simply increases with the relative length of the limb segment, then it would be expected that swimmers would invest the most muscle mass in the thigh, while jumpers would invest the most in the shank and proximal foot (Table 2.2). Vice versa, walkers would have the smallest relative thigh muscle mass, and burrowers would have the smallest relative shank and proximal foot muscle mass. However, the only significant difference in overall hindlimb composition is that arboreal jumpers have a larger total relative shank muscle mass than walker-hoppers (Figure 3.7). The way in which locomotor modes invest differently into the total muscle mass in each segment may simply reflect the relative importance of the functional muscle groups in each segment. Walker-hoppers have the highest relative thigh muscle mass, followed by burrowers, swimmers and jumpers (Figure 3.7). Since the present study examines relative proportions, this does not necessarily mean that walkerhoppers have stronger thighs than other locomotor modes; they may just not invest as much muscle into their other segments. In alignment with my expectations, jumpers and swimmers invest most strongly into shank musculature (Figure 3.8), driven primarily by the large size of the plantaris longus due to the strong requirements for ankle entension (Figure 3.9; Figure 3.11; Přikryl et al., 2009; Vera et al., 2022). Despite their short tarsals, burrowers invest more muscle mass into the proximal foot, presumably to achieve the large forces required for scooping dense substrates (Vidal-García et al., 2014). These findings all hold wider significance for palaeontological studies, as inferring behaviour from fossils involves using the shape and size of bones to estimate the size of muscles. There is likely another functional explanation besides muscle size for why there are significant differences in segment lengths between locomotor modes (Chapter 2). This knowledge gap has inspired the work carried out in Chapters 5 and 6, where I quantify how different hindlimb proportions impact hindlimb mechanics using computational models.

3.4.4 Variation in the mass of the largest muscles is not sufficient to predict locomotor function

The cruralis is the most well-studied thigh muscle and has been described as the functional mediator between jumping and swimming (Peplowski & Marsh, 1997; Gillis & Biewener, 2000; Nauwelaerts et al., 2007; Danos & Azizi, 2015; Astley, 2016; Marsh, 2022; Garcia-Pelagio et al., 2023). As the largest and most pinnate muscle in the thigh (Figure 3.8; Carlow & Alexander, 1973; Nauwelaerts et al., 2007, Přikryl et al., 2009), the cruralis generates considerably large forces (Gillis & Biewener, 2000; Astley, 2016). As expected, the cruralis is the strongest driver of myological variation, particularly for terrestrial jumpers and burrowers (Figure 3.9). The knee extension group (cruralis, gluteus magnus, tensor fascia latae) is much larger on average in terrestrial jumpers compared to other locomotor modes (Figure 3.10). It was expected that this functional group would be small in burrowers, since the only large difference to jumping motion is supposedly the lack of femur extension during burrowing and the asynchronous movement of the hindlimbs (Emerson, 1976), but this is not the case. Additionally, given that the primary selection pressure acting on jumping is predation (Nauwelaerts et al., 2007), while climbing/walking is primarily a method for traversing the canopy, it is surprising to find that arboreal jumpers have significantly smaller knee extensors in the thigh (Figure 3.8). An enlarged cruralis and gluteus magnus might somehow impede the function of other thigh muscles which are important for climbing/walking, but functional analyses would be needed to test this.

The adductor magnus, gracilis major and semimembranosus are the next largest thigh muscles (Figure 3.8, Gillis & Biewener, 2000; Nauwelaerts *et al.*, 2007), and are responsible for femur protraction, adduction, and retraction (Figure 3.10; Přikryl *et al.*, 2009). Femur protraction is important for obtaining the crouched position prior to jumping and reducing the recovery phase during swimming (Nauwelaerts *et al.*, 2007; Přikryl *et al.*, 2009; Astley, 2016), while efficient femur retraction is vital for power amplification during jumping, which is particularly important for small frogs (Roberts & Marsh, 2003; Astley & Roberts, 2014). Adduction has been linked to jumping performance, while abduction is more important for swimming (Nauwelaerts *et al.*, 2007). While there are some significant differences between some locomotor modes for the adductor magnus (smaller in burrowers than terrestrial jumpers and walker-hoppers) and semimembranosus (smaller in burrowers than arboreal jumpers; Figure 3.8), there are no significant differences between locomotor modes for any of the functional groups these large muscles occupy (Figure 3.10). The lack

of significant differences in these evidently important thigh muscles suggests that either all locomotor modes require all of these functions to a similar extent, or that physiological muscle properties besides just relative mass and overall length need to be considered, such as the length of tendinous attachments (Roberts & Azizi, 2011), fibre lengths, and degree of pennation (Kargo & Rome, 2002; Rabey *et al.*, 2015; Astley, 2016; see Chapter 4). For example, the femur retractors in many jumping mammals have a more proximal insertion onto the tibia (Emerson, 1985).

The plantaris longus is the most well-studied shank muscle, and the most frequently used hindlimb muscle for quantifying how contractile properties vary with locomotor performance (Roberts et al., 2003; Wilson et al., 2004; James et al., 2005; Richards & Biewener, 2007; James & Wilson, 2008; Azizi & Roberts, 2010; 2014; Roberts et al., 2011; Clemente & Richards, 2013; Richards & Clemente, 2013; Sawicki et al., 2015; Astley, 2016; Mendoza & Azizi, 2021; Marsh, 2022; Garcia-Pelagio et al., 2023). Its large mass, pinnate fibre architecture, and long tendon have all been correlated with variation in jump performance (Roberts & Marsh, 2003; James et al., 2005; Roberts et al., 2011; Azizi & Roberts, 2014; Sawicki et al., 2015; Marsh, 2022). Additionally, it is known to have long electromyographic activity bursts important for the propulsive phase of swimming and for balancing hydrodynamic forces while the foot rotates (Gillis & Biewener, 2000; Richards & Biewener, 2007; Richards & Clemente, 2013; Astley, 2016). The plantaris has even been shown to vary across two populations of the same invasive species, where frogs at the edge of the locality invest in larger, more pinnate ankle extensors as an adaptation for range expansion (Padilla et al., 2019). In the present study, swimmers have considerably larger ankle extensor muscles than arboreal jumpers, burrowers and walker-hoppers (Figure 3.11), driven primarily by the size of the plantaris longus (Figure 3.9; Figure 3.12). Swimmers also show the smallest amount of variation in shank anatomy (Figure 3.9; Figure 3.11), implying that there are strong selective pressures on shank muscle composition. This aligns with previous work by Richards (2010), who found that swimmers rely more on rotational thrust powered by the ankle than translational thrust powered by the thigh musculature.

Despite the importance of the plantaris longus in determining jump performance in tree frogs (Roberts *et al.*, 2011; Mendoza & Azizi, 2021), arboreal jumpers surprisingly have significantly smaller ankle extensors than burrowers and swimmers (Figure 3.12). However, this does not necessarily mean that arboreal taxa

are bad at jumping. This group has invested muscle mass into a significantly larger knee extension group in the shank instead, driven primarily by the peroneus (Figure 3.12). This could be to account for their significantly smaller thigh-based knee extensors. Arboreal jumpers also invest the most muscle into overall shank mass (Figure 3.7), and their plantaris longus, peroneus, tibialis posticus, and tibialis anticus longus are all longer on average relative to tibiofibula length compared to the other locomotor modes (Appendix Figure D.2). These differences in the distribution of muscle mass throughout the hindlimb between terrestrial and arboreal jumpers may be because arboreal taxa must compensate for a displaced centre of gravity (de Oliveira- Lagôa *et al.*, 2019) and may need to be able to climb as well as jump (Simons, 2008). To conclude, the properties of one large muscle are not sufficient to accurately predict locomotor function, and each locomotor mode may achieve similar functions by changing different muscle parameters, indicating many-to-one mapping of form to function.

3.4.5 Small muscles may have an underappreciated role in locomotor function

There is very little information in the literature about the significance of the smaller muscles in the thigh and shank, particularly those near the hip, due to the difficulty associated with extracting them intact using traditional dissection methods. This chapter presents the first evidence that small hindlimb muscles can differ significantly between locomotor modes. This likely represents the different strategies employed by each locomotor mode in how they modulate the function of the large muscles. For example, the muscle which stabilises the femur, the pectineus, is significantly larger in terrestrial jumpers compared to both walkerhoppers and arboreal jumpers (Figure 3.10). A larger pectineus may be important in terrestrial jumping to influence the position of the femur with relatively little force, and hence alter the moment arm, and therefore function, of the thigh knee extensors with greater efficiency (Figure 3.10). Meanwhile, the muscle responsible for ankle dorsiflexion, the tibialis anticus brevis, is considerably larger in arboreal jumpers compared to terrestrial jumpers and swimmers (Figure 3.12). These instances also provide another example of the impact of differences in habitat requirements on hindlimb myology.

The obturator internus, the muscle responsible for long-axis rotation of the femur, is significantly smaller in burrowers than the other locomotor modes, supporting hypothesis 4 and suggesting that there is a less important function for this muscle in burrowing. This, and the significant differences across the principal components of the thigh (Figure 3.9), contrasts with Emerson's (1976) hypothesis that thigh modifications for jumping are suitable exaptations for burrowing. The structure of small shank muscles in burrowers are also unique. The extensor cruris brevis, which is part of the knee extension group, inserts more distally onto the tibiofibula in burrowers compared to jumpers (Appendix Figure D.2). This is said to increase the amount of force generated at the distal end of the shank during knee extension and lateral rotation (Emerson, 1976). Similarly, the tibialis anticus longus always has two very distinct heads in burrowers (Supplementary Dataset 5), which has been suggested to increase the force of ankle extension without involving movement of the hip, unlike the other muscles in this functional group (Emerson, 1976). The importance of these two muscles is supported by their considerably larger size in burrowers (Figure 3.11) and the tighter clustering of burrowers in shank morphospace (Figure 3.9) compared to the other locomotor modes. This important variation in shank composition cannot be observed when the tibialis anticus longus is grouped with the other ankle extensors (Figure 3.12). This supports my prior conclusion that one muscle alone should not be used to represent the functionality of a limb, as a functional group may not have a completely synergistic influence on locomotor function. Functional analyses will be needed to directly determine how much the variation in these small muscles can influence behaviour.

3.4.6 Burrowing style does not noticeably impact pelvis and hindlimb anatomy

Interestingly, forward burrowers (*Hemisus guineensis, Rhinophrynus dorsalis*) are not clustered separately from the backward (*Breviceps poweri, Neobatrachus pictus*), and non-descript (*Bufo bufo, Phrynomantis annectans*) burrowers for both the pelvis (Figure 3.6) and hindlimb muscles (Figure 3.9). Since backwards burrowing is the basal condition (Nomura *et al.,* 2009) and prevalent in ~95% of burrowing frogs (Emerson, 1976), these results suggest that changes in the forelimbs and pectoral girdle may be all that differentiates forward burrowers from their ancestral condition (Engelkes *et al.,* 2020; Keeffe & Blackburn 2020, 2022).

Unfortunately, there is no information on the exact function of pelvis muscles during burrowing in the literature, making this an area worth studying in more detail.

3.4.7 The driver of variation in muscle anatomy depends on the hindlimb segment

Muscle number may change in line with evolution (hypothesis 5.1), locomotor requirements (hypothesis 5.2), or a combination of the two (hypothesis 5.3). The results of the present study indicate that these relationships differ between each part of the anuran anatomy. The pelvis and the thigh, which have the most variation in muscle number, both have a higher degree of muscle separation in more derived taxa (Figure 3.14; Table 3.2), supporting hypothesis 5.1. Though lacking significance, there is a moderate phylogenetic signal for both pelvic pPCA axes, as well as the first thigh pPCA axis, suggesting that evolutionary history impacts muscle size as well as separation in these parts. Shank muscle number and muscle size have no phylogenetic signal, instead showing significant differences between locomotor modes, supporting hypothesis 5.2 (Table 3.3). Specifically, walkers and swimmers are more likely to have an unseparated tibialis anticus longus (Figure 3.14), which functions as an ankle extensor. Although the number of muscle heads in the proximal foot was not evaluated, phylogenetic signal for muscle size is also zero and there is evidence of differences between locomotor modes in terms of muscle composition (Figure 3.9). Therefore, these results support hypothesis 5.2, as well as the findings of a previous study, which suggests that the muscle architecture of more distal limbs segments is labile across evolution and is more closely correlated to locomotor performance (Astley, 2016). The proximal-distal sequence of increasing variation in muscle composition across segments found in the present study further supports this hypothesis (Figure 3.9).

3.4.8 Increases in muscle separation could afford greater range of motion and motor control

Muscle separation is thought to contribute towards more precise motor control and to create a larger area of functionality within which the limb can perform as it allows for separate nerve innervation and an increase in the range of external moment arms (Gans & Bock, 1965; Collings & Richards, 2019). This raises the question of why a species would undergo subsequent muscle fusion - are there any trade-offs associated with muscle separation? For example, both *Telmatobius thompsoni*

(swimmer) and *Paedophryne verrucosa* (walker-hopper) show fusion of the tibialis anticus longus, despite the ancestral condition having two separate heads (Figure 3.14). Does muscle fusion permit larger forces to be generated during ankle extension? Can two heads be activated at once to produce the same or more force than if they were fused? Or does asynchronous activation of different heads mean the muscle experiences less fatigue when contracting over long periods of time? Additionally, there are some instances where entire muscles are lost, such as the tensor fascia latae in burrower *Breviceps poweri* and arboreal jumper *Hyperolius ocellatus*, two distantly related species (Supplementary Dataset 5). As muscle is an energetically expensive tissue (Perry & Prufrock, 2018), this loss of 'residual complexity' could be to reduce energetic costs and could be an example of selection for more efficient and effective function (McShea & Hordijk, 2013). It would be interesting to explore why other species with specialist locomotor functions have not always followed suit.

3.4.9 Limitations

lodine cannot stain tendons, so tendinous structures cannot be visualised or measured using diceCT, thus limiting the functional inferences that can be made from soft tissue. Tendinous attachments impact elastic energy storage, metabolic energy conservation, muscle power amplification and mechanical feedback mechanisms (Roberts & Azizi, 2011). Therefore, tendons are expected to show significant differences between locomotor modes. Abdala et al. (2018), for example, used electron microscopy to show that jumpers have collagen fibrils with a greater cross-sectional area than walker-hoppers, which could reflect the role of tendons to absorb forces during landing in frogs. Tendons also permit the locomotor system to function beyond the physiological limits of isotonic muscle contraction, which is essential for the spring-actuated jumping mechanism in small frogs (Roberts et al., 2011; Sutton et al., 2019; Mendoza & Azizi, 2021). Additionally, tendons can be very long, making the origin and insertion points of muscles hard to determine without supplementary traditional dissection (e.g., the iliofibularis; Appendix Figure C.1). Finally, tendinous inscriptions, such as those in the gracilis major and semimembranosus, are important to examine as they permit separate nerve innervations to different parts of the muscle, and therefore the fine-tuning of motion (Collings & Richards, 2019).

Some key inferences about the relationship between form and function could not be explored because relative muscle sizes had to be used to account for variation in the extent of muscle shrinkage, as the specimens in this dataset differ in how they were preserved and stained. Total hindlimb mass, for instance, is an important explanatory variable for differences in maximum jump distance (James et al., 2005) as it determines how much force is needed for linear acceleration (Nauwelaerts et al., 2007). It is therefore strongly associated with locomotor mode – swimmers have the largest muscles, followed by jumpers, then walkers (Moen, 2019; Vera et al., 2022). Arboreal species have considerably longer (Appendix Figure D.1; Appendix Figure D.2; Appendix Figure D.3) and slimmer muscles, which is likely to have functional consequences on jump performance (Moen, 2019). Since total hindlimb length and muscle mass are both strongly correlated with locomotor mode, dividing the variables examined in this chapter by these parameters for normalisation, instead of SVL and total body mass, might be diluting the trends I have observed. Additionally, the mass of an individual muscle might be correlated to the mass of synergistic muscles within the same functional group, or even across hindlimb segments. The assumption that there is a positive correlation between absolute bone and muscle size must be tested before attempting to make functional interpretations from the fossil record (Bates et al., 2021).

3.4.10 Future directions

Digitising museum specimens has been increasing in popularity over the last decade, resulting in large collections of 3D data in repositories such as MorphoSource and iDigBio. However, this chapter has highlighted the need for a change in the way specimen and µCT data are currently recorded. Standard body size measurements at the time of capture (e.g., SVL length, body weight) and information on the time between capture and fixation, fixation duration, ethanol storage duration, staining concentration, and staining duration are not available for most taxa. Consequently, the present study was limited to making interpretations from relative measurements, as variation in the level of soft tissue shrinkage could not be reliably controlled for. While the inclusion of rare, endangered, and/or recently extinct species necessitates the use of preserved museum specimens (Leonard *et al.*, 2021), future studies should aim to digitise specimens that have been captured within a year of the original fixation to limit the amount of shrinkage caused by alcohol storage (Gignac *et al.*, 2016). Additionally, all scans uploaded to digital Page 106 of 286

repositories should be supplemented with metadata containing all preservation, staining, and scanning parameters, as well as specimen measurements which enable body size corrections.

Future studies should include traditional dissection or different staining techniques to enable the visualisation of tendons, especially those between distinct heads of same muscle and the tendinous inscriptions described for semimembranosus and gracilis major (Přikryl et al., 2009). Then, innervation experiments should be performed to determine whether these distinct areas of a muscle involve separate nerve stimulation. Dynamics simulations (e.g., Kargo & Rome, 2002) could then be built to directly test the impact of this anatomical variation on locomotor performance – does the separation of muscles into distinct heads increase range of motion, thereby enabling specialised functions? If the second muscle head is removed from the dynamics model, will the frog no longer be able to perform certain tasks? Does the muscle have to be entirely separate, or is partial separation sufficient to perform certain functions? If muscle separation increases the ability to perform multiple tasks, the number of muscle heads relative to other species could be a potential indicator of locomotor specialisation. This investigation would enable us to determine the functional significance of separate areas of muscle, thus directly addressing the question of whether anatomical complexity is a prerequisite for functional complexity.

There is currently very little information on how muscle activation varies in muscles besides the largest ones in the thigh and shank, especially for locomotor modes besides jumping and swimming (Reynaga *et al.*, 2019). Here, I describe new evidence of which muscles could be the functional mediators between arboreal and terrestrial habitats. It would be particularly interesting to determine how the function of previously untested muscles (i.e., the coccygeoiliacus, iliacus externus, and pectineus) changes in response to different locomotor functions within the same species/individual, or in response to differences in substrate compliance. Computational models may be the way forward (e.g., Astley *et al.*, 2015), since many muscles are too small for more invasive techniques such as electromyography. For instance, femur stabilisers and long-axis rotators show significant differences between locomotor modes, but their actions can be difficult to quantify. Burrowing is another understudied locomotor mode, where the pelvis and hindlimb myology has received little attention besides the present study since Page 107 of 286

1976 (Emerson). How muscle activation differs in forward- and backward-burrowers and how burrower morphology differs from walkers are lines of enquiry which would also benefit from functional analyses.

3.4.11 Conclusion

This chapter contributes to the building body of evidence that there is no unique combination of musculoskeletal characteristics for each locomotor mode (Přikryl *et al.*, 2009; Fabrezi *et al.*, 2014; Marsh, 2022; Vera *et al.*, 2022). The results indicate that most myological features serve multiple functions, reflecting the complex mechanics of anuran hindlimbs. Musculoskeletal anatomy often varied in response to factors besides locomotor requirements and phylogenetic history, such as habitat type. Furthermore, the size and topology of muscles within each segment of the hindlimb is likely shaped by different selection pressures - the shank appears to be influenced more strongly by locomotor mode compared to the pelvis and thigh. This labile relationship between anatomy and function could provide the means for species to be able to perform multiple locomotor modes, albeit sub-optimally (Moen, 2019). In an everchanging world, natural selection may favour the resultant intermediate phenotype for its ability to adapt to different locomotor requirements and environmental conditions (Nauwelaerts *et al.*, 2007).

4 Fibre architecture of the anuran hindlimb muscles in relation to locomotion

Jessica Arbour (Middle Tennessee State University) assisted with the automated fibre tracking R package, 'GoodFibes'. Dr Laura Porro and Dr Chris Richards provided comments on draft versions of this chapter.

4.1 Introduction

In Chapter 2, I found that hindlimb skeletal proportions differed significantly between frogs which specialised in different locomotor modes. Since changes in muscle size and shape as a response to habitual mechanical loading is the primary mechanism driving bone growth (Zumwalt, 2006), this trend was also expected across the majority of hindlimb muscles. Functional studies which use electromyography to analyse muscle dynamics have found that the masses of several key hindlimb muscles are important predictors of force output, and therefore locomotor performance in frogs (Calow & Alexander, 1973; Emerson, 1978; Choi & Park, 1996; Gillis & Biewener, 2000; James et al., 2007; Nauwelaerts et al., 2007; Astley, 2016). However, there were several instances highlighted in Chapter 3 where muscle mass and length did not differ significantly between locomotor modes, implying that there is more influencing the relationship between locomotor mode and pelvic/hindlimb musculature than gross muscle size. When examined in isolation, muscle mass has been shown to be an inappropriate proxy for muscle force (Rabey et al., 2015), which instead depends largely on the cross-sectional area (CSA) of the muscle (Biewener, 1989; Nauwelaerts et al., 2007). To measure CSA accurately, it is important to consider fibre architecture. Muscle fibres can be arranged in complex ways, differing in how they are angled relative to the force-producing axis (i.e., degree of pennation) and rarely stretching along the entire length of the muscle from origin to insertion, even within parallel-fibred muscles (Lieber & Fridén, 2000; Rabey et al., 2015; Perry & Prufrock, 2018). Physiological cross-sectional area (PCSA) is likely more representative of muscle function, as it incorporates pennation angle and fibre length into estimates of a muscle's force-producing capacity (Sacks & Roy, 1982; Powell et al., 1984).

For a given volume, muscles with parallel fibres have higher maximum excursions, creating larger functional ranges of motion, and can produce faster contractile

velocities (Lieber & Fridén, 2000). Muscles of the same volume with a higher pennation angle tend to have shorter, more tightly packed fibres which enables them to produce higher forces (Gans, 1982; Sacks & Roy, 1982; Powell et al., 1984). Muscles cannot be optimised for both contractile velocity and maximum force generation without incurring detrimental functional trade-offs (Rabey et al., 2015). Specifically, if a frog has muscles built for high fatigue resistance (i.e., short fibres with low/no pennation), then it will not be able to produce powerful movements (Wilson et al., 2004). Equally, a frog with muscles designed for high power output will suffer more quickly from fatigue. This will have consequences for the ability to perform endurance tasks (e.g., walking, hopping) compared to explosive movements (e.g., jumping, swimming), respectively (James et al., 2007). Muscle architecture is therefore likely under strong selection as it has important implications for ecologically relevant performance traits. However, with the exception of Astley (2016) who analysed two muscles across 14 species, differences in muscle fibre architecture in frogs have usually only been examined within one muscle across a small number of species (Mendoza & Azizi, 2021), or between many muscles within the same species (Calow & Alexander, 1973; Lieber & Brown, 1992; Kargo & Rome, 2002). Additionally, all of these studies only measured a small number of fibres (<25), which can have significant consequences for estimates of muscle function (Charles et al., 2022).

Much of the reason behind this scarcity of frog muscle architecture studies is because individual muscle fibres are notoriously difficult to isolate intact using physical dissection, especially in particularly small animals and/or muscles (Lieber & Fridén, 2000). In the last decade, significant progress has been made in attaining sufficient contrast-enhanced μCT scan resolution to examine minute internal structures, including muscle fibre arrangement (Gignac & Kley, 2014; Nyakatura *et al.*, 2019; Dickinson *et al.*, 2020). Furthermore, methods for automated fibre recognition and tracking have been recently developed in ImageXd (Kupczik *et al.*, 2015; Dickinson *et al.*, 2018; Nyakatura *et al.*, 2019), Amira/Avizo (Sullivan *et al.*, 2019; Peeters *et al.*, 2020; Holliday *et al.*, 2022) and Python (Püffel *et al.*, 2021; see Katzke *et al.*, 2022 for a review). These techniques have never been applied to frogs, presenting a unique opportunity to study the complex relationship between anatomy and function using a high number of fibres, muscles and species.

Given these knowledge gaps and recent advancements in fibre tracking technology, the overarching aim of this chapter is to determine the link between hindlimb muscle fibre architecture and locomotor mode, specifically for frogs that specialise in jumping, swimming, or walking/hopping. Figure 4.1 describes how muscle function can be inferred from fibre architecture, and explains the hypotheses addressed in this chapter. This type of plot separates out muscles (and, in this case, species with different locomotor modes) that are likely specialised for different functions producing high forces (large PCSA and short fibres), high power (large PCSA and long fibres), or high contractile velocities (small PCSA and long fibres) (Böhmer et al., 2018; Martin et al., 2020). The final category, 'generalists', describes muscles with no specialisation for these functions (small PCSA and short fibres; Figure 4.1). For instance, since frogs that primarily walk/hop have smaller, less muscular legs than frogs which specialise in jumping and swimming (Chapter, 3; Astley, 2016), walker-hoppers are expected to occupy this generalist section of a functional space plot (Figure 4.1). Additionally, where each species places on the functional plot may depend on the muscle being examined. For example, the size and structure of the plantaris longus, a pennate ankle extensor, is positively associated with both swimming and jumping performance via its role in power amplification (Gillis & Biewener, 2000; James et al., 2007; Astley, 2016), while the semimembranosus, a parallel-fibred femur retractor, has faster contractile properties in jumpers than in swimmers (Figure 4.1; Astley, 2016). Therefore, the hypotheses addressed in this chapter are:

- H1) The trade-off between PCSA (muscle force) and fibre length (muscle contractile speed, range of movement) for each muscle will differ between locomotor modes.
- H2) Differences in fibre architecture between locomotor modes will depend on the muscle being examined.
- H3.1) Pennation angle is larger and fibre lengths are shorter in smaller muscles.
- H3.2) Pennation angle is larger and fibre lengths are shorter in larger muscles.

The final set of hypotheses address the aforementioned result of Chapter 3, where I did not find as many significant correlations between locomotor modes and muscle size as I expected. If hypothesis 3.1 is supported by the results of the present chapter, this would suggest that muscles can be specialised towards force

production without the high metabolic costs associated with growing and maintaining large muscle size. If hypothesis 3.2 is supported, then pennate muscles may be built with the purpose of maximising potential force output. Similarly, if the fibres are longer in larger parallel-fibred muscles, they would be adapted to maximise range of motion and contractile speed.

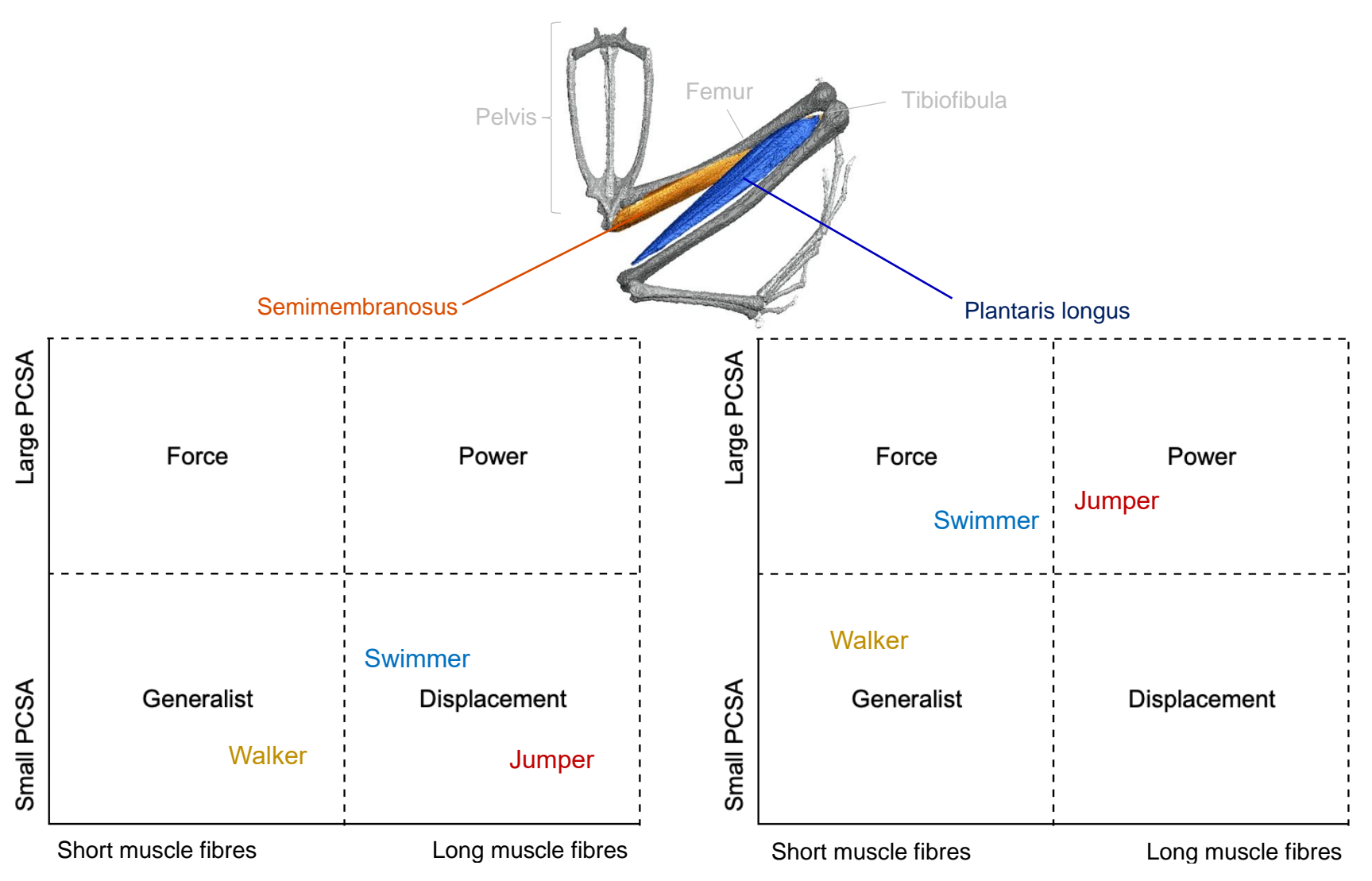


Figure 4.1 - Functional space plots hypothesising how the trade-off between fibre length and physiological cross-sectional area (PCSA) can differ between both locomotor modes (hypothesis 1) and muscles specialising in different functions (hypothesis 2), using a parallel-fibred femur retractor (semimembranosus) and pennate ankle extensor (plantaris longus) as an example (dorsal view). The anatomical model is of *Leptodactylus poecilochilus* (voucher number: CAMZN R.16735.A) and was created in Amira (Version 2020.2).

4.2 Methods

4.2.1 Data selection

A review of the literature indicated which hindlimb muscles were the most important determinants of locomotor performance, resulting in a priority list of muscles to test (Calow & Alexander, 1973; Lieber & Brown, 1992; Gillis & Biewener, 2000; Kargo & Rome, 2002; Nauwelaerts *et al.*, 2007; Azizi & Roberts, 2014; Enriquez-Urzelai *et al.*, 2015; Astley, 2016; Mendoza & Azizi, 2021). Four muscles from a range of functional groups most consistently showed high fibre resolution in the μCT scans from Chapter 3 – the cruralis (pennate knee extensor), gluteus magnus (parallel-fibred knee extensor), semimembranosus (parallel-fibred femur retractor) and plantaris longus (pennate ankle extensor). Out of the 30 scans digitally dissected in Chapter 3, ten have a suitable resolution for visualising individual fibres - two walker-hoppers, three swimmers and five terrestrial jumpers. An effort was made to scan more arboreal jumpers and burrowers at the University of Florida, but none with sufficient scan resolution for fibre tracking were obtained.

4.2.2 Exporting and preparing muscle image stacks

To prepare an image stack of each muscle for analysis, muscles were first aligned with the global Z axis so that a cross-section through the fibres could be visualised. In VGStudio Max, the muscle of interest can be exported directly as an image stack, while scans segmented in Amira required use of the arithmetic module to first isolate the muscle from the rest of the scan using the formula A * (B > 0) (where A is the original image stack and B is the label field of the muscle of interest). Image stacks were then imported into ImageJ. To prevent the tracking algorithm passing between neighbouring fibres, the number of grayscale values were minimised by using the 'unsharp mask' filter (Figure 4.2). This sharpening operator enhances the edges in an image by subtracting a smoothed version of the image from the original image, and ultimately increases the contrast between the muscle fibres and interstitial spaces (Jaimi Gray, pers. comms). The mask weight (i.e., the strength of the filtering) was set to 0.9.

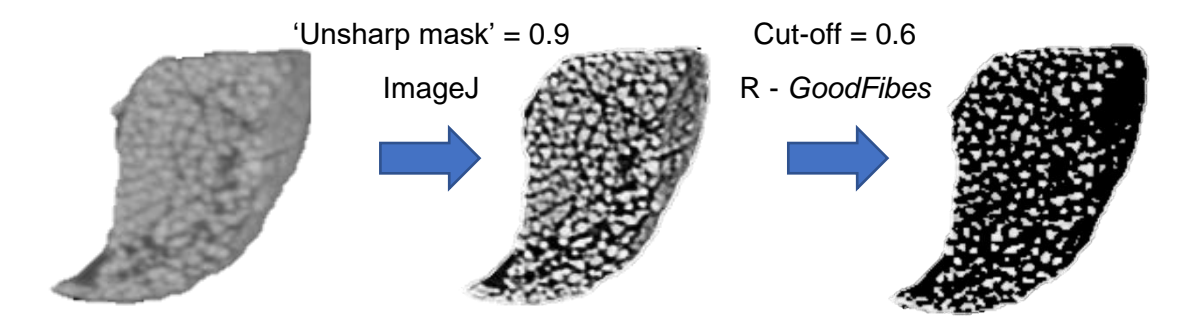


Figure 4.2 - The process of muscle image stack preparation, using the gluteus magnus muscle from *Eupsophus roseus* (voucher number YPM:HERR:005002) as an example. The first step involves the use of a filter to increase contrast in ImageJ, while the second step defines the grayscale values below which voxels will be considered black by the fibre tracking algorithm utilised by the 'good.fibes' function in R.

4.2.3 Automated fibre tracking

Fibre extractions and measurements were carried out in R (Version 4.3.1) using the GoodFibes package (Arbour, 2023). First, histogram equalization ('equalise.stack' function) was used to remove all intermediate grayscale values, as the automated fibre tracking algorithm works by not passing through black spaces. The appropriate grayscale cut-off was determined on a case-by-case basis for each specimen, where fibres needed to appear isolated from each other as much as possible without disappearing too early (Figure 4.2). Fibres were tracked using the 'good.fibes' function - fifty starting points known as 'seeds' were used, with each set of seeds starting from five equally distanced scan slices across the muscle length. The algorithm then traces fibres backwards and forwards from each seed until the fibre disappears (i.e., 95% of the surrounding voxels are black). A 'bound buffer' of three was used to prevent fibres from running along the edge of the muscle where the iodine is often more concentrated (Arbour, 2023). The 'quality.check' function was then used to remove any low-quality fibres (i.e., fibres with high grayscale variation compared to fibre length, and fibres below one-tenth of the muscle belly length, as this was never reported in traditional dissections; Astley, 2016). Mean fibre length was then calculated from the output of the 'fibre lengths' function. The number of high-quality fibres extracted from each muscle ranged from 40 to 168 (Supplementary Dataset 6), which meets the sample size requirement for statistical The evolution of musculoskeletal anatomy and locomotor mode in frogs analysis of mean fibre length (i.e., >25 fibres; Charles *et al.*, 2022). 3D mesh files of the fibres were exported for the creation of Figure 4.3.

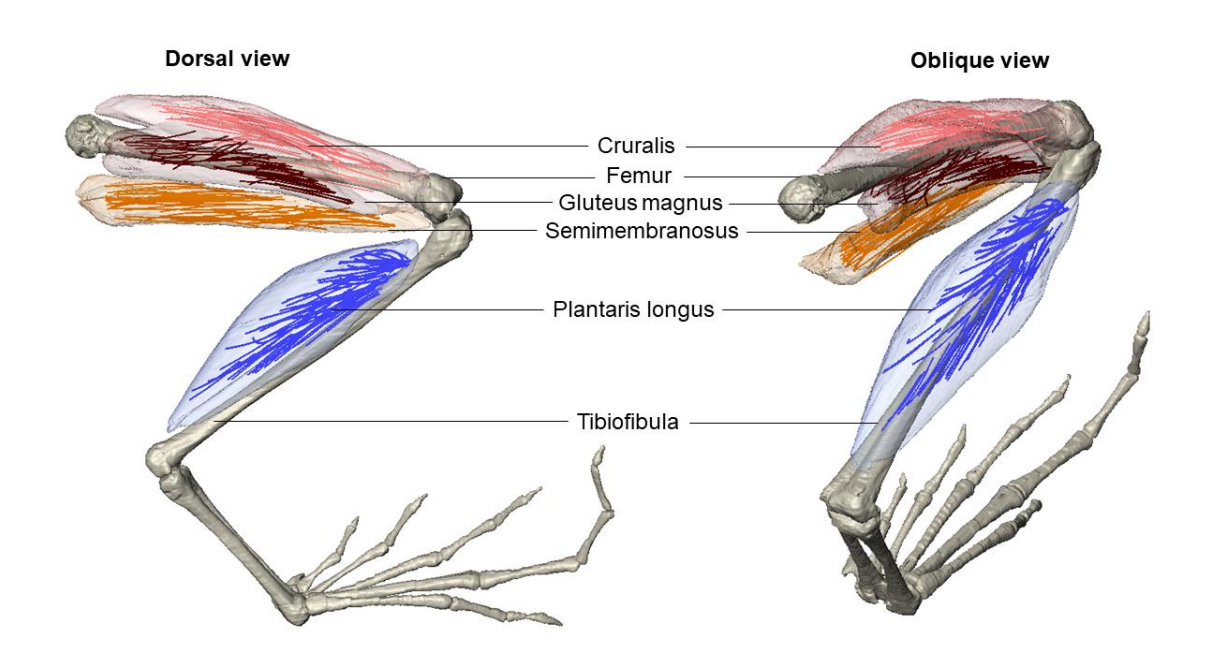


Figure 4.3 - 3D visualisation of *Arthroleptis tanneri* (voucher number CAS:HERP:168823) fibres from the four muscles used for analysis, extracted in R (*GoodFibes* package) and visualised in Amira (Version 2020.2).

4.2.4 Pennation angle

As pennation angle cannot yet be reliably extracted using the *GoodFibes* package (Arbour, 2023), pennation angle of the traced fibres was measured manually within Amira/VGStudio Max. First, the 2D scan plane was aligned with the force-generating axis (i.e., along the length of the muscle belly) and positioned in the centre of the muscle (Figure 4.4). Five measurements of the fibre angle relative to the tendon were taken and averaged to improve accuracy. In line with previous studies, pennation angle was assumed to be constant in all positions and across different layers of muscle (i.e., deep vs. superficial; Kargo & Rome, 2002; see section 4.4.7).

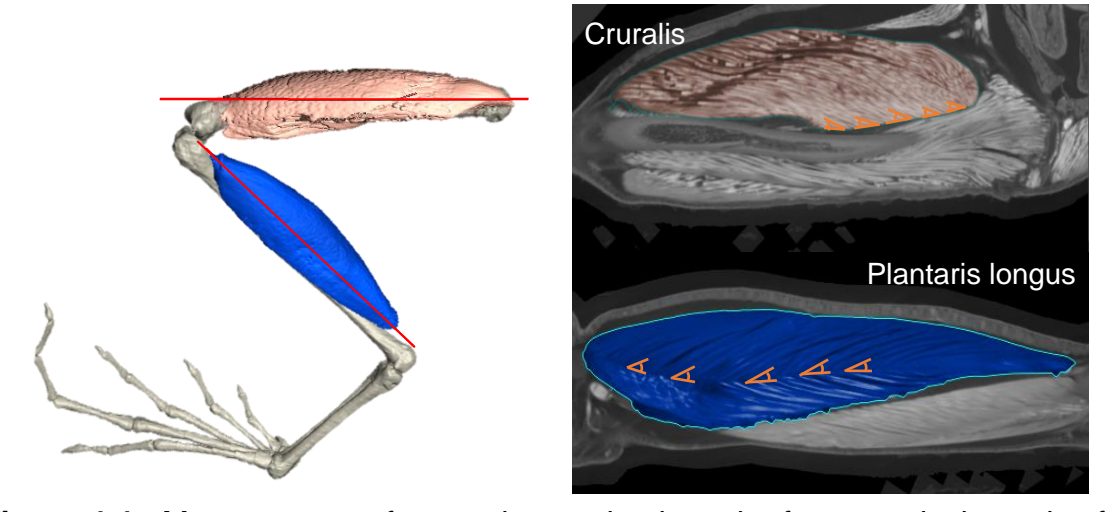


Figure 4.4 - Measurement of pennation angle along the force-producing axis of the cruralis and plantaris longus, using *Arthroleptis tanneri* (voucher number CAS:HERP:168823) in VGStudio Max (Version 3.4) as an example. The red lines on the 3D model (left) represents where the views in the 2D plane are from (right).

4.2.5 Statistical analyses

Muscle belly volume (MBV) divided by fibre length (FL) calculates the physiological cross-sectional area (PCSA) as a measure of a parallel-fibred muscle's force-producing capacity. For a pennate muscle, PCSA is calculated through incorporation of the cosine of the average pennation angle (φ; Sacks & Roy, 1982):

$$PCSA = \frac{MBV \cdot cos\phi}{FL}$$

(Equation 4.1)

PCSA was corrected for body size by log-transformation followed by regression against log-transformed total hindlimb muscle mass from thigh to proximal foot, which was obtained in Chapter 3 (total body mass was only available for four frogs). The resulting residuals were used for subsequent statistical tests, all of which were performed in R (Version 4.3.1). Relative fibre length (i.e., the ratio of mean fibre length to muscle belly length; FL:MBL) is a dimensionless architectural variable and thus does not require any further size corrections prior to analysis (Allen *et al.*, 2010).

Small sample size meant that phylogenetic signal could not be accurately estimated (Münkemüller *et al.*, 2012; Astley, 2016), so supplementary phylogenetic versions of all analyses were carried out using a Brownian motion model of evolution (see

The evolution of musculoskeletal anatomy and locomotor mode in frogs

Appendix E:). To address hypotheses 1 and 2, ANOVA were used to compare the relative fibre lengths and size-corrected PCSAs across locomotor modes and muscles, since these variables were normally distributed (Appendix Table E.1). The grayscale cut-offs used in the fibre tracking algorithm were incorporated as a potential explanatory factor into the comparative models addressing these hypotheses to ensure that any lower cut-offs required for the algorithm to run did not result in bias leading to abnormally longer fibres in some muscles/species. As sample size is small, the corrected Akaike Information Criterion (AICc) was used to determine which models best fit their data.

To address hypothesis 3, Pearson's correlation tests were performed to determine if there is a relationship between the muscle mass relative to total hindlimb mass and its relative fibre length and, for the pennate muscles, pennation angle. Two additional ANOVAs were run to evaluate which of these variables have the greatest impact on PCSA across locomotor modes (i.e., whether muscle size, fibre length, or pennation angle is the best indicator of functional specialisation). The first test accounts for the potential bias induced into analyses of PCSA, in that both pennate muscles are frequently much larger than the parallel-fibred muscles, by using a version of PCSA where muscle volumes were all made equal to 1mm³. The second test involves removing pennation angle from the PCSA calculation for the pennate muscles (i.e., the anatomical cross-sectional area of the muscle; ACSA) to determine the importance of including pennation angle in the model (as this matter is under debate; Lieber, 2022).

4.3 Results

4.3.1 Comparisons of relative fibre length

All of the raw data from the present chapter can be found in Supplementary Dataset 6. Generally, relative fibre length increases significantly with the relative length of the muscle (Pearson's correlation = 0.40, p = 0.011). However, there are no significant relationships between relative fibre length and relative muscle length when the data are divided into the different locomotor modes, but the general trends are still positive, especially for jumpers (Figure 4.5). In addition, swimmers show a considerably smaller range of relative fibre lengths across muscles compared to jumpers (Figure 4.5). When grouped by the specific muscles, relative fibre length increases significantly with the relative length of the gluteus magnus (Pearson's

The evolution of musculoskeletal anatomy and locomotor mode in frogs

correlation = 0.71, p = 0.022). While there is also a general, non-significant increase for the semimembranosus and cruralis, the relative fibre length of the plantaris longus does not increase with relative muscle length (Figure 4.5).

The best model of relative fibre length uses only locomotor mode as the explanatory factor (AICc₍₄₎ = -65.93; muscle only AICc₍₅₎ = -61.55), though there are no significant differences between locomotor modes (ANOVA: $F_{(2)}$ = 1.85, p = 0.17). Adding the grayscale cut-off does not improve the fit of the model (AICc₍₁₄₎ = -38.41), thus assuring there is no bias in fibre extraction affecting the results. The model which includes the interaction between muscle type and locomotor mode also has a weaker fit to the data (AICc₍₁₃₎ = -38.53), indicating that the relationship between fibre length and locomotor mode does not depend on the muscle being examined, and vice versa. The best model for the phylogenetic ANOVA also includes locomotor mode only, and it too shows no significant differences between locomotor modes (Appendix Table E.2).

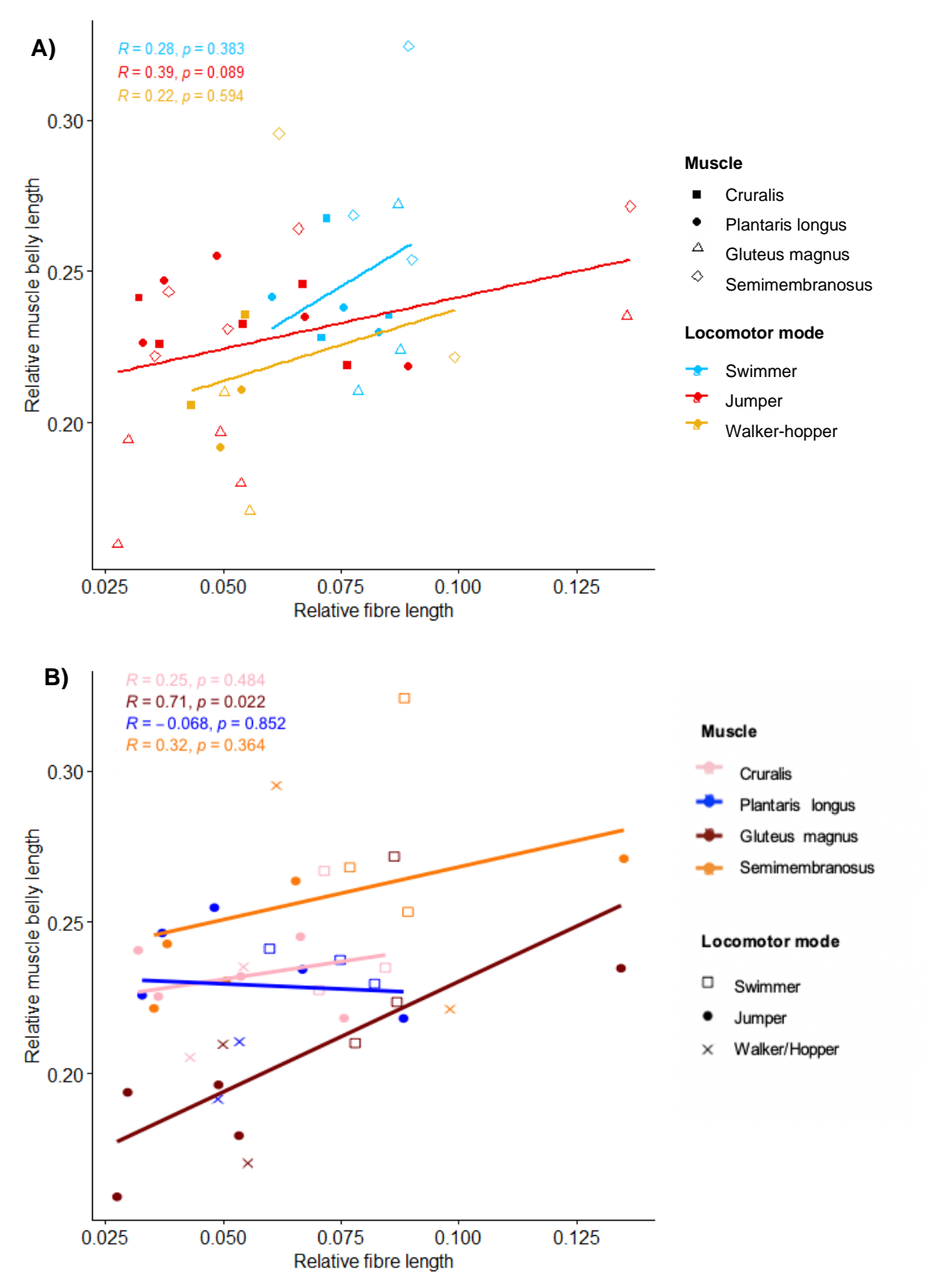


Figure 4.5 - The relationship between relative fibre length and muscle belly length relative to total hindlimb length. There are four points per species; one for each muscle. The data are the same across the two plots, with points colour coded according to either A) locomotor mode or B) muscle type. In A), filled shapes

represent pennate muscles and empty shapes represent parallel-fibred muscles. The statistics reported refer to Pearson's correlation tests.

4.3.2 Comparisons of PCSA

Size-corrected PCSA is significantly higher when relative fibre length is shorter (Figure 4.6), indicating a trade-off between muscle force and contractile speed that is consistent with the findings of previous studies (Lieber & Fridén, 2000; Wilson *et al.*, 2004; Rabey *et al.*, 2015). The best model of this relationship includes both locomotor mode (ANOVA: $F_{(2)} = 4.17$, p = 0.02) and the specific hindlimb muscle (ANOVA: $F_{(3)} = 17.25$, p < 0.001) as explanatory variables (AICc₍₇₎ = 89.95), but not the interaction between them (AICc₍₁₃₎ = 110.81), nor grayscale cut-off (AICc₍₁₄₎ = 115.53; Appendix Table E.3). The parallel-fibred muscles have a significantly smaller PCSA than both the pennate muscles, while there are no significant differences within each muscle type (Table 4.1; Figure 4.6). In addition, terrestrial jumpers have muscles with significantly larger PCSAs than swimmers, but not walkers (Table 4.1; Figure 4.6). When species relatedness is taken into account using a phylogenetic ANOVA, both terrestrial jumpers and walkers have significantly higher PCSA values for the cruralis specifically (Appendix Table E.4).

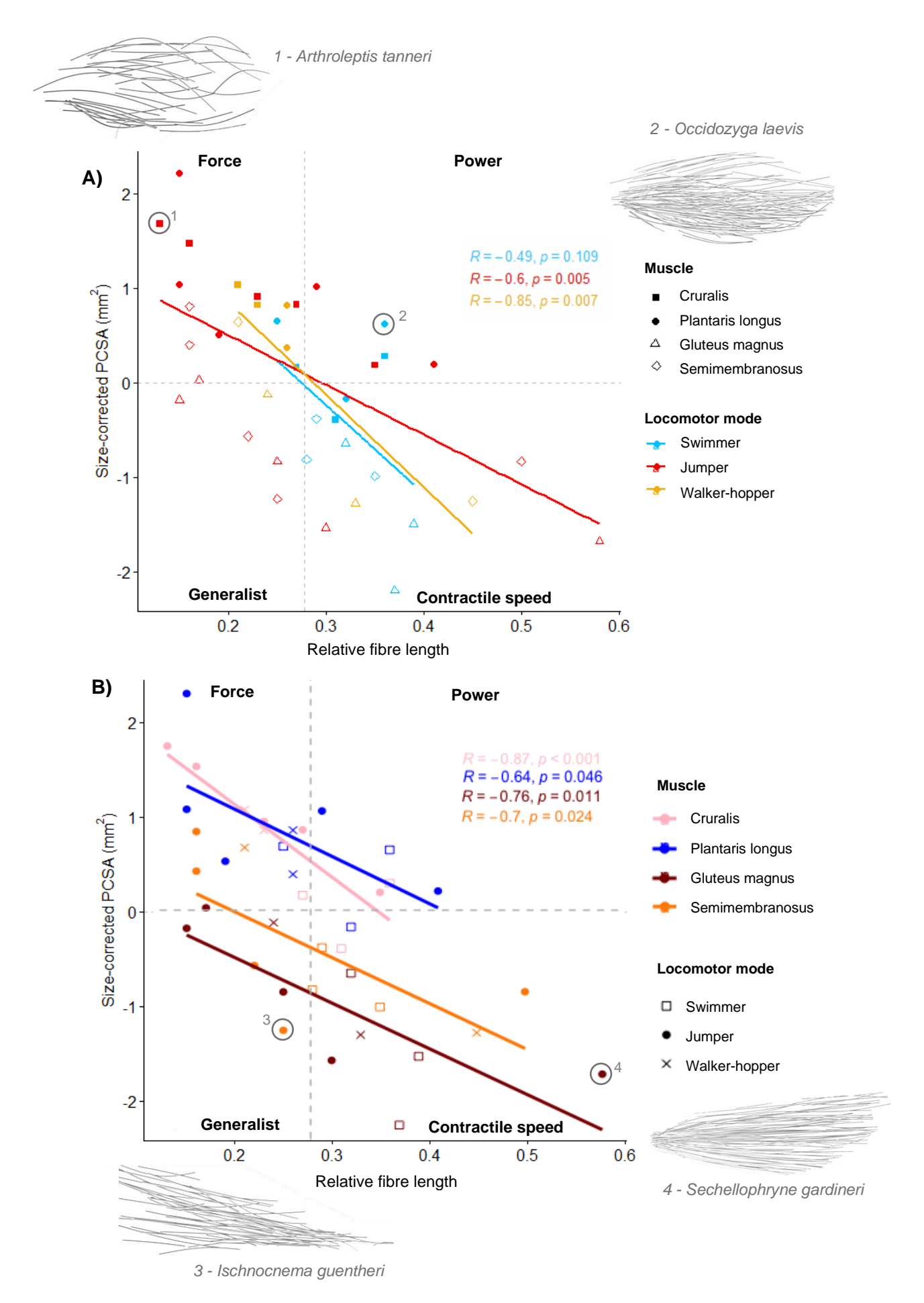


Figure 4.6 - The relationship between size-corrected physiological cross-sectional area (PCSA) and relative fibre length. There are four points per species; one for each muscle. The data are the same across the two plots, with points colour-coded according to either A) locomotor mode or B) muscle type. In A), filled shapes represent pennate muscles, and empty shapes represent parallel-fibred muscles. The PCSA for the parallel-fibred muscles simply represents the anatomical cross-sectional area (i.e., pennation angle = 0). The grey dashed lines represent the means across each axis, which divide the plot into the four areas of functional space. Each area has an encircled example depicted by the corresponding fibre silhouette. The statistics reported refer to Pearson's correlation tests.

Table 4.1 - Pairwise Tukey results from the best ANOVA model for size-corrected physiological cross-sectional area. Results meeting the p < 0.05 significance threshold have been highlighted in bold.

Pair	Difference in means	Adjusted p- value			
Muscle type					
Cruralis – Gluteus magnus	1.691	< 0.001			
Cruralis – Semimembranosus	1.118	0.003			
Cruralis – Plantaris longus	0.03	1			
Plantaris longus – Gluteus magnus	1.721	< 0.001			
Plantaris longus – Semimembranosus	1.148	0.002			
Gluteus magnus – Semimembranosus	0.573	0.218			
Locomotor mode					
Jumpers – Swimmers	0.669	0.021			
Jumpers – Walkers	0.092	0.939			
Swimmers – Walkers	-0.577	0.141			

To address hypothesis 3, two additional ANOVAs were performed to evaluate which variables have the greatest impact on PCSA. In the first test, where PCSA was calculated with a fixed volume of 1mm³ for all species, there are no significant differences between muscles (ANOVA: $F_{(3)} = 0.495$, p = 0.688; Appendix Figure E.1), but there are between locomotor modes (ANOVA: $F_{(2)} = 3.704$, p = 0.035). Specifically, jumpers have a significantly higher PCSA than swimmers (Tukey: difference = 0.9, p = 0.034) even when muscle volumes are equal, largely because jumpers have significantly shorter relative fibre lengths (Tukey: difference = -0.022, p = 0.048). In the second test, size-corrected ACSA was evaluated for differences

between locomotor modes and each hindlimb muscle, i.e., pennation angle is not considered in the calculation of cross-sectional area. The pairwise results for ACSA are very similar to those for PCSA (Table 4.2). The only difference between the analyses is that the relationship between ACSA and relative fibre length is not significant for the plantaris longus (Pearson's correlation = 0.63, p = 0.052).

Table 4.2 - Pairwise Tukey results from the best ANOVA model for size-corrected anatomical cross-sectional area. Results meeting the p < 0.05 significance threshold have been highlighted in bold.

Pair	Difference in means	Adjusted p- value				
Muscle type						
Cruralis – Gluteus magnus	1.77	< 0.001				
Cruralis – Semimembranosus	1.23	< 0.001				
Cruralis – Plantaris longus	0.029	1				
Plantaris longus – Gluteus magnus	1.741	< 0.001				
Plantaris longus – Semimembranosus	1.201	< 0.001				
Gluteus magnus – Semimembranosus	0.54	0.227				
Locomotor mode						
Jumpers – Swimmers	0.625	0.024				
Jumpers – Walkers	0.073	0.957				
Swimmers – Walkers	-0.552	0.14				

4.3.3 The relationship between muscle size and architecture

Generally, relative fibre length decreases with increasing relative muscle mass in the pennate muscles and increases with mass for the parallel-fibred muscles, but these relationships are not significant (Figure 4.7). There are also no significant differences in pennation angle between locomotor modes for both the plantaris longus (ANOVA: $F_{(2)} = 0.748$, p = 0.508) and cruralis (ANOVA: $F_{(2)} = 0.330$, p = 0.73). In jumpers, pennation angle increases with relative muscle mass for both the cruralis and plantaris longus, while swimmers and walkers show no trend (Figure 4.8). The supplementary phylogenetic ANOVAs show very similar results (Appendix Table E.5).

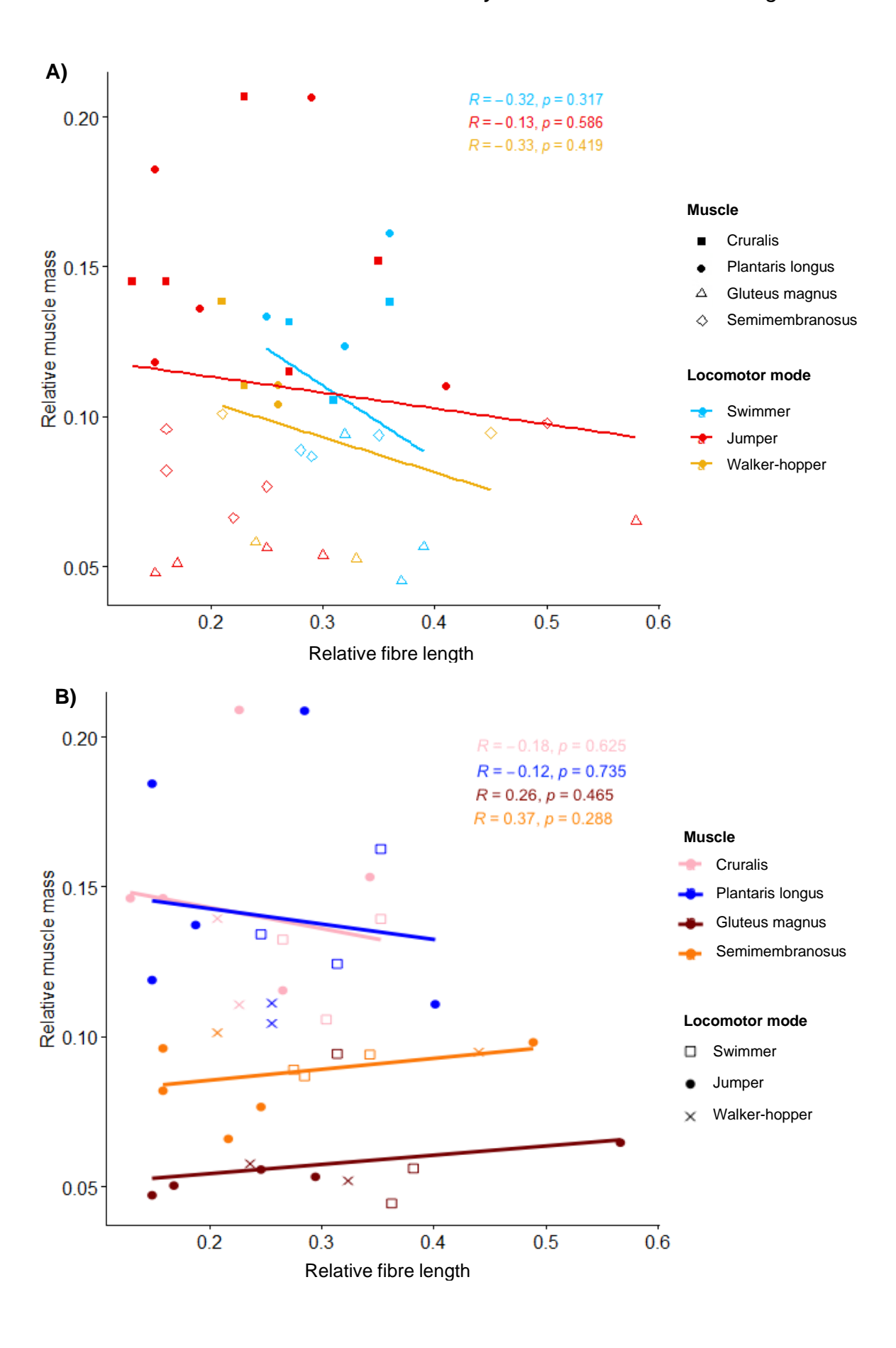


Figure 4.7 - The relationship between relative fibre length and relative muscle mass. There are four points per species; one for each muscle. The data are the same across the two plots, with points colour-coded according to either A) locomotor mode or B) muscle type. In A), filled shapes represent pennate muscles, and empty shapes represent parallel-fibred muscles. The statistics reported refer to Pearson's correlation tests.

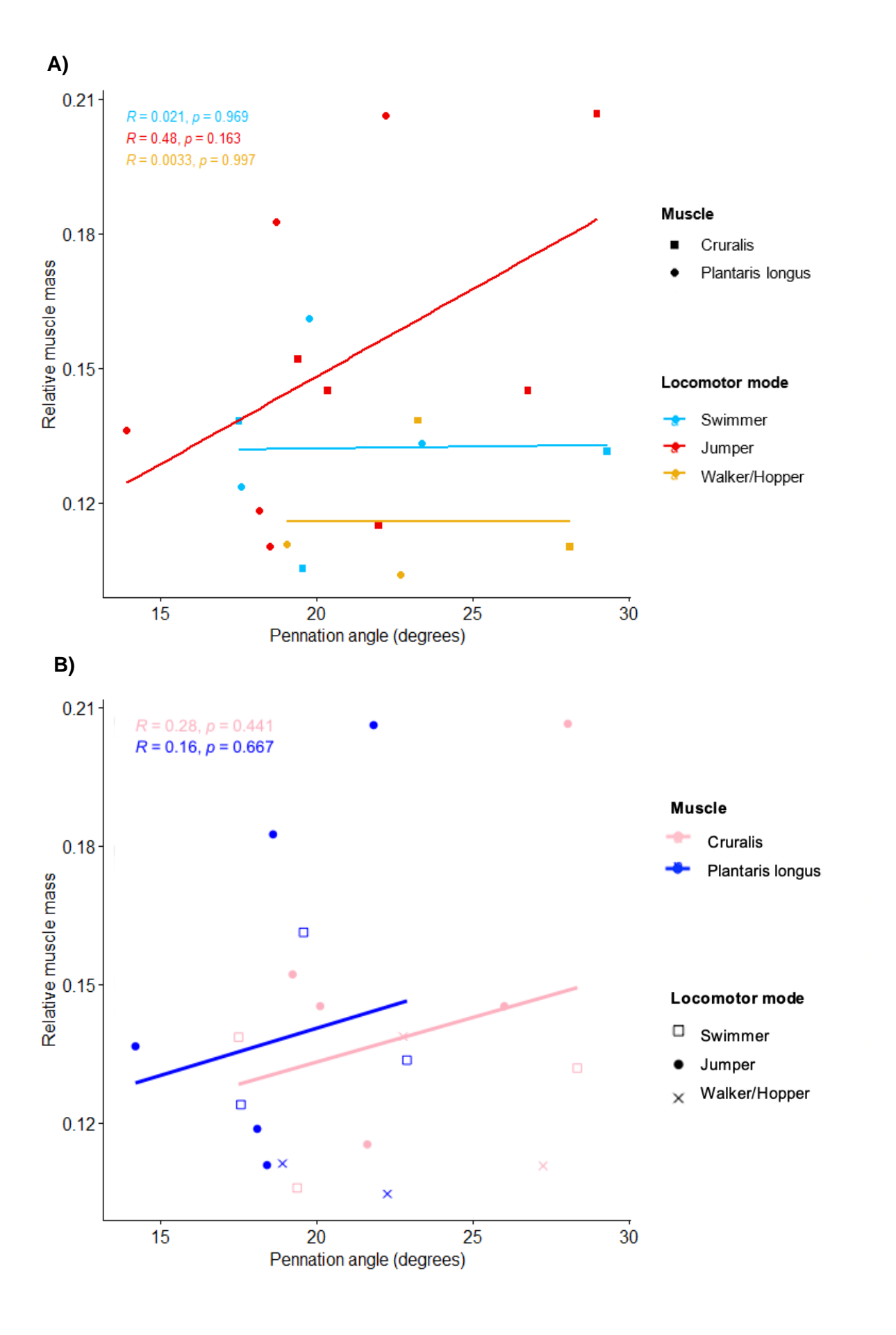


Figure 4.8 - The relationship between average pennation angle and relative muscle mass. There are four points per species; one for each muscle. The data are the same across the two plots, with points colour-coded according to either A) locomotor mode or B) muscle type. In A), filled shapes represent pennate muscles, and empty shapes represent parallel-fibred muscles. The statistics reported refer to Pearson's correlation tests.

4.4 Discussion

Despite fibre architecture being an important determinant of muscle function, it is understudied across a wide range of taxa, largely due to a lack of technology capable of accurately extracting and measuring lots of fibres, especially in small organisms (Charles et al., 2022). Here, I present the first digital fibre analysis of frogs in relation to their locomotor mode. I find that the trade-off between physiological cross-sectional area (PCSA) and fibre length, and thus muscle force output, contractile speed, and range of motion, differs significantly between jumpers and swimmers, but not walker-hoppers (partially supporting hypothesis 1). Where species place on this functional spectrum of fibre architecture does largely depend on the muscle being examined (supporting hypothesis 2). Finally, results suggest that frogs could potentially adjust fibre length to increase muscle force without undertaking the metabolically expensive process of growing and maintaining larger muscle masses (partial support for hypothesis 3.1). In contrast, pennation angle could increase with muscle mass in jumpers, suggesting their architecture is potentially able to maximise potential force output (partial support for hypothesis 3.2). Overall, this chapter presents novel insights into how frogs utilise fibre architecture to address the requirements of different locomotor modes.

4.4.1 Jumpers may increase performance via modifications in fibre architecture more than other locomotor modes

Frogs specialising in different locomotor modes may adapt their fibre architecture to perform functions efficiently in different ways. The results presented in this chapter support the conclusions of earlier chapters and of previous studies, where jumping is the primary driver of changes in frog musculoskeletal physiology (Nauwelaerts *et al.*, 2007). Jumpers are the only group to show a positive relationship between pennation angle and muscle size (Figure 4.8), suggesting that their muscles have

more fibres per unit volume (Rabey *et al.*, 2015). This implies that jumpers are prioritising the maximisation of potential muscle power output more highly than other locomotor modes. In comparison, swimmers show no significant relationships across analyses. However, their comparatively narrow range of fibre lengths suggests that their fibres are under stronger selection than jumpers, or that the range of fibre lengths in swimmers are constrained by some other factor (Figure 4.7). Swimmers may invest more strongly into longer fibres because they require larger ranges of motion, since swimming is used to navigate their environment, while jumping is a one-off, consistent movement. Alternatively, swimmers could afford to rely primarily on increases in muscle mass to increase force ouput, as spending the majority of their life in a buoyant medium could reduce the considerable metabolic costs associated with growing and maintaining muscle mass.

Jumpers have a significantly higher PCSA across muscles than swimmers (Table 4.1; Figure 4.6), even when all muscles are scaled to the same volume (Appendix Figure E.1), suggesting that the fibre architecture of jumpers increases the forcegenerating capacity of their muscles (Mendoza & Azizi, 2021). This supports previous studies of function, where smaller muscle forces and lower rates of muscle shortening were found during swimming compared to jumping, even within the same frog (Calow & Alexander, 1973). This difference between PCSAs is mainly driven by the cruralis, which corroborates the findings of Nauwelaerts *et al.* (2007), who found that a larger cross-sectional area of the cruralis had a negative effect on swimming performance.

4.4.2 Fibre architecture may be an example of many-to-one mapping of morphology to function

Unexpectedly, there are no other significant differences between locomotor modes in fibre architecture. This could indicate that there is high plasticity in muscle use across species (Figure 4.6; Vera et al., 2022). Using two jumpers as an example, Sechellophryne gardineri has muscles occupying each of the three areas of functional specialisation (Figure 4.6; Appendix Figure E.1) due to the high variation in relative fibre length across its muscles. In comparison, Arthroleptis tanneri has a small range of short fibres, with the only significant variation between the PCSA of each muscle being due to volume. S. gardineri is therefore likely to have greater range of contractile velocities, as well as versatility in the functional workspace of

the hindlimb (Lieber & Fridén, 2000). Since this variation in fibre architecture occurs even when the locomotor mode is the same, frogs could be using different fibre anatomies to achieve similar functions, thus alleviating any selection pressures to alter larger components of muscle or bone structure. Fibre architecture could therefore be an example of many-to-one mapping (Moen, 2019). Direct functional studies are needed to test that this is not just a case of differences in jumping ability (see section 4.4.8). Alternatively, there is likely to be other determinants of muscle architecture which could be driving this variation within locomotor groups, such as phylogenetic history, habitat type, location within a dispersal range (Padilla *et al.*, 2019), and body size (see section 4.4.3).

4.4.3 Frogs with a minute body size may experience different selection pressures on fibre architecture

Unlike jumping, walking performance has been shown to be uncorrelated with the contractile properties of the semimembranosus and plantaris longus, and is strongly associated with small hindlimb mass (Astley, 2016). However, in the current study, there are no significant differences in PCSA between jumpers and walker-hoppers. This could simply reflect the small sample size of the walker-hopper group. However, this could also be an interesting insight into how body size might impact fibre architecture, as this result is largely driven by *Paedophryne verrucosa* (Figure 4.6). This species is one of the smallest frogs in the world (Rittmeyer et al., 2012), with the specimen analysed here measuring just 8.36mm in snout-vent length. Despite its poor jumping abilities (Rittmeyer et al., 2012), its muscles place more highly in the force specialist region of the functional plot than many other taxa (Figure 4.6). This is primarily due to the relatively short fibre lengths, since even the parallel-fibred muscles place in the force specialist region when all volumes are equal (Appendix Figure E.1). Since fibre visualisation in this specimen is among the best of the dataset, and the grayscale cut-off is not included in any of the best models, this appears to be a novel insight into how these frogs may adapt their fibre architecture to life as an extremely small vertebrate.

Previous studies have established that PCSA generally increases with body size across animals (Martin *et al.*, 2020; Bishop *et al.*, 2021a), largely due to an increase in the number of muscle fibres, and therefore energy output, per unit mass (Emerson, 1978). Consequentially, larger frogs can afford to have less pennate

muscles (James et al., 2007). Small frogs may have to rely more strongly on fibre architecture than muscle size to increase power output because they are more limited by constraints on body size. In *Paedophryne*, there is a comparatively small number of fibres in the muscles compared to the other species (Appendix Figure E.2). Their higher-than-average pennation angles (Supplementary Dataset 6) and short fibre lengths could be a 'space-saving strategy' (Lieber, 2022) that this tiny frog uses to compensate for body size restrictions. It is worth noting, however, that the fibre anatomy of the next smallest frog in the present study (snout-vent length: 11.71 mm), terrestrial jumper S. gardineri, is very different to that of P. verrucosa (Figure 4.6). This suggests that locomotor mode is still an important factor influencing how small frogs adapt via changes fibre architecture, or that there could be a critical size threshold below which the selection pressure on fibre architecture increases. Additional analyses of allometry were not possible in the present study due to the unavailability of body mass data, highlighting the need for specimen metadata to be uploaded alongside CT scans. Overall, these preliminary findings present the opportunity for an interesting future study on the anatomical trade-offs experienced by miniaturised frogs using digital dissection.

4.4.4 Where species place in functional space depends on the muscle being examined

Long fibres enable parallel-fibred muscles greater range and control of hindlimb motion (Collings & Richards, 2019), while large pennate muscles with short fibres are important for generating explosive movement due to the dense packing of muscle fibres (Calow & Alexander, 1973; James et al., 2007; Bishop et al., 2021a). These functional trends are reflected in the fibre architecture of all species, regardless of locomotor mode. For instance, pennate muscle fibre lengths decrease with increasing muscle mass, while parallel-fibred muscles show an increase (Figure 4.7). The contractile speed specialist area of the functional space plot is occupied only by parallel-fibred muscles for all but one species, Telmatobius thompsoni (swimmer), which has the cruralis and plantaris longus near the upper limits of this region (Figure 4.6). Most of the pennate muscles occupy the force specialist region of the plot, along with the semimembranosus from three species -Paedophryne (walker-hopper), Rana and Arthroleptis (jumpers). The 'generalist' region is only ever occupied by parallel-fibred muscles, while the power specialist region only contains pennate muscles (Figure 4.6; Böhmer et al., 2018). Functional Page 131 of 286

studies will be needed to check whether the trends observed here reflect *in vivo* locomotor performance, e.g., whether the better jumpers within the jumper group have a more highly adapted fibre architecture.

4.4.5 Reducing fibre length to amplify force production could reduce the need to grow and maintain high muscle mass, regardless of the degree of pennation

Two lines of questioning were established in the future directions suggested in Chapter 3 - does changing architectural properties in favour of increasing force production reduce the large metabolic costs associated with increasing muscle size (hypothesis 3.1), or is fibre length smaller and pennation angle larger in bigger muscles, thus maximising the potential for force generation (hypothesis 3.2)? Similarly, does fibre length increase with muscle length in parallel-fibred muscles to maximise contractile speeds and ranges of motion? Ultimately, optimising fibre length and pennation angle alone is likely not sufficient for muscles to produce power outputs that match or exceed a muscle of larger volume (Figure 4.6; Appendix Figure E.1). However, there is some evidence that relative fibre length, independent of pennation angle, is a strong determinant of muscle function.

Regarding force-specialisation, examining PCSA when all volumes are equal shows that the decreasing the length of muscle fibres can still result in force specialisation for any of the four muscles examined (Appendix Figure E.1). The lack of a significant negative trend between the relative mass and fibre length of pennate muscles (Figure 4.7) further supports this, as fibres might not be experiencing strong selection pressure to decrease in length alongside increases in muscle mass to maximise potential force production. Regarding specialisation in contractile speed and functional range, the parallel-fibred muscles both show increases in fibre length with muscle length. The gluteus magnus shows a significant relationship irrespective of body size (Figure 4.5), indicating that it might experience stronger selection pressures for specialisation in high contractile speed and range of knee extension than the semimembranosus. Overall, these trends support Astley's (2016) hypothesis that the evolutionary lability of muscle contractile properties allows organisms to increase muscle power output without increasing muscle mass, thus supporting hypothesis 3.1. Similar to that study, the sample size used here is not high enough to extract phylogenetic signal to confirm this (Münkemüller et al., 2012),

so how fibre length changes throughout evolutionary history continues to be an interesting area for future research.

Analysing pennation angle and its relationship with muscle mass independently tells a slightly different story, where each locomotor mode may use different strategies. Mendoza & Azizi (2021) found that larger mass-specific forces, and thus better jumping ability, was largely explained by increases in plantaris longus pennation angle. Here, terrestrial jumpers are the only group of frogs which show an increase in pennation angle with muscle size (Figure 4.8), meaning that they increase the number of muscle fibres per unit volume. Though this is not a statistically significant relationship, this could indicate that selection favours the maximisation of potential force output for jumpers, thus providing some partial support for hypothesis 3.2. In contrast, swimmers and walkers do not show any trends in pennation angle, so these groups may rely more strongly on increases in muscle mass or the reduction of fibre lengths to exert higher forces.

4.4.6 Pennation angle: to measure or not to measure?

Lieber (2022) has claimed that measuring pennation angle in just a few areas within a static muscle can lack functional significance. This is largely because muscle fibres can differ in orientation throughout the muscle, particularly when comparing deep and superficial regions (Azizi & Deslauriers, 2014; Charles et al., 2022), and will rotate during contraction such that the shortening of the fibres is smaller than the total shortening of the muscle (Roberts et al., 2019). This creates regional variation in mechanical output both throughout the muscle and throughout any movement (Azizi & Deslauriers, 2014). Additionally, any pennation angles below 30 degrees, which is common for most pennate frog muscles (Kargo & Rome, 2002; Supplementary Dataset 6), is likely to have little effect on force calculations, as the cosine variable is then typically very close to one ((Equation 4.1); Martin et al., 2020). Therefore, since extensive fibre extractions and measurements is a very time-consuming process, many studies have treated pennation angle as constant throughout the muscle (Calow & Alexander, 1973; Kargo & Rome, 2002; Astley, 2016; Mendoza & Azizi, 2021; the present study), or all muscles are treated as parallel-fibred (Nauwelaerts et al., 2007). Here, I found that while the results for analyses of PCSA are largely very similar to the results for ACSA, the relationship with relative fibre length of the plantaris longus is significant when using PCSA, but not ACSA (Table 4.2). More detailed sensitivity tests are needed to estimate how much this variation in fibre orientation directly affects force production (see section 4.4.8).

4.4.7 Limitations

Fibre tracking is only as successful as the quality of the contrast-enhanced μCT scan. The primary limitation of this chapter is sample size, which is limited by scan resolution to ten species across three locomotor groups. Considering the findings of Chapter 3, muscle architecture could be another functional mediator between arboreal and terrestrial habitats. For instance, the forelimb muscles in arboreal pine martens (Böhmer et al., 2018) and hindlimb muscles in arboreal squirrels (Nyakatura et al., 2019) have been shown to have greater force-producing capabilities compared to their close terrestrial relatives due to differences in fibre architecture. Architectural variables from previous frog studies would have ideally been included in my analyses to expand the range of taxa, but the mean fibre lengths obtained here appear smaller than those recorded in studies whose method for body size correction (or lack thereof) allowed for more direct comparisons (Kargo & Rome, 2002; Astley, 2016). This difference could potentially be because the present study uses formalin-fixed and iodine-stained specimens, which are known to suffer from tissue shrinkage (Martin et al., 2020), while previous studies have used fresh specimens. However, most studies also do not disclose exactly how many fibre measurements they took. Compared to those that did (Lieber & Brown, 1992; Nauwelaerts et al., 2007), I measured considerably more fibres, making PCSA estimations less prone to error (Charles et al., 2022). Additionally, the GoodFibes package has undergone substantial testing to ensure that comparable results are obtained between the traditional and digitally automated methods for fibre extraction (Arbour, 2023). For the purposes of the present study, the differences in the results presented here to those from previous research did not affect the ability to address the hypotheses tested. The same fibre tracking technique is used for all muscles/specimens and there are no statistical models where the addition of grayscale cut-off improved the fit to the data. Furthermore, since I examine relative fibre length, differences in the level of shrinkage experienced by the individual fibres due to differences in preservation and staining procedures would be proportional to that of the entire muscle. Similar to Chapter 3,

it is important to note that because measurements had to be normalised using total hindlimb length and muscle mass, which are already strongly correlated with locomotor performance (James *et al.*, 2005; Nauwelaerts *et al.*, 2007), rather than snout-vent length and total body mass, the trends observed in fibre architecture might be diluted. To conclude, the relative differences between architectural variables still provide useful insights, but future comparisons made using the raw data from the present study should be taken with caution.

Another well-studied limitation is how examining fibre architecture in isolation may not relate to muscle function in the same way once placed in the skeletal system. For example, the amount of change in fibre length that occurs as a joint rotates depends on the muscle moment arm, i.e., the "mechanical advantage" that a muscle has at a particular joint (Lieber & Fridén, 2000). Additionally, pennate muscles experience variable gearing throughout movement (i.e., fibres act differently depending on the mechanical load), which can affect how muscle moment arms change with changes in joint angle, as well as the size of a muscle's functional range (Azizi *et al.*, 2008; Azizi & Roberts, 2014). To correctly estimate joint dynamics during locomotion, the interaction between joint moment arms and fibre architecture needs to be fully understood (Lutz & Rome, 1996) especially since the outputs from musculoskeletal models (e.g., maximal muscle torques) can be highly sensitive to variation in fibre length (Charles *et al.*, 2016).

4.4.8 Future directions

Given the primary limitation of the present study being sample size, scan resolution and staining techniques are important areas requiring improvement for future studies comparing fibre architecture across vertebrates. Several muscles were unable to be included in this study as their resolution was not clear enough for fibre tracking across all species. For example, while the extensor muscles analysed here are important for both swimming and jumping, it would have been ideal to investigate whether the adductors (important during jumping, e.g., adductor magnus) and abductors (important during swimming, e.g., iliacus externus) are a key point of difference in fibre anatomy between these locomotor modes (Nauwelaerts *et al.*, 2007). Improvements in the ability to visualise fibre structure in muscles which are too small to extract fibres using traditional methods would also be very beneficial. This will be vital for comparatively analysing muscle function across miniaturised

frogs (see section 4.4.3). Furthermore, it would be interesting to see whether the tibialis anticus longus and extensor cruris brevis, which are small pennate muscles in the shank (Collings & Richards, 2019), differ in their fibre architecture between locomotor modes in the same ways as they significantly differ in size (Chapter 3). Examining these muscles in more detail would determine whether the distal hindlimb segments have fibre architectures more highly adapted for force production. Previous studies have observed muscles becoming increasingly pennate when moving distally down the limb across other vertebrates (Powell *et al.*, 1984; Allen *et al.*, 2010; Charles *et al.*, 2016; Bishop *et al.*, 2021a), which is said to improve energy conservation during locomotion (Sacks & Roy, 1982). Having smaller distal segments is important for reducing moments of inertia (i.e., the forces required for limb acceleration; Nauwelaerts *et al.*, 2007), so the shank may be more limited in how much it can increase force/power output through increases in muscle mass. The muscles in the shank may therefore be under stronger selection pressures to optimise fibre architecture than those in the thigh.

A potential solution for addressing the issue of fibre resolution could be to induce muscle shrinkage by prolonged dehydration and/or higher iodine concentrations during staining, as this has been observed to result in better separation of individual fibres (Ed Stanley, pers. comms.). However, facilitating easier fibre detection in this way would have consequences for accurately measuring muscle mass, volume, and length. Future studies could attempt staining for gross measurements first, then increasing the concentration of the staining solution so that fibres can be better examined in subsequent μ CT scans. For subsequent statistical analyses, the appropriate size correction would then be included to account for the additional muscle shrinkage.

As suggested in Chapter 3, computational models may also be key to quantifying the impact of variation in musculoskeletal anatomy on function. Previous studies have used fibre architecture to better inform and validate biomechanical models (Sánchez et al., 2014; Sellers et al., 2017; Orsbon et al., 2018), which is particularly important for estimating locomotor performance in extinct taxa (Bishop et al., 2021b), but this has not been done in frogs before. Muscle volume, fibre length and pennation angle can be systematically varied while keeping all other features of anatomy the same to examine how these model parameters impact motion. Additionally, variation in pennation angle throughout the layers of an individual

muscle, and its effect on mechanical output, could be explored through a series of sensitivity tests without the need for extensive dissection (Azizi & Deslauriers, 2014). This is also likely to be the most efficient way to address the calls for more research on the complex relationship between muscle architecture and bone biomechanics in relation to locomotor function more easily (Marchi *et al.*, 2018). In turn, a computational approach will facilitate future advances in "palaeomyology" (Perry & Prufrock, 2018), where researchers can virtually graft different potential fibre anatomies onto fossilised remains and test how they impact function.

4.4.9 Conclusion

By examining a combination of musculoskeletal variables (muscle mass, fibre length, physiological cross sectional area, skeletal structure) using digital techniques, we can derive the best possible estimates of muscle function during locomotion, and therefore their ecological relevance. This chapter completes the comparative anatomical investigation presented in this thesis by exploring how the functional spectrum of architectural properties in frog muscle fibres differs between four hindlimb muscles with varying roles in locomotion. Jumpers show specialisation towards producing higher forces than other locomotor modes. The high plasticity in fibre architecture observed within each locomotor group indicates that many-to-one mapping of fibre form to function is occurring, and that there are other determinants of fibre architecture besides locomotor mode. I also exemplify how digital techniques can enable the quantification of muscle architecture in some of the world's smallest vertebrates, providing the foundation for future studies to determine the effects of miniaturisation on anatomy and function. Ways in which the acquisition of this anatomical information can be improved, and how it can be incorporated into musculoskeletal dynamics models, have also been suggested.

5 Modelling the effect of different skeletal proportions on hindlimb kinematics

Dr Chris Richards assisted in project design and provided the Mathematica packages, 'Biomechanics Bootcamp' tutorials and coding assistance, as well as comments on draft versions of this chapter along with Dr Laura Porro.

5.1 Introduction

In Chapter 2, hindlimb proportions were shown to differ between frogs utilizing different locomotor modes across a broad phylogenetic spectrum, suggesting that individual segments may have a discrete role in locomotion. Currently, direct mechanical evidence for how variations in frog limb segment proportions influence locomotor function is lacking (Enriquez-Urzelai et al., 2015). Most comparative research on anuran locomotor mode has considered the hindlimb as a single functional unit (e.g., Gomes et al., 2009), neglecting important biomechanical properties of hindlimb morphology. Furthermore, biomechanical analyses of locomotor performance usually compare individuals of the same species (Nauwelaerts et al., 2007; James & Wilson, 2008; Herrel et al., 2014), or a small number of species from select locomotor modes (Roberts et al., 2011; Robovska-Havelkova et al., 2014; Reynaga et al., 2018) or phylogenetic groups (Reilly et al., 2015). Comparative studies of the ability to perform more than one locomotor function across species with different primary locomotor modes are rare (Astley, 2016; Vassallo et al., 2021). No known studies have analysed anuran mechanics with a large sample size of representative species from all the locomotor modes analysed in Chapter 2. Similarly, no literature has been found which quantifies how hindlimb proportions impact locomotor mechanics across multiple species. Jumping performance is arguably the best starting point, as this locomotor mode is strongly correlated with morphology (Chapter 2; Nauwelaerts et al., 2007) and has the most experimental data available (e.g., Richards et al., 2017; Porro et al., 2017). Additionally, hindlimb motion during jumping is linear compared to the cyclical motions involved in swimming (Robovska-Havelkova et al., 2014) and walking (Reynaga et al., 2018; Collings et al., 2019; Collings et al., 2022), and is therefore more straightforward to record, model and analyse.

To fully comprehend energy flow through the hindlimbs, the locomotor system can be viewed as a hierarchy of system properties and constraints (Figure 5.1; Richards, 2019). Experimental approaches involving animal behaviour suffer from measurement noise, individual variation, and the difficulty of replication, while a modelling approach does not. and is therefore more appropriate for detecting subtle shifts in behaviour, causal relationships and underlying mechanisms (Richards & Porro, 2018). Kinematics forms the foundation of this multi-step framework – it describes the motion of a rigid body in 3D space, and considers the constraints of limb geometry (i.e., joint ranges of motion and limb segment lengths) without considering the forces (e.g., moments of inertia, ground reaction forces) that cause limb motion. Muscles are assumed to be able to produce enough force to produce the desired kinematics (Richards et al., 2017). Previous papers have used kinematics to study anuran walking mechanics (Ahn et al., 2004; Collings et al., 2019; Collings et al., 2022) and determine how each joint contributes to hindlimb motion during jumping (Richards et al., 2017; Richards & Porro, 2018). Theoretical kinematics can isolate specific parameters, such as take-off angle, to determine how each one contributes towards motion (Richards & Porro, 2018). The results can then be compared to in vivo performance data and extrapolated to other species. Ultimately, kinematics provides a non-invasive and innovative technique which can be utilised to enhance our understanding of the mechanisms behind jumping in frogs.

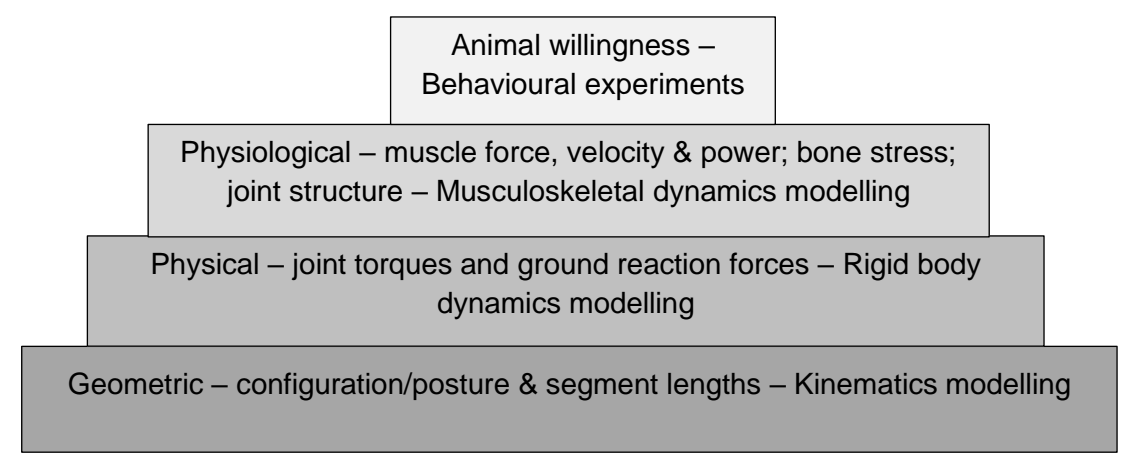


Figure 5.1 - Hierarchy of system properties in limb modelling. The general format is property/constraint – insights gained – approach.

In this chapter, I create an inverse kinematics (IK) model to determine how hindlimb geometry influences locomotion. Specifically, this model tests how the relative

length of the thigh, shank, and proximal foot affects how each hindlimb segment rotates during the take-off sequence. IK is the calculation of the minimal segment rotations needed at each time step to place the hindlimb at a given end position and orientation relative to its starting posture (Richards et al., 2017; Richards, 2019). For the take-off sequence to be 'kinematically parsimonious', the hindlimb should follow the shortest possible path to a hypothetical target at the point of take-off, i.e., the frog should minimise the rotation of each segment (Richards et al., 2017). Therefore, the amount the hindlimb muscles are working is suggested to be minimised, making jumping more efficient, as there is the implicit assumption that the muscles will provide the necessary force to achieve the desired kinematics (Richards et al., 2017). This also implies that longer hindlimb segments are expected to have more potential to influence the endpoint of the limb. Even subtle differences in segment rotations can have profound effects on hindlimb motion due to changes in muscle function from differences in moment arms (Collings et al., 2022), and the accumulation of motion down the joints (Richards & Porro, 2018).

In Chapter 2 and earlier studies (Nauwelaerts *et al.*, 2007; James & Wilson, 2008; Jorgensen & Reilly, 2013; Lires *et al.*, 2016; Gómez & Lires, 2019), arboreal jumpers (AJ) and terrestrial jumpers (TJ) are shown to have a longer shank relative to the thigh and total hindlimb length, as well as a longer proximal foot relative to total hindlimb length compared to burrowers (BWH), walker-hoppers (WH), and swimmers (AQ) (Table 5.1). The highly elongated proximal foot (formed by extreme elongation of two of the tarsal bones) is a distinguishing feature of the anuran body plan and essentially represents a novel limb segment from an evolutionary standpoint, so it is likely to hold some mechanical advantage. However, this segment is never longer than the thigh and shank (Chapter 2). Therefore, I predict that the take-off sequence is more kinematically parsimonious when:

- H1) The shank is long relative to the thigh and total hindlimb length.
- H2) The proximal foot is long relative to total hindlimb length, but no longer than the more proximal segments.

The effect of different hindlimb proportions on joint positioning, and how that may potentially affect jump performance is also discussed. The results obtained will serve as a direct input for more complex dynamics models, in terms of both data and hypotheses to test (see Chapter 6).

Table 5.1 - Summary of the relationship between average relative hindlimb segment length and locomotor mode for the 164 frogs spanning all recognised anuran families from Chapter 2. See Table 2.2 for more detailed descriptive statistics.

Segment	Length relative to the hindlimb					
	Shortest -			Lo	ngest	
Thigh	WH	TJ	BWH	AJ	AQ	
Shank	AQ	BWH	WH	TJ	AJ	
Proximal foot	AQ	BWH	WH	TJ & AJ		

5.2 Methods

5.2.1 Model organism

To estimate take-off kinematics across all 164 study taxa, I used *Phlyctimantis maculatus* (formerly known as *Kassina maculata*) as a model because there are abundant kinematics and dynamics data from *in vivo* jumps available from previous studies (Ahn *et al.*, 2004; Porro *et al.*, 2017; Richards *et al.*, 2017; Richards *et al.*, 2018; Collings *et al.*, 2019; Collings *et al.*, 2022). Furthermore, compared to other frogs, this species is a 'generalist' in terms of locomotor mode, in that it performs swimming, jumping, climbing, burrowing, walking, and running.

5.2.2 Inverse kinematics model construction and validation

To explore the theoretical impact of hindlimb geometry on jumping motion, I have developed an IK model which allows manipulation of the hindlimb proportions of a model frog. IK models are fast to run and, compared to forward dynamics (FD) models, involve less computationally demanding simulations since they require fewer parameters (e.g., degrees of freedom) and do not require optimisation for every anatomical variant of the model. The initial XYZ coordinate data used to build the IK model were extracted from high-speed videos of *P. maculatus* jumps by Richards *et al.* (2017), where skin markers were used to represent the centres of joint rotation. To best compare across species, the data from the most average jump in terms of jump angle (34.46 degrees) were used. The take-off sequence – from the onset of motion in the initial crouched position to the moment the last toe leaves the substrate - occurs across 16 time steps (0.04 seconds each) and a total distance of 0.0539 m. The model frog is a simplified 'stick-figure', where XYZ coordinates for the hip, knee, ankle and tarsometatarsal (TMT) joints and the point of contact (POC)

between the heel of the foot and the ground were joined by straight lines representing each hindlimb segment (Figure 5.2). The left hindlimb was mirrored to create the right hindlimb as this model assumes that the legs act symmetrically during jumping. Kinematic constraints (Murray *et al.*, 1994) were implemented to keep the hip joints at a fixed distance apart, which was the same as the distance between the hips of *P. maculatus* (0.016 m) (Appendix Figure F.1).

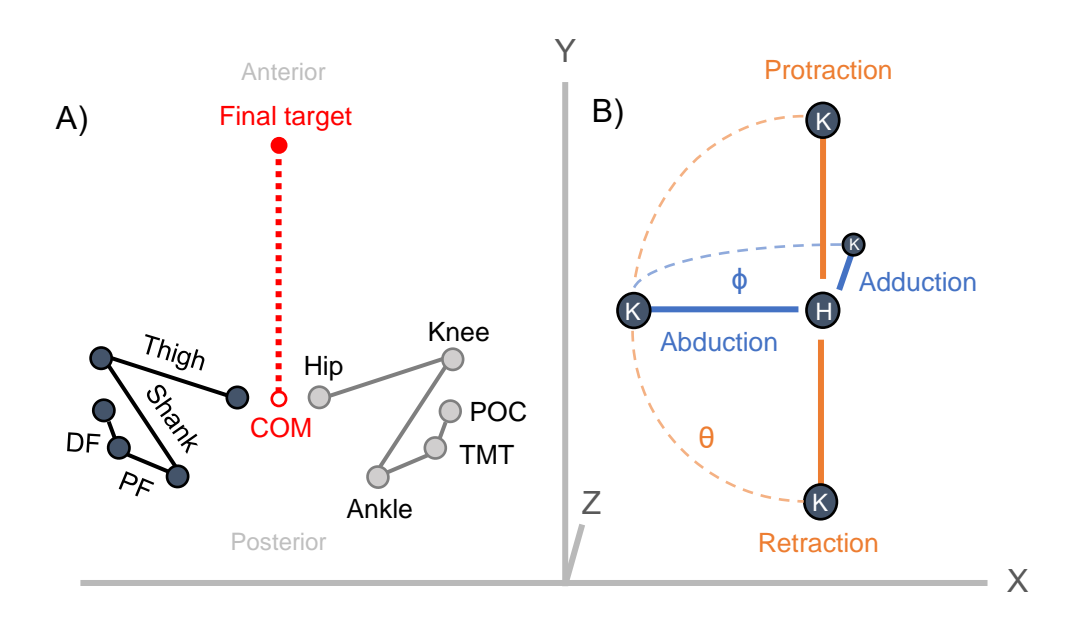


Figure 5.2 - A) Dorsal view of the frog 'stick-figure' model, where ball joints, each with three degrees of freedom, are connected by lines to represent each segment of the hindlimb. The red dashed line represents the jump trajectory along the global Y axis from the initial centre of motion (COM) to a final target distance of 0.0539 m. The right hindlimb is a mirror image of the left hindlimb. PF = proximal foot; DF = distal foot; TMT = tarsometatarsal joint; POC = point of contact with the ground. B) On the same axis in dorsal view, the hip joint (H) acts as the centre of segment rotation, where movement of the knee joint (K) about the vertical Z axis in the XY plane causes the segment to protract/retract (flex/extend; θ), while abduction/adduction (\$\phi\$) occurs about the caudal axis in the XZ plane. The same geometry applies to all joints where the proximal joint is the centre of the local coordinate system.

Mathematica (Version 13.0, Wolfram Research, 2022) was used to build and run the IK model (see workflow in Figure 5.3). First, the model frog was rotated and scaled to ensure it takes off along the global Y axis (consistent with how the *in vivo*

frog jump data were processed). During initialisation, the XYZ coordinates were then converted to 'twist parameters', which are a way of representing rigid body motion that easily allows for segment lengths or orientations to be changed (see section 3.2 of Murray *et al.*, 1994). FK was used to convert the twist parameters back into XYZ coordinates. If the hindlimbs remain unaltered (i.e., during model validation), then the XYZ coordinates would be identical to the initial data (Figure 5.3).

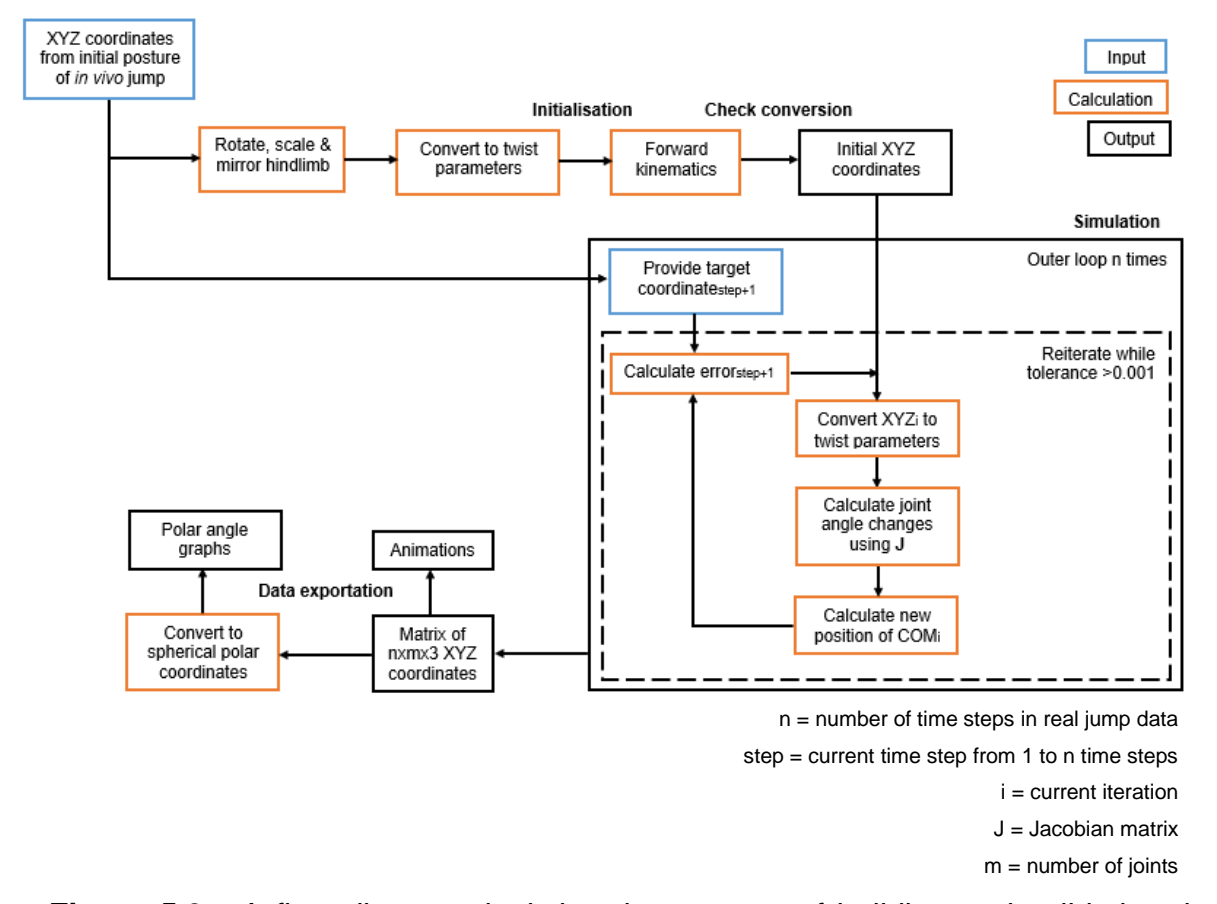


Figure 5.3 - A flow diagram depicting the process of building and validating the kinematics model based on *in vivo Phlyctimantis maculatus* jump data.

A well-known challenge in robotics and biomechanics is that joints are coupled, creating a nonlinear system, i.e., the rotations occurring at each joint do not relate directly to the movement of the limb's 'endpoint' (Murray *et al.*, 1994; Richards, 2019). The Jacobian matrix (*J*) is widely used to solve this issue (Kargo & Rome, 2002; Richards *et al.*, 2017; Richards & Porro, 2018, Richard, 2019), as it relates incremental changes in joint angles to the velocity of the limb endpoint in Cartesian space. Essentially, joint angle changes are made to be small so that the relationship between joint velocities and endpoint velocity is linear (Murray *et al.*, 1994). *J*

accounts for multiple joints, interacting effects of hindlimb posture, segment proportions and joint axis orientation, all within a single step (Equation 5.1):

$$dI * dq = dP$$

(Equation 5.1)

where J is a matrix of 3 x 6, q is the joint angles, P is the list of X, Y and Z coordinates representing the endpoint position and d symbolises a small change. The pseudoinverse of J is dP. In this model, the endpoint at each point in time was the model frog's current centre of motion (COM, i.e., the midpoint between the hip joints).

This model consists of a loop which calculates the most minimal Euclidean distance, known as the 'error', between the model frog's current COM and the COM at the next time step according to the real *P. maculatus* jump data (Figure 5.3). The model incrementally moves the frog in the direction of the next target until the error is less than a predefined tolerance, which is defined as the distance between the hips of P. maculatus. For the frog to accurately reach and not overshoot that target, the model moves by 0.001 m at each timestep, referred to as the 'gain'. This process repeats itself until the final target is reached (time step 16). This model produces a 16 x 5 x 3 matrix - the XYZ coordinates for each joint at each of the sixteen time frames (Figure 5.3). These XYZ coordinates situate the joint positions in a global reference frame, which can make hindlimb motion difficult to describe (Richards et al., 2017). Thus, the XYZ coordinates were converted into polar angles, which quantifies the orientation of the thigh, shank, and proximal foot as a series of local reference frames anchored at the hip, knee, and ankle respectively, as depicted in Figure 5.2B. The most proximal joint of a limb segment acts as the centre of rotation in a 3D sphere. The relative position of the distal joint is represented by the associated segment length r (Equation 5.2) and two angles – a protraction-retraction angle θ (Equation 5.3) and an abduction-adduction angle φ (Equation 5.4):

$$r = \sqrt{x^2 + y^2 + z^2}$$

(Equation 5.2)

$$\theta = tan^{-1}(\frac{y}{x})$$

(Equation 5.3)

$$\phi = \cos^{-1}(\frac{x}{r})$$

(Equation 5.4)

Conversion from radians into degrees and a combination of negating and offsetting by a factor of *Pi*/2 was used for convenience, e.g., the rotation axis direction of the shank is opposite that of the thigh and proximal foot, so the shank orientation was not negated. If the resulting polar angles showed a similar trend and magnitude to the real jump kinematics, then the model was successfully validated.

5.2.3 Modelling different frog species

Using the skeletal measurements of the femur, tibiofibula and calcaneum from Chapter 2 to represent the thigh, shank, and proximal foot segments, I investigated the effects of differences in hindlimb proportions on take-off kinematics for 164 taxa, thus 'mapping' the route of feasible segment kinematics across a wide range of locomotor modes, habitat types and phylogenetic groups. There are several key differences between this IK model and the original model used for validation (Figure 5.4). Firstly, the hindlimb proportions were altered to reflect different species during the conversion of P. maculatus XYZ coordinates to twist parameters in the initialisation stage. Pelvis size, total hindlimb length (0.0763 m) and the initial hindlimb segment orientations remained identical to the P. maculatus model throughout all simulations to enable the effects of relative hindlimb segment lengths to be considered in isolation. Secondly, the same method of predefined time steps using COM targets cannot be used in species-specific models. Instead, the error was the distance between the current COM and the final target, which was calculated using the *P. maculatus* jump angle and take-off sequence distance. Tolerance and gain were kept the same. The resulting data points were resampled to 100 time steps using the time interval from the *P. maculatus* take-off sequence (0.000525 s) to make the velocity profile identical across simulations (Figure 5.4).

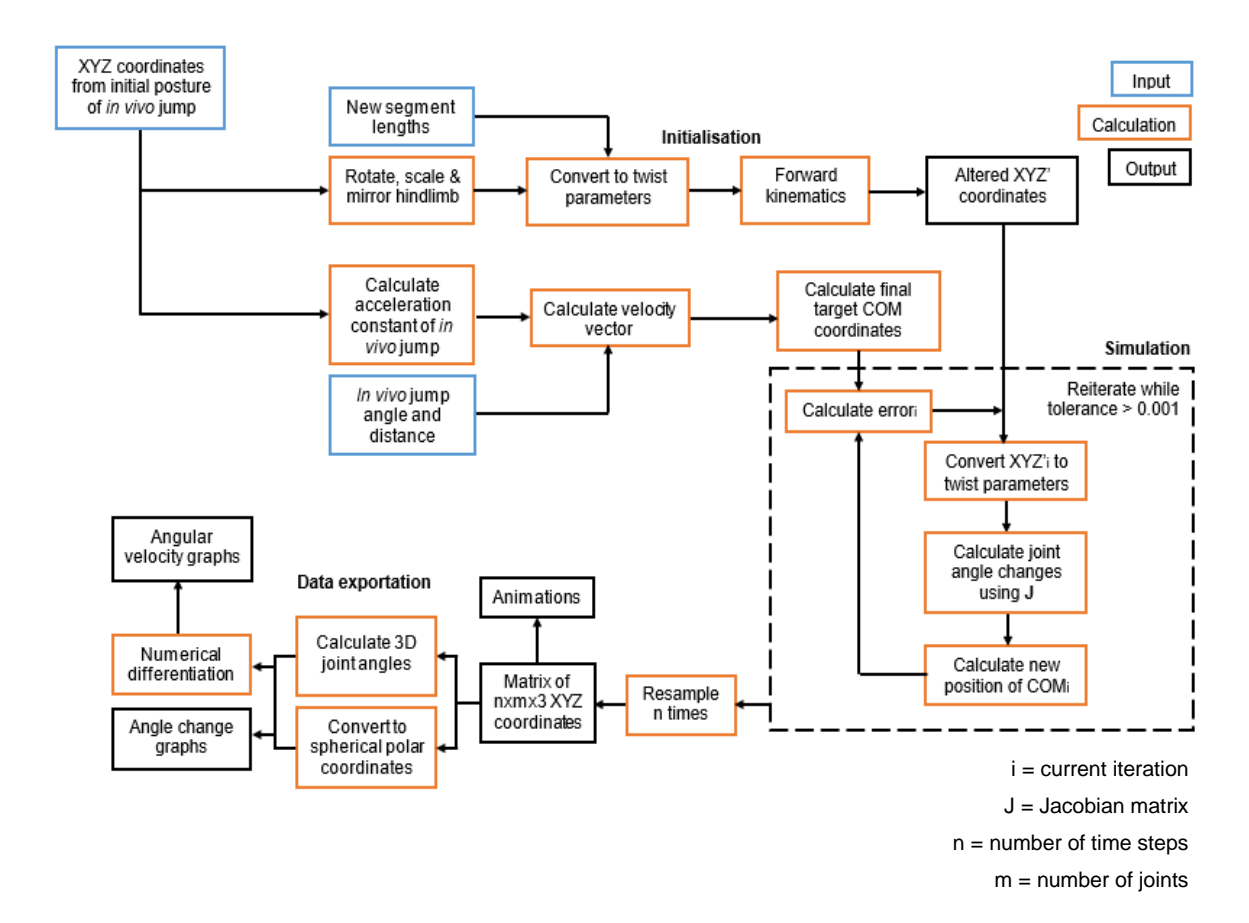


Figure 5.4 - A flow diagram depicting the process of building the model for testing the effect of different segment proportions on hindlimb kinematics based on *in vivo Phlyctimantis maculatus* jump data.

In addition to polar angles, which describe how the orientation of each hindlimb segment changes throughout the take-off sequence, 3D joint angles were examined to determine how joint configurations change to gain further insight into how the muscles spanning each joint may be acting. Hip, knee, and ankle angles were calculated using vectors defined by the endpoint of the proximal (V_{prox}) and distal (V_{dist}) segments (Equation 5.5). The 'body vector' used to calculate the hip angle was of arbitrary length directly along the cranio-caudal axis. An offset of Pi and subsequent conversion from radians into degrees was used for convenience, same as in the polar angle calculation:

3D joint angle =
$$\left(\frac{Vprox.Vdist}{||Vprox|| ||Vdist||} \times -1\right) + \pi$$

(Equation 5.5)

Species where the relative length of one segment differed significantly while the remaining segments' proportions were highly similar were overlapped on graphs and animations of take-off to directly compare and quantify the effects of varying the length each segment on hindlimb motion. To examine how fast joints were opening, the angular velocity of each segment and joint throughout the take-off sequence was calculated using numerical differentiation (Figure 5.4; see Appendix G:).

5.2.4 Hypothetical models

To fully establish the relationship between segment length and hindlimb motion, this kinematics model was modified to test hypothetical combinations of hindlimb proportions, including extreme examples not found in nature (Figure 5.4). While total hindlimb length were kept constant, hindlimb segments were systematically prescribed a set of realistic and extreme arbitrary lengths in isolation (Table 5.2) based on the range of hindlimb proportions found in the 164 real frogs (Table 5.3). The strength of this approach is the ability to explore the link between anatomy and function in unoccupied areas of morphospace. The use of hypothetical models could also show the extent to which elongating a segment makes take-off more kinematically parsimonious before that segment becomes a hindrance. It is important to note that the segment lengths were modelled relative to each other, meaning this does not directly translate to being relative to the total length of the hindlimbs. For example, although the models 'thigh x 0.5' and 'shank x2' both mean that the shank is double the length of the thigh, the overall hindlimb proportions are not the same, resulting in slightly different kinematics (Table 5.2).

Table 5.2 - Relative hindlimb proportions for each hypothetical frog model. PF = proximal foot. *Note that the model 'PF x 0.5' has the same proportions for what would be 'Thigh x 1' and 'Shank x 1'.

Model	Thigh	Shank	PF	Graph colour
Thigh x 0.5	0.005	0.01	0.005	Red
Thigh x 0.75	0.0075	0.01	0.005	Blue
Thigh x 1	0.01	0.01	0.005	Purple
Thigh x 1.5	0.015	0.01	0.005	Magenta
Thigh x 2	0.02	0.01	0.005	Cyan
Shank x 0.5	0.01	0.005	0.005	Red
Shank x 0.75	0.01	0.0075	0.005	Blue
Shank x 1	0.01	0.01	0.005	Purple
Shank x 1.5	0.01	0.015	0.005	Magenta
Shank x 2	0.01	0.02	0.005	Cyan
PF x 0.25	0.01	0.01	0.0025	Black
PF x 0.5*	0.01	0.01	0.005	Red
PF x 0.75	0.01	0.01	0.0075	Blue
PF x 1	0.01	0.01	0.010	Purple
PF x 1.5	0.01	0.01	0.015	Magenta

Table 5.3 - The range of hindlimb segment ratios for the 164 study species.

Ratio	Maximum	Minimum
Thigh:Shank	1.19	0.73
Shank:Thigh	1.37	0.83
PF:Thigh	0.92	0.40
PF:Shank	0.75	0.40

5.2.5 Statistical analyses

All statistical analyses were carried out in R (Version 4.2.2). The take-off sequence is deemed more kinematically parsimonious when changes in hindlimb segment polar angles and 3D joint angles are comparatively smaller, so maximum-minimum angle change was calculated for each segment and joint in each model. The total protraction-retraction, abduction-adduction, and 3D joint angle change across all three segments/joints were used to represent overall hindlimb motion. The data for most angle changes were not normally distributed (Appendix Table G.1) and could not be normalised through transformation. In order to analyse the relationship

between angle change and locomotor mode, a permutational phylogenetic ANOVA was performed (anova.lm.rrpp function in the *RRPP* package; Collyer & Adams, 2018). The same phylogeny as in Chapter 2 was used (Jetz & Pyron, 2017; see section 2.2.3).

5.3 Results

5.3.1 Simulated versus observed kinematics

Given that the IK model only uses the initial limb configuration and a set of COM targets, the close resemblance between the segment rotations from the IK model and the in vivo take-off sequence indicates successful model validation for the thigh, shank, and proximal foot (Figure 5.5). However, the distal foot does not resemble the *in vivo* kinematics in the abduction-adduction plane. The primary reason for this is the distal accumulation of movement down the limb, and because this landmark represents a point of contact, i.e., as the foot peels off of the ground, the distal foot elongates (Richards et al., 2017). Therefore, the length and position of the distal foot has been fixed according to the first frame of the take-off sequence for subsequent simulations. Exclusion of the distal foot from biomechanical analyses of frog jumping is a common practice due to the complexity of modelling this 'peeling' motion and is not considered to significantly weaken model predictions, given the scope of this and other studies (Kargo & Rome, 2002; Wang et al., 2014; Richards et al., 2017, Richards et al., 2018). Additionally, as the in vivo frog data are from centres of joint rotation estimated from external skin markers, the lengths of the limb segments appear to vary slightly throughout the jump. To better reflect reality, limb segment lengths remain constant throughout the take-off sequence in the IK model (from the initial time frame) and subsequent models of different species use limb lengths measured directly from µCT scans.

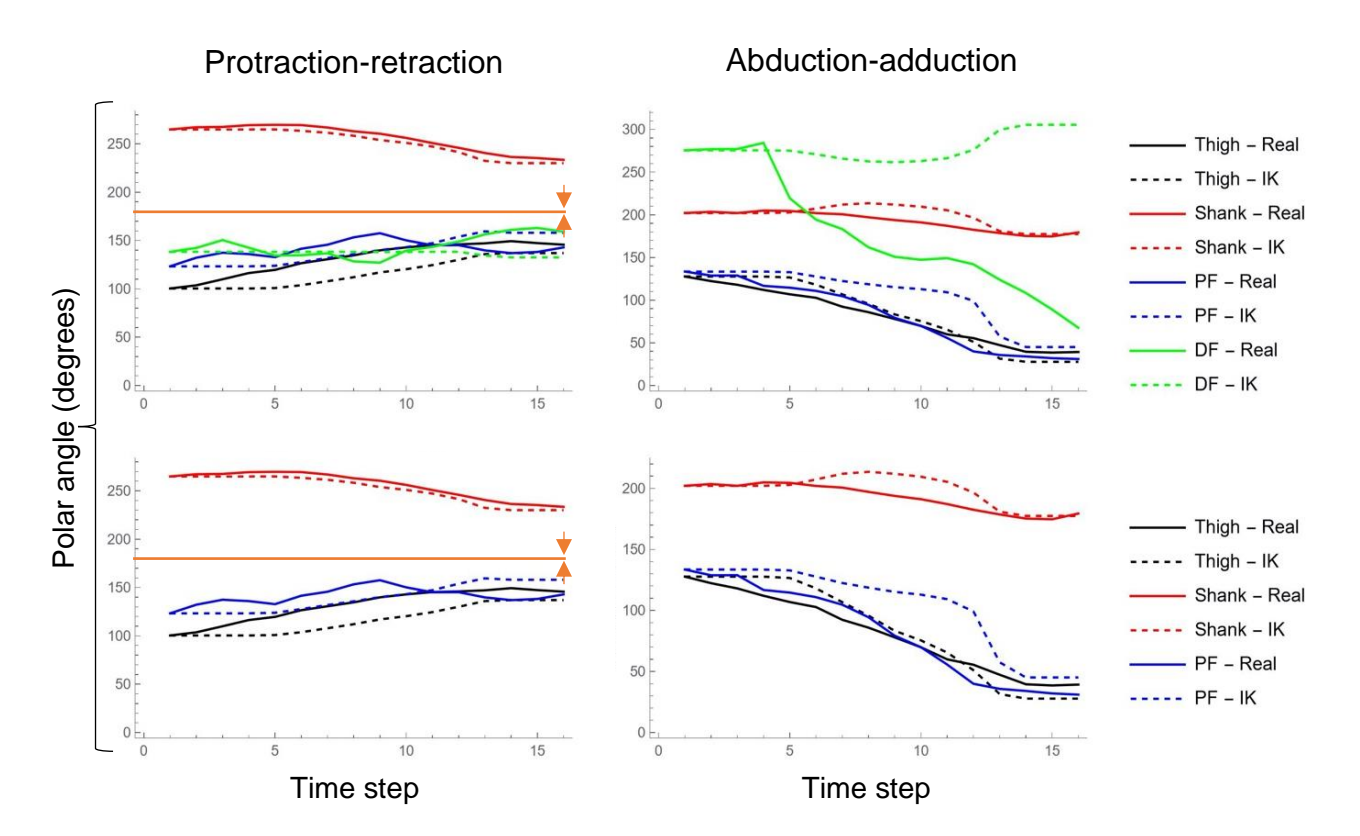


Figure 5.5 - Polar angle graphs from validation of the inverse kinematics (IK) model. The data from the *in vivo P. maculatus* jump (solid lines) and IK model (dashed lines) are coloured according to hindlimb segment, where PF denotes the proximal foot, and DF the distal foot, which is excluded in the second set of graphs for clarity. Movement of protraction-retraction traces towards 180 degrees denotes retraction (orange line). In the abduction-adduction traces, ventral adduction is indicated by downward slopes.

5.3.2 Comparative analysis of hindlimb kinematics in real frogs

Overall limb motion reflects the stereotyped kinematics found for *P. maculatus* regardless of which species' proportions are used – all limb segments retract and adduct throughout the take-off sequence (Figure 5.6; Figure 5.7; Figure 5.8), which propels the body forwards and upwards (Richards *et al.*, 2017). In terms of protraction-retraction, the orientation of the shank remains relatively constant until ~30% of the take-off sequence duration (i.e., the end of the 'preparatory' phase) where it retracts for take-off, while the thigh and proximal foot begin to retract from the onset of motion.

In terms of the differences observed between models, the effects of changing the length of each segment have been summarised in Table 5.4. Most notably,

kinematics are more sensitive to changes in proximal foot length (Figure 5.8) than changes to the lengths of the thigh and shank (Figure 5.7). For example, the largest variation across models is in proximal foot adduction in the final ~40% of the take-off sequence, while thigh retraction is the least sensitive to changes in thigh:shank ratio. When the proximal foot is longer, proximal foot retraction is initially greater, though the proximal foot then begins protracting immediately prior to take-off when it is very long, to the point where the final proximal foot orientation is less retracted compared to the other species (Figure 5.8). The polar angle for shank retraction and adduction also converges prior to take-off, though large differences are present in the middle of the take-off sequence. In terms of 3D joint angles, differences between the models of different hindlimb proportions are marginal (Figure 5.9).

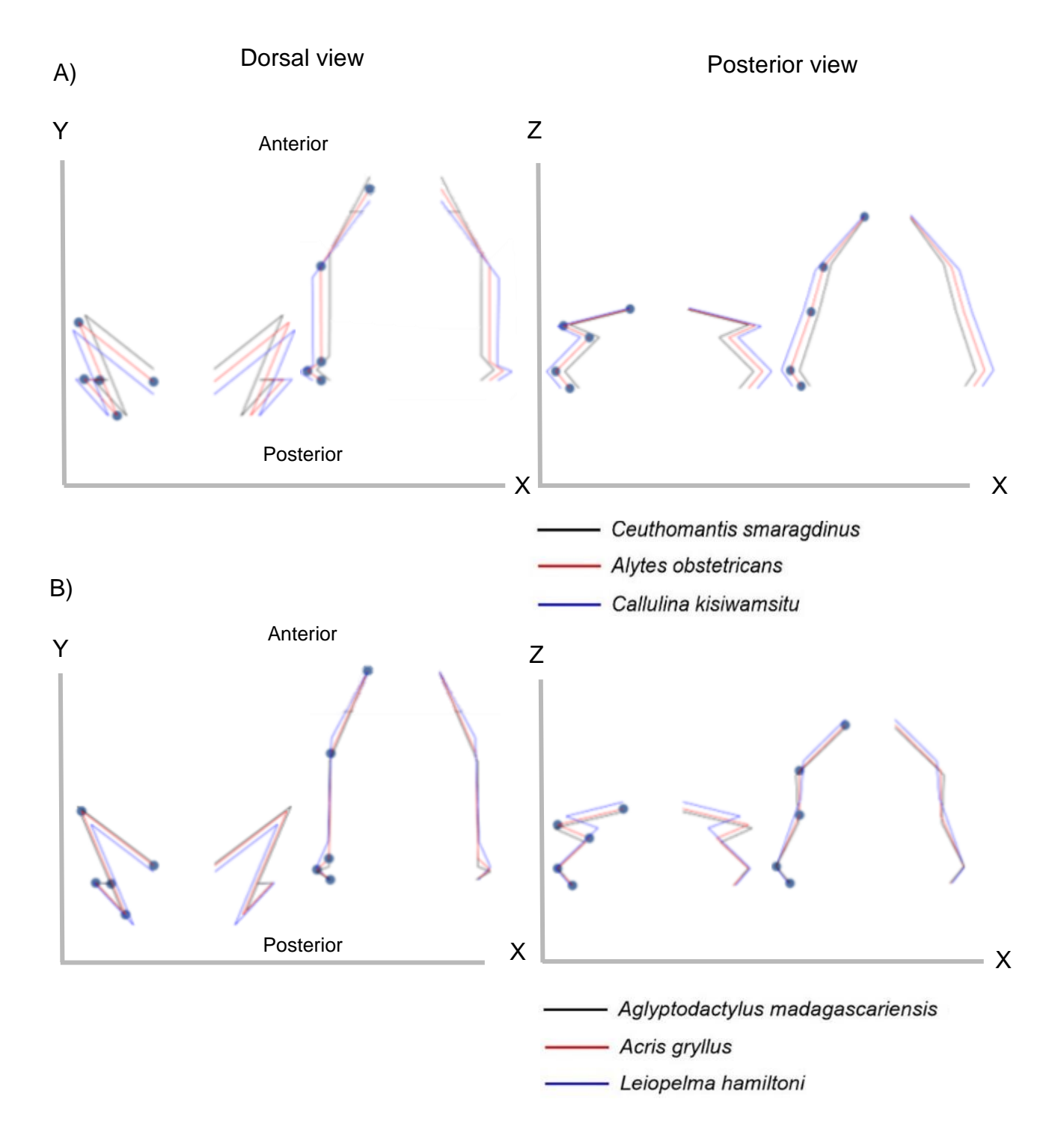


Figure 5.6 - The first and final frames of the take-off sequence for two sets of three species exemplifying variation in A) thigh:shank length ratio and B) proximal foot:total hindlimb length ratio. Blue represents the species with the longest thigh and proximal foot, respectively. The jump occurs along the global Y axis and the distance between the hip joints is identical across simulations. The hindlimbs differ in how they propel the body forwards (dorsal view) and upwards (posterior view).

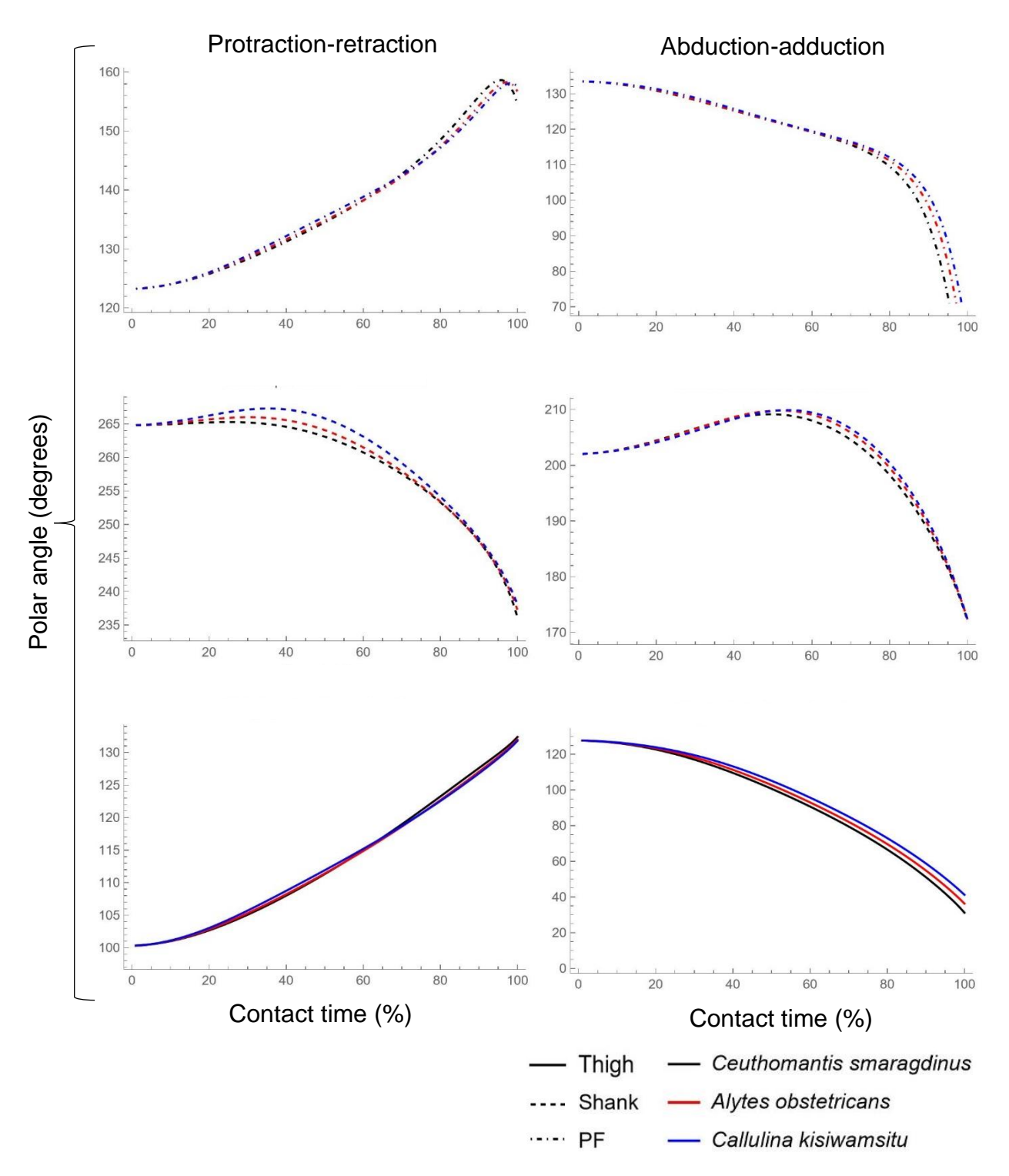


Figure 5.7 - Hindlimb segment kinematics for three species exemplifying variation in thigh:shank length ratio in the form of polar angles. Blue and black represent the species with the longest thigh and shank, respectively. Retraction (left column) is indicated by motions towards 180 degrees (upwards for the thigh and proximal foot (PF), downwards for the shank). Ventral adduction (right column) is indicated by downward slopes for all hindlimb segments. See Appendix Figure G.1 for polar angle velocities.

Page 153 of 286

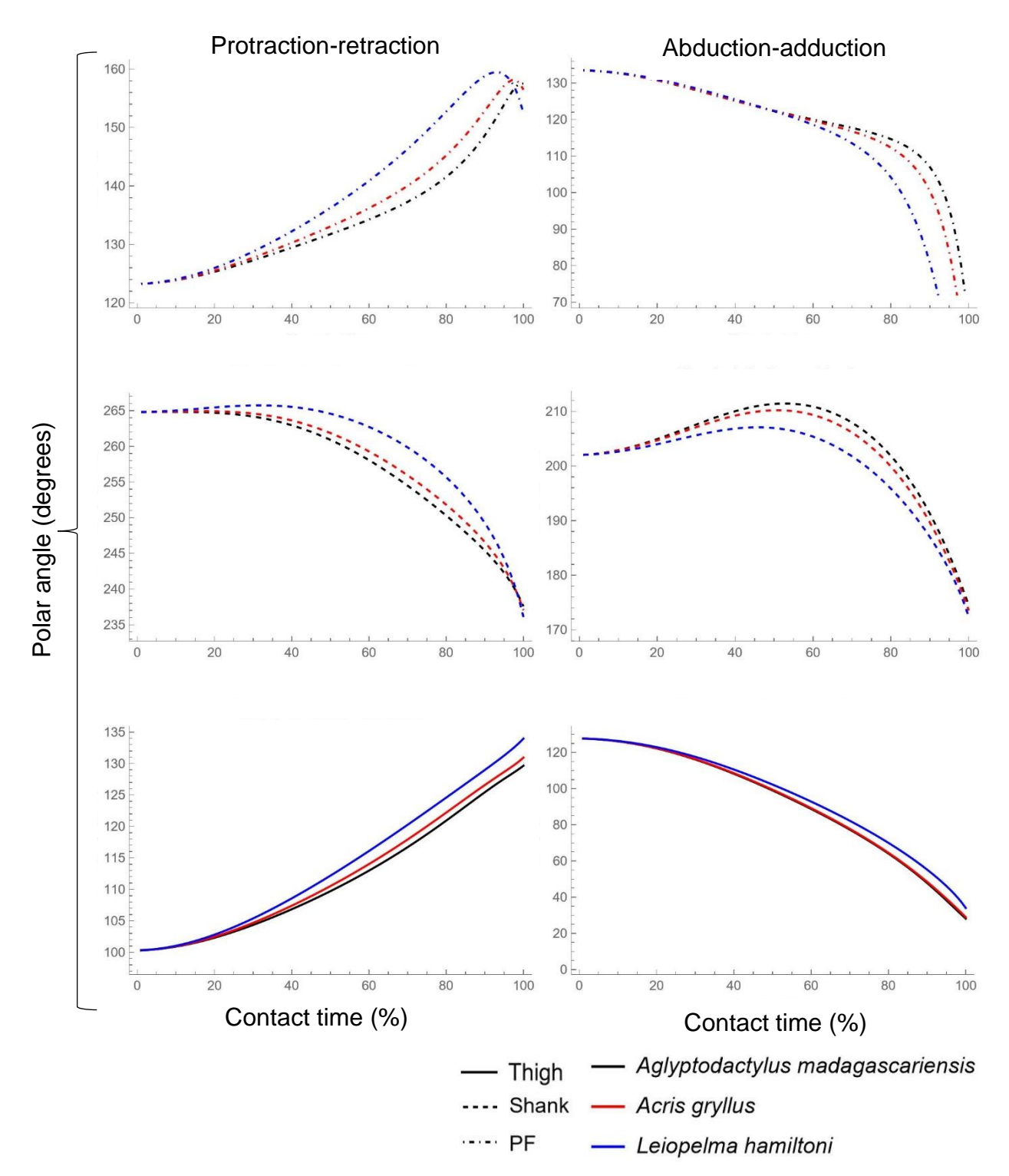


Figure 5.8 - Hindlimb segment kinematics for three species exemplifying variation in proximal foot (PF):total hindlimb length ratio in the form of polar angles. Blue represents the species with the longest PF. Retraction (left column) is indicated by motions towards 180 degrees (upwards for the thigh and PF, downwards for the shank). Ventral adduction (right column) is indicated by downward slopes for all hindlimb segments. See Appendix Figure G.2 for polar angle velocities.

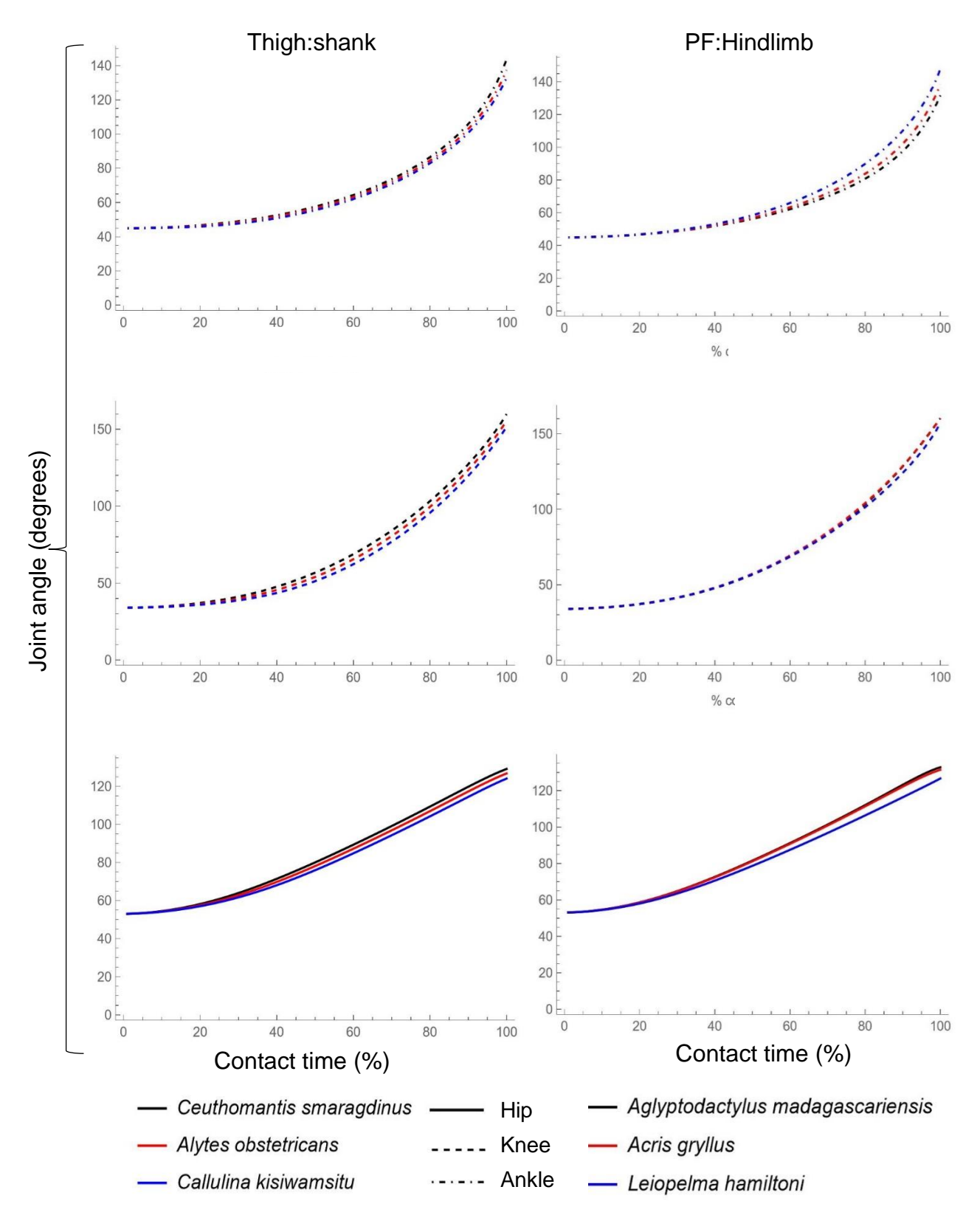


Figure 5.9 - 3D joint angles for two sets of three species exemplifying variation in the ratio between A) thigh and shank length, and B) proximal foot (PF) and total hindlimb length. Blue represents the species' with the longest thigh (A) and PF (B), while black represents the species' with the longest shank (A) and shortest PF (B). Upward slopes indicate greater joint opening. See Appendix Figure G.3 for angular velocities.

Page 155 of 286

Table 5.4 - A summary of the most prominent kinematic effects of elongating or shortening each hindlimb segment. Specific details are in parentheses. Conclusions drawn from both real and hypothetical frog models are in black, while conclusions evidenced only by hypothetical models are in blue. Exceptions to the general trends stated are numbered accordingly and underlined.

Segment change	Effect						
	Thigh retraction is the least sensitive to changes in anatomy						
	(<u>see exception below</u> 1)						
All changes	PF adduction is most sensitive to changes in anatomy						
	Shank initially protracts (<u>see exceptions below</u> ²) and abducts						
	Shank polar angles converge by the final time-step						
	Hip is positioned further posteriorly						
	• Knee is positioned lower to the ground (excluding hypothetical						
	shank models), and further laterally and posteriorly						
Longer	Ankle is positioned lower to the ground in thigh models but						
thigh/shorter	higher in shank models						
shank	Ankle is positioned further laterally						
	Shank initially protracts and abducts more strongly, then						
	shows faster retraction/adduction than other models						
	Shank adducts faster						
	 Ankle initially closes (thigh x 2 and shank x 0.5 only) 						
	Thigh retraction slows towards the end ¹						
	Thigh adducts to a greater extent and faster						
	Shank does not initially protract (hypothetical shank models						
	only) ²						
Shorter	PF retraction peak is earlier and larger, but changes to						
thigh/longer	protraction just before take-off (excluding hypothetical shank						
shank	models)						
	PF adducts earlier and faster (excluding shank models)						
	Hip opens more and faster						
	Knee opens more						
	Ankle opens more (excluding hypothetical shank models)						
	All joints are positioned higher from the ground and further						
	posteriorly						
	Knee and ankle are positioned slightly further medially						
Longer	Thigh retracts more and faster						
proximal	Shank initially protracts more, then retracts faster						
foot (PF)	PF peak retraction is earlier						
	PF changes to protraction just before take-off						
	PF adducts earlier and faster						
	Hip opens faster in final time-steps						

Shorter proximal foot (PF)

- Thigh adducts more
- Shank does not initially protract²
- Shank initially abducts more, then adducts faster
- PF retracts faster close to take-off
- Hip opens more and initially faster
- Ankle for PF x 0.25 opens considerably less and slower

In terms of maximum-minimum angle change, all angles excluding shank abduction-adduction and the knee differed significantly overall between taxa with different primary locomotor modes (Table 5.5). Pairwise tests show that walkerhoppers significantly differ in all angles from arboreal jumpers, terrestrial jumpers, and burrowers (Appendix Table G.2). Both types of jumpers always have significant separation from swimmers in angle changes except for proximal foot abduction-adduction and, for terrestrial jumpers only, thigh abduction-adduction. Terrestrial jumpers never significantly differ from arboreal jumpers and burrowers, and swimmers never significantly differ from burrowers and walkerhoppers for any angles. In terms of evolutionary relationships, the maximumminimum angle changes with the strongest phylogenetic signal are the ankle, sum of all joint angles, and the sum of abduction-adduction angles (Appendix Table G.4). The most evolutionarily labile angle changes are thigh and shank protraction-retraction, as well as the sum of all the protraction-retraction angles. Archaeobatrachia differ from all other phylogenetic groups for all angles, as do the Neobatrachia except for the proximal foot adduction angle, which is not significantly different from both Hyloidea and Ranoidea (Appendix Table G.5). There are never any significant differences between the Hyloidea and Ranoidea.

Table 5.5 - The results of the permutational phylogenetic ANOVAs testing the relationships between angle change and locomotor mode for 164 frogs. Angles which vary significantly among locomotor modes are highlighted in bold. PR = protraction-retraction angle; AA = abduction-adduction angle; PF = proximal foot.

Angle	Sum of	Mean	F-value	Z-value	<i>p</i> -value
	Squares	square			
Thigh PR	0.071	0.018	3.475	2.298	0.011
Thigh AA	1.856	0.464	5.098	3.028	0.002
Shank PR	0.024	0.006	2.529	1.601	0.053
Shank AA	0.059	0.015	1.321	0.621	0.271
PF PR	0.015	0.004	2.894	2.028	0.019
PF AA	5.813	1.453	3.026	2.027	0.017
PR sum	0.214	0.054	3.214	2.108	0.020
AA sum	6.490	1.623	3.272	2.231	0.010
Hip	0.429	0.107	3.164	2.227	0.012
Knee	0.449	0.112	2.217	1.558	0.061
Ankle	1.402	0.350	5.302	3.299	0.001
Joint sum	2.680	0.670	2.884	2.105	0.020

The relationship between each angle change and the length of each segment relative to total hindlimb length is also evaluated. When the relationship is negative, then the motion is more kinematically parsimonious when the segment is longer. All correlations are significant, excluding shank protraction-retraction angle with proximal foot:hindlimb ratio, proximal foot protraction-retraction angle with shank:hindlimb ratio, and 3D hip and knee angle with thigh:hindlimb ratio (Appendix Table G.3). The most prominent trends are as follows (Figure 5.10; Figure 5.11; Figure 5.12):

- When the thigh becomes longer relative to the overall hindlimb, the change
 in thigh and proximal foot protraction-retraction, proximal foot abductionadduction, and ankle angle becomes smaller, while the change in shank
 protraction-retraction and abduction-adduction becomes larger.
- When the shank becomes longer relative to the overall hindlimb, the change in thigh and shank protraction-retraction becomes smaller, while the change in thigh abduction-adduction and all three joint angles becomes larger.
- When the proximal foot becomes longer relative to the overall hindlimb, the change in thigh and shank abduction-adduction, and hip and knee angle becomes smaller, while the change in thigh and proximal foot protraction-

retraction, proximal foot abduction-adduction, and ankle angle becomes larger.

Regardless of locomotor mode, the direction of the significant correlations (i.e., positive or negative relationship with relative segment length) is almost always the same (Figure 5.10; Figure 5.11; Figure 5.12; Appendix Figure G.8; Appendix Figure G.9). The notable exceptions are swimmers, which often have trends in the opposite direction (Figure 5.10; Figure 5.11) and only have significant correlations between relative segment length and some 3D joint angles (Figure 5.12; Appendix Figure G.9). However, these results could be due to insufficient sampling (n = 9). There are also no significant correlations between shank:hindlimb ratio and shank abduction-adduction angle for any locomotor modes (Figure 5.11), despite the significant general correlation when all locomotor modes are considered (Appendix Table G.3). Similarly, while there is no general trend for proximal foot protraction-retraction with shank:hindlimb ratio, this relationship is significant for terrestrial and arboreal jumpers (Figure 5.10).

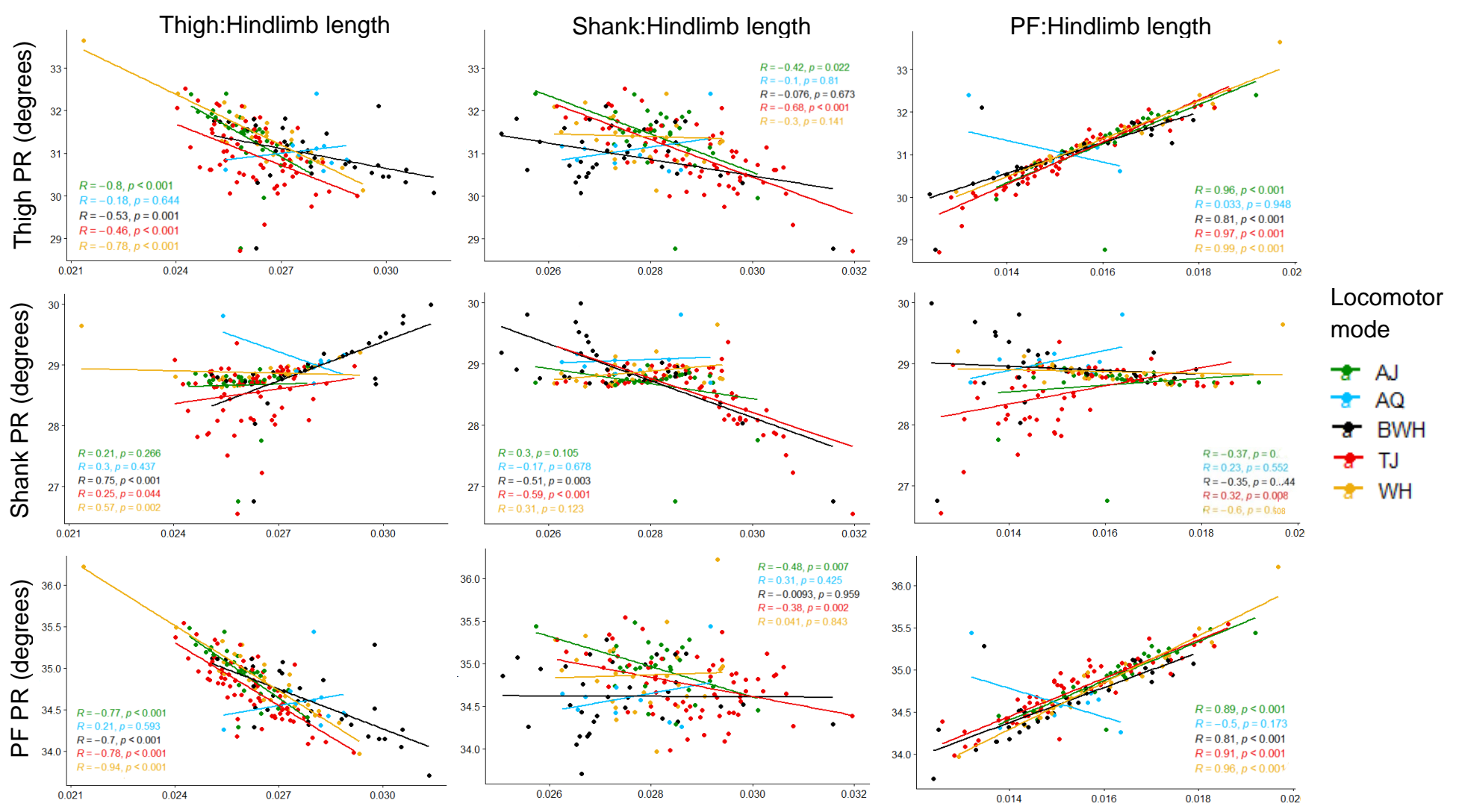


Figure 5.10 - Maximum-minimum protraction-retraction (PR) angle against relative segment length for 164 frog taxa. The data are colour coded according to locomotor mode. The statistics reported refer to Spearman's rank tests for the thigh and shank PR angle, and Pearsons's correlation tests for the proximal foot (PF) PR angle.

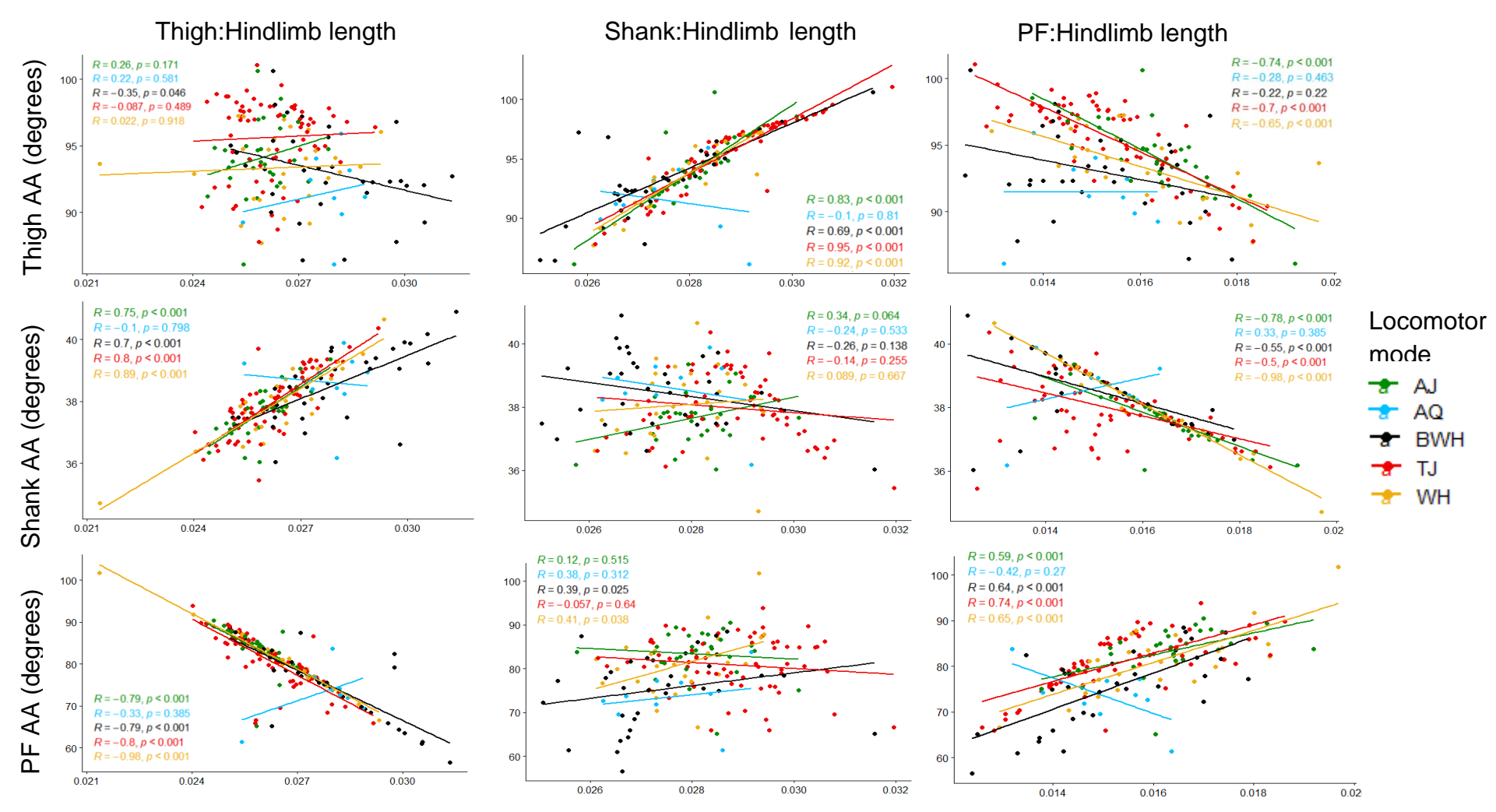


Figure 5.11 - Maximum-minimum abduction-adduction (AA) angle against relative segment length for 164 frog taxa. The data are colour coded according to locomotor mode. The statistics reported refer to Spearman's rank tests for the thigh and proximal foot (PF) AA angle, and Pearsons's correlation tests for the shank AA angle.

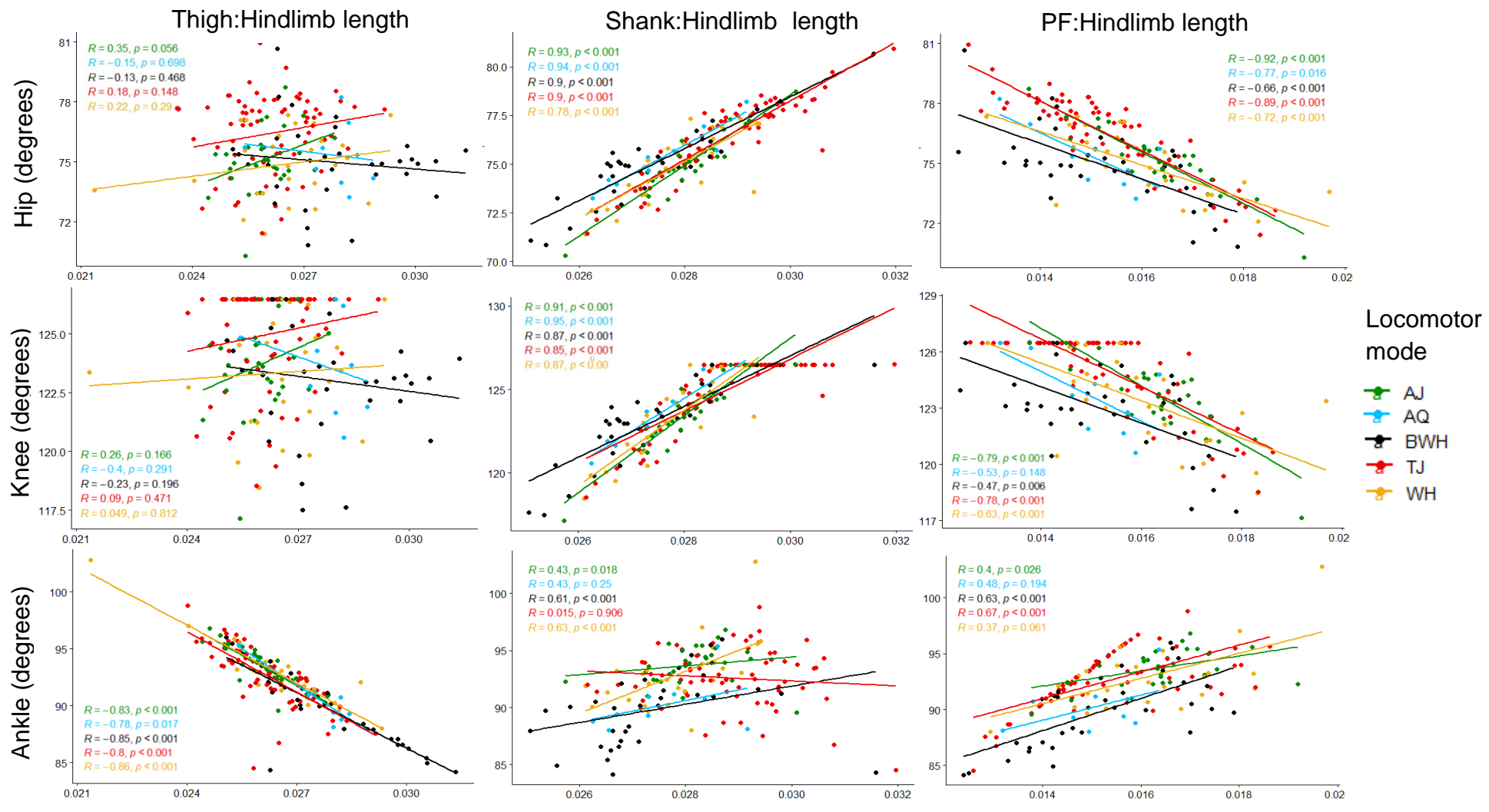


Figure 5.12 - Maximum-minimum 3D joint angle for in degrees against relative segment length for 164 frog taxa. The data are colour coded according to locomotor mode. PF = proximal foot. The statistics reported refer to Pearson's correlation tests for the hip angle, and Spearmen's correlation tests for the knee and ankle angle.

5.3.3 The effect of different hindlimb proportions on kinematics in hypothetical frog models

The hypothetical models yield results very similar to the models of real frog proportions (Table 5.4). The only contrast in terms of joint position is that ankle is positioned higher above the ground both when the thigh is long and when the shank is long relative to total hindlimb length in each respective model (Figure 5.13). For polar angles, the effect of changing the relative length of the thigh and shank are much more distinct (Figure 5.14; Figure 5.15). While protraction-retraction kinematics of the thigh appear to remain relatively robust to changes in any segment length, the retraction and adduction kinematics of the proximal foot are the most variable (Figure 5.16). Hypothetical shank models differ from real models in that the shank does not initially protract when the shank is longer, and there are highly variable retraction kinematics in the middle of the take-off sequence, followed by a convergence by the point of take-off for both the proximal foot and shank (Figure 5.15). In terms of 3D joint angles, differences can be seen much more clearly in hypothetical models (Figure 5.17). For instance, the hip, knee, and ankle all show smaller rotations when the thigh is longer than the shank. In addition, the initial closure of the ankle when the thigh is longest, or shank is shortest, is not detectable in real frog models. The differences in maximum-minimum polar and 3D joint angles for each hypothetical model can be found in Table 5.6 and Table 5.7, respectively.

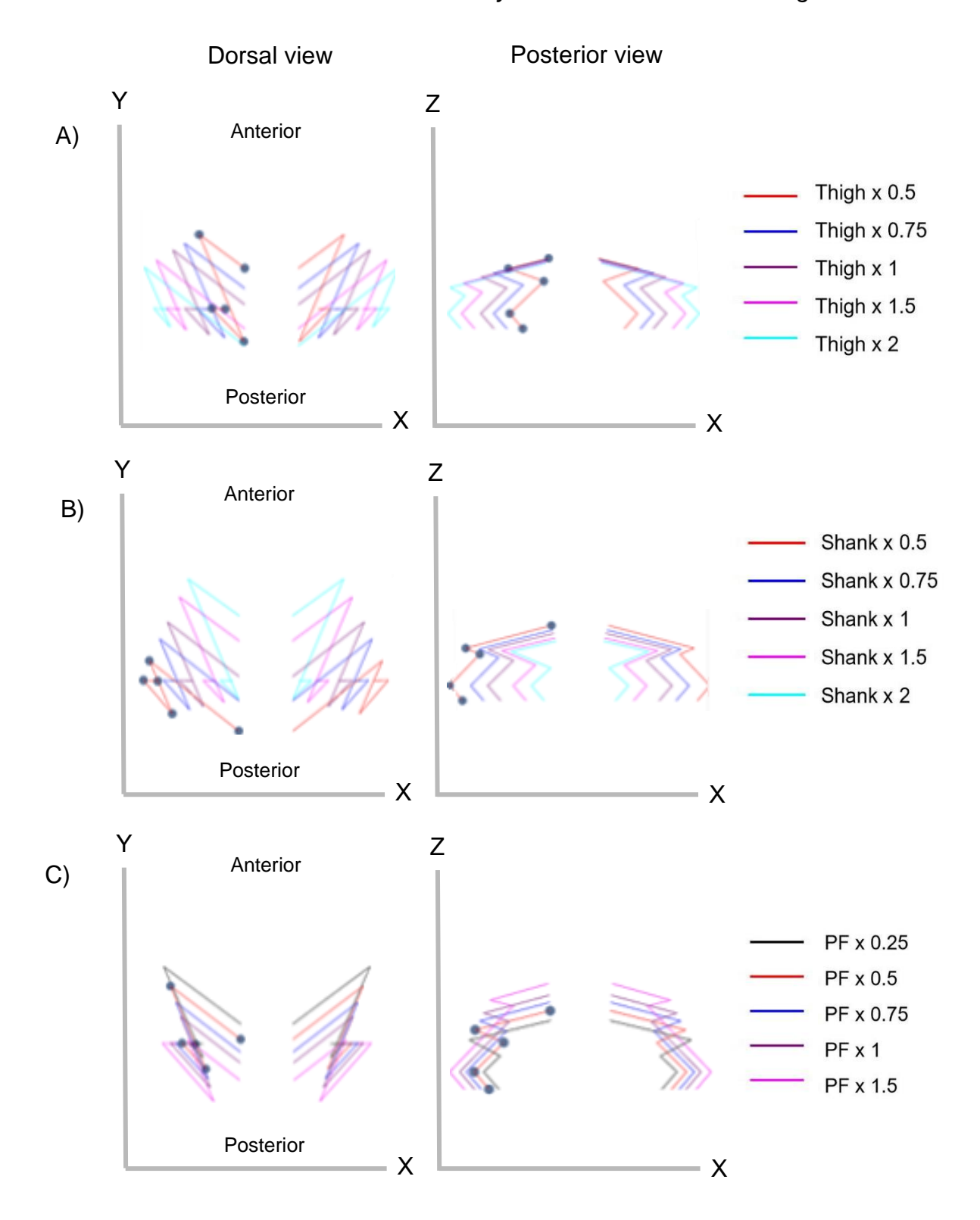


Figure 5.13 - The first frame of the take-off sequence for hypothetical thigh (A), shank (B) and proximal foot (PF) (C) proportions to illustrate how hindlimbs differ when propelling the body forwards (dorsal view) and upwards (posterior view). The jump occurs along the global Y axis and the distance between the hip joints is identical across simulations.

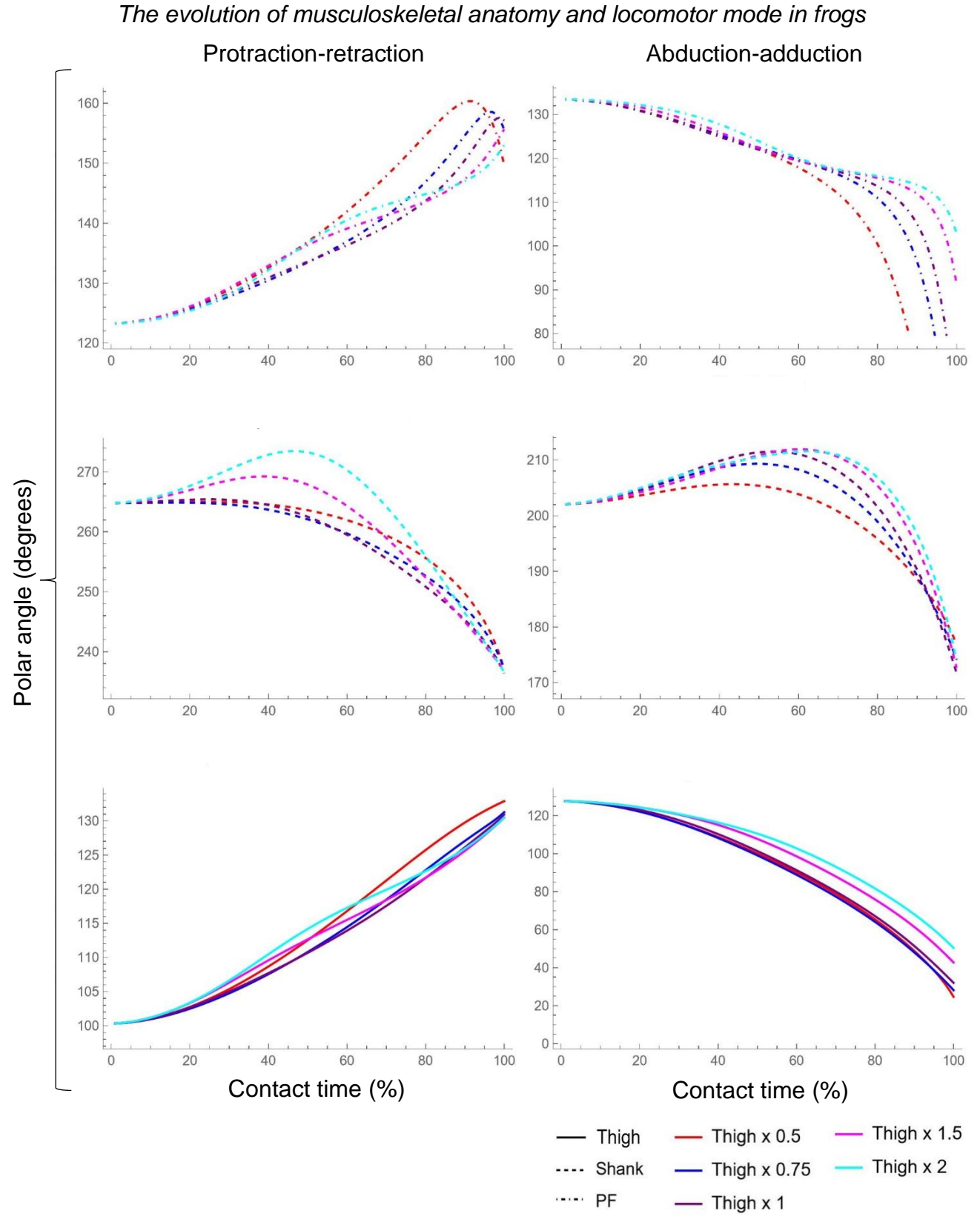


Figure 5.14 - Hindlimb segment kinematics for hypothetical thigh proportions in the form of polar angles. Each colour represents a different model of thigh length relative to shank length. Retraction (left column) of the thigh and proximal foot (PF) is indicated by upward slopes, while negative slopes indicate shank retraction. Ventral adduction (right column) is indicated by downward slopes for all segments. See Appendix Figure G.4 for polar angle velocities.

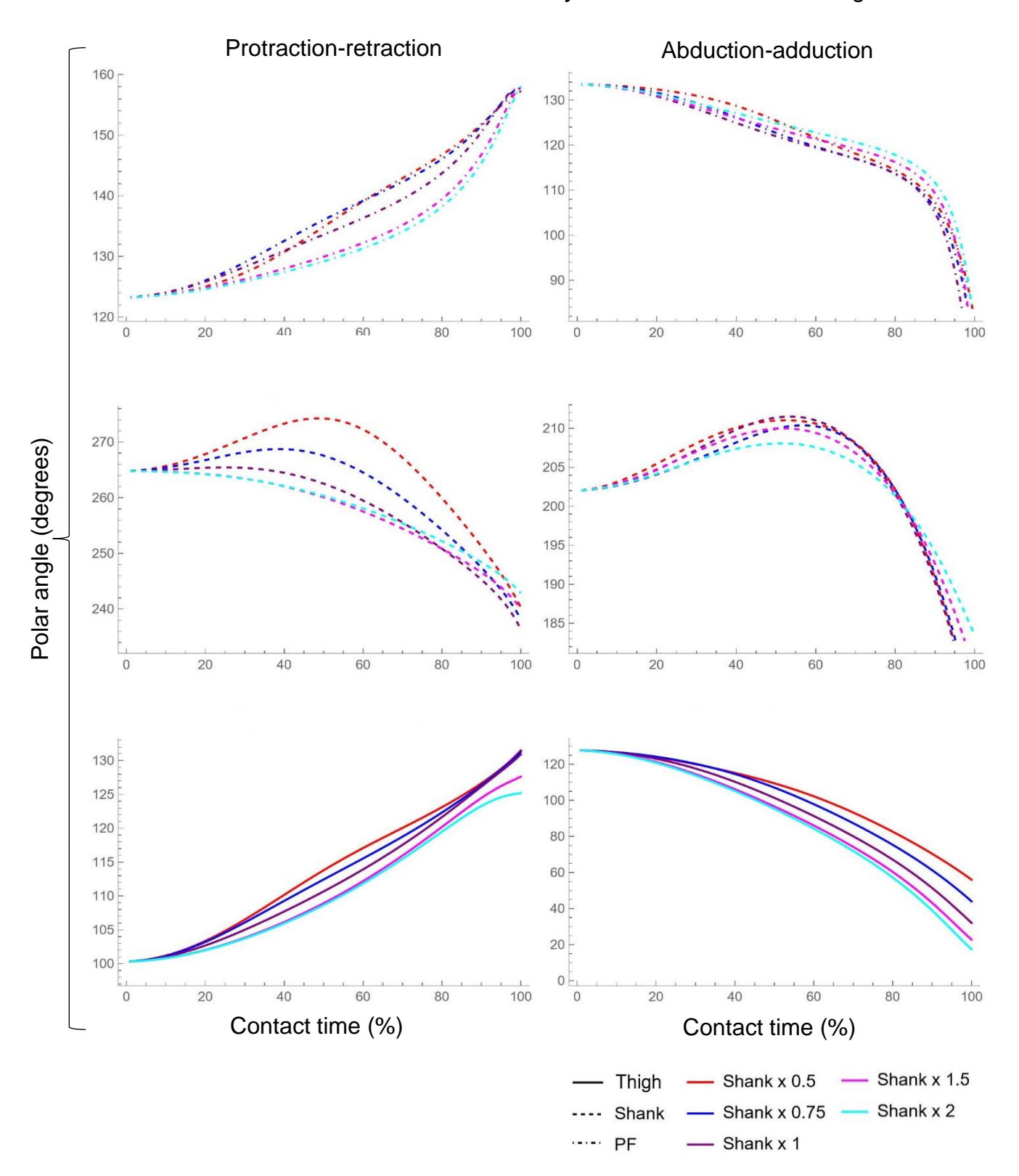


Figure 5.15 - Hindlimb segment kinematics for hypothetical shank proportions in the form of polar angles. Each colour represents a different model of shank length relative to thigh length. Retraction (left column) of the thigh and proximal foot (PF) is indicated by upward slopes, while negative slopes indicate shank retraction. Ventral adduction (right column) is indicated by downward slopes for all segments. See Appendix Figure G.5 for polar angle velocities.

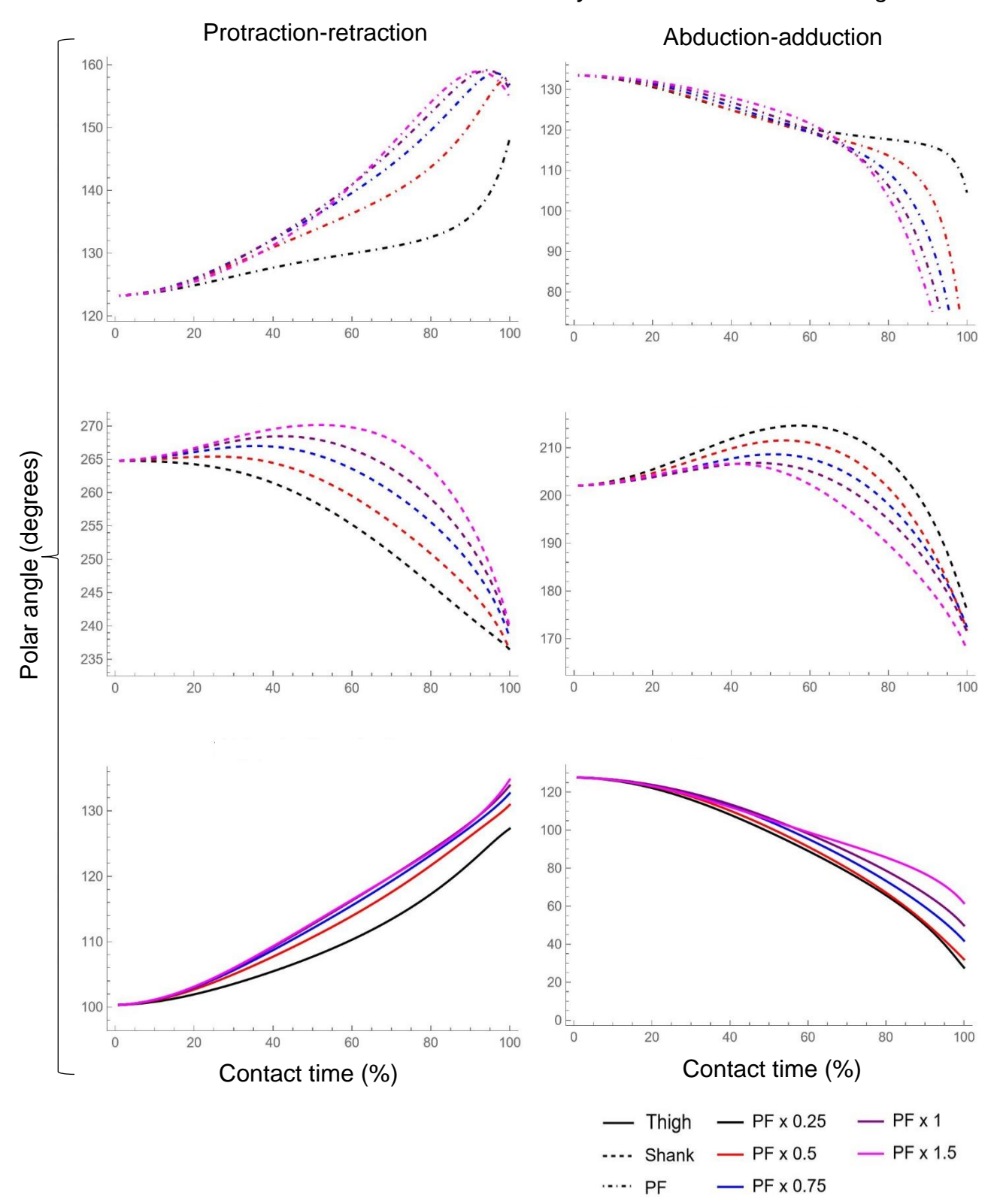


Figure 5.16 - Hindlimb segment kinematics for hypothetical proximal foot (PF) proportions in the form of polar angles. Each colour represents a different model of PF length relative to proximal segment length (thigh and shank are the same length). Retraction (left column) of the thigh and proximal foot (PF) is indicated by upward slopes, while negative slopes indicate shank retraction. Ventral adduction (right column) is indicated by downward slopes for all segments. See Appendix Figure G.6 for polar angle velocities.

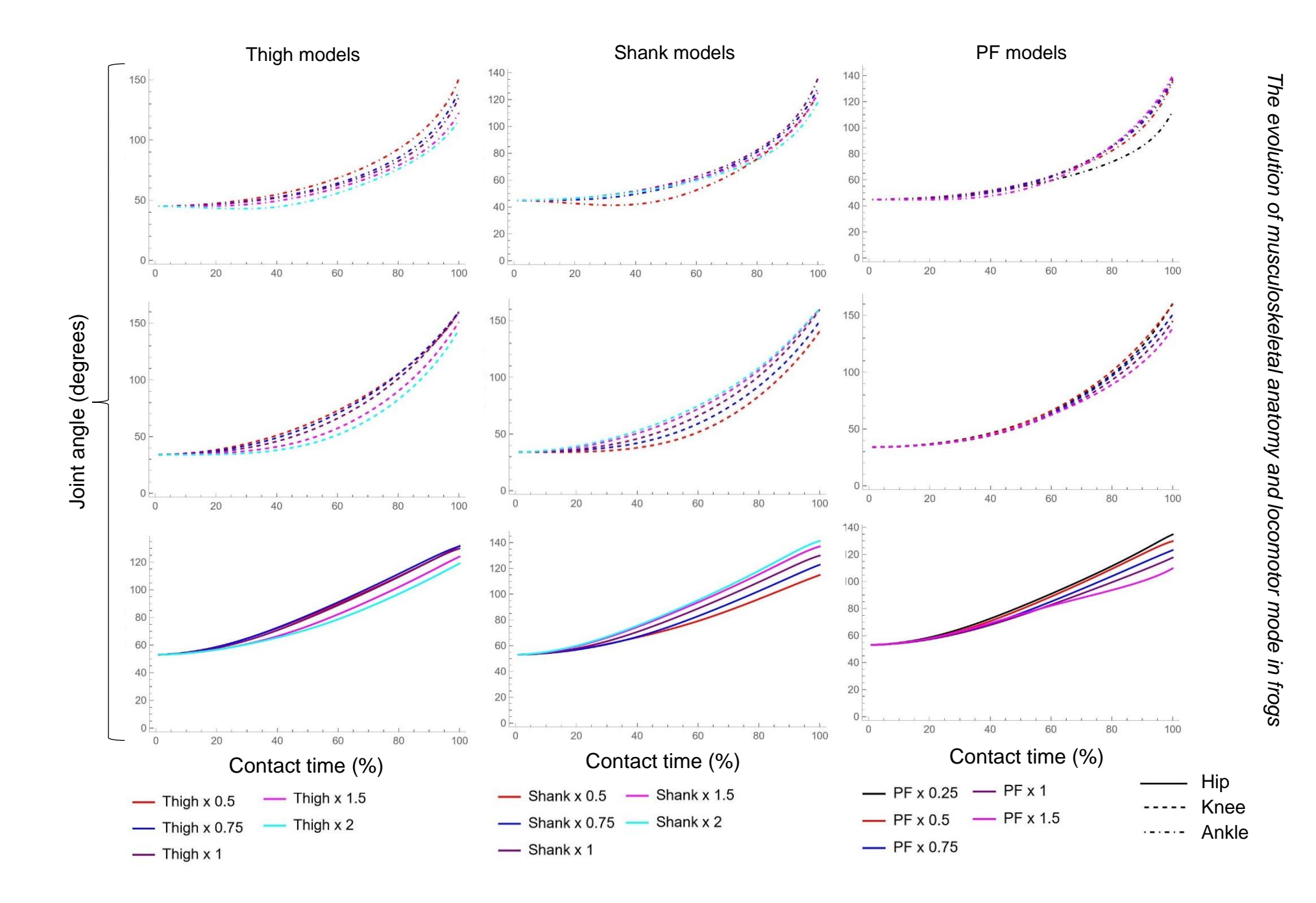


Figure 5.17 - 3D joint angles for hypothetical thigh (A), shank (B) and proximal foot (PF) (C) proportions. Upward slopes indicate greater joint opening. See Appendix Figure G.7 for angular velocities.

Table 5.6 - The difference between maximum and minimum protraction-retraction (PR) and abduction-adduction (AA) polar angles during the take-off sequence for each hindlimb segment in each model of hypothetical hindlimb proportions. The smallest angle changes for each set of models are highlighted in grey, and the smallest overall angle change across all models is in bold. PF = proximal foot. *Note that model 'PF x 0.5' results in the same values as what would be for 'Thigh x 1' and 'Shank x 1'.

	Measu	rement d	ata (m)	Polar angle (degrees)							
Model	Thigh	Shank	PF	Thigh PR	Thigh AA	Shank PR	Shank AA	PF PR	PF AA	PR total	AA total
Thigh x 0.5	0.005	0.01	0.005	32.57	103.03	27.98	28.78	37.09	112.65	97.65	244.45
Thigh x 0.75	0.0075	0.01	0.005	30.95	99.54	27.71	35.21	35.28	91.57	93.95	226.31
Thigh x 1.5	0.015	0.01	0.005	30.15	84.93	32.60	39.26	32.39	42.19	95.14	166.38
Thigh x 2	0.02	0.01	0.005	30.17	77.29	36.84	37.53	29.77	30.60	96.79	145.42
Shank x 0.5	0.01	0.005	0.005	31.16	71.69	33.96	40.21	34.02	52.32	99.15	164.22
Shank x 0.75	0.01	0.0075	0.005	30.98	83.70	30.54	37.96	34.50	59.94	96.02	181.60
Shank x 1.5	0.01	0.015	0.005	27.29	104.90	24.77	31.01	34.75	62.75	86.81	198.65
Shank x 2	0.01	0.02	0.005	24.88	110.22	21.94	24.60	34.82	54.82	81.64	189.64
PF x 0.25	0.01	0.01	0.005	26.96	100.01	28.33	38.66	25.06	28.95	80.35	167.62
PF x 0.5*	0.01	0.01	0.005	30.60	95.64	29.07	39.83	34.32	73.91	93.99	209.38
PF x 0.75	0.01	0.01	0.0075	32.37	85.83	28.72	36.22	35.41	83.06	96.50	205.11
PF x 1	0.01	0.01	0.01	33.55	77.82	29.11	35.43	35.86	87.41	98.53	200.67
PF x 1.5	0.01	0.01	0.015	34.45	66.07	30.33	38.91	35.68	88.97	100.46	193.95

Table 5.7 - The difference between maximum and minimum 3D joint angles during the take-off sequence for each hindlimb joint in each model of hypothetical hindlimb proportions. The smallest angle changes for each set of models are highlighted in grey, and the smallest overall angle change across all models is in bold. PF = proximal foot. *Note that model 'PF x 0.5' results in the same values as what would be for 'Thigh x 1' and 'Shank x 1'.

	Measurement data (m)			3D joint angle (degrees)			
Model	Thigh	Shank	PF	Hip	Knee	Ankle	Joint total
Thigh x 0.5	0.005	0.01	0.005	78.70	126.50	105.97	311.17
Thigh x 0.75	0.0075	0.01	0.005	78.46	126.49	95.86	300.81
Thigh x 1.5	0.015	0.01	0.005	70.92	117.10	77.60	265.61
Thigh x 2	0.02	0.01	0.005	65.96	110.26	73.51	249.73
Shank x 0.5	0.01	0.005	0.005	61.73	106.79	82.79	251.31
Shank x 0.75	0.01	0.075	0.005	69.68	115.59	83.32	268.59
Shank x 1.5	0.01	0.015	0.005	83.86	126.50	80.23	290.59
Shank x 2	0.01	0.02	0.005	88.16	126.50	73.04	287.70
PF x 0.25	0.01	0.01	0.0025	81.75	126.49	68.05	276.29
PF x 0.5*	0.01	0.01	0.005	76.78	125.93	90.57	293.28
PF x 0.75	0.01	0.01	0.0075	70.15	116.92	91.92	279.00
PF x 1	0.01	0.01	0.01	64.65	111.13	93.12	268.90
PF x 1.5	0.01	0.01	0.015	56.68	105.01	95.28	256.98

5.4 Discussion

To understand the evolutionary origins of locomotion, behaviour should be analysed across broader ecological and phylogenetic contexts (Robovska-Havelkova et al., 2014). Until now, there have been no studies which explore the effect of different hindlimb proportions on anuran jumping motion across taxa representing all primary locomotor modes and major phylogenetic groups. Inverse kinematics (IK) models provide the ideal approach for detecting subtle changes in a complex, multi-jointed system for many taxa in a relatively short time frame (Richards & Porro, 2018). This chapter uses the skeletal morphometrics data collected in Chapter 2 to build and validate an IK model which can simulate the take-off sequence for all 164 taxa, as well as hypothetical frog morphologies which cover both realistic and unrealistic hindlimb proportions. This IK model was used to test two hypotheses: there will be smaller segment rotations during the take-off sequence (i.e., take-off is more kinematically parsimonious) when 1) the shank is longer than the thigh and 2) the proximal foot is long relative to the more proximal hindlimb segments. In summary, I find that kinematic parsimony is segment-specific, and that biomechanical tradeoffs may be occurring. Patterns in the sensitivity of segment kinematics to anatomical changes indicate that there may be a functional advantage to having kinematics remaining constant even as hindlimb proportions change. Some locomotor modes differ significantly in their kinematics while others do not, suggesting complex interactions between form and function. Furthermore, joint positions are likely changing with varying segment lengths, which could have large consequences for joint dynamics.

5.4.1 Take-off kinematics varies with hindlimb proportions, but not entirely as hypothesised

Results from Chapter 2 and other studies have indicated that elongation of the shank and proximal foot is strongly associated with frogs specialising in jumping locomotion (Table 5.1; James & Wilson, 2008; Jorgensen & Reilly, 2013; Lires *et al.*, 2016; Gómez & Lires, 2019). These findings are supported when examining 3D joint angles, as a longer proximal foot results in smaller joint rotations throughout the jump (Table 5.7; Appendix Figure G.9). However, in terms of segment polar angles, a longer thigh and shorter proximal foot appears to generally result in the most kinematically parsimonious overall hindlimb motion (Table 5.6; Appendix

Figure G.8; Appendix Figure G.9). In terms of locomotor mode, the species with the smallest total change in hindlimb abduction-adduction angle (Appendix Figure G.8) and overall joint angles (Appendix Figure G.9) are mostly burrowers, which have a relatively short shank and proximal foot compared to jumpers (Table 5.1). However, it is important to note that the initial hypotheses refer only to overall hindlimb motion - it is only when the segment-specific kinematics are examined that it becomes clear that there are more complex interactions between anatomy and kinematics than initially hypothesised.

5.4.2 Kinematic trade-offs between segments may be key to optimising the take-off sequence

The segment-specific results of this chapter ultimately support the conclusion made in Chapter 2 – that examining only total hindlimb anatomy is not a reliable way of inferring locomotor mode, and that the examination of deeper trends are required to fully understand the relationships between anatomy and function. What is best for jumping in terms of kinematics will likely differ between segments, as each segment is hypothesised to have a different function (Enriquez-Urzelai et al., 2015). For example, increasing the length of the shank generally results in more parsimonious shank kinematics (Figure 5.7; Figure 5.10; Figure 5.11; Figure 5.14; Figure 5.15; Table 5.6). If shank motion is more important to keep minimised (i.e., the muscles moving the shank are having to work less to achieve the same motion), then the other segments could either afford to compensate, or be less constrained, i.e., their anatomy is able to vary more while performance is maintained. Similarly, each joint has different roles in locomotion. The muscles spanning the hip and ankle are the most prominent contributors to hindlimb extension in the cranio-caudal plane (i.e., driving the body forwards), while the knee drives the body upwards, allowing finetuning of jump trajectory (Porro et al., 2017). Although a longer proximal foot results in larger ankle rotation, this could enable the hip and knee to have more kinematically parsimonious motion (Figure 5.9). Additionally, as an optimal jump requires both forward thrust and upward elevation, there could be a morphological configuration that optimises both retraction and adduction.

Another indicator of the presence of kinematic trade-offs is that hindlimb segment kinematics differ in their sensitivity to length changes at different points during the take-off sequence. Shank (and occasionally proximal foot retraction) kinematics vary most in the middle of the take-off sequence, before converging by the point of

take-off (Figure 5.7; Figure 5.8; Figure 5.14; Figure 5.15; Figure 5.16). If the final shank polar angles are being conserved, does this mean that what happens in the middle of take-off is less important? Or is this where more morphological variation is "allowed" to occur? Future studies should further investigate what point during the take-off sequence is most important for overall jump performance.

Proximal foot abduction-adduction kinematics show considerable changes whenever any segment changes in length (including when relative proximal foot length itself remains identical in the hypothetical models), while the protractionretraction kinematics of the thigh are the most conserved across simulations. Normally, this would be unsurprising as frogs experience a proximal to distal accumulation in joint motion (Astley & Roberts, 2014; Richards et al., 2017). However, this IK model has been built using the hip as the base of motion (rather than the foot) to simplify the mathematics. Therefore, these results occur despite the model not incorporating the proximal to distal pattern found in real frogs. Less sensitive kinematics could represent a motion which is more important to conserve through coordinated changes in morphology and, by extension, evolutionary history. As the proximal foot has the most variable kinematics, it may be kinematically compensating for the reduced motion in other segments which may experience greater restraints on morphology. Investigating this relationship further could provide substantial insights into the relationship between form and function - are distal limb segments having a disproportionally greater impact relative to their size because distal bones are more labile to changes in response to selection (Wyngaarden & Hopyan, 2008; Stepanova & Womack, 2020)? Using the present findings as a foundation, future studies may wish to investigate whether greater variation in the shape of a distal segment also creates greater variation in terms of mechanical performance.

5.4.3 Hindlimb proportions affect joint positioning and direction of movement, potentially influencing jumping dynamics

The position of the joints in 3D space are important to consider because their proximity to the ground reaction force (GRF) vector will determine the amount of rotational force (torque) produced by that joint. For example, GRF orientation is posterior and medial to the knee, which plays a significant mechanical role in jumping (Porro *et al.*, 2017). As proximal foot length increases, knee position is moved further posteriorly and aligns more closely with the body midline (Figure 5.6;

Figure 5.13). If this causes the GRF to pass closer to the knee, the external moment arm will be reduced, thus increasing the effective mechanical advantage of the muscles crossing the knee throughout the take-off sequence (Porro *et al.*, 2017). However, it is not yet known whether a shift in joint positions also shifts the orientation of the GRF vector, which could disrupt any beneficial shortening of the external moment arm.

Additionally, there are some instances where segments and joints change their direction of motion which could impact the direction of joint torques throughout the take-off sequence. For example, the shank abducts during the preparatory phase the take-off sequence (i.e., until ~60-65%) before adducting. However, the hypothetical models reveal some instances where this change does not occur, as well as new instances of directions changing. Firstly, the shank does not initially protract during the preparatory take-off phase when the shank is considerably longer than the thigh (Figure 5.15) or when the proximal foot is a quarter of the length of the more proximal segments (Figure 5.16). Secondly, a shorter thigh and longer proximal foot can result in proximal foot retraction slowing to the point where it begins to protract in the final ~5-10% of the take-off sequence (Figure 5.14; Figure 5.16). Finally, the ankle closes slightly before opening when the shank length is half of the thigh length (Figure 5.17).

5.4.4 The route to take-off differs significantly between locomotor modes

Several interesting similarities and differences are identified between locomotor modes. Firstly, terrestrial and arboreal jumpers did not show any significant differences in angle changes across the entire hindlimb during the take-off sequence. Considering the findings of Chapter 3, differences in hindlimb myology, rather hindlimb kinematics, appear to be the primary driver of functional differences between habitat types in jumpers. Secondly, despite previous studies stating that there is no trade-off in performance for jumping and swimming (Nauwelaerts *et al.*, 2007), jumping kinematics are significantly different for frogs who specialise in swimming. This aligns with the findings of Robovska-Havelkova *et al.* (2014), who found important differences in swimming kinematics between frogs with different lifestyles. Since thigh and proximal foot abduction-adduction show the only non-significant comparisons between jumpers and swimmers, this implies that these motions are potentially similar for both functions. Surprisingly, burrowers do not differ from terrestrial jumpers nor swimmers for any of the angles, but they did differ

from walker-hoppers (Appendix Table G.2). Compared to non-burrowers, burrowers generate significantly less jumping power in behavioural experiments, especially when frogs have a higher body mass (Mendoza *et al.*, 2020). Additionally, burrowing species tend to have a shorter tibiofibula relative to total hindlimb length (Table 5.1; Enriquez-Urzelai *et al.*, 2015), which is said to increase the force generated while scooping substrate (Emerson, 1976; Vidal-García *et al.*, 2014), but is detrimental to jump performance. There are other factors besides hindlimb proportions that differentiate between these two locomotor modes, such as bone thickness (Chapter 2) and hindlimb myology (Chapter 3). More studies on burrowing mechanics are needed to make sense of the similar kinematics observed between jumpers and burrowers during take-off.

5.4.5 Testing unoccupied areas of morphospace

Hypothetical models were tested to identify causal relationships and underlying mechanisms more easily, because a group of frogs with identical relative hindlimb proportions excluding one small difference is not likely to exist. A variety of models with both realistic and unrealistic proportions were tested to explore unoccupied areas of morphospace. The hypothetical models were also designed to enable comparisons between models where the length of two segments relative to each other is the same while their lengths relative to the overall hindlimb are different (Figure 5.18). By comparing these kinds of complementary models, the different impacts of relative segment lengths on hindlimb kinematics can be examined. For instance, in the two models where the shank is half the length of the thigh, the shank's length relative to the proximal foot differs (i.e., in 'shank x 0.5, the shank is the same length as the proximal foot, whereas it is double the length of the proximal foot in 'thigh x 2'). When the shank is half the length of the thigh, kinematics are almost identical across both hypothetical thigh and shank models (Appendix Figure H.1). However, when the thigh is half the length of the shank, there are comparatively large differences, i.e., the 'shank x 2' model generally has much smaller rotations than the 'thigh x 0.5' model. This means that changing the length of the shank relative to the proximal foot has a larger impact on jump kinematics compared to the thigh, which could potentially be because the shank and proximal foot share the ankle joint. Dynamics models will be required to test whether these complementary hypothetical models show similar patterns in the production of ankle torque.

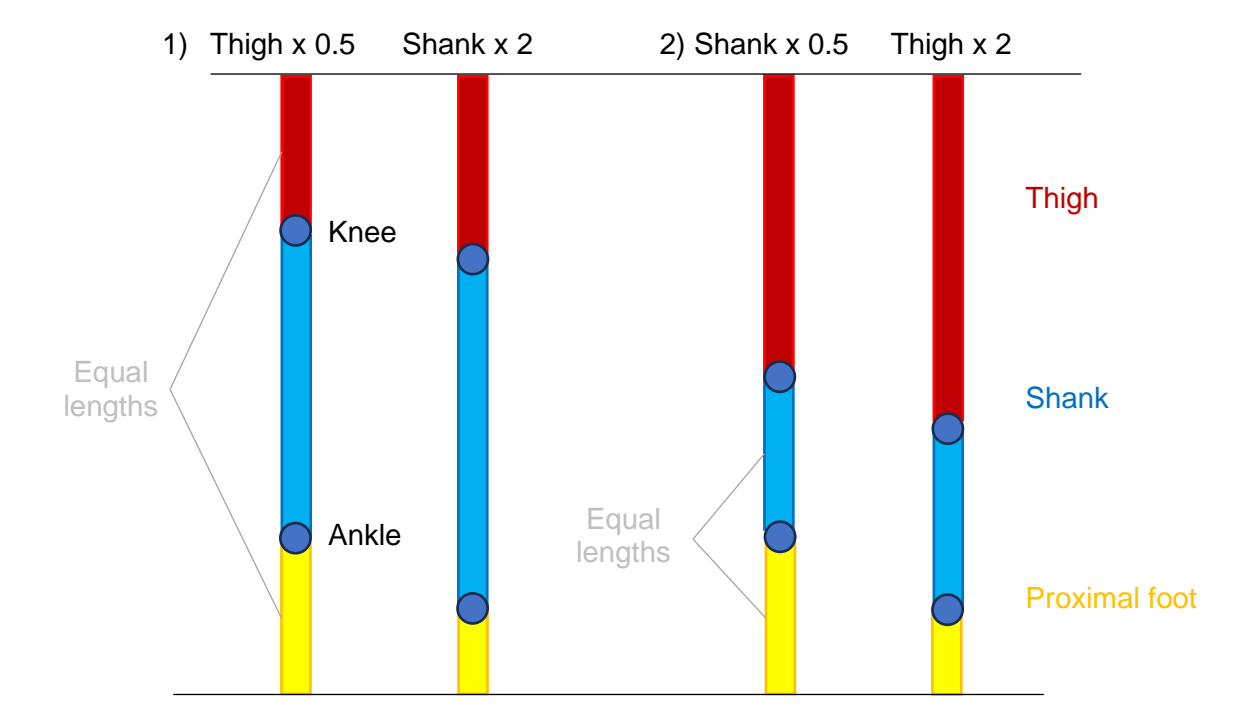


Figure 5.18 - A visual representation of the hindlimb in the two sets of 'complementary' hypothetical models, where 1) the thigh is exactly half the length of the shank, and 2) the shank is exactly half the length of the thigh. In the 'x 0.5' models, the segment being referred to is the exact same length as the proximal foot. The total hindlimb length is the same across models, as shown by the black lines, so the only difference within each set of complementary models is the length of the thigh and shank relative to the proximal foot and the total hindlimb length.

5.4.6 Limitations

The biological significance of the differences between complementary models and between hypothetical and real frog models is potentially overshadowed by the occurrence of singularities towards the end of some simulations. When the shank is very long, or the thigh or proximal foot are very short, the 3D knee angle reaches a maximum of 160 - 160.5 degrees (Figure 5.17). While this could appear as diminishing returns on the effects of increasing shank length or decreasing thigh and proximal foot length, examination of the Jacobian matrix shows very small error distances and huge angular changes as the knee angle approaches 160 degrees, which the simulation cannot process. This point matches the maximum performance of frogs *in vivo*, as frog hindlimb joints have been suggested to have a maximum flexion-extension range of 160 degrees (Kargo *et al.*, 2002). As knee singularities

only happened in unoccupied areas of morphospace in the hypothetical models, one could infer that this why these morphologies are not seen in nature. However, knee singularities also occurred for 46 real frog species (Figure 5.12). Interestingly, this happened most often for terrestrial jumpers, indicating that singularities are not an indicator of poor jumping ability. It is likely that these frogs would have different initial postures to compensate for differences in hindlimb proportions and prevent the knee from reaching maximal extension before take-off, which should be considered in future modelling work (see section 5.4.6).

Inverse kinematics models, by definition, prescribe a standardised performance for a modified morphology to achieve in the most 'optimal' way possible. In other words, these models assume that the required torques produce sufficient force to achieve the desired kinematics. Kinematics data are only meaningful as far as this assumption of minimising movement in Cartesian space is valid (Richards *et al.*, 2017; Richards, 2019). Consequentially, IK modelling in isolation can only indicate how each hindlimb segment is *potentially* contributing towards overall motion, rather than how the frog is actually acting. Therefore, it is important to note that kinematics analyses cannot be directly related to real-life performance and can only suggest how each segment *may* affect hindlimb motion (Richards, 2019).

IK models also assume that the frog will always jump 'optimally' in the context of kinematics, i.e., the frog will take the shortest route to achieve the jump, so segment rotations will be minimal (Richards *et al.*, 2017). In real life, frog jumps are not always optimal, but to integrate variability in jump performance would overcomplicate the model – incorporating too much detail at this point would preclude examination of the mechanical impact of relative hindlimb proportions in isolation. This is also the reason for keeping initial posture (i.e., the orientation of each segment) and the distance between the hips the same across all frog models (although there is an unavoidable [at the sub-millimetre scale] drift in pelvis width throughout the take-off sequence, which differs slightly for some models [Appendix Figure F.1]). Additional limitations include mirroring the left limb to creating the right limb for ease of interpretation, and modelling all joints as ball joints, which rotate freely but cannot translate. Furthermore, using external landmarks meant that joint centres of rotation were only estimated and long-axis rotation could not be inferred (Richards *et al.*, 2017), meaning that there is likely some element of 'cross-talk' between all degrees

of freedom, i.e., motion around one axis is accidentally interpreted (at least in part) as being around another axis (Piazza & Cavanagh, 2000).

The present study also prioritised a more in-depth analysis of the more proximal hindlimb segments by keeping the distal foot fixed in place, mainly because the 'peeling' motion that takes place as the foot leaves the ground is difficult to model (see section 5.3.1). However, there is much ground to be covered regarding the role of the foot and tarsometatarsal joint in jump performance. Wang *et al.* (2008) state that the design of the frog foot permits rapid and controlled limb extension by maximising contact of the broadest part with the ground and making continuous adjustments in balance, so that rapid changes in trajectory can be made. Future models could potentially include the distal foot by calculating the rate at which foot length incrementally increases throughout the take-off sequence during the *in vivo* simulation and incorporating this into the model. Alternatively, the foot could be divided into multiple smaller segments and confined to the appropriate curvature. Despite these limitations, IK modelling is a powerful tool which provides a foundation in building a more comprehensive understanding of limb multifunctionality.

5.4.7 Future directions

Previous studies have used ancestral state reconstructions to estimate how well extinct frogs may have jumped, but there is currently no strong consensus (Herrel et al., 2016; Mendoza et al., 2020). Both hindlimb segment and joint kinematics show evidence of a phylogenetic signal (Appendix Table G.4), Archaeobatrachia show consistently different kinematics to more recently derived phylogenetic groups (Appendix Table G.5). Therefore, inverse kinematics has strong potential for investigating the jumping kinematics of rarely observed extant taxa, as well as extinct frogs using fossil data, which has never been done before. However, the next step is to use inverse dynamics (ID) models, which measure joint torques and ground reaction forces, to test the assumptions made by kinematics models and confirm whether the conclusions made in this chapter can be related to performance. Firstly, this approach can be used to examine whether the effect of increasing relative segment length on kinematics is due to an increased or decreased contribution of the proximal or distal joints. Secondly, dynamics models could be utilised to better understand the presence of potential biomechanical tradeoffs during the take-off sequence, namely whether there are consistent differences in the sensitivity of joint dynamics to anatomical changes. Thirdly, further work is needed to quantify how shifts in joint positioning impacts GRF orientation, and therefore the size and direction of the external moment arms and torques about each joint. The ability to test these outcomes with dynamics models has inspired the next stage of this thesis (Chapter 6).

Investigating how the timing of peaks in retraction/adduction and joint opening impacts jump dynamics would be another interesting avenue for future research. For example, proximal foot retraction peaks earlier when the thigh is shorter and proximal foot is longer (Figure 3.8; Figure 3.14). If the frog model was not required to continue until a fixed distance, would earlier peaks in polar angle, or angular velocity, result in an earlier take-off? Given the ballistic nature of jumping, and a similar take-off angle and amount of limb extension, a jump with a shorter take-off sequence duration should result in greater jump distances because COM acceleration is higher (Wang et al., 2008). If certain hindlimb proportions enable a frog to achieve the necessary power needed for take-off in a shorter time frame, this could make it faster and more efficient at jumping away from predators, which would have evolutionarily significant consequences. Additionally, there are some instances where segments change their direction of motion in both real frog and hypothetical models. How these changes in direction impact the torques produced at each joint is not yet known.

Starting posture is another area requiring further exploration. Different hindlimb proportions are likely to cause the frog to adopt a different crouching posture at the start of the take-off sequence. This will have important consequences for locomotion, as disproportionately retracted limbs can increase the muscle forces and joint moments required to support body weight (Biewener, 1989; Reynaga *et al.*, 2018). Frogs could potentially change their posture to keep the GRF at the minimum distance from the joints required for sufficient jump performance if altered by changes in segment lengths. For example, walking species are said to make kinematic adjustments for walking rather than alter the asymmetry of the anuran body too drastically, so that sufficient hopping performance is preserved for use as a predator avoidance strategy (Reynaga *et al.*, 2018). Additionally, frogs of different body sizes are likely to adopt different postures to avoid overloading the bones and muscles beyond their respective mechanical tolerances (Perry & Prufrock, 2018). An extension to the study presented here could record and incorporate various

postures into the model by placing external markers on each joint. Posture data can be obtained from existing 3D models such as those available at digitallife3d.org.

5.4.8 Conclusion

Morphometrics studies spanning several decades have evidenced how a longer shank and proximal foot is positively associated with jumping performance (Chapter 2; Zug, 1972; Dobrowolska, 1973; James & Wilson, 2008; Enriquez-Urzelai et al., 2015; Gómez & Lires, 2019). By quantifying the jumping kinematics of taxa spanning a broad range of locomotor modes and phylogenetic groups, this chapter has shown that overall hindlimb kinematics are not sufficient to explain these trends in frog morphology. Kinematics are segment-specific, further supporting the conclusion that each hindlimb segment and joint has different roles during locomotion (Enriquez-Urzelai et al., 2015). Furthermore, I have shown how hypothetical models can remove the noise present when using real taxa and provide a "cleaner" picture of how changing one segment in isolation impacts performance. Shifts in joint positioning and differing levels of kinematic sensitivity to changing hindlimb proportions has raised additional questions regarding the effect of segment elongation on motion which can only be solved by examining joint dynamics (see Chapter 6). In light of both the outcomes and limitations of IK, I have ultimately gained insight into more specific hypotheses requiring testing, and the data required to test them, to answer the overarching question: what is the contribution of each hindlimb segment to jumping motion in anurans?

6 Modelling the effect of different skeletal proportions on hindlimb joint dynamics

Dr Chris Richards provided the initial code for inverse dynamics modelling and, along with Dr Tiina Murtola, helped with troubleshooting. Chris and Dr Laura Porro provided comments on draft versions of this chapter.

6.1 Introduction

Frogs represent a classical model of comparative functional anatomy, especially their hindlimbs (Richards, 2019). The function of the hindlimbs at both a musculoskeletal (Kargo & Rome, 2002; James & Wilson, 2008; Azizi & Roberts, 2010) and mechanical (Nauwelaerts & Aerts, 2003; Astley & Roberts, 2014; Porro et al., 2017; Richards et al., 2018) level have been studied intensely across a select number of species. However, traditional functional approaches are often not able to measure the change in force demands that occurs in response to evolutionary changes in anatomy. It is difficult to isolate the precise anatomical difference that is causing the change in function, and these approaches often involve time-consuming invasive procedures, such as those used in electrical stimulation studies (e.g., Přikryl et al., 2009). Consequently, several fundamental questions pertaining to the anatomical diversity observed among frogs with similar functional niches remain unanswered (Richards, 2019).

Despite differences in skeletal proportions having important links to locomotor mode (Chapter 2; James *et al.*, 2005; Enriquez-Urzelai *et al.*, 2015; Lires *et al.*, 2016; Gómez & Lires, 2019), comparisons of hindlimb dynamics between species with different hindlimb proportions have not been made. Elongation of a particular bone could act as a longer external lever arm, resulting in the generation of larger forces about its joints, and therefore greater mechanical advantage, which has been shown to enhance jumping performance (Choi *et al.*, 2003; Nauwelaerts *et al.*, 2007; Enriquez-Urzelai *et al.*, 2015; Porro *et al.*, 2017). Therefore, frogs with a longer shank and proximal foot were expected to have more 'optimal' take-off kinematics (i.e., the hindlimb orientation changes less over a set take-off distance), as these segments are longer in jumpers compared to non-jumpers (Chapter 2). However, the inverse kinematics (IK) model built in Chapter 5 showed that, although variation in hindlimb proportions does influence kinematics during the take-off sequence, it is not in the ways that were initially expected. Overall hindlimb motion was not

minimised when the shank and proximal foot were longer, but instead shank rotation was minimised at the expense of thigh and proximal foot rotation. What is still unknown is how this translates to the forces that are being produced during take-off, which are important for making inferences about performance from anatomy. For example, it is currently unknown how the shifts in joint positioning that occur as hindlimb proportions change impacts the ground reaction force (GRF), which is linked to jump performance (Nauwelaerts *et al.*, 2007). While IK has provided some useful insights, its inherent limitations mean that IK is a tool which should not be used in isolation.

Inverse dynamics (ID) modelling has become an increasingly utilised technique for investigating the relationship between anatomy and locomotor function in frogs (Astley & Roberts, 2014). ID is the calculation of the joint torques needed to achieve the prescribed kinematics and is therefore the natural next step in biomechanical modelling after IK analyses (Chapter 5). IK relates segment motion to locomotor behaviour, but determining whether that motion is driven by the action of the proximal or distal joint requires ID analyses (Richards, 2019). The ability to fix certain parameters permits investigation of individual muscle and joint function, which is often not possible in experimental set ups. Previous studies have used this technique to determine the roles of the iliosacral joint (Richards et al., 2018), hindlimb joints (Porro et al., 2017; Kargo et al., 2002), and elastic energy storage at the ankle (Astley & Roberts, 2014) in anuran jumping. Using kinematics and GRF as inputs, ID calculates the segment inertial properties, external moment arms (i.e., the perpendicular distance from the joint to the GRF vector) and torques (i.e., rotational forces) acting at a joint, thus indicating how the muscles spanning that joint may be performing (Richards, 2019). When the external moment arm is larger, more joint torque is produced for a given input force (Porro et al., 2017).

Using the kinematics data from the hypothetical frog models in Chapter 5 and *in vivo* force plate measurements from a *Phlyctimantis maculatus* jump (Porro *et al.*, 2017), I create an ID model to address the overarching question: How do hindlimb proportions influence joint dynamics during take-off? Ground reaction forces, and the external moment arms and joint torques at the hip, knee, and ankle are compared to test three hypotheses based on the findings from Chapter 2 and Chapter 5:

- H1) Smaller external joint torques are required to take-off over a set distance as the relative length of the shank increases.
- H2) Smaller external joint torques are required to take-off over a set distance as the relative length of the proximal foot increases.
- H3) Shifts in joint positioning will impact GRF orientation, and therefore the size and direction of the torques acting about each joint.

This research will demonstrate how inverse dynamics can be used to predict the performance capabilities of different species without the need to carry out time-consuming *in vivo* data collection. This will be particularly important for future studies of extinct taxa, which can then estimate performance based on the hindlimb proportions measured from fossils. With this, we can attain a more comprehensive overview of the functional implications of the anatomical changes observed throughout the evolution of the anuran hindlimb.

6.2 Methods

6.2.1 Model set up

MuJoCo ('Multi-Joint dynamics with Contact') is a physics engine which can be used to extract force data from biomechanical models (Version 2.1.1; Todorov *et al.*, 2012). Given sound kinematics data and a simple rigid floor, MuJoCo can perform inverse dynamics without force plate data (Richards *et al.*, 2018; Richards, 2019), so it is the ideal tool for examining how hindlimb proportions affect jumping behaviour without *in vivo* jump experiments for real (both extant and extinct) and hypothetical frog species. Several steps are required to build an ID model in MuJoCo, as well as two key data inputs – the XML file and the kinematics data (Figure 6.1). The source code that was edited for use in this chapter (Collings *et al.*, 2022) and the initial force plate measurements (Porro *et al.*, 2017) and kinematics (Richards *et al.*, 2017) are based on *in vivo* data from *Phlyctimantis maculatus*, a 'generalist' species in terms of locomotor mode.

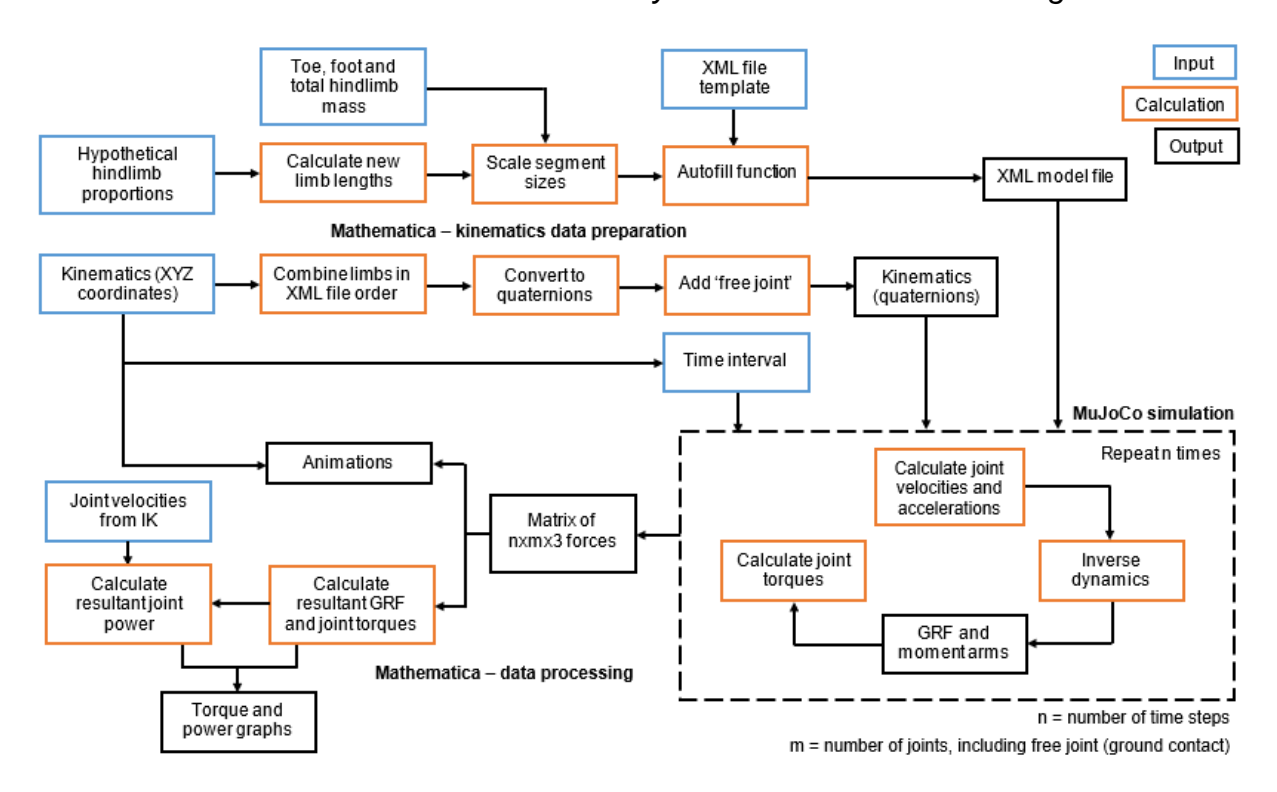


Figure 6.1 - A flow diagram depicting the process of building the inverse dynamics model for testing the effect of different segment proportions on hindlimb dynamics based on *in vivo Phlyctimantis maculatus* data.

The XML file contains all the information relating to the structure of the model, while kinematics data are loaded seperately to animate the model. An XML template file describes the generalised hierarchy of the frog model's anatomy, starting at the 'free joint' (i.e., the ball joint which describes the contact of the left toe with the substrate), moving proximally up to the pelvis, then distally back down through the segments to the right toe. Anatomical information is input into this template using Mathematica to generate a unique XML model for each set of hindlimb proportions (Figure 6.1). MuJoCo requires data on the length and radius of each segment in the limb to calculate the mass and inertial properties of each segment. To be able to examine the effects of varying relative hindlimb lengths in isolation, the mass of each segment (and therefore total hindlimb mass) is kept constant by scaling the radius (*R*) of each segment accordingly:

$$R_{thi} = \sqrt{\frac{M_{total\ hindlimb} - M_{toe} - M_{DF}}{\pi \rho (l_{PF}C_1^2C_2^2 + l_{sha}C_2^2 + l_{thi})}}$$

(Equation 6.1)

$$R_{shank} = C_2 * R_{thigh}$$
 (Equation 6.2)

$$R_{PF} = C_1 * R_{shank}$$
 (Equation 6.3)

Since only total body mass data was available for the specimen used in Chapter 5 (0.01455kg; Porro et al., 2017; Richards et al., 2017), the total hindlimb, toe and distal foot (DF) masses (M) were calculated as proportions of total body mass based on data from Collings et al. (2022), who estimated the mass of each segment and total body mass from their μ CT scan. Hindlimb density (ρ) is based on the standard value for mammalian skeletal muscles (1.056 g/cm³; Mendez & Keys, 1960), which has been shown to be representative of most vertebrates, including anurans (Biewener, 2003; Ward & Lieber, 2005). This density was adjusted to represent how the model contains only the hindlimbs (5.603 g/cm³), which makes up approximately 25% of a frog's body mass (Dr Laura Porro, unpublished data). As in Chapter 5, segment lengths (I) were calculated as the distance between joint coordinates in the kinematics model. Hindlimb segment widths were not recorded for the specimen from the behavioural studies (Porro et al., 2017; Richards et al., 2017), so constants C_1 and C_2 were calculated using measurements of the thigh, shank and proximal foot radii from the 3D volume of P. maculatus from the µCT scan dissected in Chapter 3. Note that the methods used in this chapter allow investigation of the dynamics of any frog species, extant or extinct, so long as the data are in the same format.

XML models contain only information which defines frog geometry, and thus lacks any data for segment orientations or posture. The second key input required to run a simulation in MuJoCo is kinematics data (i.e., XYZ coordinates for each joint). As in the previous chapter, the take-off sequence is defined as being from the onset of movement to the point at which the fixed distal foot would leave the ground. The time interval used is the same as the one used for the IK model (0.000524743 s) to ensure that the velocity is identical across simulations. The only difference between this version and the kinematics data from the hypothetical models from Chapter 5 is that the distal-foot segment was first aligned with the jump axis as a precautionary step to avoid large artefacts in the dynamics output. As in Chapter 5, the distal foot is fixed, so the origin of the GRF vector cannot translate. Additionally, to remove

artefacts from resampling the kinematics data to create 100 time steps, the kinematics data were fit with a fifth order polynomial fitler. These kinematics data are then converted from a matrix of XYZ coordinates into quaternions (Equation 6.4) using Mathematica (Version 13.0, Wolfram Research, 2022):

$$Unit\ quaternion = \{ \cos(\theta/2), X \cdot \sin(\theta/2), Y \cdot \sin(\theta/2), Z \cdot \sin(\theta/2) \}$$
 (Equation 6.4)

X, Y and Z correspond to the coordinates for each axis of rotation, where θ is the rotation angle about that axis. Quaternions are the 4D mathematical units that MuJoCo requires to describe the rotation of an object.

6.2.2 Running the dynamics simulation

The XML file and kinematics data (in quaternions) are called by the MuJoCo code to calculate the joint velocities and accelerations, which are then used to calculate the inverse dynamics, i.e., the combined internal and external joint torques at each time step of the kinematics (Figure 6.1):

Inverse dynamics:
$$t = Ma + c - J^T \times f$$
 (Equation 6.5)

where t are the net joint torques, M is the mass/inertia matrix, a are the joint accelerations, c describes bias forces such as gravity, and J^T is the Jacobian which maps f into joint space. MuJoCo mathematically solves f as the ground reaction force (GRF) at each time step, which enables realistic simulations of how a substrate may respond to a contact force (Todorov et al., 2012). External torques for the hip, knee, and ankle are estimated using the GRF and external moment arms (V_{MA}), which are estimated using the vectors defined by the GRF (V_{GRF}) and the joint (V_{Joint}) (Equation 6.6; (Equation 6.7):

$$V_{MA} = \frac{\left|\left|V_{GRF} \times V_{Joint}\right|\right|}{\left|\left|V_{GRF}\right|\right|}$$
 (Equation 6.6)

$$V_{Torque} = V_{MA} \times GRF$$
 (Equation 6.7)

The ID model produces a $100 \times 5 \times 3$ matrix – the GRF and the external torques produced at each joint across 100 time steps in each of the X, Y and Z components.

The resultant GRF and external joint torques were calculated using (Equation **6.8** to compare the magnitude of these forces:

$$Resultant = \sqrt{X^2 + Y^2 + Z^2}$$
 (Equation 6.8)

As the ID model produced resultant torques and GRFs at magnitudes similar to *in vivo* force plate data, the model produces realistic results (Porro *et al.*, 2017). This entire process was repeated using the same hypothetical hindlimb proportions as in Chapter 5 (Table 5.2) to enable investigation of the morphospace occupied by a large range of frog species.

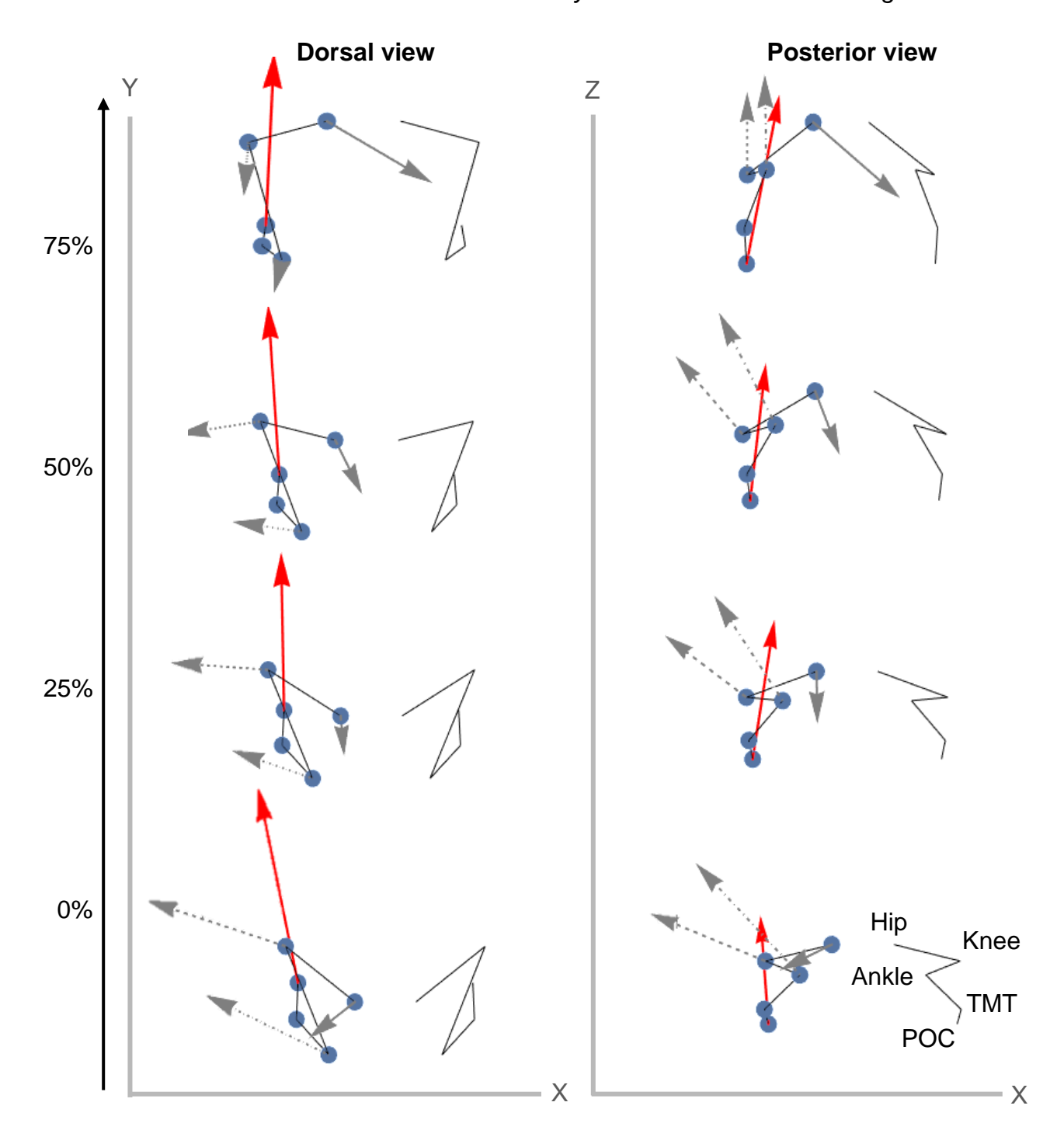


Figure 6.2 - The take-off sequence for *Phlyctimantis maculatus* with the ground reaction force (red arrow, scaled down by 10) and joint torques (grey arrows, scaled up by 2) generated from MuJoCo, shown using Mathematica. The jump occurs along the global Y axis. The dorsal view depicts the process of forward propulsion, which is driven by limb retraction, while the posterior view depicts upward elevation, which is driven by limb adduction. The numbers on the left represent the time point during the take-off sequence. TMT = tarsometatarsal joint; POC = point of contact with the ground.

6.3 Results

6.3.1 Ground reaction forces

The variation between models in ground reaction force (GRF) is most evident at ~80% of the take-off duration, especially for the proximal foot models (Figure 6.3). For thigh and shank models, the GRF required during the take-off sequence is relatively similar, with the most prominent differences being that the GRF is lowest when the shank is double the length of the thigh, and highest when the segments are equal in length (Figure 6.3). Changing the length of the proximal foot has a less straightforward effect. The model of the shortest proximal foot requires the smallest GRF, but the largest GRF is associated with the next shortest proximal foot model, with longer proximal foot models placing in the middle with *P. maculatus*.

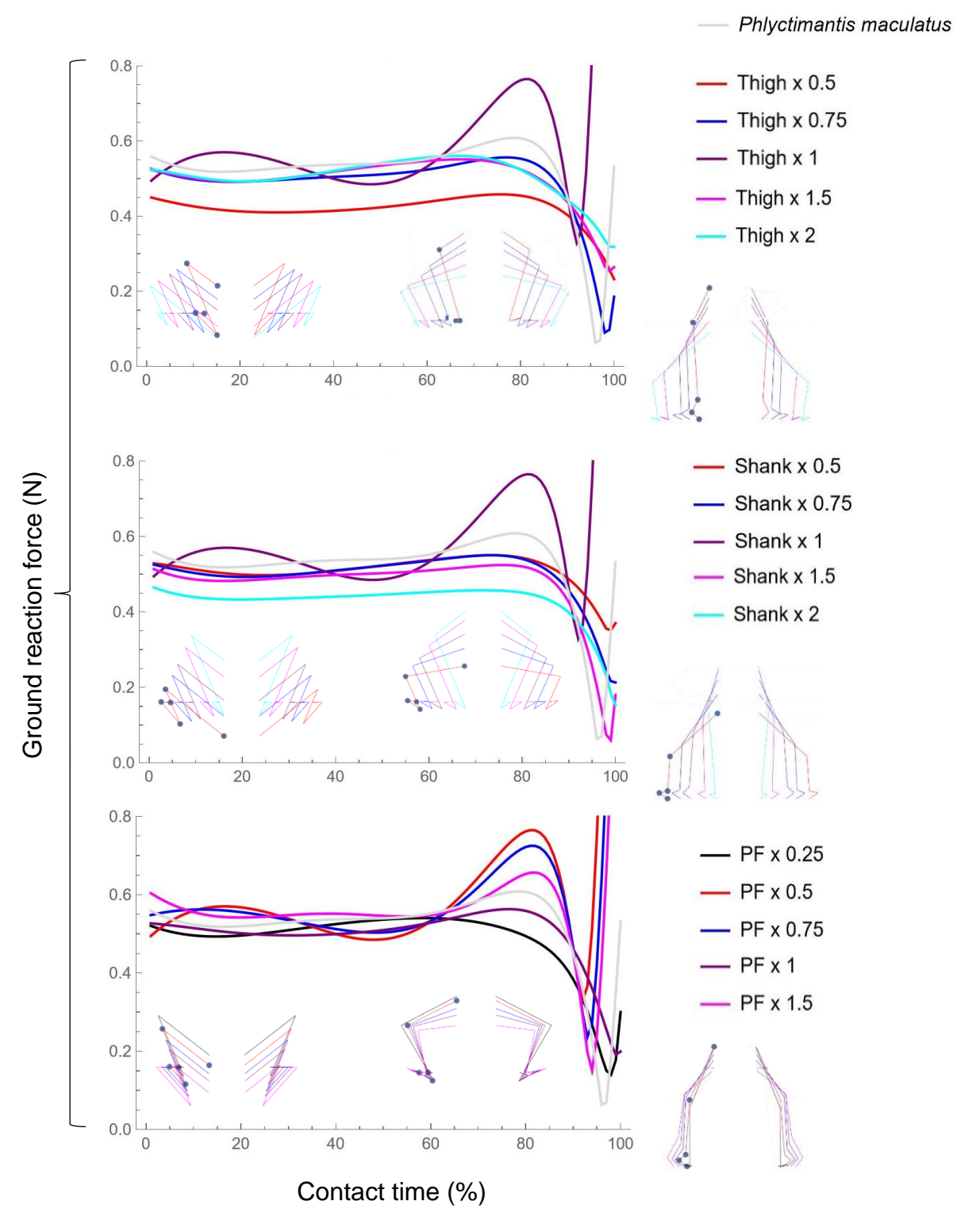


Figure 6.3 - Resultant ground reaction forces for hypothetical hindlimb proportions. Each colour represents a different model of segment length – the thigh relative to the shank, the shank relative to the thigh, and the proximal foot (PF) relative to the more proximal segments. *P. maculatus* is identical across graphs. The stick figures (dorsal view) show how different hindlimb proportions look at 0%, 70% and 100% of the take-off sequence duration.

6.3.2 Proximity to the ground reaction force

External moment arms and joint torques often peak in magnitude just before the point of take-off, likely due to the constraint that the foot remains glued to the ground (Figure 6.4; Figure 6.5; Figure 6.6), unlike real jumps where the foot gradually peels off (Porro et al., 2017). Therefore, only the moment arms and torques in first 90% of the take-off sequence are compared throughout this chapter. Table 6.1 describes the key differences in external moment arms between the different models of hindlimb proportions. There are, however, some notable exceptions. When the thigh length is equal to that of the shank in the hypothetical thigh models, the knee moment arm is the longest, and the ankle moment arm is the shortest (Figure 6.4). Additionally, the hip moment arm is slightly shorter than when the thigh is threequarters the length of the shank (Figure 6.4). This same result occurs for the ankle moment arm in the hypothetical shank models (Figure 6.5). Although the hip and ankle moment arms generally become longer as the proximal foot length increases, the shortest moment arm for these joints occurs when the proximal foot is half the length of the thigh and shank (Figure 6.6). Furthermore, the longest moment arm is when the proximal foot length is equal to that of the thigh and shank. There are also several cases where models of longer segments are initially showing considerable differences to the other models, but then converge in moment arm length around 80% of the take-off duration (Table 6.1).

Table 6.1 - A summary of the key changes to external moment arms and joint torques when the relative length of each hindlimb segment increases. The percentages mentioned refer to the take-off duration. A * denotes an exception which is discussed in the main text.

Length change	Joint	Effect on moment arm length	Effect on torque magnitude
Thigh becomes longer	Hip	Longer *	Larger
relative to shank (Figure	Knee	Longer *	Larger
6.4)	Ankle	Shorter *	Larger
	Hip	Shorter	Initially smaller, then
Shank becomes longer	er Tip	Shorter	all similar by 80%
relative to thigh (Figure	Knee	Initially shorter, then	Smaller
6.5)	Trice	longer by 80%	
	Ankle	Shorter *	Smaller
	Hip	Longer *	Initially smaller, then
Proximal foot becomes	ן ווף	Longer	all similar by 80%
longer relative to thigh	Knee	Initially longer, then	Larger
and shank (Figure 6.6)	MICE	all similar by 80%	
	Ankle	Longer *	Larger

As illustrated by Figure 6.2, the GRF vector rotates from being lateral to the hip and ankle joints to being more medial, resulting in a general decrease in their external moment arms across all models (Figure 6.4; Figure 6.5; Figure 6.6). The GRF vector is generally medial and posterior to the knee (Figure 6.2). In *P. maculatus* and many of the hypothetical models, the knee and the GRF vector move closer together during the take-off sequence, as in previous studies (Porro *et al.*, 2017). However, they initially move further apart when the shank is equal to or longer than the length of the thigh (Figure 6.4; Figure 6.5). Knee moment arms are also observed to be considerably lower in the hypothetical thigh models (Figure 6.4) compared to the shank models (Figure 6.5), regardless of whether the thigh is shorter or longer than the shank. However, this does not result in a significant difference in the joint torques. Additionally, the knee of *P. maculatus* comes very close to the GRF at 90% of the take-off sequence duration, as does the model where the thigh is three-quarters of the length of the shank (Figure 6.4). When the shank is 1.5 times the

length of the thigh, the hip also comes very close to the GRF towards the end of the take-off sequence (Figure 6.5).

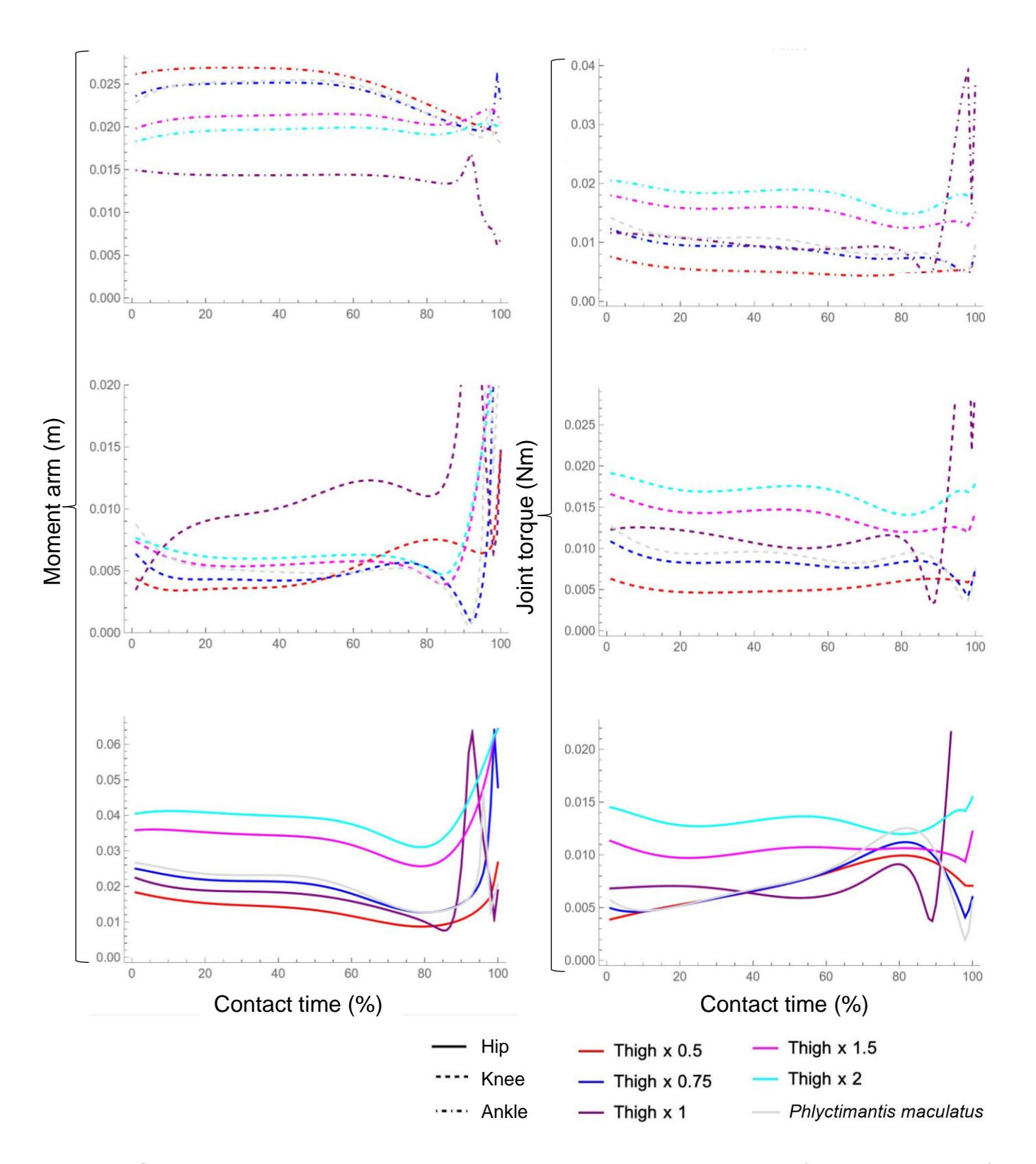


Figure 6.4 - External moment arms and resultant joint torques for each model of hypothetical thigh proportions. Line types represent each joint. Each colour represents a different model of thigh length relative to shank length.

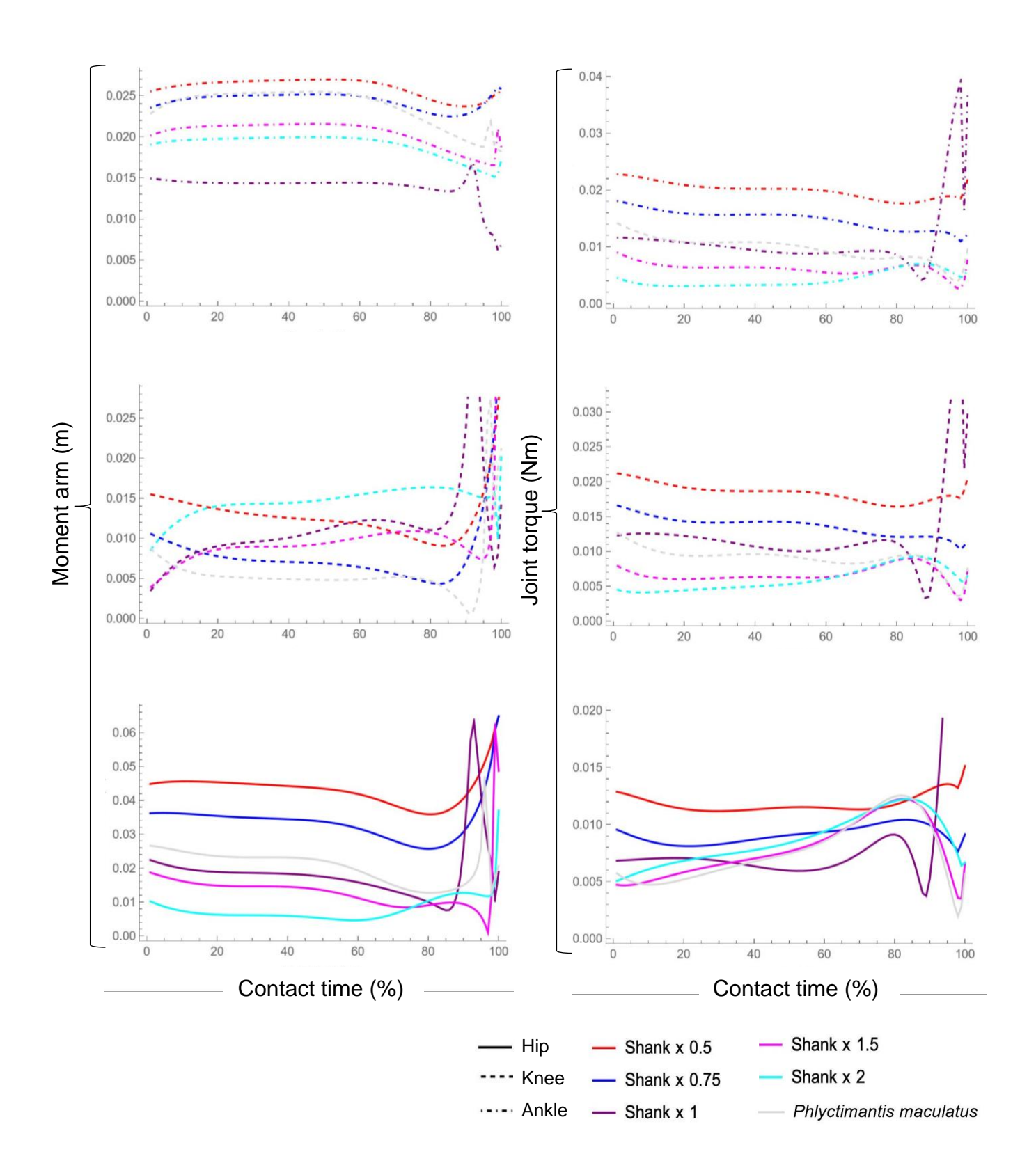


Figure 6.5 - External moment arms and resultant joint torques for each model of hypothetical shank proportions. Line types represent each joint. Each colour represents a different model of shank length relative to thigh length.

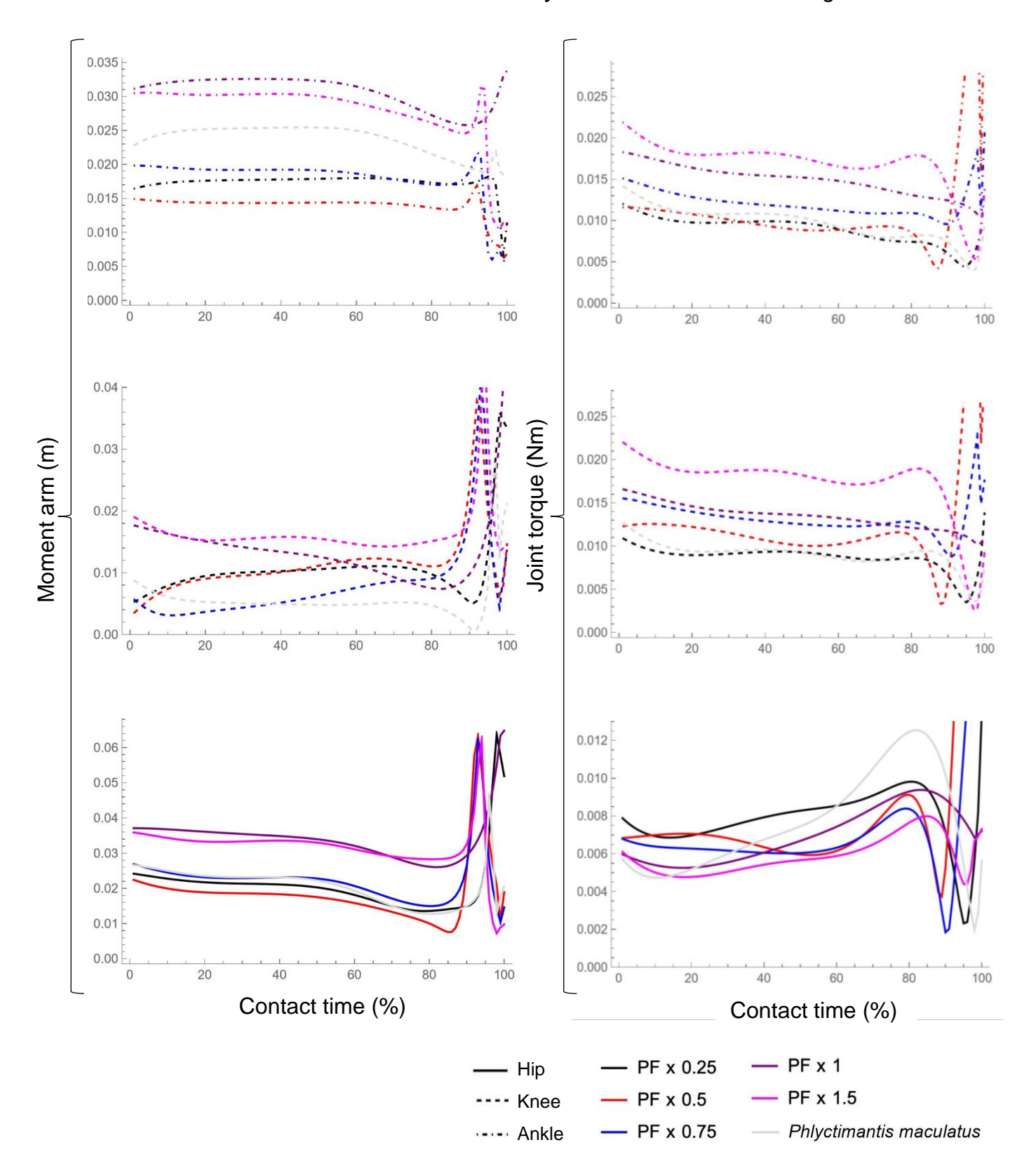


Figure 6.6 - External moment arms and resultant joint torques for each model of hypothetical proximal foot (PF) proportions. Line types represent each joint. Each colour represents a different model of PF length relative to the length of the thigh and shank, which are the same length.

6.3.3 External joint torques

The magnitudes of the external joint torques are determined by external moment arm length and GRF magnitude (Equation 6.7). In contrast to Porro *et al.* (2017), who found that torque magnitudes were largest for the hip and ankle, the knee and ankle torques are often slightly larger than those at the hip, despite the proximity of the knee to the GRF vector being generally smaller compared to the hip across all models (Figure 6.4; Figure 6.5; Figure 6.6). Table 6.1 shows the most prominent trends in 3D external joint torques as segment proportions change, with much fewer exceptions compared to the external moment arms. Hip torques are initially smaller when the shank and proximal foot are longer compared to the other models, before torque magnitudes converge to similar values by 80% of the take-off sequence duration (Figure 6.5; Figure 6.6). It is also interesting to note that the ankle in the thigh models (Figure 6.4) and the hip in the proximal foot models (Figure 6.6) show opposite trends in torque magnitudes as they do in moment arms, e.g., the ankle moment arm is smaller but the torque magnitude is larger as the thigh lengthens.

6.4 Discussion

As the primary mode of terrestrial locomotion in frogs, jumping is an energetically expensive and explosive movement (Emerson, 1978; Astley & Roberts, 2014; Porro et al., 2017). Better understanding the mechanisms behind jumping provides crucial insight into how these animals adapt their morphology to increase their likelihood of escaping predators (James et al., 2007). This chapter utilises inverse dynamics modelling to determine how variation in hindlimb skeletal proportions affects joint forces during jumping. Increasing the length of the shank results in a smaller ground reaction force (GRF) and external joint torques being required to take-off (support for hypothesis 1), but a longer proximal foot does not have the same effect (contrasting hypothesis 2). Similar to the hindlimb kinematics in Chapter 5, this could indicate that there are potentially biomechanical trade-offs in joint dynamics. Shifts in joint positioning with changing segment lengths are found to impact the orientation of the GRF, but not always by the same amount as the distance each joint shifts, i.e., increases in external moment arms are not always consistent with increases in segment length (partial support for hypothesis 3). Overall, this investigation has contributed new knowledge towards understanding how hindlimb geometry impacts

locomotor function, which will facilitate future research into the lifestyles of extinct frogs.

6.4.1 A longer shank, but not proximal foot, reduces the forces needed to take off

An elongated limb segment creates a longer external lever arm about its joints, which has been shown to improve jump performance by increasing effective mechanical advantage (Choi et al., 2003; Nauwelaerts et al., 2007; Enriquez-Urzelai et al., 2015). Terrestrial and arboreal jumpers tend to have a significantly longer shank and proximal foot than non-jumpers (Chapter 2), so these morphologies are expected to require smaller forces to perform the task simulated in this chapter take-off over a fixed distance at a fixed take-off angle with a constant acceleration. The results presented here partially align with these expectations, since the longest shank model requires a smaller GRF (Figure 6.3) and smaller joint torques (Figure 6.5), supporting hypothesis 1. The distal joints in particular contribute more towards motion when the shank is longer than the thigh, as there is a large jump up in knee and ankle torque magnitudes for these models, while hip torques are less sensitive to changes in segment length by the second half of the take-off seguence (Figure 6.5; Figure 6.5). A smaller proximity of the joints to the GRF enables the muscles crossing these joints to have a larger effective mechanical advantage, assuming that muscle moment arms do not change (Lieber & Brown, 1992; Kargo & Rome, 2002; Astley & Roberts, 2011), resulting in the requirement for smaller joint torques to complete the simulation task. These results may also indicate that frogs with longer shanks are capable of producing larger a GRF, which produces higher takeoff speeds and therefore increases jump distance (Nauwelaerts et al., 2007).

In contrast to expectations, a longer proximal foot requires larger joint torques to perform the simulation task (Figure 6.6). Interestingly, the relative proximal foot lengths most similar to that of real frogs (Table 5.3) required the largest GRF to perform the take-off sequence (Figure 6.3). Similar to the conclusions of Chapter 5, the proximal foot may be shaped in a way that enhances the function of another segment, which is most likely the shank, as they connect via the ankle joint. Alternatively, having a proximal foot that is equal to, or longer than the more proximal segments might impede a more important function, such as shank extension. It might also be that a longer proximal foot has a different function in jumping not explored here, though the results of digital musculoskeletal dissections indicate that

it is not to support larger tarsal muscles compared to frogs specialising in other locomotor modes (Figure 3.7). It is also important to consider that minimising the torques required for this simulation in all three joints may not be the end-goal for adaptation – a frog may want to have variability in performance to facilitate unpredictability in jump trajectory, as this could increase the chances of survival from predation (Kargo *et al.*, 2002). Therefore, wide variation in the possible ranges of motion, rather than simply the maximisation of potential jump distance, may also be selected for.

6.4.2 Segment length relative to total hindlimb length has significant impacts on joint dynamics, even if proportions are similar

In Chapter 5, I introduced two sets of 'complementary' hypothetical models which describe how take-off mechanics change when the length of each segment changes relative to total hindlimb length, even if the lengths of two segments relative to each other remain the same. Specifically, I examined what happens to the kinematics when the length of thigh relative to the shank is kept fixed, but their lengths relative to the proximal foot and total hindlimb length is varied (Figure 5.18). Considering subtle differences in anatomy in this way is a powerful approach, as it considers the geometric interactions of multiple segments working together, rather than as isolated segments which may not affect jumping mechanics in isolation. In Chapter 5, I observed that hindlimb kinematics are very different between the two models where the thigh is half the length of the shank (1), but are almost identical when the shank is half the length of the thigh (2), regardless of length relative to the proximal foot (Appendix Figure H.1). I hypothesised that this is because the difference in length between the shank and the proximal foot is larger in complementary models (1) than complementary models (2). This could be because the shank and proximal foot share an ankle joint. Therefore, it was expected that there would also be a larger difference in ankle torques between models where the thigh is half the length of the shank (1), compared to the models where the shank is half the length of the thigh (2). However, the differences (or lack thereof) observed in the kinematics data are not reflected in any of the joint torques (Appendix Figure H.2). In other words, having a shank four times the length of the proximal foot (1) did not impact joint torques more than having a shank that is double the length of the proximal foot (2). This indicates that the length of each segment relative to the total hindlimb length impacts

joint force production during the take-off sequence, and is therefore also important for jump performance, even if thigh and shank proportions are similar.

6.4.3 The ground reaction force vector orientation changes with different hindlimb proportions

Prior to the present study, it was not known whether shifts in joint positions also impact the orientation of the GRF vector in frogs. Adjusting the GRF vector to be closer to the joints could be a potential strategy to compensate for the disadvantageous lengthening of the external moment arms that can occur when joints become further away with increasing segment lengths. Dynamics models were used here to test this theory. I find that shifts in joint positioning with changing segment proportions does impact the orientation of the GRF, but not always according to the distance each joint shifts. This is indicated by the external moment arms of many closely related models being far apart, while others are very similar (e.g., the hip moment arm when the shank is equal to and three-quarters the length of the thigh; Figure 6.5).

The change in the direction of knee motion when shank and proximal foot proportions differ provides additional evidence for this 'GRF shift' theory. When the proximal foot is equal to or longer than the thigh and shank, the knee and GRF vector move further apart throughout the take-off sequence (Figure 6.6). When the proximal foot is relatively short, the knee and GRF instead move closer together. Increasing relative shank length has the opposite effect on knee moment arms (Figure 6.5). Essentially, there is a convergence of the knee moment arms towards a specific range of distances from the GRF at ~80% of the take-off sequence duration. In comparison, the ankle and the hip remain relatively parallel to the GRF for the first ~60% of the take-off sequence, before moving closer together (excluding the final stage of the take-off sequence). Since the magnitude of the knee torques does not appear to be significantly impacted by the direction in which the knee and GRF move relative to one another (Figure 6.4; Figure 6.5; Figure 6.6), these results support the conclusion that the knee has an important role in fine-tuning take-off trajectory (Kargo et al., 2002; Porro et al., 2017). It would be interesting to see whether these functional shifts in GRF orientation are still observed when different variations in hindlimb posture are considered in future dynamics models (see section 6.4.6).

6.4.4 Additional factors may be influencing the relationship between hindlimb anatomy and dynamics

There are some instances where results did not align with expectations, indicating that there are other factors besides external moment arms, joint torques, and GRF which determine the impact of anatomical changes on hindlimb dynamics. For instance, despite the GRF appearing relatively robust to changes in hindlimb proportions for most of the take-off sequence (Figure 6.3), there is broad variation in external moment arms and joint torques (Figure 6.4; Figure 6.5; Figure 6.6). Additionally, some trends across moment arms are different to those for joint torques. For example, the ankle moment arm is considerably shorter when the thigh is longer (Figure 6.4), but the ankle torques required to take-off are higher, thus showing the opposite trend to what I would expect, given that shorter moment arms provide higher effective mechanical advantage (Porro et al., 2017). Furthermore, some models have very similar moment arms throughout the entire take-off sequence, but then their joint torque profiles would be very distinct, e.g., the hip when the thigh is equal in length and x1.5 longer than the shank (Figure 6.4). The opposite also occurs. When the shank is three-quarters of and equal to the length of the thigh, the knee and ankle moment arms of these two models are both very distinct, but the torque profiles are very similar (Figure 6.5).

Since the mass of each segment and the total hindlimb mass are kept the same, these results may be explained by differences in joint angular accelerations ((Equation 6.5). All simulations have been constrained to have the same COM acceleration, so the joints may be accelerating differently to account for changes in segments lengths to maintain that COM acceleration. The influence of acceleration on motion depends on the instantaneous position of the hindlimb joints and the interactions of all of the limb segments at each point in time (Richards, 2019) and was therefore not possible to investigate in the present study. Internal joint torques may also be having an effect, though previous studies have found that their magnitudes relative to the external joint torques are an order of magnitude lower at distal hindlimb joints, and could therefore be considered negligible (Porro et al., 2017). However, they could be important to examine to understand the impact of inertial limb properties on the inverse dynamics results seen here.

6.4.5 Limitations

This dynamics model provides considerable insights into the drivers of hindlimb motion during jumping, but there are assumptions that are important to consider. In line with previous studies, the kinematics model from Chapter 5 assumes that frogs jump with a constant acceleration for ease of interpretation (Juarez et al., 2020). This is often not the case (Marsh & John-Alder 1994), which could explain why the shape of the force traces plotted here are different from in vivo force plate data (Porro et al., 2017). However, acceleration profiles are often similar across different species (James & Wilson 2008; Moen et al., 2013) and this thesis focuses on comparing the *relative* impact of different hindlimb proportions on jumping dynamics. Additionally, the force magnitudes produced by the MuJoCo model are within 10-20% of the *in vivo* data, and the kinematics are qualitatively similar (Chapter 5). Another limitation of both the kinematics and dynamics models is that it assumes that there is no long-axis rotation occurring as this cannot be measured using one pair of joint markers (Richards et al., 2018). Take-off angle can be sensitive to longaxis rotation of the femur at the hip (Kargo et al., 2002), but its contribution to motion is rather minimal relative to other rotations (Astley & Roberts, 2014). X-ray Reconstruction of Moving Morphology (XROMM; Brainerd et al., 2010) will be required to accurately determine the contribution of long-axis rotation to jumping in frogs (Richards et al., 2017).

Another reason why the *in vivo* force plate data (Porro *et al.*, 2017) would not have matched the dynamics obtained from my ID model is due to differences in anatomy. Firstly, the model did not consider forelimb and body kinematics or inertial properties, which would influence overall dynamics. Secondly, segment widths were kept constant across the models to enable the investigation of the impact of different hindlimb length proportions on take-off dynamics in isolation. To do this, segment widths were measured from a μ CT scan of *P. maculatus* to create constants C_1 and C_2 (see section 6.2.1). However, segment widths will differ between species and individuals within a species, according to observations made during digital dissections (Chapter 3). Future users of this model should also note that the C_1 and C_2 calculation is based on the hindlimb segments being the shape of cylinders, when MuJoCo actually represents hindlimb segments as 'capsules' (Appendix Figure I.1). The small difference in mass would have incurred the same relative effect on the forces produced, as each model is treated the same, so this was not a concern for the purposes of the present study. It is also worth considering that segment widths

had to be measured using a different individual to the frog that was used for *in vivo* jump trials (Porro *et al.*, 2017; Richards *et al.*, 2017). Future research on hindlimb dynamics should carry out all processes using the same animal to be able to make the most direct comparisons between function and anatomy. In other words, carrying out behavioural experiments first, followed by anesthetisation of the same frog for contrast-enhanced scanning and traditional dissection. Then, the only differences between the MuJoCo simulation and *in vivo* data would be due to the use of simulated ground rather than jumping from a force plate, and how much the upper body contributes towards the generation of GRF, which is not included in this current study.

6.4.6 Future directions

This chapter has contributed towards our understanding of the ways in which frogs adapt their morphology to achieve the requirements for jumping performance demanded by their lifestyle. However, there are several more steps future functional comparative analyses can take to build a more comprehensive understanding of the relationships involved. Previous studies have shown that hip and ankle torque are the largest determinants of forward thrust, while the ankle is largely responsible for upward elevation (Astley & Roberts, 2014; Porro *et al.*, 2017). The balance of forces determining these two planes of motion ultimately determines whether a jump is successful for escaping predation (Kargo *et al.*, 2002). Future studies could use the Jacobian matrix to infer how the action of each joint contributes to body movement direction (i.e., XY torques indicating limb retraction, and XZ torques indicidating limb adduction; Porro *et al.*, 2017) as hindlimb proportions change. Additionally, how joint accelerations and internal joint torques differ between frogs with different hindlimb proportions is an area that future studies could explore further (see section 6.4.4).

As first stated in Chapter 5, the kinematics used to design the inverse dynamics simulations in this chapter do not consider the differences in posture that likely occur when hindlimb proportions change. Jump angle, for example, is determined by how the pelvis is rotated relative to the femur, as well as the position of the knee (Porro et al., 2017). Incorporating these data may provide more realistic estimations of the role of hindlimb proportions in jumping, as muscles have different roles depending on the orientation of the limbs (Kargo & Rome, 2002). For instance, the model where the shank is double the length of the thigh requires the lowest GRF to perform the simulation, but the fixed posture designated across all the models might not be

achievable for frogs with this morphology. As this extreme difference in segment lengths is not seen in nature (Table 5.3), there is likely a trade-off between optimal hindlimb proportions and posture that prevents frogs from elongating their shanks in this way to minimise force requirements. It would be interesting to explore how posture differs between species in relation to hindlimb proportions, and whether the adjustment of posture is an adaptive response to enable the alignment of their GRF vector so that optimal joint torques are produced during the take-off sequence.

Biomechanical modelling of jumping, a high energy burst along a linear trajectory, is relatively straightforward compared to modelling cyclical movements like walking (Reynaga *et al.*, 2018; Collings *et al.*, 2022), vertical climbing (Young *et al.*, 2023) and swimming (Richards, 2010; Robovska-Havelkova *et al.*, 2014). For example, the balance of external forces is completely different between air and water, which means functional demands differ between jumping and swimming (Nauwelaerts & Aerts, 2003). Future studies should compare how one species might vary joint motion to perform two different behaviours, as well as how two species with similar skeletal proportions could specialise in different locomotor modes, to see if hindlimb proportions are another example of one-to-many mapping. Future studies will need to consider other locomotor modes to fully understand of the effect of anatomy on function, though this may require more complex models.

Incorporating muscles into dynamics models will give a more accurate depiction of the effect of differences in anatomy on motion. Even small alterations made by the muscles could change jump dynamics to facilitate variability in jump response (Kargo *et al.*, 2002). Also, a muscle could exert the same force but not need to contract as far, or as fast, because it can have a flexor moment about one joint and an extensor moment about another (Carlow & Alexander, 1973). Furthermore, muscles have physiological limits which affect locomotor performance (e.g., 483 W/kg muscle-mass-specific power; Astley, 2016), which may explain why the torques and GRFs produced by the present dynamics model are slightly higher than some of the *in vivo* force plate data (Porro *et al.*, 2017). Differences in hindlimb proportions will likely affect these limitations (e.g., there could be a segment configuration where the jump is not as good as expected because the joint torque requirements are too high for the muscles to produce), so future studies should incorporate these as parameters into the MuJoCo model.

By further investigating the questions raised by kinematics models (Chapter 5), this thesis presents a more complete picture of the contribution of each hindlimb segment to jumping motion in anurans. Using a novel application of an inverse dynamics model, I have demonstrated several reasons why we tend to see a longer shank in frogs which specialise in jumping. With this new information on the role of anuran skeletal structure, we have a better understanding of how geometry can impact function irrespective of muscle design. This dynamics model therefore shows huge potential for contributing towards our knowledge of the possible locomotor behaviours performed by rarely observed extant species, as well as extinct anurans, through simulations based on museum specimens and fossil data. Furthermore, this final thesis chapter completes the list of techniques required to build musculoskeletal models which can further test some of the functional capabilities of frogs. With these musculoskeletal dynamics models and more advanced phylogenetic techniques (e.g., ancestral state reconstruction), future studies could finally determine whether the hindlimb anatomy of frogs was originally adapted for walking, jumping, or multifunctionality (Porro et al., 2017; Richards, 2019), which has been debated since the early studies of frog locomotion (Emerson, 1979; Přikryl et al., 2009; Jorgensen & Reilly, 2013).

7 Thesis discussion

7.1 Thesis summary

Anatomical complexity is defined by the number of different parts in an organism, and the regularity with which these parts are arranged (McShea, 2000). Frog anatomy exemplifies many different aspects of complexity including, but not limited to, the size and shape of their bones and muscles, the presence or absence of osteological crests, where muscles originate and insert onto bone, the number of different muscle heads and muscle fibre architecture. How variation in these anatomical structures relates to functional complexity (i.e., the number of different functions an organism can perform, and how efficiently they can be performed) across an organisms' phylogenetic history is a fundamental question challenging evolutionary biologists to this day (McShea, 2000; Adami, 2002). Using a cuttingedge combination of interdisciplinary techniques, this thesis contributes toward the growing understanding of how functional complexity - in terms of locomotion - and complexity in musculoskeletal anatomy can be related, using frogs as model organisms. The overarching aims were to 1) characterise and compare the musculoskeletal anatomy of a wide variety of species that specialise in arboreal and terrestrial jumping, swimming, walking/hopping, or burrowing; and 2) directly quantify and assess the functional significance of anatomical variation in hindlimb proportions on jumping mechanics. To address these aims, I applied the theoretical workflow outlined by Richards (2019), which describes the creation of a musculoskeletal model for biomechanical analyses of function, to a broad range of species in terms of both locomotor mode, habitat type, and phylogenetic placement. Using a combination of anatomical, phylogenetic, experimental, and theoretical data, I have presented several detailed comparative analyses of anuran morphology and function over 160 million years of evolution (Jetz & Pyron, 2017; Portik et al., 2023).

Firstly, I characterised the skeletal anatomy of 164 species spanning all extant anuran families to quantify and explore skeletal diversity (Chapter 2). The findings of this initial investigation led to two main paths of enquiry. Firstly, how bone anatomy is related to muscular anatomy, and how this relationship might change depending on a frog's locomotor mode. The muscle anatomy of 30 specimens was digitally dissected to enable the first quantitative evaluation of anuran pelvis and

hindlimb muscle anatomy across multiple representative species from all five primary locomotor modes, and to create the largest digital library of 3D musculoskeletal models of anurans to date (Chapter 3). For ten species, I went one step further, and performed the first digital comparative analysis of muscle fibre architecture in frogs (Chapter 4). The second line of enquiry resulting from the observations made in Chapter 2 involved exploring the biomechanical implications of variation in hindlimb geometry for locomotor function, specifically jumping mechanics. Bone measurements were combined with real kinematics recorded from an *in vivo* experiment (Richards *et al.*, 2017) to simulate theoretical hindlimb motions for all 164 species (Chapter 5). Joint torques and ground reactions forces were then estimated for a range of hypothetical models spanning both realistic and extreme hindlimb proportions (Chapter 6). This discussion chapter summarises the most important findings concluded from this thesis, how they address the knowledge gaps outlined in Chapter 1, and how they lay the foundation for some new directions in the fields of functional morphology and evolutionary biology.

7.2 Key findings

7.2.1 Novel insights into how musculoskeletal anatomy differs between frogs specialising in different locomotor functions could provide the means to predict the lifestyle of extinct species

Throughout this thesis, I have analysed skeletal and muscular data on several different anatomical scales to determine how the anuran body plan has evolved in relation to locomotor mode. In summary, sacral shape, limb proportions, and bone thickness were found to be good predictors of Archaeobatrachia versus more phylogenetically derived frogs, as well as jumping versus non-jumping frogs, which will have important consequences for interpreting behaviour from anatomy for extinct species (see section 7.3.2). The differences between the locomotor modes within these broad groups is better described by muscle anatomy. This includes many interesting observations which have never been quantified before, such as size differences in the small hip and tarsal muscles, as well as differences in the number of muscles in the pelvis and hindlimb. Here, I bring together all of these key insights to form a comprehensive summary of the strongest functional mediators in frogs.

Frogs specialising in jumping are characterised by narrow sacral bones, and long hindlimbs with elongated shank and proximal foot segments (Table 2.2; Figure 2.2). As hindlimb proportions are similar across jumpers from both arboreal and terrestrial habitats (Table 2.2; Figure 2.2), frogs specialising in jumping show similar kinematics when taking-off from solid ground, regardless of habitat type (Figure 5.10; Figure 5.11; Figure 5.12). In general, jumpers are also characterised by muscular shank segments (Figure 3.7), as well as muscles with shorter, more pennate fibres (Figure 4.6), which are thought to facilitate the production of higher forces (James et al., 2007; Rabey et al., 2015; Mendoza & Azizi, 2021). Although this trend in fibre architecture could only be shown in terrestrial jumpers here (Chapter 4), this result aligns with similar investigations using arboreal jumpers (Mendoza & Azizi, 2021). There are, however, several functional mediators between jumpers from different habitats in muscle anatomy. Terrestrial jumpers have large knee extensors in the thigh (Figure 3.10), while arboreal jumpers have large knee extensors in the shank (Figure 3.11), as well as thinner limb bones (Table 2.2). This could reflect adaptations to traversing an arboreal environment, which requires a different centre of gravity (de Oliveira-Lagôa et al., 2019), and the ability to climb as well as jump (Simons, 2008). Therefore, this disparity in hindlimb musculature presents new evidence of the anatomical consequences of varying locomotor requirements across habitats.

Both jumpers and swimmers invest highly into the size of ankle extensor muscles such as the plantaris longus (Figure 3.11), which amplifies power production for longer and faster jumps, as well as higher swim speeds (Gillis & Biewener, 2000; Azizi & Roberts, 2014; Astley, 2016). Unlike jumpers, swimmers have a large sacral expansion and long femurs relative to total hindlimb length (Table 2.2; Figure 2.2). Both swimmers and walkers also have a lower degree of muscle separation in the shank than other locomotor modes (Figure 3.14), which likely decreases their range of ankle motion. Walker-hoppers are largely characterised by short hindlimbs that are comparatively more even in length to their forelimbs (Table 2.2), which aligns with the findings of previous literature (Reynaga *et al.*, 2018). They sit in the centre of the skeletal morphospace (Figure 2.2), supporting the concept that walker-hopper morphology could represent the ancestral body plan in frogs (see section 7.3.2). Their thigh musculature is relatively conserved (Figure 3.8), while their shank and tarsal musculature is the most variable compared to other locomotor modes (Figure

3.11; Figure 3.13). Finally, burrowers are characterised by short, thick limb bones, with particularly large humeral crests (Table 2.2; Figure 2.2, Keeffe & Blackburn, 2020). Their hindlimbs have the most variable thigh muscle composition (Figure 3.8; Figure 3.9), as well as the most muscular tarsal segments (Figure 3.7). The shanks of burrowers are characterised by a considerably larger tibialis anticus longus than other locomotor modes, indicating that a specific type of ankle extension that excludes motion at the hip is vital for burrowing (Figure 3.11).

In terms of evolutionary trends, Archaeobatrachia are characterised best by a larger sacral expansion, and shorter and thicker hindlimbs than the more recently evolved clades, Hyloidea and Ranoidea (Table 2.2). The femur and tibiofibula of earlier diverging taxa tend to be more even in length, meaning that their hindlimb kinematics always differ significantly from the more phylogenetically derived taxa (Appendix Table G.5). This may all be because the Archaeobatrachia primarily consist of walker-hoppers, swimmers, and burrowers (Figure 2.5). Irrespective of locomotor mode, Archaeobatrachia have a lower degree of muscle separation in the thigh compared to more derived taxa (Figure 3.14), which indicates that their range of hindlimb motion might be more limited (Collings & Richards, 2019). Interestingly, there was only one significant difference across phylogenetic groups in muscular anatomy - Archaeobatrachia have a considerably larger iliacus externus muscle (Figure 3.6). This could suggest that muscles are a more evolutionarily labile element of frog anatomy than the skeleton.

7.2.2 Frogs demonstrate high anatomical complexity that could be linked to 'many-to-many' mapping of form to function

This thesis has highlighted how there is no unique combination of musculoskeletal characteristics for any locomotor mode, habitat type, or phylogenetic group (Fabrezi et al., 2014; Soliz et al., 2017; Marsh, 2022; Vera et al., 2022). There are several cases where there is an unexpected lack of significant differences in musculoskeletal anatomy between these groups, contrasting findings from previous anatomical studies and functional experiments. For example, pelvis and hindlimb morphology often do not fit into the discrete categories of anatomical specialisation prescribed for each locomotor mode (Figure 2.6) by previous literature (Emerson, 1979; Reilly & Jorgensen, 2011). Knee extensors, femur adductors and femur retractors, which take up a large proportion of thigh muscle mass, have crucial roles in jumping and swimming (Peplowski & Marsh, 1997; Gillis & Biewener, 2000;

Nauwelaerts *et al.*, 2007; Přikryl *et al.*, 2009; Danos & Azizi, 2015; Astley, 2016; Marsh, 2022; Garcia-Pelagio *et al.*, 2023), yet the only functional muscle groups in the thigh that differed significantly between locomotor modes in the present study were femur stabilisers and long-axis rotators (Figure 3.10). Correspondingly, several functional studies have found distinct differences in jumping performance between frogs specialising in different locomotor modes, but a lack of consistent differences in muscle power output, likely due to the role tendons play in power amplification (Roberts *et al.*, 2011; Astley & Roberts, 2014; Astley, 2016; Mendoza *et al.*, 2020). Asides from the role of other elements of morphology linked to locomotor function not explored here (elastic storage mechanisms, neural control, etc.), this general outcome of high morphological plasticity among frogs within the same locomotor group has two key explanations.

Firstly, frogs have shown convergence of phenotypes across broad temporal and geographical scales due to similar microhabitats and locomotor requirements, rather than phylogenetic constraints (Moen et al., 2013; Moen et al., 2016). The high anatomical variation observed throughout this thesis supports the concept that there could be an evolutionary lag in the convergence of phenotypes (Moen et al., 2016). If frogs utilising the same locomotor mode had all converged onto the 'optimal' phenotype, then I would expect to see less variation, and potentially more significant differences between each locomotor mode. This could be because frogs have not had enough time specialising in that specific locomotor function to reach its estimated anatomical optimum (Moen et al., 2016). A more likely explanation is that functional trade-offs do not permit frogs to reach their 'optimal' phenotype (Moen, 2019). More digital dissections will be needed to extract an accurate phylogenetic signal for muscle anatomy (Münkemüller et al., 2012). A similar approach to Moen et al. (2016) should then be used, where the data acquired throughout this thesis would be run through Orstein-Uhlenbeck models of evolution to identify the adaptive optima for each locomotor mode.

Secondly, it is highly likely that frogs can use many different, overlapping variations of bone and muscle anatomy to meet their performance requirements. For example, pelvis and tarsal musculature (Figure 3.6; Figure 3.9), and fibre architecture (Figure 4.6) show very few differences between locomotor modes. These two observations could therefore provide examples of many-to-one mapping of form to function in frogs (Figure 1.1B; Wainwright *et al.*, 2005). This thesis has also uncovered

examples of one-to-many mapping (Figure 1.1A), where many functions likely benefit from similar morphologies (Wainwright et al., 2005; Moen, 2019). For instance, there are similar skeletal proportions in both arboreal and terrestrial jumpers (Figure 2.2) and overall hindlimb muscle composition is relatively similar across all locomotor modes (Figure 3.7). These kinds of complex, labile relationships have been suggested to alleviate functional trade-offs, and therefore allow for diversity in function, i.e., the ability to perform multiple locomotor modes, albeit sub-optimally (Kargo & Rome, 2002; Nauwelaerts et al., 2007; Herrel et al., 2014; Soliz et al., 2017; Moen, 2019). Having an intermediate phenotype which can adapt to multiple locomotor requirements may therefore be favoured by natural selection (Nauwelaerts et al., 2007), especially since environmental conditions can fluctuate often, and the majority of frog species are required to return to water to breed (Gomez-Mestre et al., 2012). The work from Chapters 5 and 6 exemplify this, as the function of the shank and its associated joints could potentially be prioritised over other hindlimb segments to minimise the forces required for take-off. Since multiple types of form-function relationships are interacting simultaneously in frogs, there is likely to be a highly complex matrix of 'many-to-many' mapping dictating their evolutionary trajectory, i.e., multiple phenotypic traits are influencing multiple measures of performance (Bergmann & Elroy, 2014). A future study could import performance measures across all locomotor modes and the important morphological traits identified in this thesis into an interspecific 'F-matrix' to quantify the complexity of this system in frogs with more certainty (Bergmann & McElroy, 2014).

7.2.3 The effect of hindlimb geometry on jumping biomechanics depends on which segment of the hindlimb is varied

There are a multitude of factors that contribute towards achieving 'optimal' locomotor performance which rarely act independently of one another. Variation in body proportions is one way in which frogs could adapt to their functional requirements (Rand, 1952; Zug, 1972; Emerson, 1978; Choi *et al.*, 2003; James *et al.*, 2005; James & Wilson, 2008; Gomes *et al.*, 2009; Herrel *et al.*, 2016; Reynaga *et al.*, 2018). This thesis focuses on investigating how the lengths of each hindlimb segment can differ between frogs specialising in different locomotor modes, since this element of anatomical complexity has received much less focus in previous studies (Dobrowolska, 1973; Enriquez-Urzelai *et al.*, 2015; Lires *et al.*, 2016; Gómez

& Lires, 2019). In Chapter 2, jumpers are found to have a longer shank and proximal foot relative to the total length of their hindlimb than non-jumpers (Table 2.2). The extent to which this association is reflecting adaptation in the properties of the associated muscles within each segment (length, mass, fibre architecture etc.), versus changes to limb geometry which would positively impact range of motion, is unknown. This prompted further investigation using both digital dissections of contrast-enhanced μ CT scans (Chapter 3) and biomechanical modelling (Chapters 5 and 6).

The results of Chapter 3 indicate that locomotor function is not necessarily enhanced via the elongation a limb segment for the 'purpose' of increasing muscle size. Though jumpers do have the largest total muscle mass in the shank, total proximal foot muscle mass is largest in burrowers (Figure 3.7) despite having the shortest tarsal segments (Table 2.2). Also, while shank and tarsal muscle size do increase with their associated bone lengths, the total muscle mass in the thigh does not increase significantly with the length of the femur. It is also worth noting that the length of each muscle within each hindlimb segment do not show consistent increases with bone length (Appendix Figure D.1; Appendix Figure D.2; Appendix Figure D.3).

Locomotor performance is not only determined by how much force muscles can produce and how fast the muscles can contract, but also how far and how fast the limbs can extend (Nauwelaerts et al., 2007; Danos & Azizi, 2015; Collings et al., 2019). Kinematics analyses suggest that an elongated shank and proximal foot is not optimised to minimise overall hindlimb motion during a fixed-distance take-off sequence (Appendix Figure G.8; Appendix Figure G.9), but rather to minimise shank rotation specifically (Figure 5.7; Figure 5.10; Figure 5.11; Figure 5.14; Figure 5.15; Table 5.6). This minimisation of rotation implies that the shank muscles need to work less to carry out the take-off sequence when the shank is longer. Subsequent dynamics analyses showed that frogs with an elongated shank require a smaller ground reaction force (Figure 6.3) and joint torques (Figure 6.5) to perform the takeoff sequence. However, despite being a prominent feature of jumpers (Table 2.2), an elongated proximal foot does not show minimised segment rotations (Figure 5.8; Figure 5.16; Table 5.6), nor a reduction in the forces required to perform the takeoff sequence (Figure 6.3; Figure 6.6). The elongated proximal foot in jumpers may instead act to enhance the function of the shank, or to ensure that the morphological

configuration of the entire hindlimb is balanced in a way that optimises both forward thrust and upward elevation, both of which are important for escaping predation (Kargo *et al.*, 2002). Overall, the series of investigations made in this thesis indicate that there is a complex mix of implications for muscle structure, muscle topography, and jumping biomechanics as differences in skeletal geometry have evolved. Additional dynamics analyses which directly quantify the impact of muscle anatomy on locomotor function will be needed to untangle the significance of these relationships and address the new questions that have arisen throughout this thesis.

7.3 Future directions

7.3.1 Musculoskeletal dynamics models

A recurring theme in this thesis is recognising the need for direct functional tests to confirm the inferences made about locomotor mode from musculoskeletal anatomy. For example, the natural next step after this thesis would be to address how variation in hindlimb proportions impacts muscle dynamics, so that we can better understand the relationship between bone size, muscle size, and function. This will be particularly important for studies of extinct taxa (see section 7.3.2). Another area of particular interest is how the varying degrees of muscular separation found across anurans might impact locomotion, as it provides a testable example of how anatomical complexity may influence functional complexity. Muscle separation can be in the form of entirely distinct heads, which can also remain attached at one end of the muscle, as well in the form of a tendinous insertion within the muscle body, known as intramuscular separation (Přikryl et al., 2009; Collings & Richards, 2019), both of which will likely have functional consequences. In Chapter 3, more 'primitive' taxa were found to have a more simplified musculature in the thigh, while locomotor mode drove muscle separation in the shank, with jumpers and burrowers presenting more muscle heads than walker-hoppers and swimmers (Figure 3.14). Muscle separation likely functions as a way of increasing the range of possible hindlimb motions, and thus functional versatility (Collings & Richards, 2019), but this remains untested in frogs. It is also unknown how muscle separation impacts fibre architecture, and therefore the trade-off between muscle force and contractile speed (Chapter 4).

There are several reasons why these gaps in our knowledge remain. With five pelvis muscles and over 30 hindlimb muscles which all have specific functions contributing

differently to locomotion (Kargo & Rome, 2002; Přikryl et al., 2009; Chapter 3), there are too many parameters to reliably untangle without comparative functional analyses. Frog anatomy has many instances of complex muscle pathways that pass through or wrap around other structures and cross multiple joints (Chapter 3), making their line of action difficult to determine from records of only the origin and insertion sites (Collings & Richards, 2019). The lack of mechanical independence between muscles also means that even small amounts of anatomical variation can result in large functional differences, and that it is practically impossible to accurately predict whole-animal movement from examining just a few muscles (Kargo & Rome, 2002). Moreover, frog hindlimbs move in three different planes simultaneously (Chapter 5; Chapter 6; Astley & Roberts, 2014; Richards et al., 2017; Porro et al., 2017; Collings et al., 2022), so predictions of muscle function cannot be made solely from static muscle topology. Function can also vary throughout the duration of the movement and largely depends on initial limb configuration, making the interactions between joint torques, muscle forces and joint angles across multiple structures highly complex (Chapter 6; Kargo & Rome, 2002; Collings et al., 2022).

Incorporating multiple muscles and bones into computational dynamics models will be key to addressing these challenges. Musculoskeletal dynamics modelling has frequently been used to study the locomotion of vertebrates, particularly humans (Sylvester et al., 2021) and dinosaurs (Bishop et al., 2021c). Many models are informed by diceCT (Orsbon et al., 2018; Wilken et al., 2019; Demuth et al., 2022) and, in more recent studies, muscle fibre tracking algorithms (Sánchez et al., 2014; Püffel et al., 2021), as this preserves the 3D topology and allows the interactions between muscles to be analysed with more accuracy. Theoretical simulations enable the systematic fixation of each parameter influencing motion in such a way that the individual and combined impact on function is substantially easier to elucidate, i.e., sensitivity tests can be performed with easier identification of causation compared to *in vivo* studies. This approach can track how the net action of all muscles, which are all generating different forces simultaneously, impacts movement throughout its entire duration across all planes of motion (Kargo & Rome, 2002). Ultimately, utilising this method would provide more direct evidence of how differences in muscle architecture affect hindlimb multi-functionality, and therefore versatility in locomotor function.

Despite being a powerful method for quantifying function based on anatomy, musculoskeletal modelling of anuran behaviours is relatively uncommon (Kargo & Rome, 2002; Collings et al., 2022). Comparative functional analyses of hindlimb muscle dynamics across representative species specialising in each locomotor mode have never been done in frogs before. The primary challenge facing the development of musculoskeletal dynamics models is the time-consuming process of extracting anatomical information and combining it with in vivo data. By collating a library of 3D musculoskeletal models from digital dissections of diceCT scans (Chapter 3), this thesis provides the foundation for conducting these fundamental functional analyses. This thesis also tests the kinematics (Chapter 5) and dynamics (Chapter 6) methods required to build preliminary musculoskeletal models. Using the data provided here, future studies can directly estimate muscle function during locomotion by systematically fixing and varying the relevant parameters (Collings et al., 2022). For example, to discover whether the variation in muscle anatomy I observed across species represents a division of functional roles, dynamics models should be used to selectively add and remove muscle heads and/or tendinous insertions. Then, the resultant changes in the timing of muscle activation and the magnitude of muscle moment arms and joint torques can be measured. The priority muscles to test would be the cruralis, adductor magnus, and semitendinosus thigh muscles, as well as the tibialis anticus longus and extensor cruris brevis shank muscles, as they show the most variation in muscle number (Supplementary Dataset 5). The gracilis major and semimembranosus, should also be tested, as they often display intramuscular separation. Data on the differences in mass distribution and variation in the forces generated by stretched ligaments and tendons between frogs specialising in different locomotor modes should also be incorporated for a more comprehensive evaluation (Azizi & Roberts, 2014).

7.3.2 Predicting the behaviour of extinct taxa

Since the behaviour of extinct animals cannot be observed directly, studies have relied on indirect inferences about the role of locomotion in the evolution of anurans from the anatomy of extant congruent taxa. Theoretical approaches to how geometery influences function could provide further insight into the behaviour of extinct and rarely observed taxa. This thesis lays the foundation for this approach by analysing the predictive power of skeletal morphology (Chapter 2) and running biomechanical simulations (Chapters 5 and 6) which test how skeletal variation

impacts motion. It would be interesting to see where extinct species, which all have distinct morphologies (Holman, 2003), place in skeletal morphospace. For example, the oldest known frog Triadobatrachus has a pelvic and hindlimb morphology more suitable for walking (Lires et al., 2016), while Early Cretaceous frog Wealdenbatrachus has limb proportions suggestive of a good jumper (Gómez & Lires, 2019; Figure 7.1A). Beelzebufo, a huge frog from the Late Cretaceous, has similar skeletal proportions to many backwards-burrowers (Evans et al., 2014). Furthermore, how might these species perform in the biomechanical simulations tested in this thesis? If the interpretations of anatomy in previous studies are correct, most extinct species would be expected to have kinematics and dynamics outputs within a similar functional area as non-jumpers (Figure 7.1B). Considering the new information on the differences in relative muscle size between jumpers and nonjumpers presented in this thesis (Chapter 3), future studies could also examine the fossils for evidence of muscle attachment sites (e.g., using synchrotron microtomography; Sanchez et al., 2013). Using the 3D musculoskeletal dissection for the most basal living frog, Ascaphus truei, provided in Chapter 3, muscles could then be grafted onto models of the fossil skeleton according to their hindlimb proportions and muscle attachment sites. This model can then be tested for potential functional abilities in musculoskeletal dynamics simulations (Lautenschlager, 2016). If sufficient scan resolution is acquired, the muscle fibres in Ascaphus would be another interesting variable to include (Chapter 4) using the methods from Sánchez et al. (2014). Essentially, the techniques developed throughout this thesis could easily be adapted to study extinct taxa.

These approaches would help to finally answer whether the ancestral locomotor mode of frogs was jumping or walking, which has been a matter of debate for many decades. Frogs are deemed as specialised in jumping when they can perform a leap greater than eight times their snout-vent length and choose to jump and hop more often than they walk (Emerson, 1979; Reilly *et al.*, 2015; Soliz *et al.*, 2017). Compared to salamanders, the closest relative of frogs (Jetz & Pyron, 2017), which have an undulatory walking gait (Lires *et al.*, 2016), earlier studies stated that the highly specialised body plan of frogs was designed for jumping (Gans & Parsons, 1966; Shubin & Jenkins, 1995; Přikryl *et al.*, 2009). More recent studies have shown that walking or swimming was more likely to be the basal locomotor mode, as most fossil taxa have sacral bones shaped like lateral-bender or fore-aft sliding

morphotypes and have femora that are often similar in length to, or longer than, their tibiofibulae (Pugener & Maglia, 2009; Reilly & Jorgensen, 2011; Roček, 2013; Lires et al., 2016). Ancestral state reconstructions of locomotor performance have suggested that the anuran ancestor exhibited low jump forces (Herrel et al., 2016). Additionally, Gómez & Lires (2019) demonstrate that the first known emergence of jumping and swimming abilities is likely not until the Early Cretaceous. In this thesis, skeletal morphology was shown to be an accurate predictor of jumping versus nonjumping locomotor modes (Table 2.4; Table 2.5), with the expansion of the sacral diapophyses and the relative length of the hindlimb and each of its segments being strongly associated variables (Figure 2.2; Appendix Table A.2). While there may not be enough significant differences in skeletal morphology to predict the exact locomotor lifestyle of extinct frogs, largely due to one-to-many mapping of form to function (see section 7.2.2), this thesis has shown that there should be enough information in the skeleton to determine whether extinct frogs were good jumpers using fossil scans (e.g., from Evans et al., 2014; Ascarrunz et al., 2016; Xing et al., 2018; Báez & Gómez, 2019) and the biomechanical methods tested in this thesis.

Unfortunately, some taxa have incomplete fossils, and would likely require more anatomical information to be gathered before accurate predictions of locomotor function could be made. For instance, the *Electrorana* holotype is missing the entirety of the pelvis (Xing *et al.*, 2018), which contains fundamental information for predicting locomotor function (Chapter 2; Reilly & Jorgensen, 2011). In addition, most of the extinct taxa with a good fossil record (see Roček, 2013) do not appear to have any publicly available μ CT scans (pers. obs. using MorphoSource). Scanning more fossils to perform these types of analyses will be essential for expanding the questions addressed in this thesis to deeper evolutionary time scales.

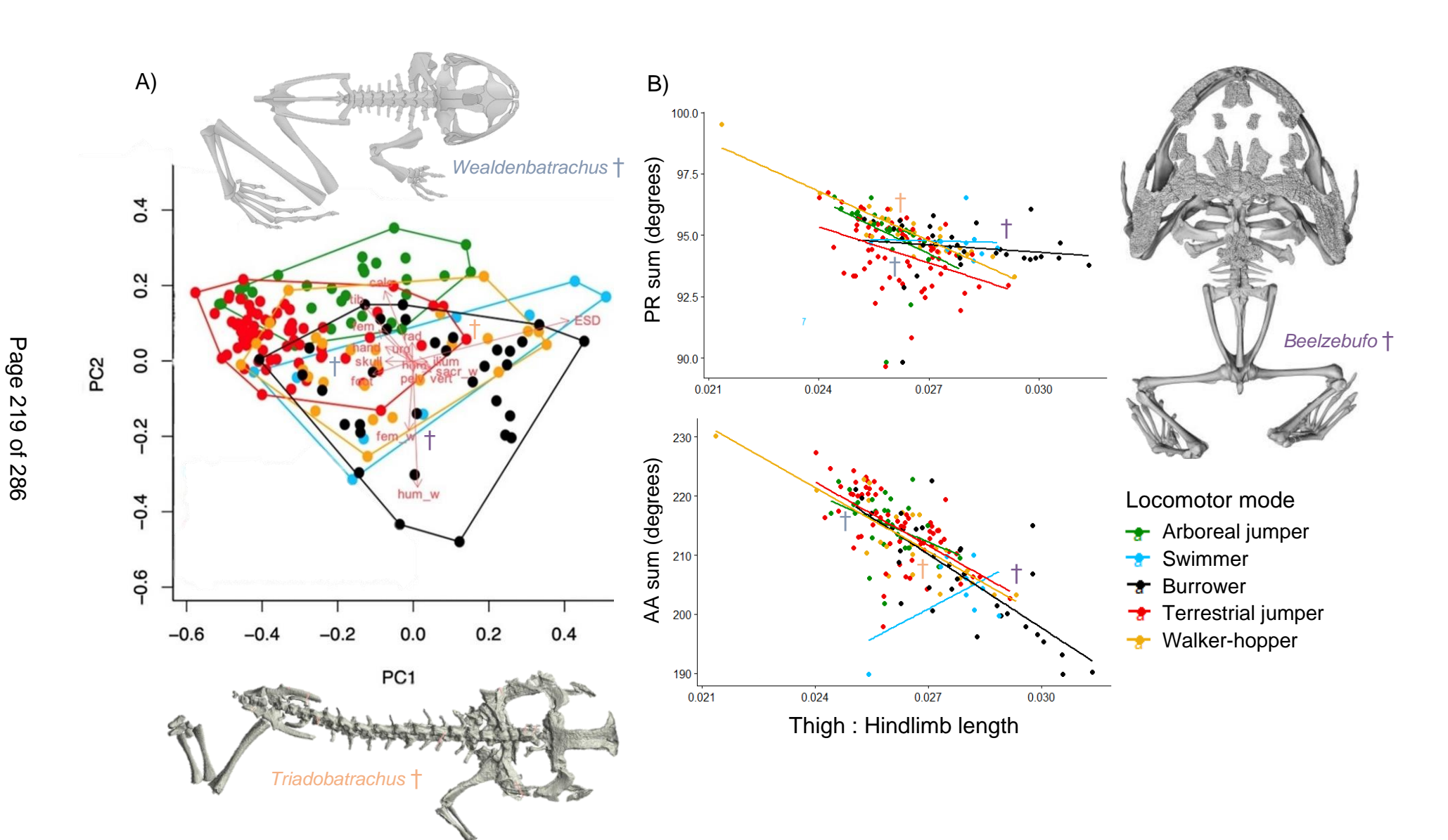


Figure 7.1 - A prediction of where three extinct frog species (†) might place in skeletal morphospace (A; adapted from Figure 2.2) and on a plot of total change in hindlimb orientation during take-off (B; adapted from Appendix Figure G.8), based on the visualisation of skeletal structure and previous studies. Each point represents a single species, coloured according to their locomotor mode in both figures. Principal component (PC) loadings are indicated by the red arrows in (A). CT images were adapted from Báez & Gómez (2019) for *Wealdenbatrachus*, Ascarrunz *et al.* (2016) for *Triadobatrachus*, and Evans *et al.* (2014) for *Beelzebufo*. PR = protraction-retraction and AA = abduction-adduction.

7.3.3 Assigning categories to continuous data

Categorising each species under one discrete locomotor mode and habitat type, though common practice in previous studies (Jorgensen & Reilly, 2013; Buttimer et al., 2020), is not straightforward. The literature and personal observations from different field biologists can sometimes be contradictory (pers. comms. Dave Blackburn, Andrew Gray, and Raúl Gómez). Since frogs are small creatures renowned for their ability to occupy difficult-to-reach places (pers. comms. Dave Blackburn), behavioural observations can be difficult, and so species long thought to belong to one specific locomotor mode can then be discovered to occupy an entirely 'new' habitat or perform an entirely 'new' behaviour. For instance, the locomotor requirements for an arboreal lifestyle can include climbing, jumping, gliding, or a combination of these modes (Wells, 2007), and the use of each mode may vary across each area of the habitat, e.g., from the ground onto the tree, along branches, and between neighbouring trees. Some categories may also be too broad, and therefore not accurately representing the variation in locomotor function, which could undermine comparative anatomical analyses. For example, burrowing locomotion can be further subdivided into taxa that burrow using their forelimbs, or their hindlimbs, but these data are not readily available for many taxa (Keeffe & Blackburn, 2020). Without the appropriate sensitivity tests addressing these subtle differences in habitat type and locomotor mode, the analytical power of comparative analyses may be undermined.

Previous studies have handled the blended nature of locomotor diversity (and diet, habitat, reproductive mode, etc.) using ordinal ranks (Nations *et al.*, 2019), relative proportions of time spent occupying each category (Soliz *et al.*, 2017), or subcategorisations of primary functions (Fratani *et al.*, 2017; Ponssa *et al.*, 2018). In Page 220 of 286

this thesis, variability was incorporated by considering potential alternative locomotor and habitat categories in predictive models (Table 2.4; Table 2.5) according to extensive searches of recent literature (e.g., Jorgensen & Reilly, 2013; Keeffe & Blackburn, 2020) and personal communications with three field biologists from different institutions. However, there is a need for more detailed and publicly accessible accounts of animal behaviour, as well as in-depth sensitivity tests of how different categorisations impact the outcomes of comparative analyses. I hypothesise that this research would find that locomotor function occupies more of an adaptive landscape than a series of discrete 'modes'. Only by filling these knowledge gaps can studies accurately define functional complexity and clarify its relationship to anatomical complexity in frogs.

7.3.4 Generalist versus specialist

The terms 'generalist' and 'specialist' have long been used to describe all kinds of animal behaviour. For instance, *Phlyctimantis maculatus* has been described as a generalist frog, as it can run, walk, jump, climb, swim, and burrow, and is known to occupy semi-aquatic and arboreal habitats (Ahn *et al.*, 2004; Danos & Azizi, 2015). Its locomotor versatility is often the basis for using *P. maculatus* to build biomechanical models of frog motion (Chapters 5 and 6; Richards *et al.*, 2017; Porro *et al.*, 2017; Collings *et al.*, 2022). Meanwhile, *Xenopus laevis* is referred to as an aquatic specialist, which may explain its highly unique muscle morphology (Porro & Richards, 2017). Similarly, burrowers such as *Rhinophrynus dorsalis* and *Nasikabatrachus sahyadrensis* are described as locomotor specialists as they have a unique set of anatomical features suited to a subterranean lifestyle (Emerson, 1976; Trueb & Gans, 1978; Keeffe & Blackburn, 2020).

However, what classifies as a locomotor 'specialist' and 'generalist' has not been consistently defined across the literature, which undermines the ability to define complexity in anatomy and function (McShea, 2000). Vassallo *et al.* (2021) found that even a terrestrial toad (*Rhinella arenarum*) can climb given the circumstances - it just uses a different type of grip than closely related arboreal and semi-arboreal species with similar anatomies. Should *R. arenarum* be classed as a locomotor generalist just because it will climb under laboratory conditions, even if it has not been observed doing so in nature? In the same way that functional specialisation depends on the circumstances an animal is in, defining anatomical specialisation depends on the region of the body being referred to. For example, though the

forelimb muscle morphology of forward burrowers is largely different to that of backwards burrowers (Keeffe & Blackburn, 2020), I found that hindlimb anatomy is relatively similar across burrowing styles (Figure 3.9). Future studies will need to analyse the locomotor skills and limitations of both 'generalist' and 'specialist' species in their natural environments to be able to fully understand how new niches originate. Furthermore, even just the inclusion of a third categorical variable which allows species to be described as a 'moderate specialist' (e.g., species with two locomotor modes, such as the semi-aquatic jumper *Rana temporaria*) would provide more insight into whether anatomical complexity is a prerequisite for functional complexity. To address whether anatomical and functional complexity increase as species evolve, a fundamental question in evolutionary biology (Adami, 2002), locomotor specialisation should be considered along a continuous spectrum once enough data are collected, rather than two or three discrete categories.

With this research, more accurate predictions of the functional capabilities for rare taxa which have anatomical descriptions, but lack behavioural data, could be made. Furthermore, future studies may then be able to explain some of the interesting results in this thesis pertaining to locomotor generalist, P. maculatus. This species is positioned near the centre of the pelvis (Figure 3.6) and shank (Figure 3.9) muscle morphospace, while their thigh and tarsal anatomy is more distinct. Does this represent the ideal intermediate phenotype suitable for performing all locomotor functions? The locomotor modes which require specialised anatomical features may influence the adaptive landscape more strongly than those with multiple anatomical solutions, in which case being in the centre of morphospace may not be representative of a 'generalised' anatomy. Additionally, P. maculatus has an average number of separate shank muscles, but has the lowest number of thigh muscles out of all the species in the more phylogenetically derived groups, Hyloidea and Ranoidea (Figure 3.14). This subsequent fusion of muscle heads could implicate that there has been a reduction in anatomical complexity to allow for more efficient function (McShea & Hordijk, 2013). In light of the main question posed by this thesis, anatomical complexity is not a prerequisite for functional complexity in this particular case. By investigating the concept of 'generalist versus specialist' further, future studies can see whether having a complex functional repertoire reduces or increases the need for a more complex anatomy across all areas of the anuran phylogeny.

7.3.5 Macroevolutionary relationships between anatomy and function

Previous studies often allocate entire families to one habitat or locomotor mode

(Reilly & Jorgensen, 2011; Jorgensen & Reilly, 2013). However, the predictive

analyses presented in Chapter 2 demonstrate how pelvic type, locomotor mode and habitat type can differ even at species-level, let alone between different genera. Similarly, muscle architecture varies widely between even closely related species (Chapters 3 and 4). This high anatomical variation indicates a wide range of complex locomotor functions, and thus suggests that diversity within families has been overlooked and underappreciated by previous studies. Many large families, such as the Hylidae, demonstrate large levels of variation, while other families are more conservative (Moen et al., 2013; Vidal-García et al., 2014; Soliz et al., 2017). Without acknowledging these differences, analyses may miss evidence for the existence of many-to-one and one-to-many mapping (see section 7.2.1). Different lineages of frogs with the same primary locomotor mode have been shown to converge in morphology (Moen et al., 2016) - does any divergence therefore indicate that there may be different biomechanical solutions to the same functional problem, or that there are less evolutionary constraints? Which families are backed into an evolutionary corner of morphological design, and which show true diversity? Furthermore, more advanced phylogenetic analyses will be needed to determine whether differences in shape are specifically linked to specialisation towards a single locomotor mode, are reflections of a greater ability to use a range of locomotor modes (i.e., higher functional complexity), or are part of a phylogenetic legacy. For example, are the unique anatomies observed in Archaeobatrachia, such as the lack of pyriformis and large, subdivided iliacus externus in specialised swimmer, X. laevis (Figure 3.6; Porro & Richards, 2017), a result of functional specialisation, or primitiveness? Is the generalised locomotor function of *P. maculatus* a culmination of abilities through its ancestors, or a set of recent adaptations in response to new environmental conditions? Do the frogs with higher muscle separation (i.e., more independently varying parts) have a higher potential of becoming more functionally and morphologically diverse than other lineages (Wainwright et al., 2005)? This thesis begins to address these questions by mapping the key features of anatomy and locomotor function onto the frog phylogeny at a species level (Figure 2.5; Figure 3.14), but more precise definitions of locomotor capabilities (see sections 7.3.3 and 7.3.4) and targeted phylogenetic approaches are needed to identify

The evolution of musculoskeletal anatomy and locomotor mode in frogs

macroevolutionary trends. With ancestral state reconstruction (Astley, 2016) and the testing of a broader range of evolutionary models (Moen *et al.*, 2016), the evolutionary origins of novel anatomies and the adaptive optima for each locomotor mode could also be identified.

7.4 Conclusion

Ultimately, this thesis advances our current understanding of how form-function relationships are related to the evolution of frogs. Performing detailed comparative anatomical analyses and testing computational tools capable of obtaining the quantitative evidence needed to elucidate the relationships between form and function has unveiled potential links between increasing anatomical complexity and limb multi-functionality. In summary, I demonstrate how there are many anatomical solutions to how frogs may traverse different environments and I provide new insights into how specialization in hindlimb proportions in favour of another primary locomotor mode can impact jumping mechanics. By showing that Richards's (2019) theoretical workflow can be applied to both extant and hypothetical frogs, I have demonstrated its potential for studying rare or extinct species without the need for invasive or destructive techniques. I have shown that any morphological, kinematics, or dynamics data, whether experimental or hypothetical, can be used to explore the relationship between anatomy and function using this modular approach. Not only has this thesis contributed a substantial amount towards our current knowledge of the anuran musculoskeletal system, but it has also unveiled a series of interesting new hypotheses to test, and the 3D musculoskeletal models required to test them. This thesis has therefore paved a path for future researchers to continue exploring the relative impacts of locomotor function, habitat type and phylogenetic history on vertebrate anatomy, and to ultimately answer the main question posed by this thesis: is anatomical complexity required for functional complexity?

References

- AmphibiaWeb (2023). https://amphibiaweb.org> University of California, Berkeley, CA, USA.
- Abdala, V., Ponssa, M.L., Tulli, M.J., Fabre, A.C. & Herrel, A. (2018). Frog tendon structure and its relationship with locomotor modes. *Journal of Morphology*, 279(7), pp.895-903.
- Ahn, A.N., Furrow, E. & Biewener, A.A. (2004). Walking and running in the redlegged running frog, *Kassina maculata*. *Journal of Experimental Biology*, 207(3), pp.399-410.
- Allen, V., Elsey, R.M., Jones, N., Wright, J. & Hutchinson, J.R. (2010). Functional specialization and ontogenetic scaling of limb anatomy in *Alligator mississippiensis*. *Journal of Anatomy*, 216(4), pp.423-445.
- Anderson, M.J (2005). *Permutational multivariate analysis of variance*. Department of Statistics, University of Auckland, Auckland, 26, pp.32-46.
- Arbour, J.H. (2023). GoodFibes: An R Package for The Detection of Muscle Fibers from diceCT Scans. *Integrative Organismal Biology*, *5*(1), p.obad030.
- Ascarrunz, E., Rage, J.C., Legreneur, P. & Laurin, M. (2016). *Triadobatrachus massinoti*, the earliest known lissamphibian (Vertebrata: Tetrapoda) reexamined by μCT scan, and the evolution of trunk length in batrachians. *Contributions to Zoology*, *85*(2), pp.201-234.
- Astley, H.C. (2016). The diversity and evolution of locomotor muscle properties in anurans. *Journal of Experimental Biology*, 219(19), pp.3163-3173.
- Astley, H.C., Haruta, A. & Roberts, T.J. (2015). Robust jumping performance and elastic energy recovery from compliant perches in tree frogs. *Journal of Experimental Biology, 218(21)*, pp.3360-3363.
- Astley, H.C. & Roberts, T.J. (2014). The mechanics of elastic loading and recoil in anuran jumping. *Journal of Experimental Biology*, *217(24)*, pp.4372-4378.
- Azizi, E. & Deslauriers, A.R. (2014). Regional heterogeneity in muscle fiber strain: the role of fiber architecture. *Frontiers in Physiology*, *5*, p.303.
- Azizi, E. & Roberts, T.J. (2014). Geared up to stretch: pennate muscle behavior during active lengthening. *Journal of Experimental Biology, 217(3),* pp.376-381.
- Azizi, E. & Roberts, T.J. (2010). Muscle performance during frog jumping: influence of elasticity on muscle operating lengths. *Proceedings of the Royal Society B: Biological Sciences*, 277(1687), pp.1523-1530.
- Azizi, E., Brainerd, E.L. & Roberts, T.J. (2008). Variable gearing in pennate muscles. *Proceedings of the National Academy of Sciences*, 105(5), pp.1745-1750.
- Báez, A.M. & Gómez, R.O. (2019). Redescription of the overlooked basal frog *Wealdenbatrachus* reveals increased diversity among Early Cretaceous anurans. *Cretaceous Research*, *99*, pp.14-29.
- Barton, K. & Barton, M.K. (2015). *Package 'mumin'*. Version, 1(18), p.439.
- Bates, K.T., Wang, L., Dempsey, M., Broyde, S., Fagan, M.J. & Cox, P.G. (2021). Back to the bones: do muscle area assessment techniques predict functional evolution across a macroevolutionary radiation? *Journal of the Royal Society Interface*, 18(180), p.e20210324.
- Baur, H. & Leuenberger, C. (2011). Analysis of ratios in multivariate morphometry. *Systematic Biology*, 60(6), pp.813-825.
- Bergmann, P.J. & McElroy, E.J. (2014). Many-to-many mapping of phenotype to performance: an extension of the F-matrix for studying functional complexity. *Evolutionary Biology*, *41*, pp.546-560.

- Biju, S.D., Garg, S., Gururaja, K.V., Shouche, Y. & Walujkar, S.A. (2014). DNA barcoding reveals unprecedented diversity in Dancing Frogs of India (Micrixalidae, *Micrixalus*): a taxonomic revision with description of 14 new species. *Ceylon Journal of Science (Biological Sciences)*, 43(1), pp.37-123.
- Bishop, P.J., Wright, M.A. & Pierce, S.E. (2021a). Whole-limb scaling of muscle mass and force-generating capacity in amniotes. *PeerJ*, *9*, p.e12574.
- Bishop, P.J., Michel, K.B., Falisse, A., Cuff, A.R., Allen, V.R., De Groote, F. & Hutchinson, J.R. (2021a). Computational modelling of muscle fibre operating ranges in the hindlimb of a small ground bird (*Eudromia elegans*), with implications for modelling locomotion in extinct species. *PLoS Computational Biology*, 17(4), p.e1008843.
- Bishop, P.J., Cuff, A.R. & Hutchinson, J.R. (2021b). How to build a dinosaur: Musculoskeletal modelling and simulation of locomotor biomechanics in extinct animals. *Paleobiology*, *47*(1), pp.1-38.
- Bishop, P.J., Bates, K.T., Allen, V.R., Henderson, D.M., Randau, M. & Hutchinson, J.R, (2020). Relationships of mass properties and body proportions to locomotor habit in terrestrial Archosauria. *Paleobiology*, *46*(4), pp.550-568.
- Biewener, A.A. (2003). Animal Locomotion. Oxford university press: Oxford, UK.
- Biewener, A.A. (1989). Scaling body support in mammals: limb posture and muscle mechanics. *Science*, *245*(*4913*), pp.45-48.
- Böhmer, C., Fabre, A.C., Herbin, M., Peigné, S. & Herrel, A., 2018. Anatomical basis of differences in locomotor behavior in martens: A comparison of the forelimb musculature between two sympatric species of *Martes*. *The Anatomical Record*, 301(3), pp.449-472.
- Brainerd, E.L., Baier, D.B., Gatesy, S.M., Hedrick, T.L., Metzger, K.A., Gilbert, S.L. & Crisco, J.J. (2010). X-ray reconstruction of moving morphology (XROMM): precision, accuracy and applications in comparative biomechanics research. *Journal of Experimental Zoology Part A: Ecological Genetics and Physiology*, 313(5), pp.262-279.
- Bribiesca-Contreras, F. & Sellers, W.I. (2017). Three-dimensional visualisation of the internal anatomy of the sparrowhawk (*Accipiter nisus*) forelimb using contrast-enhanced micro-computed tomography. *PeerJ*, *5*, p.e3039.
- Brocklehurst, R., Porro, L., Herrel, A., Adriaens, D. & Rayfield, E. (2019). A digital dissection of two teleost fishes: comparative functional anatomy of the cranial musculoskeletal system in pike (*Esox lucius*) and eel (*Anguilla anguilla*). *Journal of Anatomy*, 235(2), pp.189-204.
- Broeckhoven, C. & du Plessis, A. (2018). X-ray microtomography in herpetological research: a review. *Amphibia-Reptilia*, *39*(4), pp.377-401.
- Buttimer, S. M., Stepanova, N., & Womack, M. C. (2020). Evolution of the unique anuran pelvic and hindlimb skeleton in relation to microhabitat, locomotor mode, and jump performance. *Integrative and Comparative Biology, 60(5),* pp.1–16.
- Calow, L.J. & Alexander, R.M. (1973). A mechanical analysis of a hind leg of a frog (*Rana temporaria*). *Journal of Zoology, 171(3),* pp.293-321.
- Charles, J., Kissane, R., Hoehfurtner, T. & Bates, K.T. (2022). From fibre to function: are we accurately representing muscle architecture and performance? *Biological Reviews*, *97*(4), pp.1640-1676.
- Charles, J.P., Cappellari, O., Spence, A.J., Wells, D.J. & Hutchinson, J.R. (2016). Muscle moment arms and sensitivity analysis of a mouse hindlimb musculoskeletal model. *Journal of Anatomy*, 229(4), pp.514-535.

- Choi, I., Shim, J. H., & Ricklefs, R. E. (2003). Morphometric relationships of take-off speed in anuran amphibians. *Journal of Experimental Zoology Part A:* Comparative Experimental Biology, 299(2), pp.99–102.
- Choi, I.H. & Park, K. (1996). Variations in take-off velocity of anuran amphibians: relation to morphology, muscle contractile function and enzyme activity. *Comparative Biochemistry and Physiology Part A: Physiology, 113(4)*, pp.393-400.
- Citadini, J. M., Brandt, R., Williams, C. R., & Gomes, F. R. (2018). Evolution of morphology and locomotor performance in anurans: relationships with microhabitat diversification. *Journal of Evolutionary Biology, 31(3),* pp.371–381.
- Clemente, C.J. & Richards, C. (2013). Muscle function and hydrodynamics limit power and speed in swimming frogs. *Nature Communications*, *4*(1), 2737.
- Collings, A. J., Eberhard, E., Basu, C. & Richards, C. T. (2022). Functional analysis of anuran pelvic and thigh anatomy using musculoskeletal modeling of *Phlyctimantis maculatus. Frontiers in Bioengineering and Biotechnology, 10*, p.806174.
- Collings, A. J., Porro, L. B., Hill, C., & Richards, C. T. (2019). The impact of pelvic lateral rotation on hindlimb kinematics and stride length in the red-legged running frog, *Kassina maculata. Royal Society Open Science*, *6*(5), p.190060.
- Collings, A. J., & Richards, C. T. (2019). Digital dissection of the pelvis and hindlimb of the red-legged running frog, *Phlyctimantis maculatus*, using Diffusible lodine Contrast Enhanced computed microtomography (DICE µ CT). *PeerJ*, 7, p.e7003.
- Collyer, M.L. & Adams, D.C. (2018). RRPP: An r package for fitting linear models to high-dimensional data using residual randomization. *Methods in Ecology and Evolution*, *9*(7), pp.1772-1779.
- Cox, P.G. & Faulkes, C.G. (2014). Digital dissection of the masticatory muscles of the naked mole-rat, *Heterocephalus glaber* (Mammalia, Rodentia). *PeerJ*, *2*, p.e448.
- Dawood, Y., Hagoort, J., Siadari, B.A., Ruijter, J.M., Gunst, Q.D., Lobe, N.H.J., Strijkers, G.J., de Bakker, B.S. & van den Hoff, M.J.B. (2021). Reducing soft-tissue shrinkage artefacts caused by staining with Lugol's solution. *Scientific Reports*, 11(1), pp.1-12.
- Dahanukar, N., Modak, N., Krutha, K., Nameer, P.O., Padhye, A.D. & Molur, S. (2016). Leaping frogs (Anura: Ranixalidae) of the Western Ghats of India: An integrated taxonomic review. *Journal of Threatened Taxa, 8(10),* pp.9221-9288.
- Danos, N. & Azizi, E. (2015). Passive stiffness of hindlimb muscles in anurans with distinct locomotor specializations. *Zoology*, *118(4)*, pp.239-247.
- De Oliveira-Lagôa, S., Cruz, F.B., Azócar, D.L.M., Lavilla, E.O. & Abdala, V. (2019). Anuran forelimb muscle tendinous structures and their relationship with locomotor modes and habitat use. *Current Zoology*, *65(5)*, pp.599-608.
- Demuth, O.E., Rayfield, E.J. & Hutchinson, J.R. (2020). 3D hindlimb joint mobility of the stem-archosaur *Euparkeria capensis* with implications for postural evolution within Archosauria. *Scientific Reports*, 10(1), p.15357.
- Dickinson, E., Kolli, S., Schwenk, A., Davis, C.E. & Hartstone-Rose, A. (2020). DiceCT analysis of the extreme gouging adaptations within the masticatory apparatus of the aye-aye (*Daubentonia madagascariensis*). *The Anatomical Record*, 303(2), pp.282-294.

- Dickinson, E., Stark, H. & Kupczik, K. (2018). Non-destructive determination of muscle architectural variables through the use of dice CT. *The Anatomical Record*, *301(2)*, pp.363-377.
- Dobrowolska, H. (1973). Body-part proportions in relation to the mode of locomotion in anurans. *Zoologica Poloniae*, 23, pp.59-108.
- Duellman, W.E. & Trueb, L. (1986). *Biology of amphibians*. New York: McGraw-Hill Book Company.
- Dunlap, D.G. (1960). The Comparative Myology of the Pelvic Appendage in the Salientia. *Journal of Morphology*, 106(1), pp.1–76.
- Early, C.M., Morhardt, A.C., Cleland, T.P., Milensky, C.M., Kavich, G.M. & James, H.F. (2020). Chemical effects of diceCT staining protocols on fluid-preserved avian specimens. *PLoS One*, *15(9)*, p.e0238783.
- Emerson, S.B. (1988). Testing for historical patterns of change: a case study with frog pectoral girdles. *Paleobiology*, *14*(2), pp.174-186.
- Emerson, S.B. (1985). 'Jumping and leaping'. In Hildebrand M.E., Bramble D., Leim K., & Wake D., eds. Functional Vertebrate Morphology. Harvard University Press, 58–72.
- Emerson, S.B. (1982). Frog postcranial morphology: Identification of a functional complex. *Copeia*, *3*(3), pp.603–613.
- Emerson, S.B. (1979). The ilio-sacral articular in frogs: form and function. *Biological Journal of the Linnean Society, 11(March)*, pp.153–168.
- Emerson, S.B. (1978). Allometry and jumping in frogs: helping the twain to meet. *Evolution*, *32*(3), pp.551-564.
- Emerson, S.B. (1976). Burrowing in frogs. *Journal of Morphology*, 149(4), pp.437-458.
- Engelkes, K., Kath, L., Kleinteich, T., Hammel, J.U., Beerlink, A. & Haas, A. (2020). Ecomorphology of the pectoral girdle in anurans (Amphibia, Anura): Shape diversity and biomechanical considerations. *Ecology and Evolution, 10(20)*, pp.11467-11487.
- Enriquez-Urzelai, U., Montori, A., Llorente, G. A., & Kaliontzopoulou, A. (2015). Locomotor mode and the evolution of the hindlimb in Western Mediterranean anurans. *Evolutionary Biology*, *42*(2), pp.199–209.
- Evans, B.J., Carter, T.F., Greenbaum, E., Gvoždík, V., Kelley, D.B., McLaughlin, P.J., Pauwels, O.S., Portik, D.M., Stanley, E.L., Tinsley, R.C. & Tobias, M.L. (2015). Genetics, morphology, advertisement calls, and historical records distinguish six new polyploid species of African clawed frog (*Xenopus*, Pipidae) from West and Central Africa. *PLoS One*, 10(12), p.e0142823.
- Evans, S.E., Groenke, J.R., Jones, M.E., Turner, A.H. & Krause, D.W. (2014). New material of *Beelzebufo*, a hyperossified frog (Amphibia: Anura) from the Late Cretaceous of Madagascar. *PLoS One*, *9*(1), p.e87236.
- Fabrezi, M., Manzano, A.S., Abdala, V. & Lobo, F. (2014). Anuran locomotion: ontogeny and morphological variation of a distinctive set of muscles. *Evolutionary Biology, 41,* pp.308-326.
- Gans, C. (1982). Fiber architecture and muscle function. Exercise and Sport Science Reviews. Lexington (MA): Franklin University Press. pp.160–207.
- Gans, C. & Parsons, T.S. (1966). On the origin of the jumping mechanism in frogs. *Evolution*, *20*(1), pp.92-99.
- Gans, C., & Bock, W. (1965). The functional significance of muscle architecture a theoretical analysis. *Advances in Anatomy, Embryology and Cell Biology, 38,* pp.115-142.
- Garcia-Pelagio, K.P., Gutiérrez, B.M., Hernández, D.P., Calva, N.P., Segura-Alegria, B. & Ochoa-Ochoa, L.M. (2023). Locomotion and biomechanical

- adaptations in hind limb muscles of three Mexican anuran species. *South American Journal of Herpetology*, *26*(1), pp.37-43.
- Gignac, P.M., Kley, N.J., Clarke, J.A., Colbert, M.W., Morhardt, A.C., Cerio, D., Cost, I.N., Cox, P.G., Daza, J.D., Early, C.M. & Echols, M.S. (2016). Diffusible iodine-based contrast-enhanced computed tomography (diceCT): an emerging tool for rapid, high-resolution, 3-D imaging of metazoan soft tissues. *Journal of Anatomy*, 228(6), pp.889-909.
- Gignac, P.M. & Kley, N.J. (2014). Iodine-enhanced micro-CT imaging: Methodological refinements for the study of the soft-tissue anatomy of post-embryonic vertebrates. *Journal of Experimental Zoology Part B: Molecular and Developmental Evolution, 322(3),* pp.166-176.
- Gillis, G.B. & Biewener, A.A., 2000. Hindlimb extensor muscle function during jumping and swimming in the toad (*Bufo marinus*). *Journal of Experimental Biology*, 203(23), pp.3547-3563.
- Gomes, F. R., Rezende, E. L., Grizante, M. B., & Navas, C. A. (2009). The evolution of jumping performance in anurans: Morphological correlates and ecological implications. *Journal of Evolutionary Biology*, 22(5), pp.1088–1097.
- Gomez-Mestre, I., Pyron, R.A. & Wiens, J.J. (2012). Phylogenetic analyses reveal unexpected patterns in the evolution of reproductive modes in frogs. *Evolution: International Journal of Organic Evolution, 66(12),* 3687-3700.
- Gómez, R.O. & Lires, A.I. (2019). High ecomorphological diversity among Early Cretaceous frogs from a large subtropical wetland of Iberia. *Comptes Rendus Palevol*, 18(7), pp.711-723.
- Gray, J.A., Gignac, P.M. & Stanley, E.L. (2023). The first full body diffusible iodine-based contrast-enhanced computed tomography dataset and teaching materials for a member of the Testudines. *The Anatomical Record. Early view.*
- Hautier, L., Lebrun, R. & Cox, P.G. (2012). Patterns of covariation in the masticatory apparatus of hystricognathous rodents: implications for evolution and diversification. *Journal of Morphology*, *273*(*12*), pp.1319-1337.
- Hedrick, B.P., Yohe, L., Vander Linden, A., Dávalos, L.M., Sears, K., Sadier, A., Rossiter, S.J., Davies, K.T. & Dumont, E. (2018). Assessing soft-tissue shrinkage estimates in museum specimens imaged with diffusible iodinebased contrast-enhanced computed tomography (diceCT). *Microscopy and Microanalysis*, 24(3), pp.284-291.
- Herrel, A., Moureaux, C., Laurin, M., Daghfous, G., Crandell, K., Tolley, K.A., Measey, G.J., Vanhooydonck, B. & Boistel, R. (2016). Frog origins: inferences based on ancestral reconstructions of locomotor performance and anatomy. *Fossil Imprint*, 72(1-2), pp.108-116.
- Herrel, A., Vasilopoulou-Kampitsi, M., & Bonneaud, C. (2014). Jumping performance in the highly aquatic frog, *Xenopus tropicalis*: Sex-specific relationships between morphology and performance. *PeerJ*, 2014(1), pp.1–15.
- Herrel, A. & Bonneaud, C. (2012). Trade-offs between burst performance and maximal exertion capacity in a wild amphibian, *Xenopus tropicalis*. *Journal of Experimental Biology*, 215(17), pp.3106-3111.
- Holliday, C.M., Sellers, K.C., Lessner, E.J., Middleton, K.M., Cranor, C., Verhulst, C.D., Lautenschlager, S., Bader, K., Brown, M.A. & Colbert, M.W., (2022). New frontiers in imaging, anatomy, and mechanics of crocodylian jaw muscles. *The Anatomical Record*, 305(10), pp.3016-3030.

- Holliday, C.M., Tsai, H.P., Skiljan, R.J., George, I.D. & Pathan, S. (2013). A 3D interactive model and atlas of the jaw musculature of *Alligator mississippiensis*. *PLoS One*, *8*(6), p.e62806.
- Holman, J.A. (2003). Fossil frogs and toads of North America. Indiana University Press.
- Holzman, R., Collar, D.C., Mehta, R.S. & Wainwright, P.C. (2011). Functional complexity can mitigate performance trade-offs. *The American Naturalist,* 177(3), pp.E69-E83.
- Hudson, C.M., Brown, G.P. & Shine, R. (2016). Athletic anurans: the impact of morphology, ecology and evolution on climbing ability in invasive cane toads. *Biological Journal of the Linnean Society*, *119*(4), pp.992-999.
- James, R. S., & Wilson, R. S. (2008). Explosive jumping: Extreme morphological and physiological specializations of Australian rocket frogs (*Litoria nasuta*). *Physiological and Biochemical Zoology*, *81*(2), pp.176–185.
- James, R.S., Navas, C.A. & Herrel, A. (2007). How important are skeletal muscle mechanics in setting limits on jumping performance? *Journal of Experimental Biology*, *210*(6), pp.923-933.
- James, R. S., Wilson, R. S., De Carvalho, J. E., Kohlsdorf, T., Gomes, F. R., & Navas, C. A. (2005). Interindividual differences in leg muscle mass and pyruvate kinase activity correlate with interindividual differences in jumping performance of *Hyla multilineata*. *Physiological and Biochemical Zoology*, 78(5), pp.857–867.
- Shubin, N.H. & Jenkins Jr, F.A. (1995). An early Jurassic jumping frog. *Nature*, 377(6544), pp.49-52.
- Jetz, W., & Pyron, R. A. (2017). Diversification, evolutionary isolation, and imperilment across the amphibian tree of life. *Nature Ecology & Evolution*, 2(5), pp.850-858.
- Jones, M.E., Button, D.J., Barrett, P.M. & Porro, L.B. (2019). Digital dissection of the head of the rock dove (*Columba livia*) using contrast-enhanced computed tomography. *Zoological Letters*, *5*, pp.1-31.
- Jorgensen, M.E., & Reilly, S.M. (2013). Phylogenetic patterns of skeletal morphometrics and pelvic traits in relation to locomotor mode in frogs. *Journal of Evolutionary Biology*, 26(5), pp.929–943.
- Jungers, W.L., Falsetti, A.B. & Wall, C.E. (1995). Shape, relative size, and size-adjustments in morphometrics. *American Journal of Physical Anthropology*, 38(S21), pp.137-161.
- Kargo, W.J., Nelson, F. & Rome, L.C. (2002). Jumping in frogs: assessing the design of the skeletal system by anatomically realistic modelling and forward dynamic simulation. *Journal of Experimental Biology*, 205(12), pp.1683-1702.
- Kargo, W.J. & Rome, L.C. (2002). Functional morphology of proximal hindlimb muscles in the frog Rana pipiens. Journal of Experimental Biology, 205(14), pp.1987-2004.
- Katzke, J., Puchenkov, P., Stark, H. & Economo, E.P. (2022). A roadmap to reconstructing muscle architecture from CT data. *Integrative Organismal Biology*, *4*(1), p.obac001.
- Keeffe, R. & Blackburn, D.C. (2022). Diversity and function of the fused anuran radioulna. *Journal of Anatomy*, 241(4), pp.1026-1038.
- Keeffe, R., & Blackburn, D.C. (2020). Comparative morphology of the humerus in forward-burrowing frogs. *Biological Journal of the Linnean Society*, 131(2), pp.291–303.

- Kleinteich, T. & Gorb, S.N. (2015). Frog tongue acts as muscle-powered adhesive tape. *Royal Society Open Science*, *2*(9), p.150333.
- Kupczik, K., Stark, H., Mundry, R., Neininger, F.T., Heidlauf, T. & Röhrle, O. (2015). Reconstruction of muscle fascicle architecture from iodine-enhanced microCT images: a combined texture mapping and streamline approach. *Journal of Theoretical Biology, 382*, pp.34-43.
- Lanzetti, A. & Ekdale, E.G. (2021). Enhancing CT imaging: A safe protocol to stain and de-stain rare fetal museum specimens using diffusible iodine-based staining (diceCT). *Journal of Anatomy*, 239(1), pp.228-241.
- Lautenschlager, S. (2016). Digital reconstruction of soft-tissue structures in fossils. *The Paleontological Society Papers*, 22, pp.101-117.
- Lautenschlager, S., Bright, J.A. & Rayfield, E.J. (2014). Digital dissection—using contrast-enhanced computed tomography scanning to elucidate hard-and soft-tissue anatomy in the Common Buzzard *Buteo buteo. Journal of Anatomy*, 224(4), pp.412-431.
- Leonard, K.C., Worden, N., Boettcher, M.L., Dickinson, E. & Hartstone-Rose, A. (2022). Effects of long-term ethanol storage on muscle architecture. *The Anatomical Record*, *305(1)*, pp.184-198.
- Levy, J. (2018). Analog vs digital: Testing the comparability and compatibility of diceCT and gross dissection, with special emphasis on muscle tissue (Doctoral dissertation, Sam Houston State University).
- Li, Z., Ketcham, R.A., Yan, F., Maisano, J.A. & Clarke, J.A. (2016). Comparison and evaluation of the effectiveness of two approaches of diffusible iodine-based contrast-enhanced computed tomography (diceCT) for avian cephalic material. *Journal of Experimental Zoology Part B: Molecular and Developmental Evolution*, 326(6), pp.352-362.
- Lieber, R.L. (2022). Can we just forget about pennation angle? *Journal of Biomechanics*, 132, p.110954.
- Lieber, R.L. & Fridén, J. (2000). Functional and clinical significance of skeletal muscle architecture. *Muscle & Nerve: Official Journal of the American Association of Electrodiagnostic Medicine*, *23(11)*, pp.1647-1666.
- Lieber, R.L. & Bodine-Fowler, S.C. (1993). Skeletal muscle mechanics: implications for rehabilitation. *Physical Therapy*, *73*(12), pp.844-856.
- Lieber, R.L. & Brown, C.G. (1992). Sarcomere length-joint angle relationships of seven frog hindlimb muscles. *Cells Tissues Organs*, *145(4)*, pp.289-295.
- Lieber, R.L. & Shoemaker, S.D. (1992). Muscle, joint, and tendon contributions to the torque profile of frog hip joint. *American Journal of Physiology-Regulatory, Integrative and Comparative Physiology*, 263(3), pp.R586-R590.
- Lires, A. I., Soto, I. M., & Gómez, R. O. (2016). Walk before you jump: New insights on early frog locomotion from the oldest known salientian. *Paleobiology*, 42(4), pp.612–623.
- Lutz, G.J. & Rome, L.C. (1996). Muscle function during jumping in frogs. II. Mechanical properties of muscle: implications for system design. *American Journal of Physiology-Cell Physiology*, 271(2), pp.C571-C578.
- Manzano, A.S. & Barg, M. (2005). The iliosacral articulation in Pseudinae (Anura: Hylidae). *Herpetologica*, *61*(3), pp.259-267.
- Marchi, D., Leischner, C.L., Pastor, F. & Hartstone-Rose, A. (2018). Leg muscle architecture in primates and its correlation with locomotion patterns. *The Anatomical Record*, 301(3), pp.515-527.
- Marsh, R.L. (2022). Muscle preactivation and the limits of muscle power output during jumping in the Cuban tree frog *Osteopilus septentrionalis*. *Journal of Experimental Biology*, 225(19), p.jeb244525.

- Marsh, R.L. & John-Alder, H.B. (1994). Jumping performance of hylid frogs measured with high-speed cine film. *Journal of Experimental Biology, 188(1),* pp.131-141.
- Martin, M.L., Travouillon, K.J., Fleming, P.A. & Warburton, N.M. (2020). Review of the methods used for calculating physiological cross-sectional area (PCSA) for ecological questions. *Journal of Morphology*, 281(7), pp.778-789.
- McShea, D.W. & Hordijk, W. (2013). Complexity by subtraction. *Evolutionary Biology, 40,* pp.504-520.
- McShea, D.W. (2000). Functional complexity in organisms: parts as proxies. *Biology* and *Philosophy*, *15*, pp.641-668.
- Mendez, J. & Keys, A. (1960). Density of fat and bone mineral of mammalian muscle. *Metabolism-clinical and Experimental*, 9, pp.184-188.
- Mendoza, E. & Azizi, E. (2021). Tuned muscle and spring properties increase elastic energy storage. *Journal of Experimental Biology*, 224(24), p.jeb243180.
- Mendoza, E., Azizi, E. & Moen, D.S. (2020). What explains vast differences in jumping power within a clade? Diversity, ecology and evolution of anuran jumping power. *Functional Ecology*, *34*(5), pp.1053-1063.
- Moen, D. S. (2019). What determines the distinct morphology of species with a particular ecology? The roles of many-to-one mapping and trade-offs in the evolution of frog ecomorphology and performance. *American Naturalist*, 194(4), pp.E81–E95.
- Moen, D.S., Morlon, H. & Wiens, J.J. (2016). Testing convergence versus history: convergence dominates phenotypic evolution for over 150 million years in frogs. *Systematic Biology*, *65*(1), pp.146-160.
- Moen, D. S., Irschick, D. J., & Wiens, J. J. (2013). Evolutionary conservatism and convergence both lead to striking similarity in ecology, morphology and performance across continents in Frogs. *Proceedings of the Royal Society B: Biological Sciences*, 280(1773), p.20132156.
- Mosimann, J.E., 1970. Size allometry: size and shape variables with characterizations of the lognormal and generalized gamma distributions. *Journal of the American Statistical Association, 65(330)*, pp.930-945.
- Motani, R. & Schmitz, L. (2011). Phylogenetic versus functional signals in the evolution of form–function relationships in terrestrial vision. *Evolution*, *65(8)*, pp.2245-2257.
- Münkemüller, T., Lavergne, S., Bzeznik, B., Dray, S., Jombart, T., Schiffers, K. & Thuiller, W. (2012). How to measure and test phylogenetic signal. *Methods in Ecology and Evolution*, *3*, pp.743-756.
- Murray, R.M., Li, Z. & Sastry, S.S. (1994). A mathematical introduction to robotic manipulation. CRC press.
- Nali, R.C., Zamudio, K.R., Haddad, C.F. & Prado, C.P. (2014). Size-dependent selective mechanisms on males and females and the evolution of sexual size dimorphism in frogs. *The American Naturalist*, 184(6), pp.727-740.
- Nauwelaerts, S., Ramsay, J., & Aerts, P. (2007). Morphological correlates of aquatic and terrestrial locomotion in a semi-aquatic frog, *Rana esculenta*: No evidence for a design conflict. *Journal of Anatomy*, 210(3), pp.304–317.
- Nauwelaerts, S. & Aerts, P. (2003). Propulsive impulse as a covarying performance measure in the comparison of the kinematics of swimming and jumping in frogs. *Journal of Experimental Biology*, 206(23), pp.4341-4351.
- Neuwirth, E. & Neuwirth, M.E. (2011). Package 'RColorBrewer'. *Physical Review D,* 84, pp.1-5.

- Nomura, F., Rossa-Feres, D.C. & Langeani, F. (2009). Burrowing behavior of *Dermatonotus muelleri* (Anura, Microhylidae) with reference to the origin of the burrowing behavior of Anura. *Journal of Ethology*, 27, pp.195-201.
- Nyakatura, J.A., Baumgarten, R., Baum, D., Stark, H. & Youlatos, D. (2019). Muscle internal structure revealed by contrast-enhanced µCT and fibre recognition: The hindlimb extensors of an arboreal and a fossorial squirrel. *Mammalian Biology*, 99(1), pp.71-80.
- Orsbon, C.P., Gidmark, N.J. & Ross, C.F. (2018). Dynamic musculoskeletal functional morphology: integrating diceCT and XROMM. *The Anatomical Record*, 301(2), pp.378-406.
- Orsbon, C.P., Gidmark, N.J., Gao, T. & Ross, C.F. (2020). XROMM and diceCT reveal a hydraulic mechanism of tongue base retraction in swallowing. *Scientific Reports*, 10(1), p.8215.
- Padilla, P., Courant, J. & Herrel, A. (2019). Allocation trade-offs impact organ size and muscle architecture in an invasive population of Xenopus laevis in Western France. *Journal of Anatomy*, 235(6), pp.1057-1064.
- Pagel, M. (1999). Inferring the historical patterns of biological evolution. *Nature*, 401(6756), pp.877-884.
- Paradis, E. & Schliep, K. (2019). ape 5.0: an environment for modern phylogenetics and evolutionary analyses in R. *Bioinformatics*, *35(3)*, pp.526-528.
- Peeters, C., Keller, R.A., Khalife, A., Fischer, G., Katzke, J., Blanke, A. & Economo, E.P. (2020). The loss of flight in ant workers enabled an evolutionary redesign of the thorax for ground labour. *Frontiers in Zoology, 17,* pp.1-13.
- Peplowski, M.M. & Marsh, R.L. (1997). Work and power output in the hindlimb muscles of Cuban tree frogs *Osteopilus septentrionalis* during jumping. *The Journal of Experimental Biology, 200(22),* pp.2861-2870.
- Perry, J.M. & Prufrock, K.A. (2018). Muscle functional morphology in paleobiology: the past, present, and future of "Paleomyology". *The Anatomical Record,* 301(3), pp.538-555.
- Petrović, T. G., Vukov, T. D., & Tomašević Kolarov, N. (2017). Morphometric ratio analyses: Locomotor mode in anurans. *Comptes Rendus Biologies, 340(4)*, pp.250–257.
- Piazza, S.J. & Cavanagh, P.R. (2000). Measurement of the screw-home motion of the knee is sensitive to errors in axis alignment. *Journal of Biomechanics*, 33(8), pp.1029-1034.
- Pinheiro, J., Bates, D., DebRoy, S., Sarkar, D., Heisterkamp, S., Van Willigen, B. & Maintainer, R. (2017). Package 'nlme'. *Linear and nonlinear mixed effects models*, *3*(1), p.274.
- Ponssa, M. L., Fratani, J., & Abdala, V. (2018). Phylogenetic patterns and correlation of key structures for jumping: bone crests and cross-sectional areas of muscles in *Leptodactylus* (Anura, Leptodactylidae). *Journal of Anatomy*, 232(5), pp.870–885.
- Porro, L. B., Collings, A. J., Eberhard, E. A., Chadwick, K. P., & Richards, C. T. (2017). Inverse dynamic modelling of jumping in the red-legged running frog, *Kassina maculata. Journal of Experimental Biology, 220(10),* pp.1882–1893.
- Porro, L. B., & Richards, C. T. (2017). Digital dissection of the model organism *Xenopus laevis* using contrast-enhanced computed tomography. *Journal of Anatomy*, 231(2), pp.169–191.
- Portik, D.M., Streicher, J.W. & Wiens, J.J. (2023). Frog phylogeny: a time-calibrated, species-level tree based on hundreds of loci and 5,242 species. *Molecular Phylogenetics and Evolution*, p.107907.

- Portik, D.M. & Blackburn, D.C. (2016). The evolution of reproductive diversity in Afrobatrachia: A phylogenetic comparative analysis of an extensive radiation of African frogs. *Evolution*, *70*(*9*), pp.2017-2032.
- Powell, P.L., Roy, R.R., Kanim, P., Bello, M.A. & Edgerton, V.R. (1984). Predictability of skeletal muscle tension from architectural determinations in guinea pig hindlimbs. *Journal of Applied Physiology*, *57(6)*, pp.1715-1721.
- Přikryl, T., Aerts, P., Havelková, P., Herrel, A., & Roček, Z. (2009). Pelvic and thigh musculature in frogs (Anura) and origin of anuran jumping locomotion. *Journal of Anatomy, 214(1),* pp.100–139.
- Püffel, F., Pouget, A., Liu, X., Zuber, M., van de Kamp, T., Roces, F. & Labonte, D., (2021). Morphological determinants of bite force capacity in insects: a biomechanical analysis of polymorphic leaf-cutter ants. *Journal of the Royal Society Interface*, 18(182), p.20210424.
- Pugener, L.A. & Maglia, A.M. (2009). Developmental evolution of the anuran sacrourostylic complex. *South American Journal of Herpetology, 4(3),* pp.193-209.
- Rabey, K.N., Green, D.J., Taylor, A.B., Begun, D.R., Richmond, B.G. & McFarlin, S.C. (2015). Locomotor activity influences muscle architecture and bone growth but not muscle attachment site morphology. *Journal of Human Evolution*, 78, pp.91-102.
- Rand, A. S. (1952). Jumping ability of certain anurans, with notes on endurance. *Copeia*, 1952(1), pp.15-20.
- Reilly, S., Essner Jr, R., Wren, S., Easton, L. & Bishop, P.J. (2015). Movement patterns in leiopelmatid frogs: insights into the locomotor repertoire of basal anurans. *Behavioural Processes*, *121*, pp.43-53.
- Reilly, S. M., & Jorgensen, M. E. (2011). The evolution of jumping in frogs: Morphological evidence for the basal anuran locomotor condition and the radiation of locomotor systems in crown group anurans. *Journal of Morphology*, 272(2), pp.149–168.
- Revell, L.J. (2012). phytools: an R package for phylogenetic comparative biology (and other things). *Methods in Ecology and Evolution, 2,* pp.217-223.
- Reynaga, C.M., Eaton, C.E., Strong, G.A. & Azizi, E. (2019). Compliant substrates disrupt elastic energy storage in jumping tree frogs. *Integrative and Comparative Biology*, *59*(6), pp.1535-1545.
- Reynaga, C.M., Astley, H.C. & Azizi, E. (2018). Morphological and kinematic specializations of walking frogs. *Journal of Experimental Zoology Part A: Ecological and Integrative Physiology, 329(2),* pp.87-98.
- Richards, C.T. (2019). Energy flow in multibody limb models: a case study in frogs. *Integrative and Comparative Biology, 59(6),* pp.1559-1572.
- Richards, Christopher T., & Porro, L. B. (2018). A novel kinematics analysis method using quaternion interpolation—a case study in frog jumping. *Journal of Theoretical Biology, 454*, pp.410–424.
- Richards, C.T. & Porro, L.B. (2018). A novel kinematics analysis method using quaternion interpolation a case study in frog jumping. *Journal of Theoretical Biology, 454*, pp.410-424.
- Richards, C.T., Porro, L.B. & Collings, A.J. (2017). Kinematic control of extreme jump angles in the red-legged running frog, *Kassina maculata. Journal of Experimental Biology, 220(10)*, pp.1894-1904.
- Richards, C.T. & Clemente, C.J. (2013). Built for rowing: frog muscle is tuned to limb morphology to power swimming. *Journal of The Royal Society Interface,* 10(84), p.20130236.

- Richards, C.T. (2010). Kinematics and hydrodynamics analysis of swimming anurans reveals striking inter-specific differences in the mechanism for producing thrust. *Journal of Experimental Biology*, 213(4), pp.621-634.
- Richards, C.T. & Biewener, A.A. (2007). Modulation of *in vivo* muscle power output during swimming in the African clawed frog (*Xenopus laevis*). *Journal of Experimental Biology, 210(18),* pp.3147-3159.
- Rittmeyer, E.N., Allison, A., Gründler, M.C., Thompson, D.K. & Austin, C.C. (2012). Ecological guild evolution and the discovery of the world's smallest vertebrate. *PLoS One, 7(1),* p.e29797.
- Roberts, T.J., Eng, C.M., Sleboda, D.A., Holt, N.C., Brainerd, E.L., Stover, K.K., Marsh, R.L. & Azizi, E. (2019). The multi-scale, three-dimensional nature of skeletal muscle contraction. *Physiology*, *34*(6), pp.402-408.
- Roberts, T.J., Abbott, E.M. & Azizi, E. (2011). The weak link: do muscle properties determine locomotor performance in frogs? *Philosophical Transactions of the Royal Society B: Biological Sciences*, *366(1570)*, pp.1488-1495.
- Roberts, T.J. & Marsh, R.L. (2003). Probing the limits to muscle-powered accelerations: lessons from jumping bullfrogs. *Journal of Experimental Biology*, 206(15), pp.2567-2580.
- Roberts, T.J. (2002). The integrated function of muscles and tendons during locomotion. *Comparative Biochemistry and Physiology Part A: Molecular & Integrative Physiology*, 133(4), pp.1087-1099.
- Robovska-Havelkova, P., Aerts, P., Rocek, Z., Přikryl, T., Fabre, A.C. & Herrel, A. (2014). Do all frogs swim alike? The effect of ecological specialization on swimming kinematics in frogs. *Journal of Experimental Biology, 217(20)*, pp.3637-3644.
- Roček, Z. (2013). Mesozoic and tertiary anura of laurasia. *Palaeobiodiversity and Palaeoenvironments*, 93, pp.397-439.
- Sacks, R.D. & Roy, R.R. (1982). Architecture of the hind limb muscles of cats: functional significance. *Journal of Morphology*, *173(2)*, pp.185-195.
- Sakamoto, M. & Ruta, M. (2012). Convergence and divergence in the evolution of cat skulls: temporal and spatial patterns of morphological diversity. *PLoS One, 7(7)*, p.e39752.
- Sahd, L., Bennett, N.C. & Kotzé, S.H. (2022). Hind foot drumming: Volumetric microcomputed tomography investigation of the hind limb musculature of three African mole-rat species (Bathyergidae). *Journal of Anatomy*, 240(1), pp.23-33.
- Sánchez, C.A., Lloyd, J.E., Fels, S. & Abolmaesumi, P. (2014). Embedding digitized fibre fields in finite element models of muscles. Computer Methods in Biomechanics and Biomedical Engineering: Imaging & Visualization, 2(4), pp.223-236.
- Sanchez, S., Dupret, V., Tafforeau, P., Trinajstic, K.M., Ryll, B., Gouttenoire, P.J., Wretman, L., Zylberberg, L., Peyrin, F. & Ahlberg, P.E. (2013). 3D microstructural architecture of muscle attachments in extant and fossil vertebrates revealed by synchrotron microtomography. *PloS One*, 8(2), p.e56992.
- Santana, S.E. (2018). Comparative anatomy of bat jaw musculature via diffusible iodine-based contrast-enhanced computed tomography. *The Anatomical Record*, 301(2), pp.267-278.
- Sawicki, G.S., Sheppard, P. & Roberts, T.J. (2015). Power amplification in an isolated muscle–tendon unit is load dependent. *Journal of Experimental Biology*, 218(22), pp.3700-3709.

- Sellers, K.C., Middleton, K.M., Davis, J.L. & Holliday, C.M. (2017). Ontogeny of bite force in a validated biomechanical model of the American alligator. *Journal of Experimental Biology*, 220(11), pp.2036-2046.
- Simons, V. F. H. (2008). Morphological correlates of locomotion in anurans: Limb length, pelvic anatomy and contact structure (Doctoral dissertation, Ohio University).
- Soliz, M., Tulli, M. J., & Abdala, V. (2017). Osteological postcranial traits in hylid anurans indicate a morphological continuum between swimming and jumping locomotor modes. *Journal of Morphology*, 278(3), pp.403–417.
- Stanchak, K.E. & Santana, S.E. (2018). Assessment of the hindlimb membrane musculature of bats: implications for active control of the calcar. *The Anatomical Record*, *301*(3), pp.441-448.
- Stepanova, N. & Womack, M.C. (2020). Anuran limbs reflect microhabitat and distal, later-developing bones are more evolutionarily labile. *Evolution*, 74(9), pp.2005-2019.
- Sullivan, S.P., McGechie, F.R., Middleton, K.M. & Holliday, C.M. (2019). 3D muscle architecture of the pectoral muscles of European Starling (*Sturnus vulgaris*). *Integrative Organismal Biology, 1(1),* p.oby010.
- Sutton, G.P., Mendoza, E., Azizi, E., Longo, S.J., Olberding, J.P., Ilton, M. & Patek, S.N. (2019). Why do large animals never actuate their jumps with latch-mediated springs? Because they can jump higher without them. *Integrative and Comparative Biology*, *59*(6), pp.1609-1618.
- Sylvester, A.D., Lautzenheiser, S.G. & Kramer, P.A. (2021). A review of musculoskeletal modelling of human locomotion. *Interface Focus*, 11(5), p.20200060.
- To, K.H., O'Brien, H.D., Stocker, M.R. & Gignac, P.M. (2021). Cranial musculoskeletal description of black-throated finch (Aves: Passeriformes: Estrildidae) with DiceCT. *Integrative Organismal Biology*, *3*(1), p.obab007.
- Todorov, E., Erez, T. & Tassa, Y. (2012), October. Mujoco: A physics engine for model-based control. In 2012 IEEE/RSJ international conference on intelligent robots and systems, pp.5026-5033.
- Trueb, L. & Gans, C. (1983). Feeding specializations of the Mexican burrowing toad, *Rhinophrynus dorsalis* (Anura: Rhinophrynidae). *Journal of Zoology*, 199(2), pp.189-208.
- Tsai, H.P., Turner, M.L., Manafzadeh, A.R. & Gatesy, S.M. (2020). Contrastenhanced XROMM reveals in vivo soft tissue interactions in the hip of *Alligator mississippiensis. Journal of Anatomy*, 236(2), pp.288-304.
- Tsai, H.P. & Holliday, C.M. (2011). Ontogeny of the alligator cartilago transiliens and its significance for sauropsid jaw muscle evolution. *PloS One*, *6*(*9*), p.e24935.
- Tulli, M. J., Cruz, F. B., Kohlsdorf, T., & Abdala, V. (2016). When a general morphology allows many habitat uses. *Integrative Zoology*, 11(6), pp.483–499.
- Vassallo, A.I., Manzano, A., Abdala, V. & Muzio, R.N. (2021). Can anyone climb? The skills of a non-specialized toad and its bearing on the evolution of new niches. *Evolutionary Biology, 48(3),* pp.293-311.
- Vera, M.C., Ferretti, J.L., Cointry, G.R. & Abdala, V., 2022. Hind limb muscles influence the architectural properties of long bones in frogs. *Journal of Anatomy*, 241(3), pp.702-715.
- Vickerton, P., Jarvis, J. & Jeffery, N. (2013). Concentration-dependent specimen shrinkage in iodine-enhanced microCT. *Journal of Anatomy*, 223(2), pp.185-193.

- Vidal-García, M., Byrne, P. G., Roberts, J. D., & Keogh, J. S. (2014). The role of phylogeny and ecology in shaping morphology in 21 genera and 127 species of Australo-Papuan myobatrachid frogs. *Journal of Evolutionary Biology*, 27(1), pp.181–192.
- Wainwright, P.C., Alfaro, M.E., Bolnick, D.I. & Hulsey, C.D. (2005). Many-to-one mapping of form to function: a general principle in organismal design? *Integrative and Comparative Biology*, 45(2), pp.256-262.
- Wake, D.B. & Koo, M.S. (2018). Amphibians. *Current Biology*, 28(21), pp.R1237-R1241.
- Ward, S.R. & Lieber, R.L. (2005). Density and hydration of fresh and fixed human skeletal muscle. *Journal of Biomechanics*, *38(11)*, pp.2317-2320.
- Wang, Z., Ji, A., Endlein, T., Samuel, D., Yao, N., Wang, Z. & Dai, Z. (2014). The role of fore-and hindlimbs during jumping in the Dybowski's frog (*Rana dybowskii*). *Journal of Experimental Zoology Part A: Ecological Genetics and Physiology*, 321(6), pp.324-333.
- Weisstein, E.W. (2009). Euler angles. https://mathworld.wolfram.com/.
- Wells, K. D. (2007). *The ecology and behaviour of Amphibians*. Chicago: The University of Chicago press.
- Widrig, K.E., Bhullar, B.A.S. and Field, D.J., 2023. 3D atlas of tinamou (Neornithes: Tinamidae) pectoral morphology: Implications for reconstructing the ancestral neornithine flight apparatus. *Journal of Anatomy. Early view.*
- Wilken, A.T., Middleton, K.M., Sellers, K.C., Cost, I.N. & Holliday, C.M. (2019). The roles of joint tissues and jaw muscles in palatal biomechanics of the savannah monitor (*Varanus exanthematicus*) and their significance for cranial kinesis. *Journal of Experimental Biology*, 222(18), p.jeb201459.
- Wilson, R.S., James, R.S., Kohlsdorf, T. & Cox, V.M. (2004). Interindividual variation of isolated muscle performance and fibre-type composition in the toad *Bufo viridus*. *Journal of Comparative Physiology B*, 174, pp.453-459.
- Wilson, R.S. & James, R.S. (2004). Constraints on muscular performance: tradeoffs between power output and fatigue resistance. *Proceedings of the Royal Society of London. Series B: Biological Sciences, 271,* S222-S225.
- Wyngaarden, L.A. & Hopyan, S. (2008). Plasticity of proximal–distal cell fate in the mammalian limb bud. *Developmental Biology*, *313(1)*, pp.225-233.
- Xing, L., Stanley, E.L., Bai, M. & Blackburn, D.C. (2018). The earliest direct evidence of frogs in wet tropical forests from Cretaceous Burmese amber. *Scientific Reports*, 8(1), p.8770.
- Yapuncich, G.S., Kemp, A.D., Griffith, D.M., Gladman, J.T., Ehmke, E. & Boyer, D.M. (2019). A digital collection of rare and endangered lemurs and other primates from the Duke Lemur Center. *PloS One*, *14*(*11*), p.e0219411.
- Young, M.W., Flaim, N.D., Yarbro, J., Ragupathi, A., Guru, N., Dickinson, E. & Granatosky, M.C. (2023). Dynamics of horizontal walking and vertical climbing in the Australian green tree frog (*Ranoidea caerulea*). *Journal of Experimental Biology*, 226(7), p.jeb244833.
- Zug, G. R. (1972). Anuran locomotion: Structure and function. I. Preliminary observations on relation between jumping and osteometrics of appendicular and postaxial skeleton. *Copeia*, 1972(4), p.613.
- Zumwalt, A. (2006). The effect of endurance exercise on the morphology of muscle attachment sites. *Journal of Experimental Biology*, *209*(3), pp.444-454.

Appendix A: Ana

Page 238 of 286

Appendix A: Analysing skeletal measurements

In Chapter 2, I collected 22 skeletal measurements for 164 frog species to create 16 variables for analysis (Table A.1). Several measurements were combined to make total measurements and to calculate the iliac angle (Figure A.1). There has been variation in previous studies with how skeletal features are measured (traditional dissection, X-rays, µCT scans etc), so the first step in this thesis was to define how each element of skeletal anatomy was measured in a clear and repeatable way (Table A.1).

Table A.1 - Descriptions of skeletal measurements with their abbreviations. The name of the variable within the supplementary datasets have been given in square brackets.

	Measurement	Description
	Snout-vent length [SVL]	Skull + Gap + Vertebrae + Pelvis lengths
rements	Skull length	The most anterior point of premaxilla to the base of the skull along central line.
nren	Gap between skull and	Sometimes required for measuring snout-vent length. The space between the base of the skull to the
meası	vertebrae	most cranial point of the vertebral column along the central line.
Body m	Vertebral length [vert]	The most cranial to most caudal point (before the sacral vertebrae attach to vertebral body) of the vertebral column along the central line. When curved (or in one case, broken), this was measured in two parts.

	Pelvis length [pelv]	The most anterior point of where the sacral vertebrae attach to the vertebral column to the most		
		posterior end of the pelvis/ischium.		
	Sacral width [sacr_w]	The maximal ossified width of the sacral vertebrae at the widest point. Sesamoids and cartilaginous		
ıts		caps were not included.		
μe	Expansion of the sacral	The greatest length between the cranial and caudal edges of the left sacral diapophysis adjacent to		
<u>e</u>	diapophyses [ESD]	the vertebral centrum. Cartilaginous caps were not included.		
measurements	Ilium length [ilium]	The distance from the anterior tip of the left ilium to the lateral process of the ilium.		
ic m	Anterior iliac distance (1)	The distance between the anterior end of each ilium.		
Pelvic	Posterior iliac distance (2)	The distance between the lateral process of each ilium.		
	Urostylic length [uro]	The most anterior to most posterior end of the urostyle. When the urostyle is fused to the sacra		
		vertebrae, the measurement is from the most posterior/caudal side of sacral vertebrae to the end of		
		the urostyle.		
10	Hindlimb length [HL]	Femur + Tibiofibula + Foot		
ınts	Femur length [fem]	The maximum ossified length measured from proximal femoral head to the distal end.		
ı Be	Femur width [fem_w]	The maximum ossified width measured in the midpart of the femur.		
nre	Tibiofibula length [tib]	The maximum ossified length measured from the proximal end of the tibiofibula to the distal end.		
measurements	Calcaneum length [calc]	The maximum ossified length measured from the proximal end of the calcaneum to the distal end.		
me	Foot total length [foot]	Heel + Metatarsal + Toe total		
qu	Heel	The distance between the most distal calcaneum point to the most proximal end of the metatarsal		
<u>=</u>		(includes all the bones 'floating about' in the middle). If there is no gap between calcaneum and		
Hindlimb		metatarsal, the measurement is zero.		
_	Metatarsal	The most proximal to most distal end of the metatarsal of the longest toe (usually the fourth).		

Page 239 of 286

	The most distal end of the metatarsal to the tip of the longest toe (usually the fourth). There were usually four bones in each toe. Individual measurements were taken along each bone, from the distal		
	end of last measurement to the next bone, so including the gap prior to that bone. Sometimes the last		
	bone in a finger or toe has been dislocated. In this case, the gap between the last and penultimate		
	bone was not measured, just the length of the bone itself.		
orelimb length [FL]	Humerus + Radio-ulna + Hand total		
umerus length [hum]	The maximum ossified length of the humerus measured from the proximal end to the most distal end.		
umerus width [hum_w]	The maximum ossified width measured in the midpart of the humerus.		
adio-ulna length [rad]	The maximum ossified length of the radio-ulna measured from the proximal end to the most distal end.		
and total [hand]	Wrist + Fingers total		
/rist	The distance between the most distal radio-ulna measurement to the most proximal end of the first		
	bone of the longest finger (includes all the bones 'floating about' in the middle).		
ngers total	The most proximal end of the first bone of the longest finger to the tip (usually the third). There were		
	usually four bones in each finger. Individual measurements were taken along each bone, from the		
	distal end of last measurement to the next bone, so including the gap prior to that bone.		
u a /I	imerus length [hum] imerus width [hum_w] idio-ulna length [rad] ind total [hand]		

Page 240 of 286

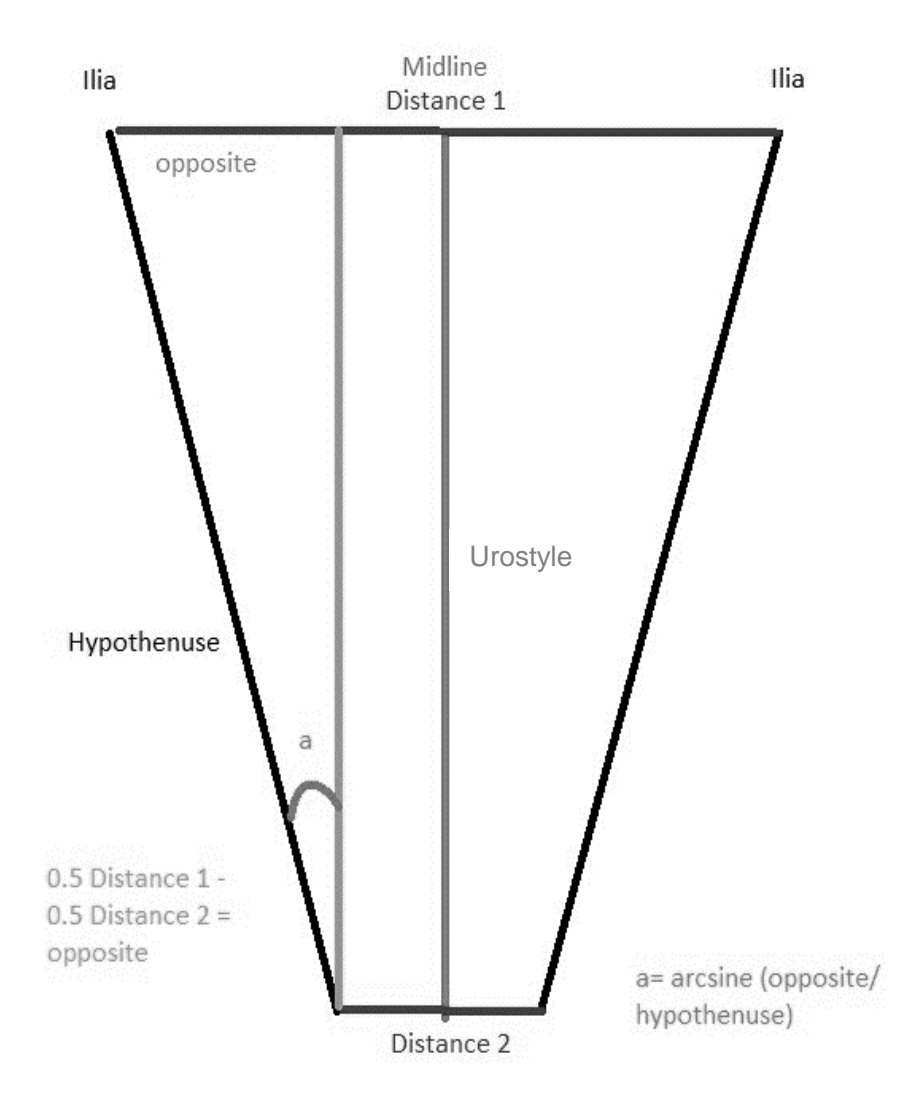


Figure A.1 - Method for Iliac angle calculation. Ilium length is the hypothenuse, and the opposite is half of anterior iliac distance (1) minus half of the posterior iliac distance (2). Arcsine (opposite/hypothenuse) was used to get the angle the ilia diverge from a line parallel to the midline.

Phylogenetic PCA analyses were used to determine where variation is driven in anuran skeletal anatomy, while factoring in locomotor mode and evolutionary history (Table A.2). The scores from this analysis were analysed in a PERMANOVA to determine whether locomotor modes, habitat types and phylogenetic groups differ significantly in morphology (Table A.3). Shape PCAs were also carried out for both the structural (Table A.5) and full (Table A.6) datasets to evaluate how grouping together individual measurements under large structural variables can affect data interpretation. A separate analysis for how the length of the dorsal crests on the ilia

and urostyle relate to locomotor mode and phylogenetic group was also carried out (Table A.4).

Table A.2 - pPCA loadings for the full dataset from the first four axes. For each PC axis, light and dark boxes highlight the largest positive and negative loadings respectively. The full names of abbreviations can be found in Table A.1.

Axis	PC1	PC2	PC3	PC4
Total variance explained (%)	34.23	21.87	9.76	7.75
skull	-0.388	-0.007	-0.421	0.122
vert	0.327	-0.139	-0.448	0.413
pelv	0.031	-0.199	-0.236	0.077
ESD	0.964	0.198	0.140	0.042
sacr_w	0.316	-0.090	-0.150	-0.345
ilium	0.322	-0.009	-0.091	0.140
uro	-0.131	0.129	-0.063	-0.157
fem	-0.611	0.475	0.411	-0.200
fem_w	-0.035	-0.673	0.348	0.189
tib	-0.609	0.565	0.440	-0.209
calc	-0.357	0.738	0.190	-0.342
foot	-0.512	-0.144	0.474	0.563
hum	-0.017	-0.018	-0.652	-0.264
hum_w	0.043	-0.894	0.102	-0.317
rad	-0.021	0.255	-0.668	-0.261
hand	-0.388	0.162	-0.331	0.496

Table A.3 - Results from the pairwise PERMANOVA analyses, which test for statistical differences between the means of locomotor modes, habitat types and phylogenetic groups for 164 frog taxa. Significant *p*-values adjusted for multiple testing have been highlighted in bold.

Pairwise comparison	R ² adonis	P adonis	P adonis adjusted
Locomotor mode		·	
AJ vs TJ	0.147	0.0001	0.001
AJ vs WH	0.158	0.0001	0.001
AJ vs BWH	0.272	0.0001	0.001
AJ vs AQ	0.196	0.0004	0.004
TJ vs WH	0.178	0.0001	0.001
TJ vs BWH	0.327	0.0001	0.001

TJ vs AQ	0.195	0.0001	0.001
WH vs BWH	0.054	0.0218	0.218
WH vs AQ	0.055	0.1230	1.000
BWH vs AQ	0.014	0.6667	1.000
Habitat type			
Arboreal vs Terrestrial	0.065	0.0001	0.0006
Arboreal vs Riparian	0.131	0.0001	0.0006
Arboreal vs Aquatic	0.201	0.0005	0.0030
Terrestrial vs Riparian	0.042	0.0044	0.0264
Terrestrial vs Aquatic	0.031	0.0295	0.1770
Riparian vs Aquatic	0.198	0.0006	0.0036
Phylogenetic group			
Ranoidea vs Hyloidea	0.020	0.0433	0.2598
Ranoidea vs	0.238	0.0001	0.0006
Archaeobatrachia			
Ranoidea vs Neobatrachia	0.041	0.0299	0.1794
Hyloidea vs	0.193	0.0001	0.0006
Archaeobatrachia			
Hyloidea vs Neobatrachia	0.325	0.0363	0.2178
Archaeobatrachia vs Neobatrachia	0.155	00073	0.0438

Table A.4 - Pairwise comparisons for the relationship between the size of dorsal crests on the iliac shaft and urostyle and locomotor mode (LM) and phylogenetic group, based on a Bonferroni-corrected Dunn's test. Only significant pairings have been included.

Model	Pairwise comparisons	Z-value	Adjusted p- value
III a series I NA	TJ vs AJ	3.493	0.005
Iliac ridge ~ LM	TJ vs BWH	5.105	<0.001
Urostylic ridge ~	TJ vs BWH	3.924	<0.001
LM	TJ vs WH	3.406	0.007
Iliac ridge ~ Phylogenetic group	Archaeobatrachia vs Ranoidea	-3.287	0.006
Urostylic ridge ~	Archaeobatrachia vs Hyloidea	-3.231	0.007
Phylogenetic group	Archaeobatrachia vs Ranoidea	-3.723	0.001

Table A.5 - Shape PCA loadings for the first four axes from the structural dataset. For each PC axis, light and dark boxes highlight the largest positive and negative loadings respectively. Full names of abbreviations can be found in Table A.1.

Axis	PC1	PC2	PC3	PC4
Total variance explained (%)	66.9	16.8	5.1	3.8
SVL	-0.144	-0.096	0.004	-0.161
ESD	0.908	-0.151	0.019	0.104
sacr_w	-0.015	-0.037	0.157	-0.694
ilium	-0.004	-0.139	-0.111	0.135
uro	-0.157	-0.230	-0.168	0.197
HL	-0.289	-0.344	-0.096	0.476
fem_w	-0.116	0.343	0.821	0.229
FL	-0.183	-0.145	-0.148	-0.372
hum_w	0.0004	0.798	-0.478	0.087

Table A.6 - Shape PCA loadings for the first four axes from the full dataset. For each PC axis, light and dark boxes highlight the largest positive and negative loadings respectively. Full names of abbreviations can be found in Table A.1.

Axis	PC1	PC2	PC3	PC4
Total variance explained (%)	54.4	17.3	6.0	4.2
skull	-0.173	0.060	0.146	-0.149
vert	0.060	0.014	0.300	-0.298
pelv	0.000	0.057	-0.001	-0.145
ESD	0.864	-0.314	-0.143	-0.006
sacr_w	0.081	0.049	0.201	0.099
ilium	0.087	-0.012	-0.039	-0.168
uro	-0.051	-0.054	-0.069	-0.074
fem	-0.176	-0.183	-0.180	0.150
fem_w	0.018	0.392	-0.214	-0.280
tib	-0.252	-0.301	-0.295	0.242
calc	-0.180	-0.414	-0.060	0.371
foot	-0.181	0.074	-0.481	-0.324
hum	-0.057	0.059	0.391	0.102
hum_w	0.140	0.651	-0.171	0.566
rad	-0.042	0.004	0.467	0.166
hand	-0.137	-0.083	0.148	-0.252

Similar to the PGLS analyses carried out in Soliz *et al.* (2017) and Tulli *et al.* (2016), I initially aimed to analyse how skeletal anatomy is affected by locomotor mode and habitat type in a phylogenetic framework by systematically examining every possible combination of each individual variable. For example, the full model would be 'PC1~TJ+AJ+AQ+BWH+WH+Terrestrial+Arboreal+Riparian+Aquatic'. The best models can then be extracted and ranked using the 'dredge' function in the R package *MuMIn* (Barton & Barton, 2015). However, multicollinearity caused NAs to be produced by coercion – every frog with a swimming locomotor mode has an aquatic habitat type, and 96% of arboreal jumper frogs had an arboreal habitat type (the rest are riparian). Despite this type of analysis being carried out by several other papers, and extensive investigation by both Dr Ruta and myself, no solution could be found for this issue. Therefore, locomotor mode and habitat type were used as independent variables in a PGLS with numerical values representing each group (Table A.7).

Table A.7 - Phylogenetic signal (λ), residual standard error (R) and Akaike Information Criterion (AIC) for each PGLS model of PC1 and PC2. The best model is highlighted in bold.

Model	λ	R	AIC
PC1 ~ Locomotor mode + Habitat type	1.024	0.225	-143.94
PC1 ~ Locomotor mode	1.039	0.232	-141.79
PC1 ~ Habitat type	1.050	0.241	-132.46
PC1~1	0.000	0.231	-133.32
PC2 ~ Locomotor mode + Habitat type	0.638	0.130	-247.70
PC2 ~ Locomotor mode	0.650	0.131	-248.02
PC2 ~ Habitat type	0.800	0.151	-224.35
PC2~1	0.000	0.185	-207.09

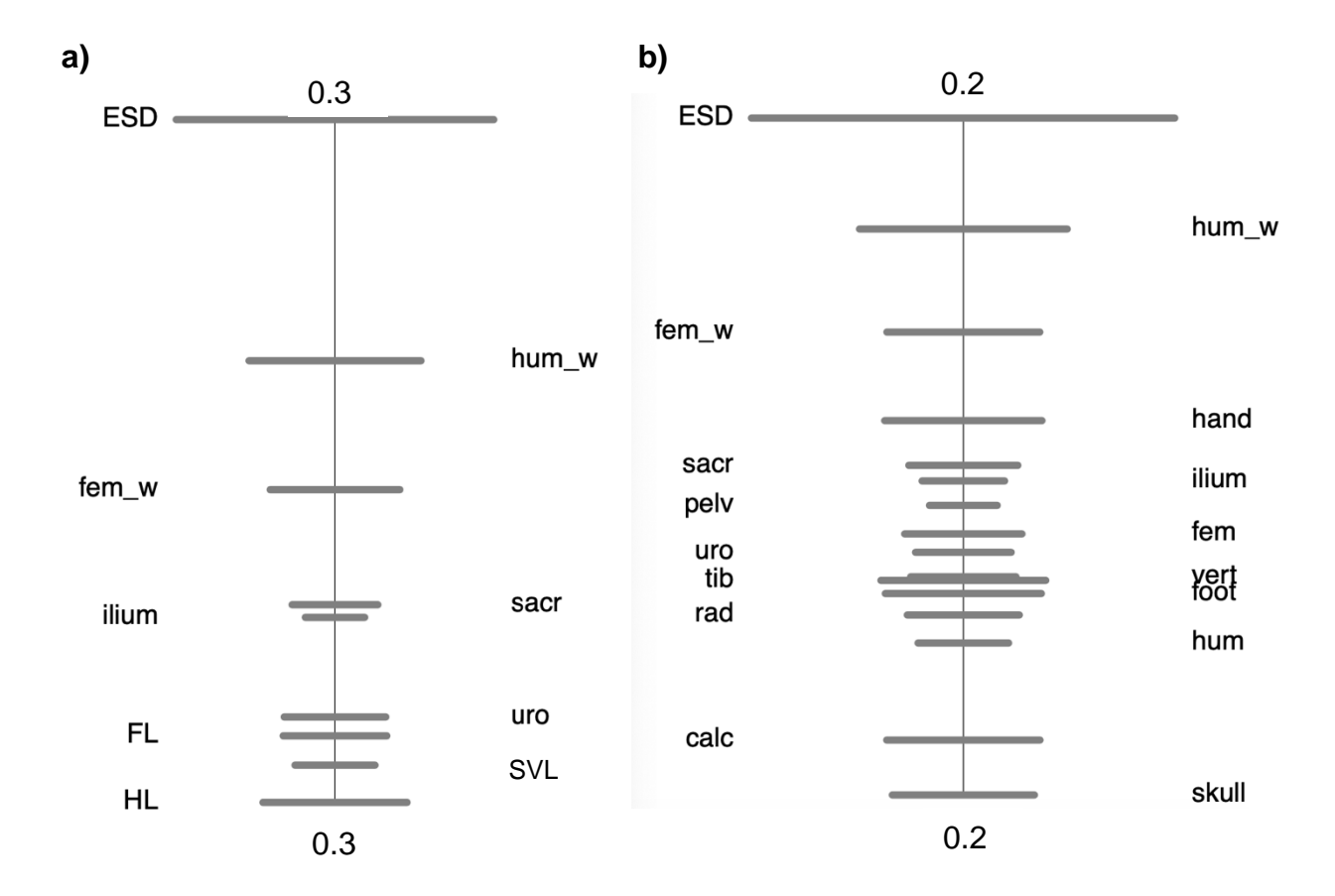


Figure A.2 - Allometry ratio spectrum (Baur & Leuenberger, 2011) for a) the structural dataset containing total body and limb lengths and b) the full dataset. The bars represent 68% confidence intervals based on 999 bootstrap replicates. As they are wide, the error bars suggest there is little allometric variation in the data.

Appendix B: Formatting the phylogeny

The phylogeny used throughout this thesis (Jetz & Pyron, 2017) required some editing to reflect the study taxa used (Table B.1). Any changes in species names were updated and the most closely related congeneric taxa were replaced by the names of three species not yet in the phylogeny. This approach was designed to preserve branch lengths.

Table B.1- Substitute taxa used in the phylogeny. A * represents where a species name has been updated.

This thesis	Jetz & Pyron (2017)	Reference
Amnirana albolabris	Hylarana albolabris *	IUCN (2020)
Amnirana	Hylarana galamensis *	IUCN (2020)
galamensis		
Cornufer guppyi	Discodeles guppyi *	IUCN (2020)
Cornufer guentheri	Ceratobatrachus	IUCN (2020)
	guentheri *	
Boana boans	Hypsiboas boans *	IUCN (2020)
Kalophrynus	Kalophrynus	No study found including
sinensis	pleurostigma	this particular species –
		chose <i>K. pleurostigma</i> as an
		estimate for branch lengths.
Lithobates vibicarius	Rana vibicaria *	IUCN (2020)
Micrixalus adonis	Micrixalus fuscus	Biju et al. (2014)
Niceforonia	Hypodactylus	IUCN (2020)
araiodactyla	araiodactylus *	
Phlyctimantis	Kassina maculata *	Portik & Blackburn (2016)
maculatus		
Sclerophrys dodsoni	Duttaphrynus dodsoni *	IUCN (2020)
Triprion spinosus	Anotheca spinosa *	IUCN (2020)
Walkerana	Indirana phrynoderma *	Dahanukar et al. (2016)
phrynoderma		
Xenopus calcaratus	Xenopus epitropicalis	Evans <i>et al.</i> (2015)

Appendix C: Troubleshooting diceCT

To familiarise myself with frog anatomy beyond the digital dissections I had performed, I dissected the hindlimb of one specimen of *Rana temporaria* using traditional dissection methods. This exercise was important considering that tendinous structures cannot be viewed using the same contrast-enhancing agents used to visualise muscles. The frog was retrieved by Dr Laura Porro, already expired with no signs of damage or disease. Dunlap (1960), Přikryl *et al.* (2009), and Dr Porro's expertise were used to identify each muscle. Muscles were photographed, removed, weighed, and measured using digital callipers (both muscle belly length and the length of the muscle-tendon unit). Any observations that would be useful to consider while carrying out the work in Chapter 3 were noted, such as those presented in Figure C.1.

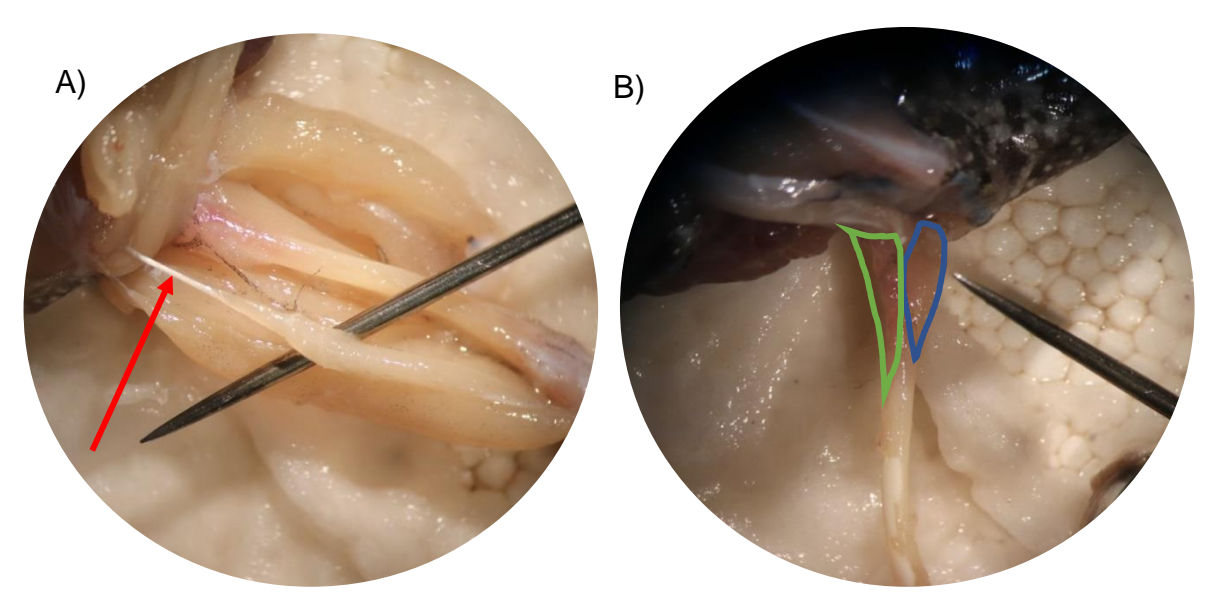


Figure C.1 - Microscope images from a traditional dissection of *Rana temporaria*. A) The long tendinous attachment of the iliofibularis (red arrow) to its origin on the ilium can result in the underestimation of muscle-tendon unit length from diceCT alone. B) Several small hip muscles were not possible to dissect in-tact, such as the gemellus (green) and obturator externus (blue), highlighting the benefits of diceCT over traditional dissection.

While on a research trip to the University of Florida, I stained and scanned ten species to complete my dataset in terms of locomotor mode and phylogeny coverage for Chapters 3 and 4. Before each full scan, I would test scan the specimens to check for that the stain had sufficiently permeated the tissues (Figure

C.2). After the scan was complete, the specimens would then be de-stained so that they could be returned to museum collections. Although the specimens appear almost identical externally to how they did before iodine-staining, μ CT scans show that tissue can remain radio-opaque for many years after the experiment (Figure C.3).

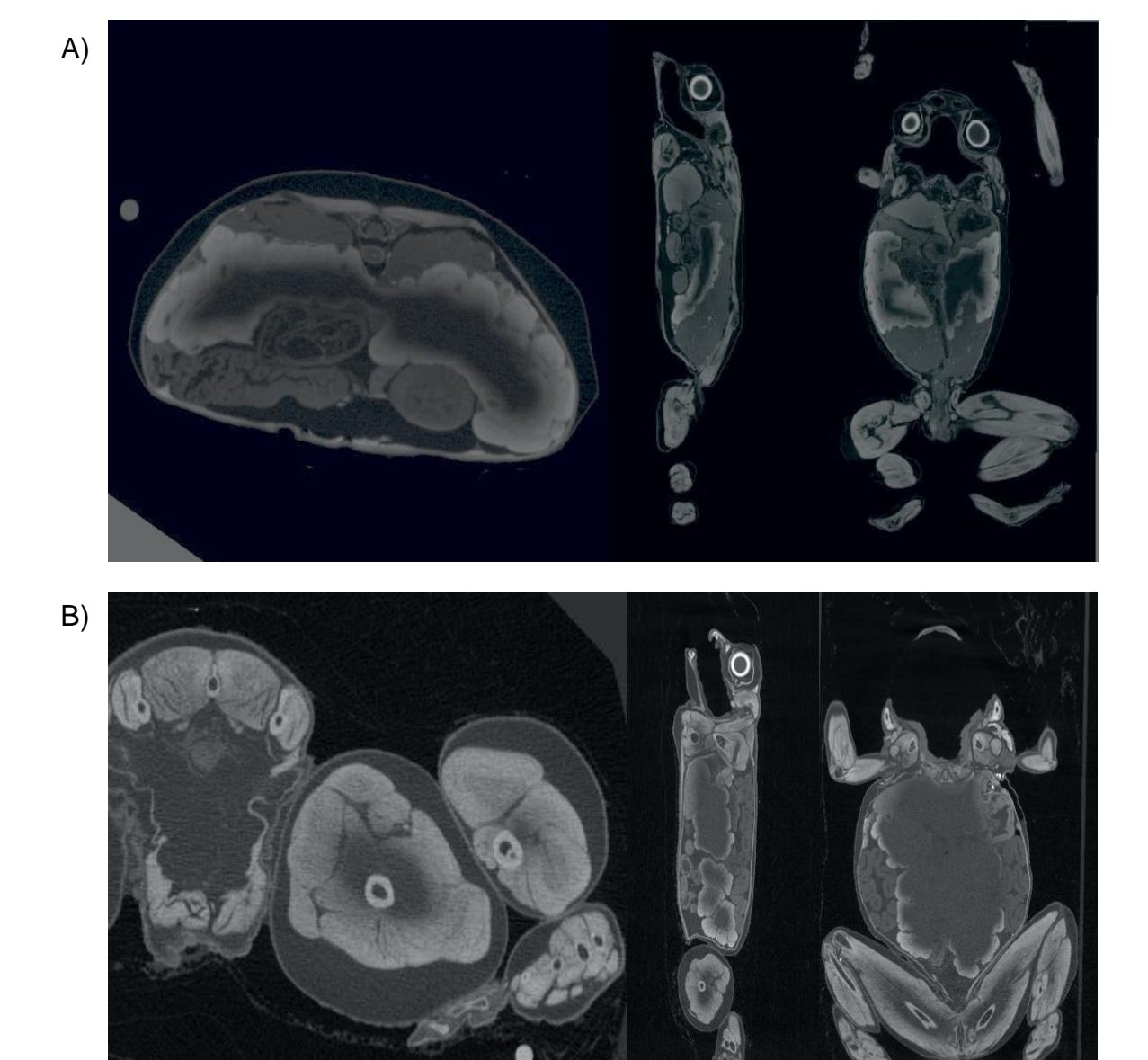


Figure C.2 - Examples of under-staining after one week in 1.25% buffered Lugol's iodine (left to right: cross-section, lateral view, dorsal view). A) *Nyctibates corrugatus* (SVL: 52.04mm) – low under-staining, requires approximately one more week of staining. B) *Leptopelis notatus* (SVL: 67.66mm) – moderate under-staining, requiring approximately one to two more weeks of staining.

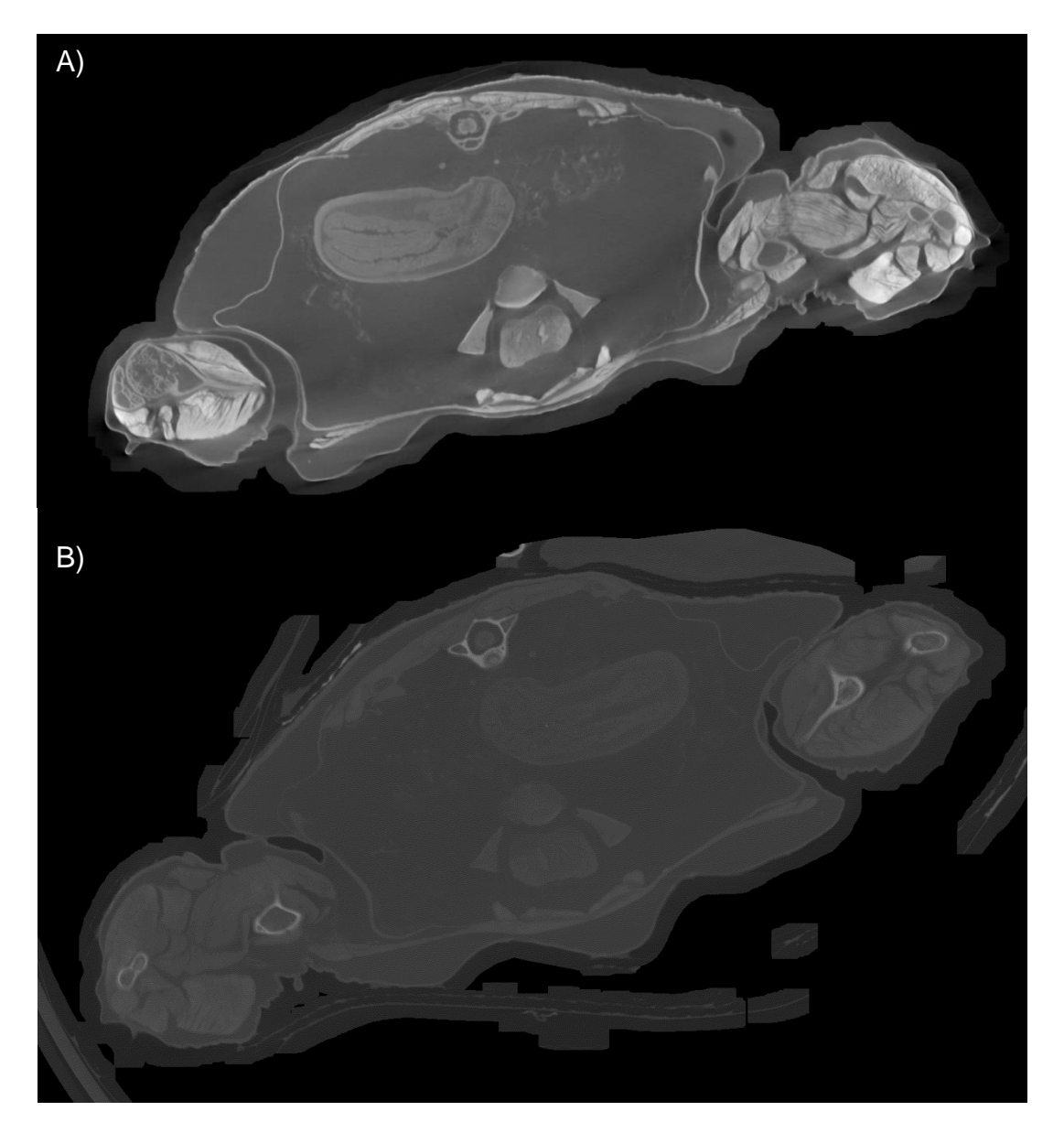


Figure C.3 - Example of radiopacity before and after iodine staining. This specimen of *Ecnomiohyla miliaris* was stained and initially scanned four years prior (A) to the second scan (B).

Previous studies have suggested that scan resolution may be a confounding variable that could impact the data obtained from μ CT scans (Broeckhoven & Plessis, 2018). Poor scan resolution can make it difficult to visualise muscle boundaries and can cause overestimations in object size, especially when examining small specimens. Therefore, voxel size, the pixel dimensions in each plane of view, was included as an explanatory factor in all the ANOVA and least-squares models in Chapter 3 to see if low scan resolution might be correlated with muscle mass (Table C.1) or the number of muscles in a segment (Table C.2). The

best model is determined by the lowest Akaike Information Criterion value, which estimates how well models fit the data they were generated from.

Table C.1 - Table of Akaike Information Criterion (AIC) for each analysis of variance (ANOVA). Rows highlighted in bold show that that adding voxel size as an explanatory variable for muscle composition across all hindlimb segments does not result in a better fit of the data.

ANOVA model	df	AIC
Total thigh muscle mass ~ LM + voxel size	10	-68.56
Total thigh muscle mass ~ LM	9	-70.48
Total shank muscle mass ~ LM + voxel size	10	-15.46
Total shank muscle mass ~ LM	9	-17.43
Total tarsal muscle mass ~ LM + voxel size	10	9.64
Total tarsal muscle mass ~ LM	9	7.77

Table C.2 - Table of Akaike Information Criterion (AIC) for each model of pelvis, thigh, and shank muscle number. Rows highlighted in bold show the models which best fit the data. All phylogenetic least squares (PGLS) models show a better fit than ordinary least squares (OLS) models, meaning that phylogenetic history is an important explanatory variable.

PGLS model	df	AIC
Pelvis muscle number ~ LM + voxel size	6	33.17
Pelvis muscle number ~ LM	5	31.38
Pelvis muscle number ~ voxel size	2	26.6
Pelvis muscle number ~ 1	1	24.65
Thigh muscle number ~ LM + voxel size	6	107.32
Thigh muscle number ~ LM	5	106.03
Thigh muscle number ~ voxel size	2	104.44
Thigh muscle number ~ 1	1	104.28
Shank muscle number ~ LM + voxel size	6	35.26
Shank muscle number ~ LM	5	33.41
Shank muscle number ~ voxel size	2	34.74
Shank muscle number ~ 1	1	33.18
OLS model	df	AIC
Pelvis muscle number ~ LM + voxel size	7	35.82
Pelvis muscle number ~ LM	6	34.08
Thigh muscle number ~ LM + voxel size	7	113.02
Thigh muscle number ~ LM	6	111.75
Shank muscle number ~ LM + voxel size	7	37.26
Shank muscle number ~ LM	6	35.41

Appendix D: pPCA loadings and muscle lengths

In Chapter 3, phylogenetic principal components analyses (pPCA) were used to evaluate how post-vertebral muscle mass varies between species (Table D.1). Muscle length was compared to the associated bone length to understand whether bone length is a suitable proxy for estimating muscle size, which would have important implications for studies which infer behaviour from fossils (Figure D.1; Figure D.2; Figure D.3).

Table D.1 - pPCA loadings from the first four pPCA axes for the pelvis, thigh, shank, and tarsal muscles. For each PC axis, light and dark boxes highlight the largest positive and negative loadings respectively. The full names for each muscle can be found in the 'List of muscle abbreviations'.

Axis	PC1	PC2	PC3	PC4		
Pelvis						
Total variance explained (%)	55.54	22.20	19.66	2.61		
LD	0.529	-0.491	0.688	0.075		
CGS	-0.061	0.970	0.207	0.115		
CGI	-0.953	-0.242	-0.167	0.067		
PY	-0.305	0.170	0.106	-0.931		
IE	0.805	-0.109	-0.581	0.047		
Thigh						
Total variance explained (%)	45.91	18.98	12.62	6.60		
II	0.444	-0.330	-0.330	-0.027		
TFL	0.094	0.140	-0.456	-0.202		
CR	-0.990	0.060	0.049	0.109		
GM	-0.243	0.528	-0.254	-0.451		
SM	0.694	0.363	0.087	0.580		
Ifib	0.483	-0.331	-0.079	-0.372		
Ifem	0.318	-0.134	-0.226	0.191		
hip_muscles	0.049	-0.636	-0.381	0.193		
SA	0.252	0.298	0.018	-0.388		
AM	0.225	0.741	-0.370	-0.110		
GRM + GRm	0.207	0.092	0.943	-0.139		
PT + AL	0.066	-0.890	-0.012	-0.029		
ST	0.431	-0.420	-0.040	-0.022		
Shank						

The evolution of musculoskeletal anatomy and locomotor mode in frogs

Total variance explained (%)	58.79	35.64	3.16	1.58
PL	0.995	-0.055	0.080	-0.009
TiP	-0.433	-0.560	-0.248	0.333
PER	-0.322	0.943	0.079	-0.034
ECB	-0.345	-0.667	-0.443	-0.489
TiAB	-0.177	0.157	-0.688	0.560
TiAL	-0.747	-0.621	0.234	0.010
		Tarsals		
Total variance explained (%)	31.90	24.07	15.32	12.94
PP	-0.799	0.046	0.443	0.358
TaP	-0.578	-0.318	-0.538	-0.281
TaA	0.491	0.288	-0.259	0.737
EBS	-0.242	-0.155	0.082	-0.281
EDCL	-0.500	-0.236	-0.178	-0.177
FDBS	0.626	-0.668	0.381	-0.070
INT	0.232	0.832	0.295	-0.380
AbdV	0.585	0.165	-0.574	-0.017

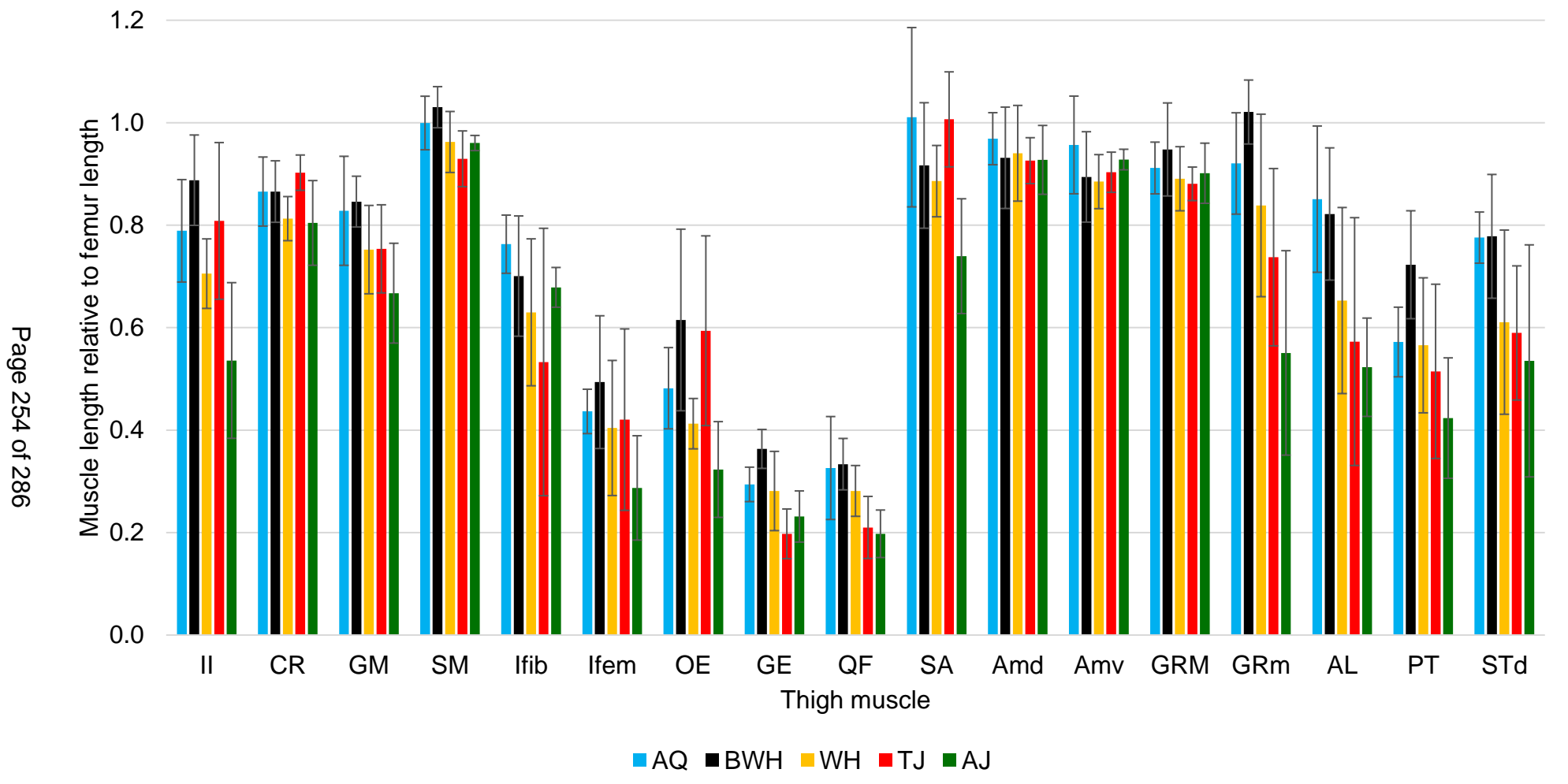


Figure D.1 - The length of each muscle in the thigh relative to the length of the femur, colour coded by locomotor mode. The full names of each muscle can be found in the 'List of muscle abbreviations'. Error bars represent standard deviation.

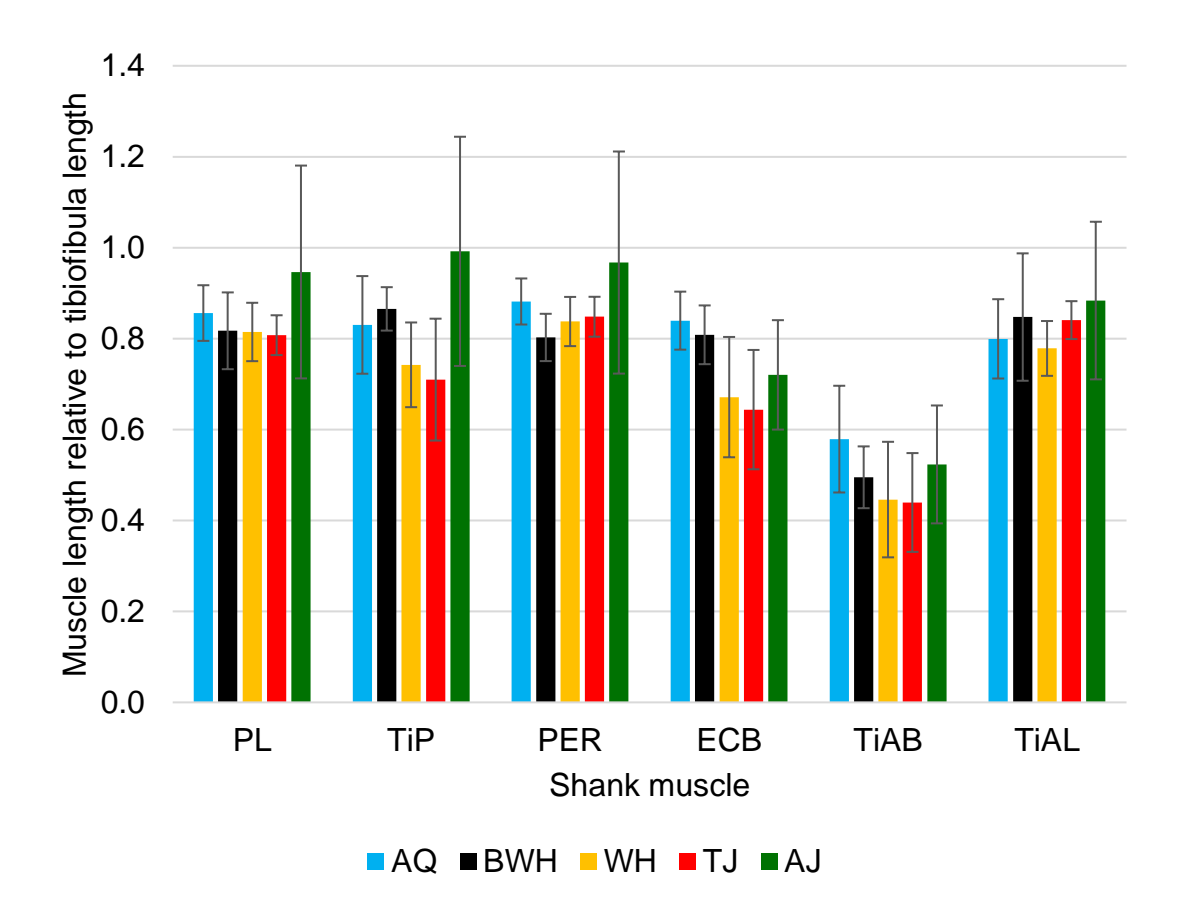


Figure D.2 - The length of each muscle in the shank relative to the length of the tibiofibula, colour coded by locomotor mode. The full names of each muscle can be found in the 'List of muscle abbreviations'. Error bars represent standard deviation.

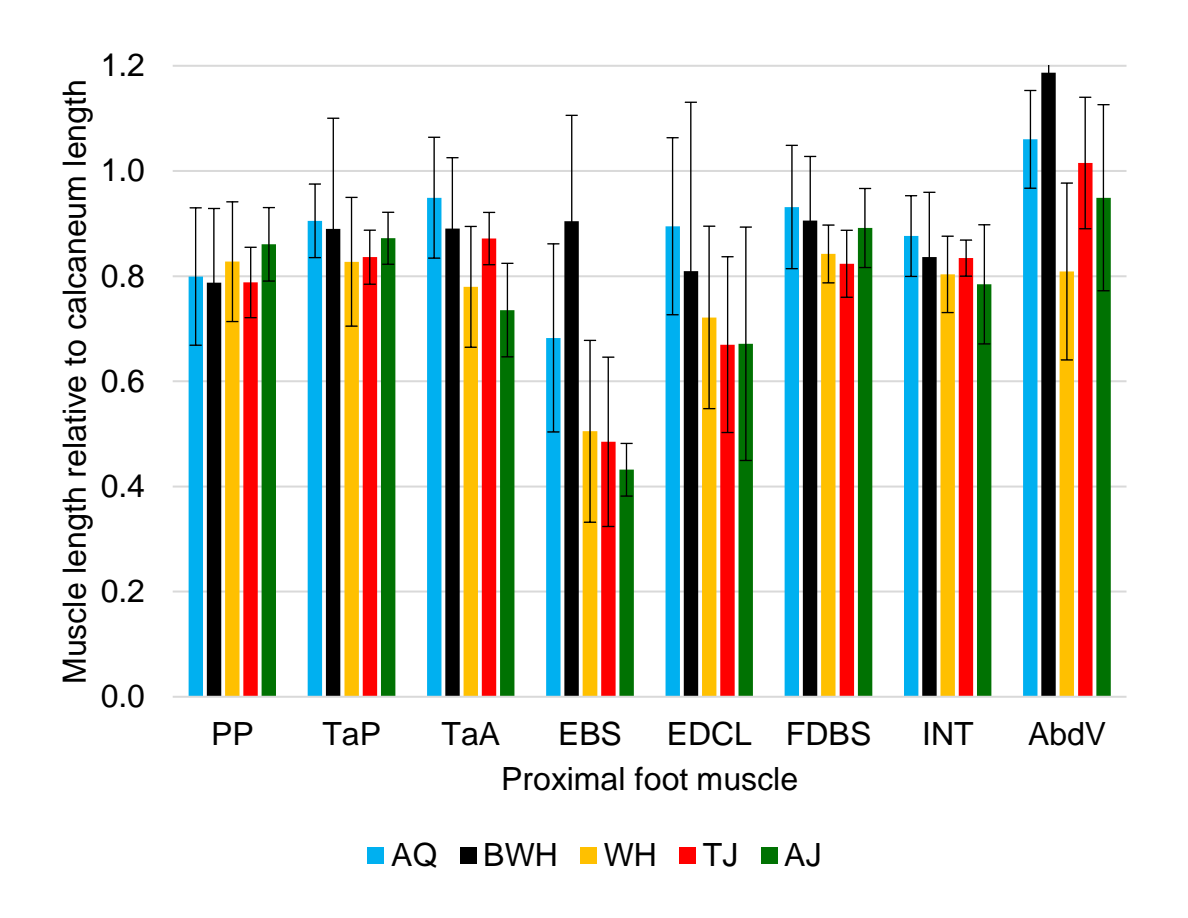


Figure D.3 - The length of each muscle in the proximal foot relative to the length of the calcaneum, colour coded by locomotor mode. The full names of each muscle can be found in the 'List of muscle abbreviations'. Error bars represent standard deviation.

Appendix E: Additional analyses of fibre architecture

In Chapter 4, several elements of fibre architecture were analysed in relation to locomotor mode and different hindlimb muscles. Data were checked for normality before subsequent statistical analyses (Table E.1). Since the sample size is very small, accurate estimates of the influence of shared phylogenetic history could not be obtained (Münkemüller et al., 2012). Indeed, all but one evolutionary model for relative fibre length and size-corrected physiological cross-sectional area (PCSA) was the 'white noise' model, i.e., no phylogenetic signal. The only exception was the semimembranosus PCSA, which had Brownian motion as the best model. When testing hypotheses 1 and 2, supplementary phylogenetic ANOVAs showed similar results to the main, non-phylogenetic analysis - grayscale cut-off does not significantly improve the fit of the model to the data for both relative fibre length (Table E.2) and PCSA (Table E.3). However, there was only one set of significant differences between locomotor modes – the PCSA of the cruralis was longer in jumpers and walkers than swimmers (Table E.4). Regarding hypothesis 3, there were no significant relationships between relative muscle mass and relative fibre length (Table E.5), which again matches the findings of the main, non-phylogenetic analysis.

Table E.1 - The test statistics (L) and *p*-values for normality tests for pennation angle (PA), relative fibre length (FL:MBL), size-corrected physiological cross sectional area (PCSA), and relative muscle belly mass (MBM).

	Semimembranosus		Glute mag			Cruralis		Plantaris Iongus	
	L	p	L	р	L	p	L	p	
Shapiro-Wilk normality test									
PA	NA	NA	NA	NA	0.878	0.124	0.966	0.853	
FL:MBL	0.895	0.191	0.880	0.130	0.985	0.987	0.933	0.480	
PCSA	0.907	0.262	0.908	0.266	0.950	0.663	0.942	0.572	
MBM	0.962	0.805	0.893	0.182	0.895	0.195	0.963	0.819	

Table E.2 - The phylogenetic ANOVA models testing for differences between locomotor modes (LM) for relative fibre length. Corrected Akaike's Information Criterion (AICc) were used to evaluate the fit of the models to the data since sample size was small. The best model was always without the grayscale cut-off, but none of the best models showed significance values above p = 0.05 besides the intercept.

Muscle	Model	Log-likelihood	AICc	AICc weights
Plantaris longus	Cut-off + LM	11.692	-14.528	0.429
T lamano longuo	LM	11.216	-15.099	0.571
Cruralis	Cut-off + LM	12.979	-17.1	0.318
Or drains	LM	12.979	-18.624	0.682
Semimembranosus	Cut-off + LM	9.869	-10.881	0.682
	LM	8.345	-9.356	0.318
Gluteus magnus	Cut-off + LM	7.928	-6.998	0.414
S.a.caeagriae	LM	7.513	-7.692	0.586

Table E.3 - The phylogenetic ANOVA models testing for differences between locomotor modes (LM) for size-corrected physiological cross-sectional area. Corrected Akaike's Information Criterion (AICc) were used to evaluate the fit of the models to the data since sample size was small. The best model was always without the grayscale cut-off.

Muscle	Model	Log-likelihood	AICc	AICc weights
Plantaris longus	Cut-off + LM	-7.786	24.429	0.32
T lamano longao	LM	-7.794	22.921	0.68
Cruralis	Cut-off + LM	-5.126	19.108	0.32
Ordrails	LM	-5.148	17.628	0.68
Semimembranosus	Cut-off + LM	-9.533	27.923	0.33
Commonword	LM	-9.568	26.47	0.67
Gluteus magnus	Cut-off + LM	-8.863	26.582	0.36
S.a.caeagriae	LM	-9.061	25.455	0.64

Table E.4 - The pairwise results of the phylogenetic ANOVA model testing for differences between locomotor modes for size-corrected physiological cross-sectional area of the cruralis. No other muscles showed significant differences between locomotor modes. SE = standard error and p-values above the 0.05 significance threshold have been highlighted in bold.

Coefficient	Estimate	SE	t-value	<i>p</i> -value
Intercept	-0.010	0.311	-0.031	0.976
Jumper	1.048	0.306	3.425	0.011
Walker	1.108	0.356	3.111	0.017

Table E.5 - The result of the phylogenetic least squares (PGLS) model testing for significant relationships between relative muscle belly length and the fibre length:muscle belly length ratio (FL:MBL) and, for pennate muscles, the pennation angle. SE = standard error and p-values above the 0.05 significance threshold have been highlighted in bold.

Muscle	Model	Estimate	SE	t	р
Semimembranosus	Intercept	0.075	0.011	7.032	< 0.001
	FL:MBL	0.046	0.031	1.492	0.174
Gluteus magnus	Intercept	0.056	0.012	4.716	0.002
Clateae magnae	FL:MBL	0.024	0.031	0.769	0.464
	Intercept	0.16	0.035	4.626	0.002
Cruralis	FL:MBL	-0.028	0.119	-0.731	0.486
or arang	Intercept	0.075	0.059	1.272	0.239
	Pennation	0.003	0.002	1.096	0.305
	Intercept	0.137	0.044	3.092	0.015
Plantaris longus	FL:MBL	0.001	0.145	0.006	0.995
	Intercept	0.07	0.094	0.744	0.478
	Pennation	0.003	0.005	0.731	0.486

Two supplementary sensitivity tests were carried out to determine what the main drivers are behind differences in PCSA between locomotor modes and muscle types, since it has been questioned whether pennation angle has any noticeable effects on estimates of muscle dynamics (Lieber, 2022). This relationship is better visualised when muscle volumes are kept equal to 1 mm³ across the dataset, especially since both pennate muscles are considerably larger than the parallel-fibred muscles. Comparing Figure 4.6 to Appendix Figure E.1 shows that differences in fibre architecture are largely driven by this difference in volume along with relative fibre length, rather than differences in pennation angle.

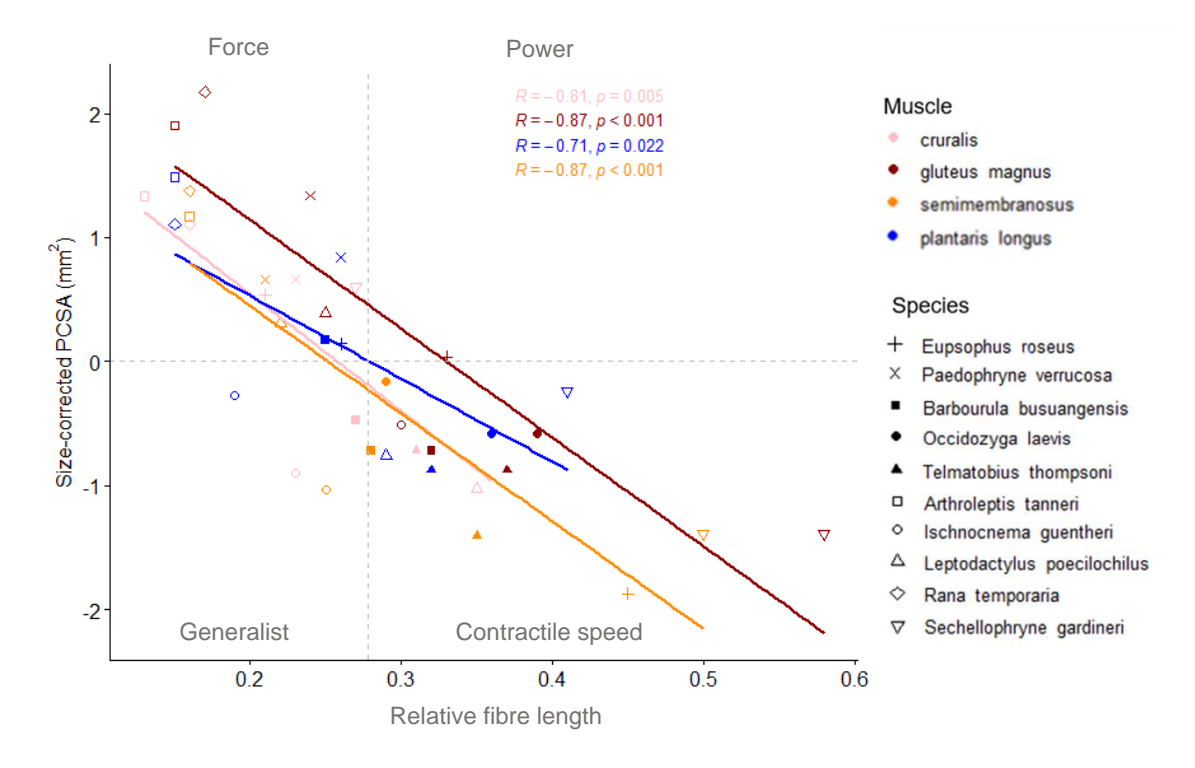


Figure E.1 - The relationship between relative fibre length and size-corrected physiological cross-sectional area (PCSA) when all muscles have a volume equal to 1mm³. Points are colour coded according to hindlimb muscle. As the gluteus magnus and semimembranosus are parallel-fibred muscles, the PCSA simply represents the anatomical cross-sectional area (i.e., pennation angle = 0). Different shaped points represent each species, where cross-type shapes represent walker-hoppers, filled shapes represent swimmers, and empty shapes represent jumpers. The grey dashed lines represent the means across each axis, which divide the plot into each area of functional space. The statistics reported refer to Pearson's correlation tests.

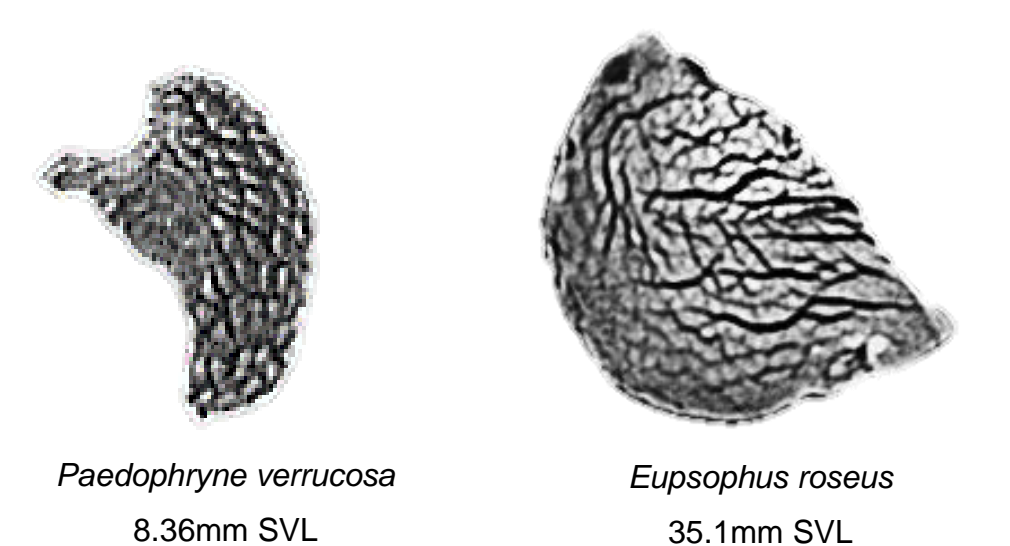


Figure E.2 - A cross-section of the plantaris longus of the two walker-hopper species, exemplifying the difference in fibre number, likely due to differences in body size. SVL = snout-vent length.

Appendix F: Inverse kinematics model pelvis displacement

Chapter 5 presents an IK model for determining the relationship between hindlimb proportions and take-off kinematics in frogs. Models of both real and hypothetical hindlimb proportions all begin with the same initial hindlimb configuration, and the limbs remain aligned throughout take-off as the left and right hips are attached to an invisible pelvis, defined by the distance between the hips of *Phlyctimantis maculatus* (0.160362 m). These hip-pelvic contacts are calculated automatically by Mathematica and experience an unavoidable small (sub-millimetre) drift as take-off progresses. The amount of drift differs slightly between the hypothetical models as more 'extreme' differences in proportions are tested (Figure F.1). The consequences of this minute variation are very unlikely to affect the interpretations made from the IK and subsequent ID models.

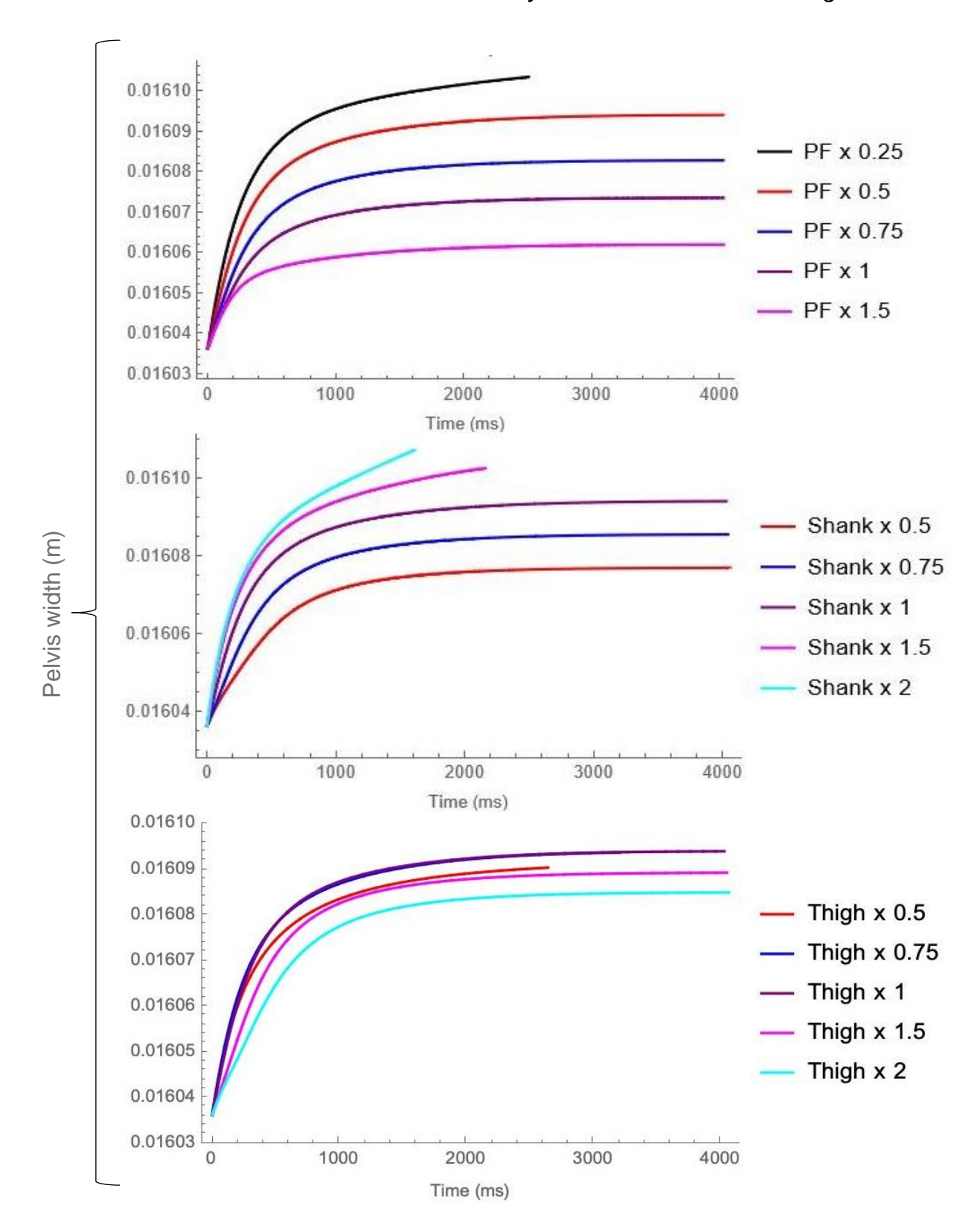


Figure F.1 - Displacement from the original pelvis width throughout take-off for the hypothetical models of frog hindlimb proportions (before the data were resampled to 100 time points). PF = proximal foot.

Appendix G: Inverse kinematics results

Another way to interpret hindlimb kinematics (Chapter 5) is to examine the rate of change of the polar angles and 3D planar angles for each joint, i.e., the angular velocity. For example, faster joint opening has previously been linked to more vertical jumps (Porro *et al.*, 2017). Angular velocity is calculated by numerically differentiating the angle data (Appendix Figure G.1 - Figure G.7).

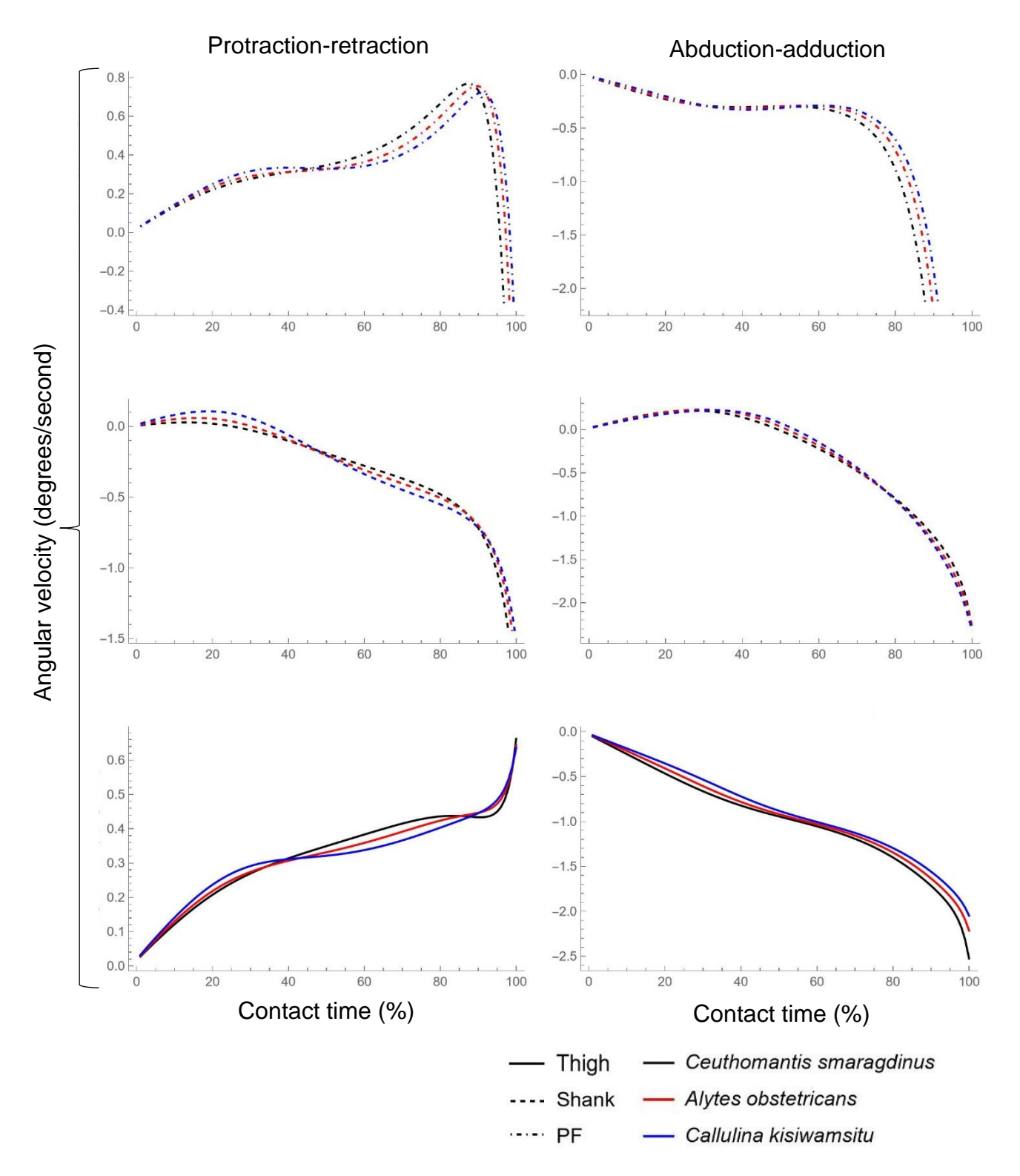


Figure G.1 - Hindlimb segment kinematics for three species exemplifying variation in thigh:shank length ratio in the form of polar angular velocities. Blue and black represents the species with the longest thigh and shank respectively. Retraction (left column) of the thigh and proximal foot (PF) is indicated by positive velocity values. Negative values indicate shank retraction. Ventral adduction (right column) is indicated by negative values for all segments. See Figure 5.7 for polar angles.

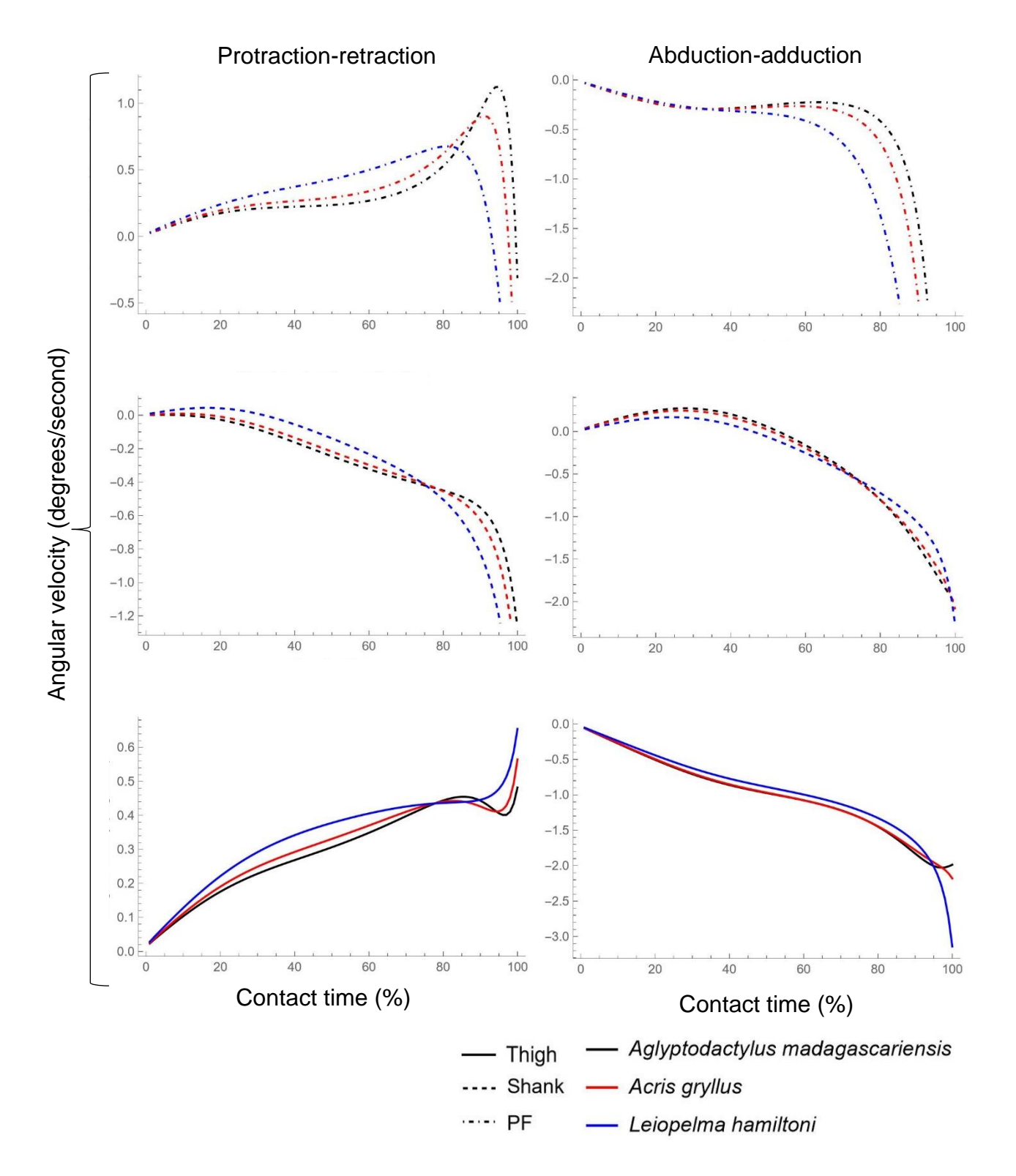


Figure G.2 - Hindlimb segment kinematics for three species exemplifying variation in proximal foot (PF):total hindlimb length ratio in the form of polar angular velocities. Blue represents the species with the longest PF. Retraction (left column) of the thigh and PF is indicated by positive velocity values. Negative values indicate shank retraction. Ventral adduction (right column) is indicated by negative values for all segments. See Figure 5.8 for polar angles.

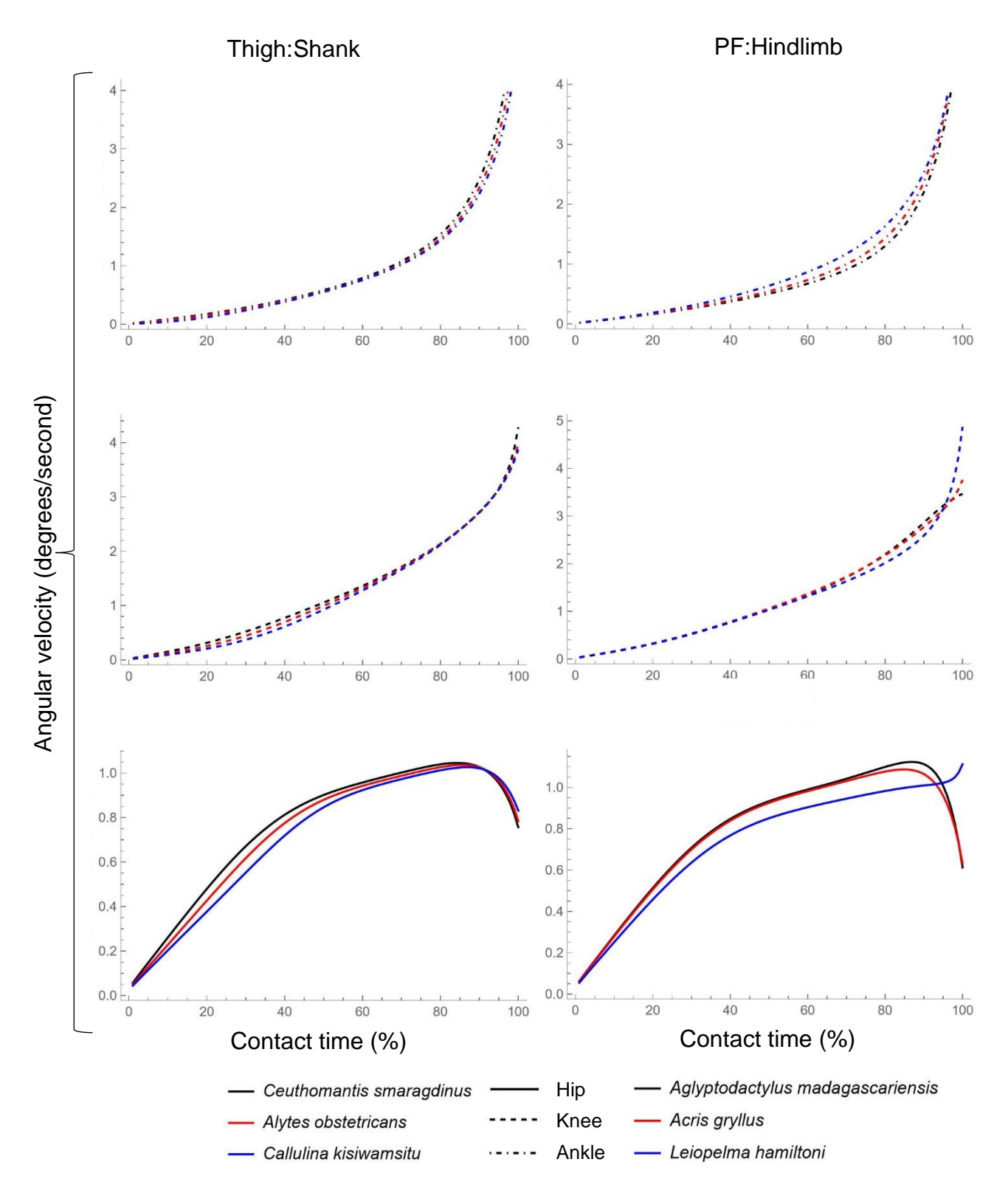


Figure G.3 - 3D joint 'extension' angle velocities for two sets of three species exemplifying variation in the ratio between A) thigh and shank length, and B) proximal foot (PF) and total hindlimb length. Blue represents the species with the longest thigh (A) and PF (B), while black represents the longest shank (A) and shortest PF (B). Positive values indicate faster joint opening. See Figure 5.9 for angular velocities.

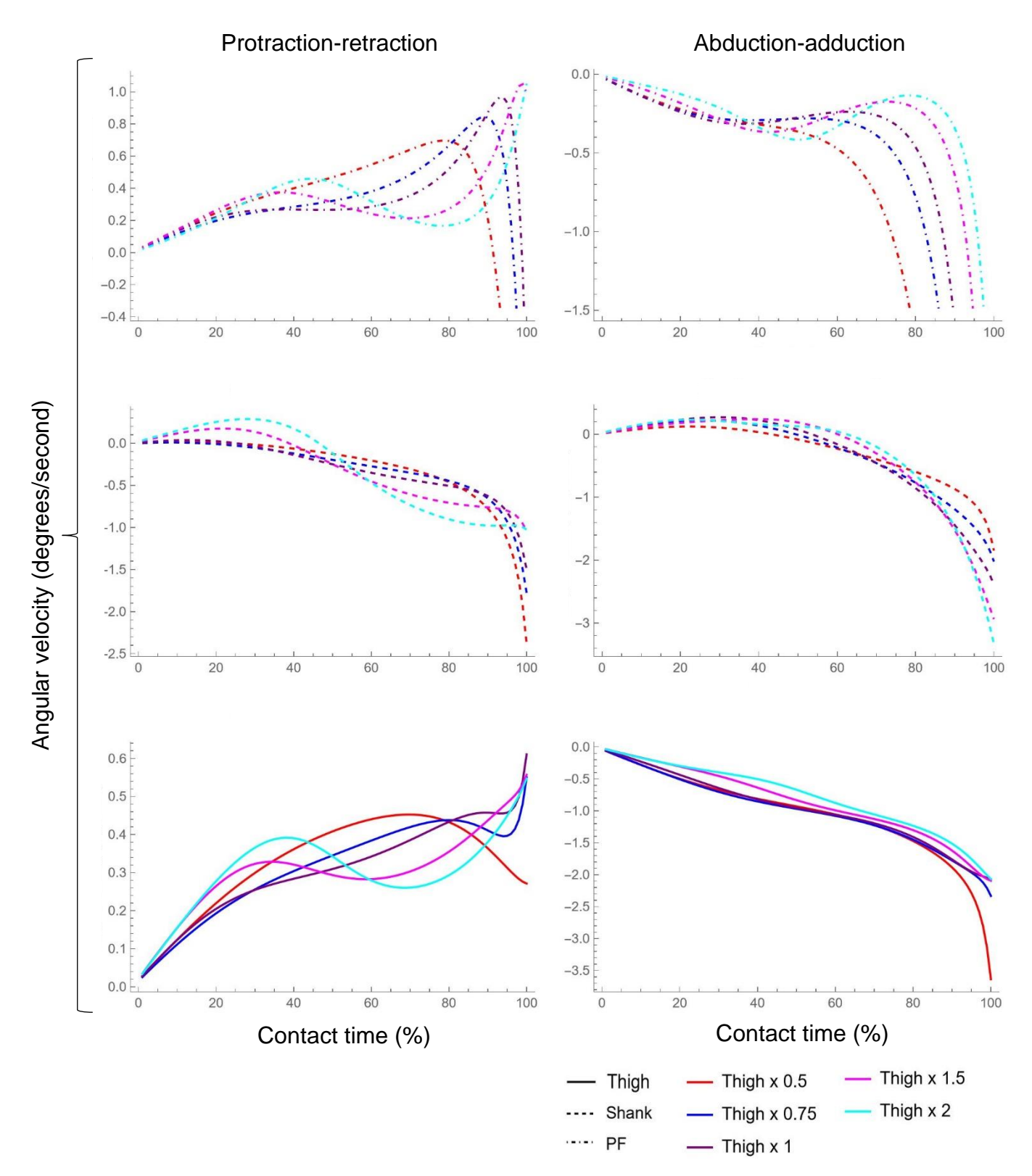


Figure G.4 - Hindlimb segment kinematics for hypothetical thigh proportions in the form of polar angular velocities. Each colour represents a different model of thigh length relative to shank length. Retraction (left column) of the thigh and proximal foot (PF) is indicated by positive velocity values. Negative values indicate shank retraction. Ventral adduction (right column) is indicated by negative values for all segments. See Figure 5.14 for polar angles.

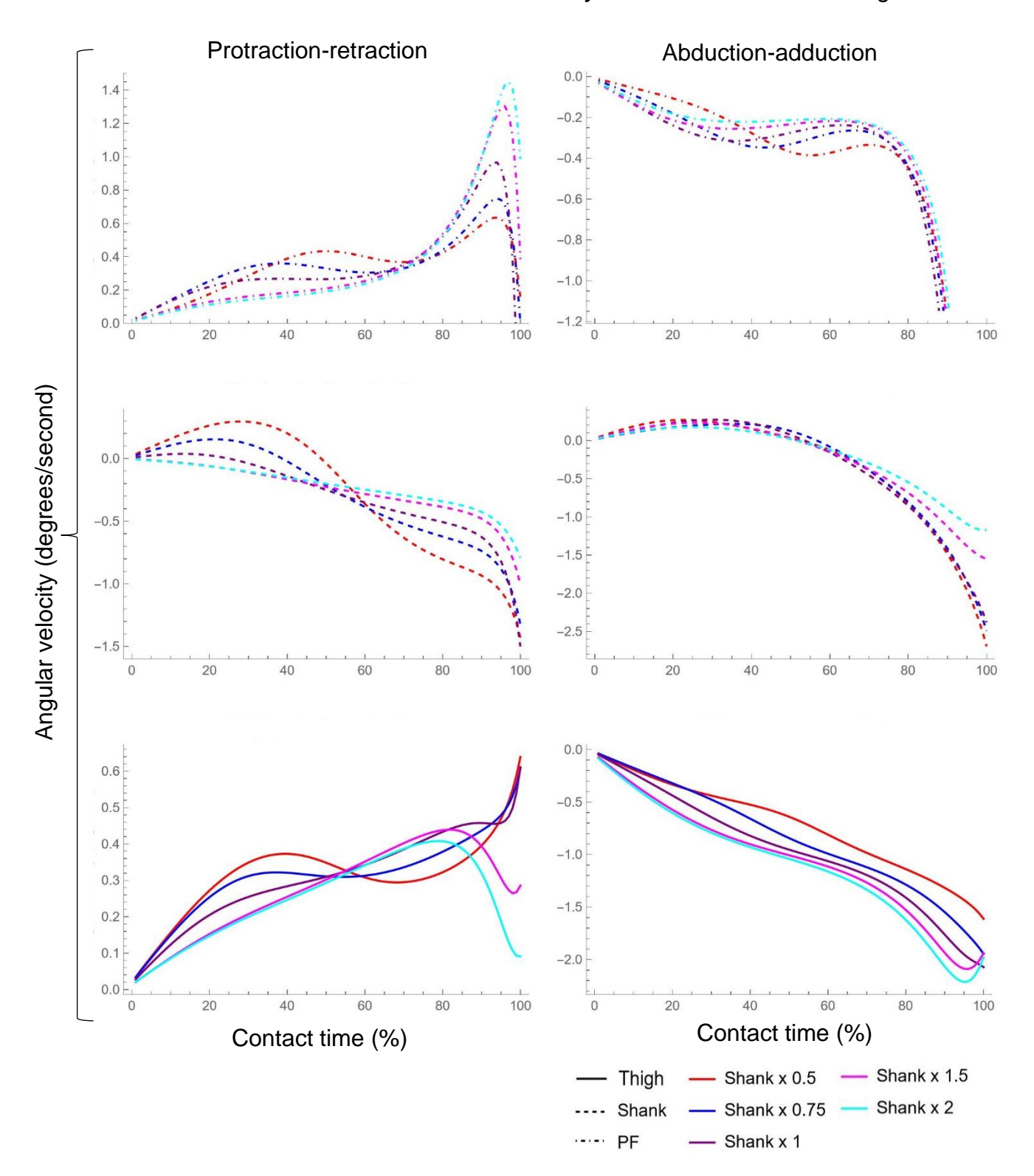


Figure G.5 - Hindlimb segment kinematics for hypothetical shank proportions in the form of polar angular velocities. Each colour represents a different model of shank length relative to thigh length. Retraction (left column) of the thigh and proximal foot (PF) is indicated by positive velocity values. Negative values indicate shank retraction. Ventral adduction (right column) is indicated by negative values for all segments. See Figure 5.15 for polar angles.

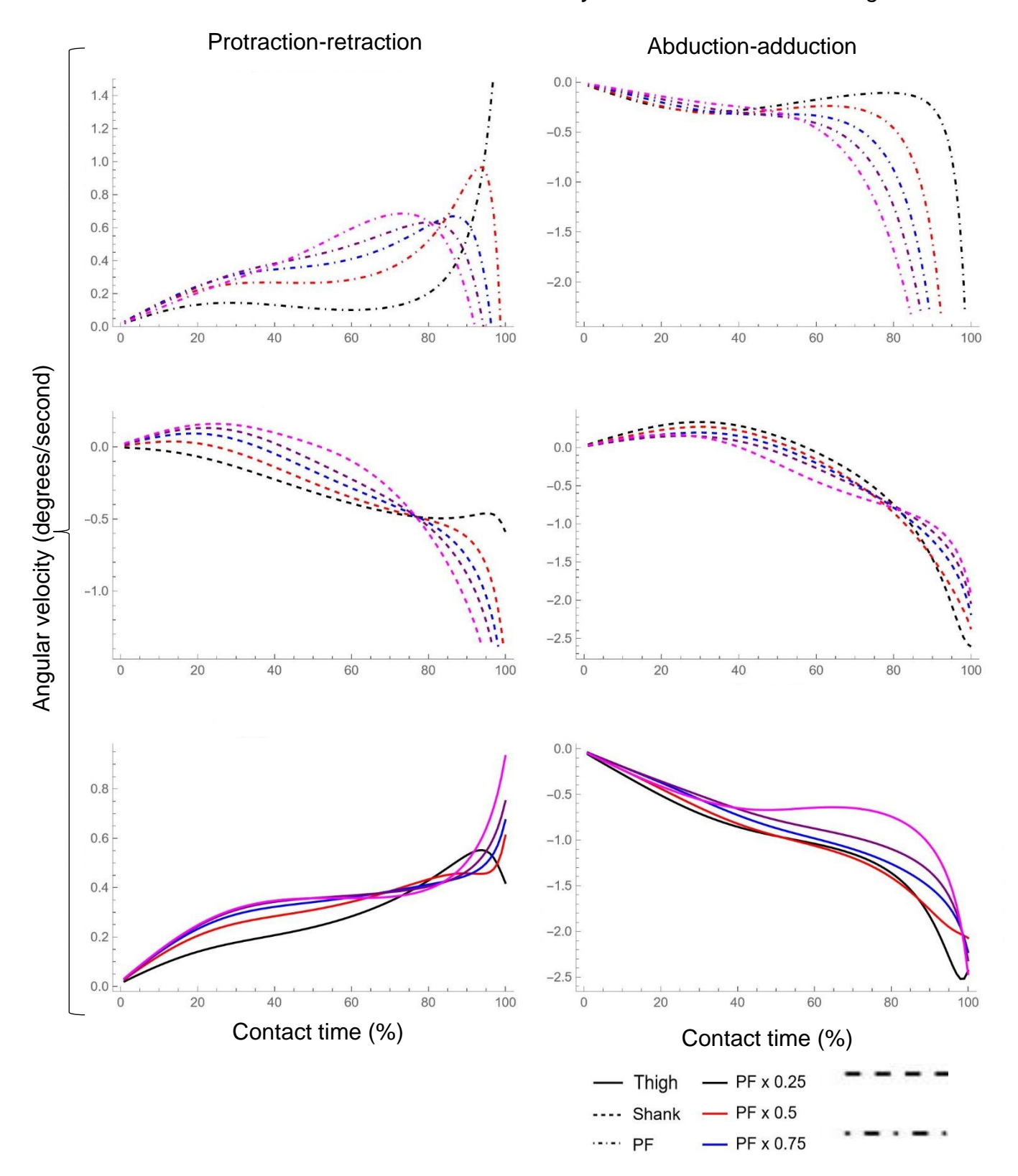
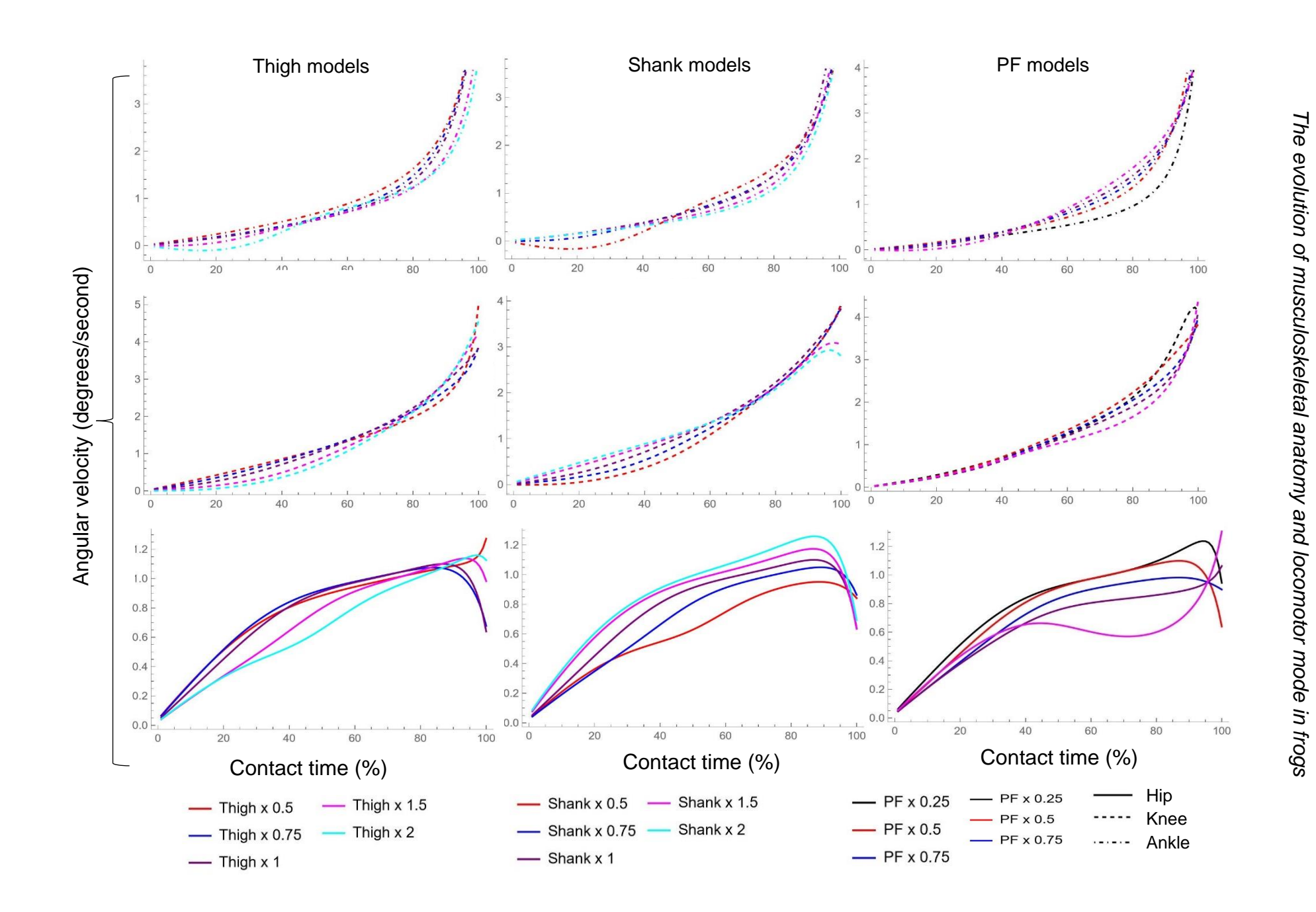


Figure G.6 - Hindlimb segment kinematics for hypothetical proximal foot (PF) proportions in the form of polar angular velocities. Each colour represents a different model of PF length relative to total hindlimb length. Retraction (left column) of the thigh and PF is indicated by positive velocity values. Negative values indicate shank retraction. Ventral adduction (right column) is indicated by negative values for all segments. See Figure 5.16 for polar angles.



The evolution of musculoskeletal anatomy and locomotor mode in frogs

Figure G.7 - 3D joint 'extension' angle velocities for hypothetical thigh (A), shank (B), and proximal foot (PF) (C) proportions. Positive values indicate faster joint opening. See Figure 5.17 for joint angles.

In Chapter 3, the maximum-minimum angle for all the polar angles and 3D joint angles was calculated and analysed in relation to locomotor mode and segment length relative to the total hindlimb length (Figure G.8; Figure G.9). As the data are not normally distributed (Table G.1), a non-parametric version of a phylogenetic ANOVA was performed (Table 5.5) which uses Residual randomization in permutation procedures (RRPP; Collyer & Adams, 2018). This was followed by pairwise post-hoc tests, to determine which locomotor modes (Table G.2) and phylogenetic groups (Table G.5) differ significantly in maximum-minimum angles. A simple linear regression was fit to the scatterplots examining angle changes versus relative segment length, and statistically analysed using either Pearson's correlation test or Spearman's rank test depending on data normality (Table G.3). The phylogenetic signal of each variable is reported in Table G.4.

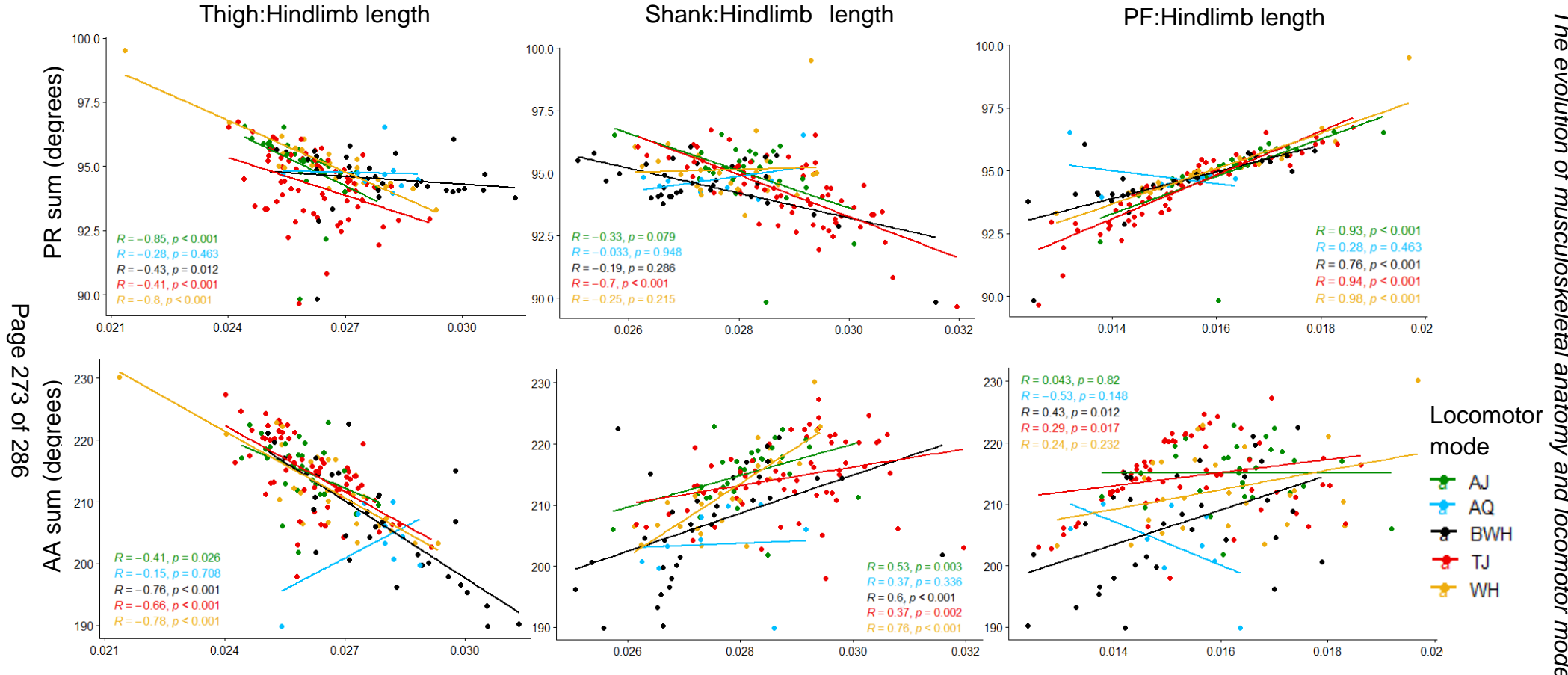


Figure G.8 - Maximum-minimum total protraction-retraction (PR) and abduction-adduction (AA) angle changes against relative hindlimb segment length for 164 frog taxa. The data are colour coded according to locomotor mode. PF = proximal foot. The statistics reported refer to Spearman's correlation tests.

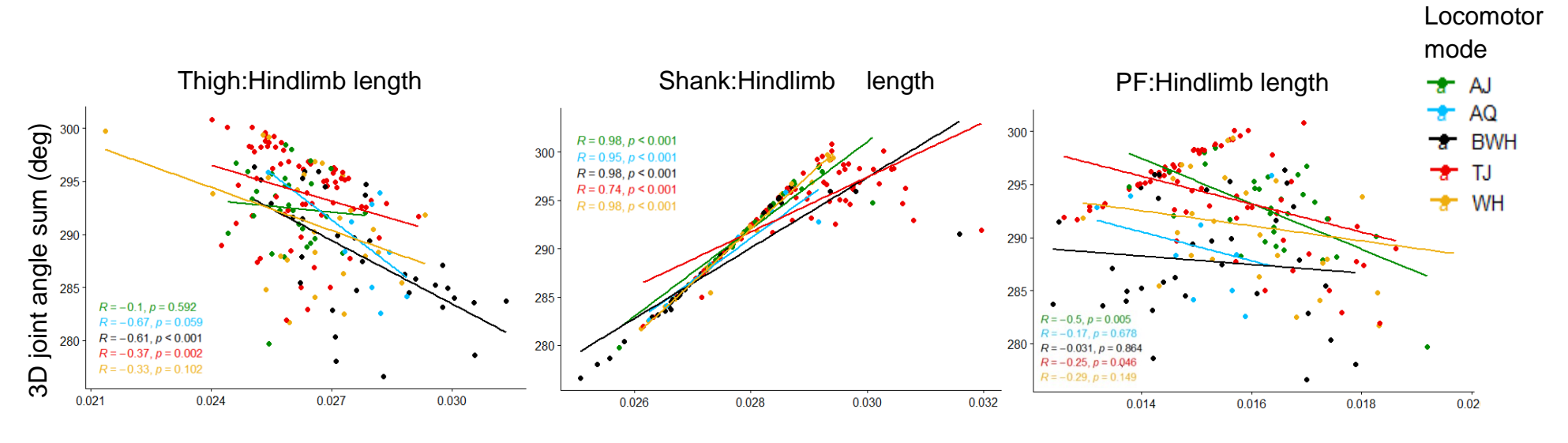


Figure G.9 - Maxi mum-minimum total 3D joint angle change against relative hindlimb segment length for 164 frog taxa. The data are colour coded according to locomotor mode. PF = proximal foot. The statistics reported refer to Spearman's correlation tests.

Table G.1 - Results of the Shapiro-Wilk normality test for maximum-minimum angle changes for each segment/joint motion for 164 frogs. Normally distributed angles are highlighted in bold. PR = protraction-retraction; AA = abduction-adduction; PF = proximal foot.

Angle	W	<i>p</i> -value
Thigh PR	0.973	0.003
Thigh AA	0.98	0.016
Shank PR	0.817	<0.001
Shank AA	0.994	0.724
PF PR	0.989	0.202
PF AA	0.966	<0.001
PR sum	0.922	<0.001
AA sum	0.976	0.005
Hip	0.991	0.398
Knee	0.896	<0.001
Ankle	0.977	0.008
Joint sum	0.963	<0.001

Table G.2 - Pairwise locomotor mode comparisons for maximum-minimum angle changes for each segment/joint across 164 frogs. Only significant relationships have been included. LMs = locomotor modes; CI = confidence interval; PR = protraction-retraction; AA = abduction-adduction; PF = proximal foot.

Angle	LMs	Difference	CI (95%)	Z-value	<i>p</i> -value
	AJ vs AQ	0.462	0.294	2.457	0.003
	AJ vs WH	0.474	0.208	3.292	0.001
Thigh PR	AQ vs TJ	0.393	0.267	2.391	0.009
	BWH vs WH	0.290	0.209	2.297	0.005
	TJ vs WH	0.405	0.182	3.367	0.001
	AJ vs AQ	1.094	0.877	1.974	0.020
Thigh AA	AJ vs WH	1.232	0.625	2.947	0.001
Thigh AA	BWH vs WH	0.633	0.606	1.653	0.041
	TJ vs WH	0.924	0.561	2.748	0.002
	AJ vs AQ	0.466	0.266	2.693	0.001
	AJ vs BWH	0.207	0.186	1.787	0.028
Shank PR	AJ vs WH	0.434	0.192	3.315	0.001
SHAHKEK	AQ vs TJ	0.390	0.240	2.609	0.005
	BWH vs WH	0.227	0.184	1.977	0.016
	TJ vs WH	0.358	0.172	3.335	0.001
	AJ vs AQ	0.625	0.350	2.794	0.001
Ola a sala A A	AJ vs BWH	0.303	0.240	2.016	0.016
Shank AA	AJ vs WH	0.555	0.252	3.183	0.001
	AQ vs TJ	0.508	0.311	2.572	0.005

	BWH vs WH	0.252	0.244	1.611	0.043
	TJ vs WH	0.437	0.220	3.114	0.001
	AJ vs AQ	0.500	0.322	2.452	0.003
	AJ vs WH	0.513	0.229	3.284	0.001
PF PR	AQ vs TJ	0.409	0.291	2.268	0.011
	BWH vs WH	0.298	0.225	2.178	0.009
	TJ vs WH	0.422	0.202	3.284	0.001
	AJ vs WH	1.122	0.647	2.704	0.001
PF AA	BWH vs WH	1.044	0.661	2.525	0.003
	TJ vs WH	1.058	0.562	2.851	0.002
	AJ vs AQ	1.428	0.864	2.540	0.001
	AJ vs WH	1.420	0.625	3.315	0.001
PR sum	AQ vs TJ	1.192	0.800	2.430	0.009
	BWH vs WH	0.814	0.610	2.178	0.011
	TJ vs WH	1.184	0.550	3.340	0.001
	AJ vs AQ	2.293	1.971	1.840	0.027
	AJ vs WH	2.908	1.429	3.029	0.001
AA sum	AQ vs TJ	1.804	1.771	1.533	0.047
	BWH vs WH	1.929	1.416	2.222	0.007
	TJ vs WH	2.419	1.233	3.065	0.001
	AJ vs AQ	1.067	0.703	2.402	0.003
	AJ vs BWH	0.486	0.476	1.611	0.048
⊔in	AJ vs WH	1.016	0.501	3.073	0.001
Hip	AQ vs TJ	0.817	0.637	2.053	0.021
	BWH vs WH	0.530	0.486	1.780	0.025
	TJ vs WH	0.765	0.435	2.806	0.001
	AJ vs AQ	1.769	1.134	2.443	0.003
	AJ vs WH	1.708	0.812	3.151	0.001
Knee	AQ vs TJ	1.391	1.023	2.164	0.018
	BWH vs WH	0.925	0.795	1.910	0.019
	TJ vs WH	1.330	0.707	2.960	0.001
	AJ vs AQ	1.138	0.865	2.109	0.017
	AJ vs WH	1.357	0.627	3.191	0.001
Ankle	AQ vs TJ	0.938	0.766	1.899	0.024
	BWH vs WH	0.949	0.623	2.475	0.003
	TJ vs WH	1.157	0.549	3.252	0.001
	AJ vs AQ	3.974	2.659	2.346	0.004
	AJ vs WH	4.081	1.909	3.148	0.001
Joint sum	AQ vs TJ	3.146	2.407	2.076	0.020
	BWH vs WH	2.404	1.879	2.102	0.011
	TJ vs WH	3.252	1.679	3.031	0.001

Table G.3 - Linear regression analyses between polar/joint angles and the relative length of each hindlimb segment. When the relationship is negative, the motion is more kinematically parsimonious when the segment is longer. Spearman rank tests are used for all variables excluding shank abduction-adduction (AA), proximal foot (PF) protraction-retraction (PR), and hip angle, which are normally distributed and therefore use Pearson's correlation tests.

Segment	Angle	Correlation	<i>p</i> -value
	Thigh PR	-0.51	<0.001
	Thigh AA	-0.16	0.039
	Shank PR	0.48	<0.001
	Shank AA	0.75	<0.001
	PF PR	-0.74	<0.001
Thigh : Uin dlimb	PF AA	-0.82	<0.001
Thigh:Hindlimb	PR sum	-0.46	<0.001
	AA sum	-0.71	<0.001
	Hip	-0.006	0.939
	Knee	-0.086	0.273
	Ankle	-0.87	<0.001
	Joint sum	-0.49	<0.001
	Thigh PR	-0.4	<0.001
	Thigh AA	0.86	<0.001
	Shank PR	-0.4	<0.001
	Shank AA	-0.16	0.043
	PF PR	-0.12	0.123
Shank:Hindlimb	PF AA	0.22	0.004
Shank.hindiinib	PR sum	-0.45	<0.001
	AA sum	0.56	<0.001
	Hip	0.89	<0.001
	Knee	0.91	<0.001
	Ankle	0.37	<0.001
	Joint sum	0.92	<0.001
	Thigh PR	0.89	<0.001
	Thigh AA	-0.54	<0.001
	Shank PR	0.089	0.258
	Shank AA	-0.62	<0.001
	PF PR	0.85	<0.001
DE: Lindlimh	PF AA	0.64	<0.001
PF:Hindlimb	PR sum	0.88	<0.001
	AA sum	0.28	<0.001
	Hip	-0.76	<0.001
	Knee	-0.66	<0.001
	Ankle	0.58	<0.001
	Joint sum	-0.23	0.004

Table G.4 - Phylogenetic signal for the maximum-minimum angle changes for each segment/joint across 164 frogs, where values closer to one indicate a stronger phylogenetic signal. PR = protraction-retraction; AA = abduction-adduction; PF = proximal foot.

Segment motion	Lambda	<i>p</i> -value
Thigh PR	0.491	0.004
Thigh AA	0.589	0.001
Shank PR	0.320	0.097
Shank AA	0.743	0.001
PF PR	0.745	< 0.001
PF AA	0.739	< 0.001
PR sum	0.418	0.012
AA sum	0.800	< 0.001
Hip	0.696	< 0.001
Knee	0.707	< 0.001
Ankle	0.900	< 0.001
Joint sum	0.844	< 0.001

Table G.5 - Pairwise phylogenetic group comparisons for maximum-minimum angle changes for each segment/joint across 164 frogs. Only significant relationships have been included. CI = confidence interval; PR = protraction-retraction; AA = abduction-adduction; PF = proximal foot.

Angle	Phylogenetic group	Difference	CI (95%)	Z-value	<i>p</i> -value
	Archaeobatrachia vs Hyloidea	0.864	0.217	4.681	0.001
	Archaeobatrachia vs Neobatrachia	0.555	0.315	2.613	0.002
Thigh PR	Archaeobatrachia vs Ranoidea	0.946	0.220	5.162	0.001
	Hyloidea vs Neobatrachia	0.309	0.249	1.924	0.020
	Ranoidea vs Neobatrachia	0.391	0.258	2.423	0.010
	Archaeobatrachia vs Hyloidea	2.576	0.668	4.632	0.001
	Archaeobatrachia vs Neobatrachia	1.671	0.977	2.626	0.003
Thigh AA	Archaeobatrachia vs Ranoidea	2.764	0.648	5.287	0.001
	Hyloidea vs Neobatrachia	0.904	0.789	1.821	0.023
	Ranoidea vs Neobatrachia	1.093	0.808	2.189	0.012
	Archaeobatrachia vs Hyloidea	0.812	0.199	4.817	0.001
	Archaeobatrachia vs Neobatrachia	0.503	0.289	2.64	0.003
Shank PR	Archaeobatrachia vs Ranoidea	0.880	0.205	5.253	0.001
	Hyloidea vs Neobatrachia	0.310	0.227	2.103	0.011
	Ranoidea vs Neobatrachia	0.377	0.234	2.545	0.007
Shank AA	Archaeobatrachia vs Hyloidea	1.071	0.266	4.813	0.001

	Archaeobatrachia vs Neobatrachia	0.641	0.382	2.553	0.004
	Archaeobatrachia vs Ranoidea	1.144	0.262	5.410	0.001
	Hyloidea vs Neobatrachia	0.429	0.305	2.191	0.010
	Ranoidea vs Neobatrachia	0.502	0.315	2.526	0.007
PF PR	Archaeobatrachia vs Hyloidea	0.960	0.235	4.676	0.001
	Archaeobatrachia vs Neobatrachia	0.610	0.351	2.604	0.002
	Archaeobatrachia vs Ranoidea	1.045	0.246	5.272	0.001
	Hyloidea vs Neobatrachia	0.350	0.275	1.988	0.017
	Ranoidea vs Neobatrachia	0.435	0.286	2.427	0.01
PF AA	Archaeobatrachia vs Hyloidea	2.065	0.658	4.066	0.001
	Archaeobatrachia vs Neobatrachia	1.615	0.994	2.533	0.003
	Archaeobatrachia vs Ranoidea	2.352	0.673	4.625	0.001
PR sum	Archaeobatrachia vs Hyloidea	2.637	0.637	4.790	0.001
	Archaeobatrachia vs Neobatrachia	1.668	0.951	2.622	0.003
	Archaeobatrachia vs Ranoidea	2.872	0.667	5.309	0.001
	Hyloidea vs Neobatrachia	0.969	0.746	2.021	0.014
	Ranoidea vs Neobatrachia	1.204	0.778	2.466	0.008
AA sum	Archaeobatrachia vs Hyloidea	5.712	1.475	4.487	0.001
	Archaeobatrachia vs Neobatrachia	3.928	2.201	2.715	0.002
	Archaeobatrachia vs Ranoidea	6.260	1.503	5.215	0.001
	Hyloidea vs Neobatrachia	1.784	1.741	1.565	0.044
	Ranoidea vs Neobatrachia	2.332	1.809	2.074	0.015
Hip	Archaeobatrachia vs Hyloidea	2.066	0.512	4.705	0.001
	Archaeobatrachia vs Neobatrachia	1.308	0.772	4.705	0.002
	Archaeobatrachia vs Ranoidea	2.211	0.525	2.611	0.001
	Hyloidea vs Neobatrachia	0.759	0.612	5.340	0.018
	Ranoidea vs Neobatrachia	0.903	0.634	2.310	0.012
Knee	Archaeobatrachia vs Hyloidea	3.403	0.847	4.732	0.001
	Archaeobatrachia vs Neobatrachia	2.166	1.235	2.631	0.002
	Archaeobatrachia vs Ranoidea	3.660	0.845	5.336	0.001
	Hyloidea vs Neobatrachia	1.237	0.995	1.957	0.017
	Ranoidea vs Neobatrachia	1.494	1.025	2.355	0.010
Ankle	Archaeobatrachia vs Hyloidea	2.501	0.656	4.552	0.001
	Archaeobatrachia vs Neobatrachia	1.697	0.970	2.665	0.002
	Archaeobatrachia vs Ranoidea	2.750	0.648	2.155	0.001
	Hyloidea vs Neobatrachia	0.804	0.765	1.627	0.038
	Ranoidea vs Neobatrachia	1.053	0.788	2.174	0.014
Joint sum	Archaeobatrachia vs Hyloidea	7.970	2.023	4.723	0.001
	Archaeobatrachia vs Neobatrachia	5.171	2.948	2.664	0.001
	Archaeobatrachia vs Ranoidea	8.621	2.033	5.306	0.001
			2.319	1.876	
	Hyloidea vs Neobatrachia	2.799	2.3191	1.070	0.022

Appendix H: Complementary hypothetical models

Chapter 5 and Chapter 6 use hypothetical models to better identify causal relationships and underlying mechanisms, as they enabled comparisons of hindlimb proportions where only one segment is varied at a time. In two sets of 'complementary models', the relative length of the thigh and shank are kept the same, while their length relative to the proximal foot and total hindlimb length are allowed to differ (Figure 5.18). By comparing these complementary models, the different impacts of relative segment length on hindlimb kinematics (Appendix Figure H.1) and dynamics (Appendix Figure H.2) during jumping can be examined.

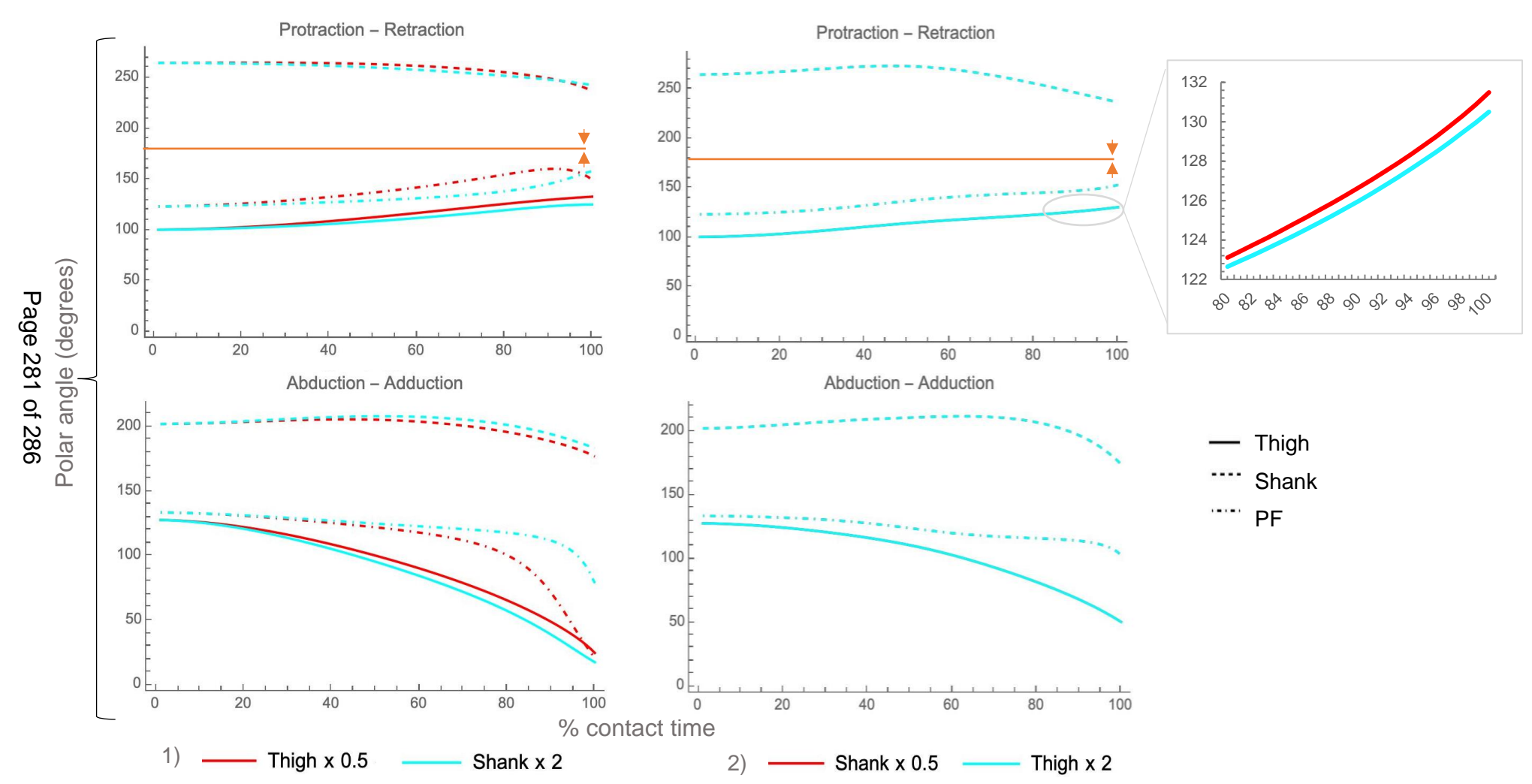


Figure H.1 - Hindlimb segment kinematics for two sets of complementary models of proximal hindlimb proportions – 1) where the thigh is half the length of the shank and 2) where the shank is half the length of the thigh. Retraction (top row) of the thigh and proximal foot (PF) is indicated by upward slopes towards 180 degrees (orange line). Downward slopes towards 180 degrees indicate shank retraction. Adduction (bottom row) is indicated by downward slopes for all segments.

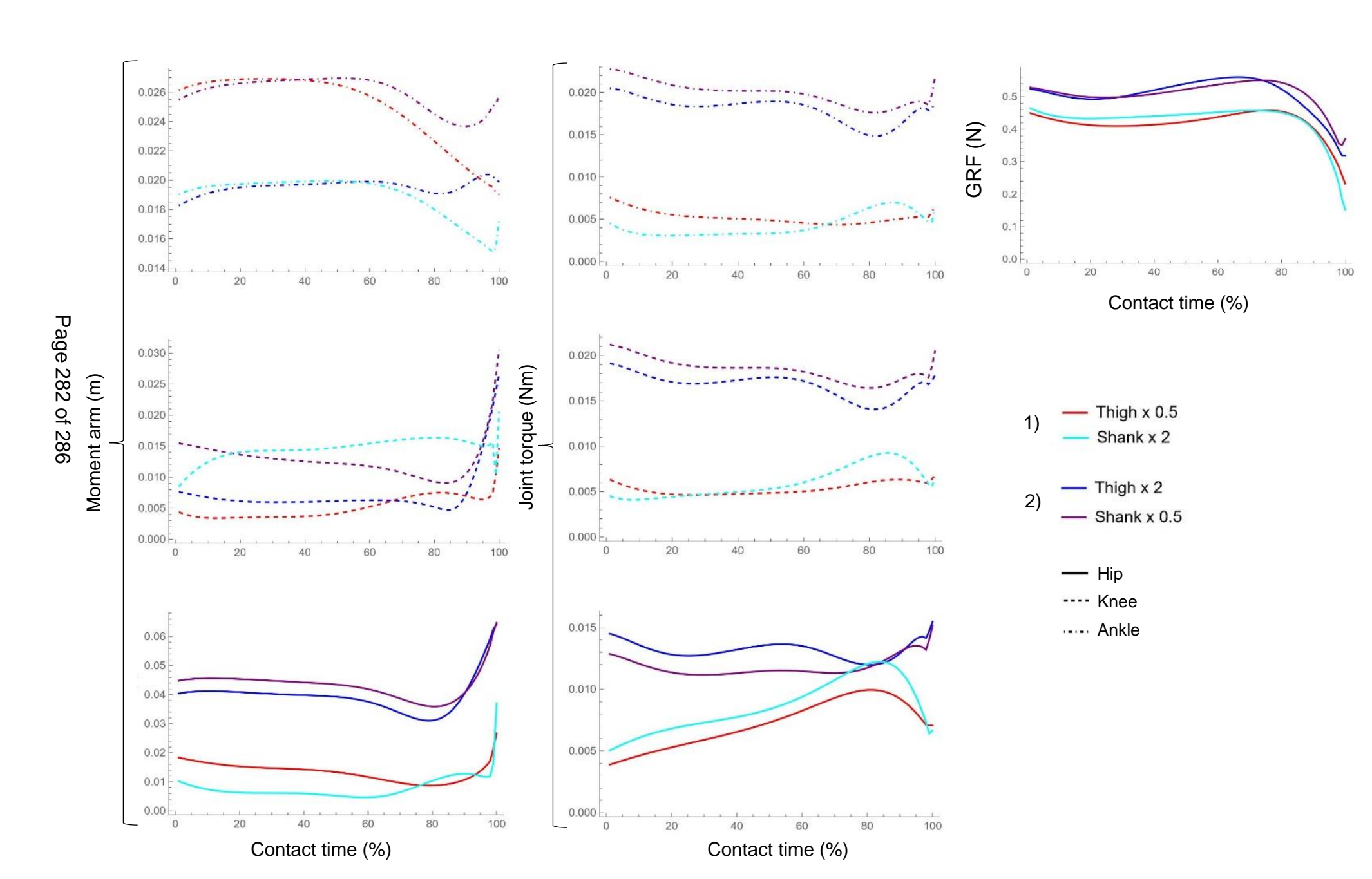


Figure H.2 - External moment arms, resultant joint torques, and ground reaction forces (GRF) for two sets of complementary models of proximal hindlimb proportions – 1) where the thigh is half the length of the shank and 2) where the shank is half the length of the thigh. The only difference between each model within these pairs is the length of the thigh and shank relative to the proximal foot and total hindlimb length i.e., the length of the thigh and shank relative to each other is the same. Line types represent each joint. Colours are different from the usual outlined in Table 5.2 for model pair (2) for the purpose of visual comparison.

Appendix I: MuJoCo environment

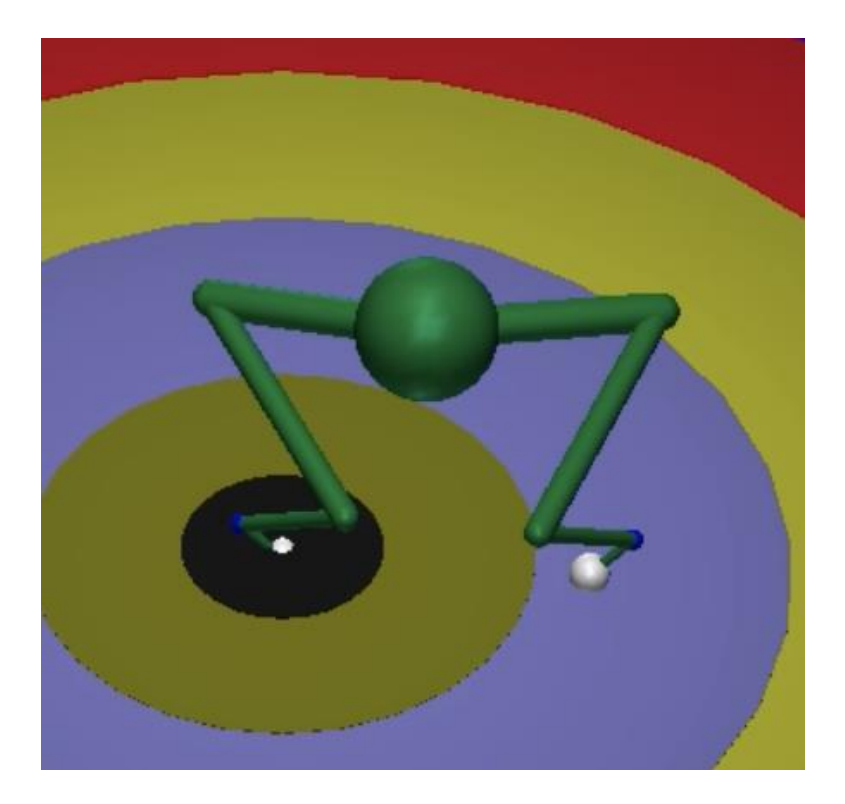


Figure I.1 – A screen capture of the frog model in MuJoCo. The sphere in the centre of the model represents the pelvis, while the white spheres represent the points of contact with the ground. The ground is simulated as a series of coloured rings to show that the model is appropriately centred within the environment.

Supplementary Datasets

All supplementary datasets have been uploaded to https://github.com/ucbtal9/ThesisSD.git with the associated metadata, which is also provided below.

Abbreviations used throughout the supplementary datasets:

LM – locomotor mode:

- AJ Arboreal Jumper
- TJ Terrestrial Jumper
- WH Walker-Hopper
- BWH Burrower-Walker-Hopper
- AQ Swimmer

HT - habitat type

- Aquatic spends the majority of its time in water.
- Arboreal spends the majority of its time in vegetation/trees.
- Terrestrial spends the majority of its time on the ground.
- Riparian spends approximately an equal amount of time in water as it does in terrestrial environments, i.e., relies on water outside of just for the purposes of reproduction.

Pelvic design:

- Sacrum shape is based on the descriptions of Emerson's (1979) three pelvic types - LB (lateral bending); FA (fore-aft sliding); SH (sagittal-hinge).
- Iliac crest
 - smooth (may have a small dorsal crest that extends no further than one-third of the way down the ilium)
 - ridge (the ilium must have a crest that extends at least halfway down the length of the ilium, occasionally tapering off towards the end)
- Urostylic crest
 - smooth (may have a small dorsal crest that extends no further than one-third of the way down the urostyle – possibly a remnant of the neural arch)
 - half (dorsal crest extends no further than halfway down the length of the urostyle)
 - o ridge (a dorsal crest that extends all the way down the length of the urostyle, occasionally tapering off at the end)
 - lateral (crest expands laterally)
 - T-shaped (crest forms the shape of a 'T' at the most proximal end of the urostyle).

Supplementary Dataset 1 - Full dataset

Introduced in Chapter 2, this data contains all of the raw measurement and categorical skeletal data acquired during the course of this PhD. Note that the variable 'gap' (the space between the base of the skull and the anterior end of the vertebral column) was measured to calculate snout-vent length (see Supplementary Dataset 2) and is not used in analyses.

Measurement data and pelvic features were collected using μ CT scans that are available on the online repository, MorphoSource. All ARK identifiers can be found under 'Scan source'.

Locomotor mode and habitat type data - determined by reading relevant literature, accessing AmphibiaWeb and IUCN websites, and personal communications with Andrew Gray (University of Manchester), Dave Blackburn (University of Florida), and Raúl Gómez (Universidad de Buenos Aires). See 'LM_citation' and 'habitat_citation'.

Phylogenetic clade - this categorisation was based on the placement of the study taxa in the Jetz & Pyron (2017) phylogeny.

* denotes the pelvis features which differ to previous findings in Reilly & Jorgensen (2011) and Jorgensen & Reilly (2013).

Supplementary Dataset 2 - Structural dataset

Introduced in Chapter 2, this dataset is the same as the full dataset, except that some measurements have been combined to form larger structural measurements of frog morphology:

- Snout-vent length (SVL): skull + gap + vertebrae + pelvis lengths
- Hindlimb length: femur + tibiofibula + calcaneum + foot lengths
- Forelimb length: humerus + radioulna + hand lengths

Supplementary Dataset 3 - Predictive analyses dataset

Introduced in Chapter 2, this dataset contains details of the potential secondary locomotor modes and habitat types tested in predictive models, and their sources.

It also contains the results of the linear discriminant analyses (LDA) and phylogenetic flexible discriminant analyses (pFDA) for locomotor mode, habitat type and phylogenetic group.

* - the alternative option was correctly predicted.

Supplementary Dataset 4 - CT data

This dataset contains all the information for each specimen used in Chapter 3, including locomotor mode, habitat type, scanning parameters, staining protocols, and sources. The 'study taxa' tab contains information for all species, while the 'UF specimens' tab provides more details about the specimens I scanned at the University of Florida, such as basic size measurements and the locality of collection.

Supplementary Dataset 5 - Muscle head counts

The number of separate muscle heads observed in the pelvis, thigh and shank for the specimens used in Chapter 3. The full names for each muscle can be found in the 'List of muscle abbreviations' at the beginning of the thesis.

Quotes and colouring are based on Přikryl *et al.* (2009). Green indicates that my findings match, red indicates that they do not. Orange means there is nothing to say this is not true, or there is suggestive wording in Přikryl *et al.* (2009), e.g., 'may be absent/separate heads in some individuals/species.'

Supplementary Dataset 6 - Fibre architecture data

The raw data collected from Chapter 4, where the fibre architecture of four muscles was analysed in ten species. This dataset includes the number of muscles fibres with high enough quality to been traced by the 'good.fibes' function in R, the grayscale cut-off used for each muscle, muscle belly volume (MBV), the resulting mean fibres lengths, pennation angle, physiological cross-sectional area (PCSA), and fibre length relative to muscle belly length (FL:MBL).